Examination of seismic models: Inhomogeneity, anisotropy, and Backus averaging

by

© Ayiaz Kaderali

A Thesis submitted to the School of Graduate Studies in partial fulfillment of the requirements for the degree of

Doctor of Philosophy

Department of Earth Sciences

Memorial University of Newfoundland

May 2025

St. John's Newfoundland and Labrador

Abstract

The thesis examines seismic models of the Earth in terms of inhomogeneity, anisotropy, and Backus averaging. Chapter One provides background information. Chapters two to four are described below. The fifth chapter provides concluding remarks. The common thread through all the chapters is the use of data acquired in the same borehole: Vertical Seismic Profiling (VSP) data and a sonic log.

A study on the estimation of inhomogeneity and anisotropy parameters from walkaway VSP traveltime data, using a multi-layered mathematical model, is presented in the second chapter. Least-squares residuals between measured and modelled traveltimes are minimized to estimate the anisotropy parameter, χ, and inhomogeneity parameters, a and b, of the layers. A two-step optimization is performed, and an adaptation of the Nelder-Mead algorithm is used to estimate the parameters. The methodology is applied to synthetic data and then to real data. An assessment of the reliability of results subject to noise shows the noise threshold to be quite low. Beyond this threshold, parameter estimates have diminishing accuracy. Using synthetic data, parameters are reliably estimated. With real data, parameter estimations indicate anisotropy to be exhibited only in the bottom layer.

The third chapter is on the use of the Bayesian Information Criterion (BIC) for the selection of a model that is most representative and has the fewest number of parameters to fit the data. Eight three-layer models, with different parameterizations, are considered that correspond to the medium in which the VSP data were acquired. The simplest model

is inhomogeneous and isotropic with six parameters. The most complicated model is inhomogeneous and anisotropic and consists of nine parameters. BIC values indicate the best model as the one with seven parameters and anisotropy in the third layer.

An adaptation of the Backus average to obtain more accurate traveltimes for obliquely propagating waves is presented in the fourth chapter. A weighting is applied that considers the distance travelled in each layer, with weights corresponding to source-receiver offsets. Traveltimes computed from the standard Backus average are compared to traveltimes computed using the modified Backus average in three cases. The first, a ten-layer synthetic model with a 30-degree take-off angle, the second, with an extreme distance of 7000 m, and the third, with real data. In all three cases, the modified Backus average performs better.

All three objectives: estimation of inhomogeneity and anisotropy parameters, use of BIC to indicate the most representative model of the medium based on the fit of the data, and modification of the Backus average to correct for non-vertical raypaths to obtain more accurate traveltimes, were successfully achieved.

To my wife Faiza and our daughters Shaleeza and Shaziana for believing in me …

ACKNOWLEDGEMENTS

I would like to thank Dr. Michael A. Slawinski for encouraging me to do this thesis and for his supervision. His patience and guidance have had a direct correlation with the successful accomplishment of this thesis, for which I am most grateful. His prompt responses and availability for discussions are also appreciated. It has been a privilege to have been a student of Dr. Slawinski.

My gratitude also extends to Dr. Charles Hurich and Dr. Colin Farquharson for their time, support, encouragement, and valuable feedback as members of my supervisory committee. Additionally, I would like to thank Dr. Farquharson for accepting to be my co-supervisor, and for sponsorship to access the Digital Research Alliance of Canada/ACENET supercomputers for some of the research that was conducted.

I want to acknowledge and thank Dr. Theodore Stanoev and Dr. David R. Dalton for the collaborative research conducted with them on some of the topics. For the many hours and days spent with Theo in discussion and research, often late into the evenings!

Last, but not least, I would like to thank my wife and children for their unwavering encouragement and moral support, as well as for foregoing family time and events to enable work on the thesis to be carried out.

Table of Contents

List of Tables

List of Figures

Chapter 1

1 Introduction

This thesis is written in traditional format and consists of five chapters. The thesis was initially submitted in manuscript format and has been rewritten to comply with Memorial University of Newfoundland guidelines.

I examine three specific issues in this thesis. I use data obtained from the same borehole for all three: a zero-offset vertical seismic profile, a walkaway vertical seismic profile, and a sonic log. The first issue examined is the estimation of parameters of the earth using a mathematical model derived from traveltimes from the walkaway vertical seismic profile: I use a new application of a widely used numerical optimization method, the Nelder-Mead algorithm, and analytical equations formulated by Dr. Michael Slawinski, in estimating the parameters. The second issue is how to select the best representative model of the earth from a number of models: For this, I use the Bayesian Information Criterion. The third issue is the accurate prediction of traveltimes using the Backus average for seismic waves propagating non-vertically through a medium: I apply a modified Backus average to obtain an equivalent medium that allows for more accurate traveltime predictions.

In this chapter, I provide definitions and descriptions of various terms and concepts used in the thesis, and a summary of the chapters that follow. I also describe the data referred to in the chapters and the geological setting.

1.1 Overview and Summary

In the second chapter, I consider a mathematical model that accounts for anisotropy and inhomogeneity to model measured walkaway vertical seismic profiling (VSP) traveltimes. The concept of the model is as described by Slawinski et al. (2004), and subsequently Rogister and Slawinski (2005), and assumes that velocity increases linearly with depth, given in terms of parameters a and b, whereas anisotropy is the result of elliptical velocity dependence given in terms of parameter χ.

An analytical equation is used to calculate the traveltime between a source and a receiver. Using traveltimes from a series of sources in a line to a single receiver, model parameters are estimated. The approach requires two steps of optimization, firstly, to find the raypaths, and secondly, to calculate traveltimes and the residual sum of squares (RSS). These steps are repeated to find parameter values of the medium by minimizing the RSS between the model and the data. The validity of this approach is assessed through synthetic traveltime data. Furthermore, the reliability of results under the influence of random noise is examined. The method is then used for a real-data case.

In the third chapter, the Bayesian Information Criterion (BIC) is presented as a means for selecting the best representative model from a number of models. Each model is composed of three layers with varied parameters. The models are generated to correspond to the multilayered medium, assumed to consist of anisotropic vertically inhomogeneous layers, that the VSP data were acquired in.

In the fourth chapter, the validity of the Backus average, whose weights are layer thicknesses, is examined. It is put forward that the validity is limited to waves whose incidence is nearly vertical and that the accuracy of this average decreases as ray paths get increasingly non-vertical, i.e., with the increase in source-receiver offsets. If, however, the weighting is adjusted by the distance travelled by a signal in each layer, a modified average can be obtained, which results in a more accurate prediction of traveltimes through these layers.

1.2. Definitions and Descriptions

All depths are from mean sea level (MSL) unless indicated otherwise.

1.2.1 Hookean solids

Hookean solids are mathematical entities, defined by Hooke's law (Chapman, 2004; Ling et al., 2016), that provide an analogy to real rocks and a means to study seismic phenomena (Brown and Slawinski, 2017). Studying theoretical perturbations of Hookean solids, for example, caused by the propagation of seismic waves, is analogous to studying the behaviour of rocks under the influence of seismic waves.

Hookean solids are defined by their mechanical properties as relating linearly the stress tensor, σ, and the strain tensor, ε, where c is the elasticity tensor (e.g., Slawinski, 2003).

$$\sigma_{ij} = \sum_{k=1}^{3}\sum_{l=1}^{3} c_{ijkl}\epsilon_{kl}, \qquad i,j = 1,2,3.$$

1.2.2 Vertical Inhomogeneity

In a medium that exhibits only vertical inhomogeneity (e.g., due to variations in lithology and pressure effects), $v = v(z)$, and a linear velocity dependence with depth, the inhomogeneity can be described by the linear velocity function:

$$v = a + bz,$$

where a is the velocity at zero depth, and b is the gradient which defines the rate of increase in velocity with depth z (Červený, 2001; Al-Chalabi and Rosenkranz, 2002; Rogister and Slawinski, 2005).

1.2.3 Anisotropy

1. Anisotropy is defined as the variation of seismic velocity depending on the direction in which it is measured (Sheriff, 1991). Figure 1.1 illustrates the terms: isotropic, homogeneous, anisotropic, and inhomogeneous. In general, stratified media, such as sedimentary rocks, exhibit anisotropy (Uhrig and Van Melle, 1955; Vander Stoep, 1966). Shales, which are the most common lithology in sedimentary basins, are anisotropic because of any or all of the following: compaction, preferential mineral alignment, cracks, and organic content (Hornby et al., 1994; Sayers, 2005). In sedimentary basins, the anisotropy of shales is caused by the preferential alignment of plate-shaped clay particles during deposition (Winkler and Murphy, 1995; Tsvankin et al., 2010). Figure 1.2 shows the wavefront geometry in an anisotropic medium. In the type of anisotropic medium typical in

sedimentary basins, e.g., shale, the horizontal velocity, v_x, is greater than the vertical velocity, v_z. In an isotropic medium, $v_x = v_z$. It is possible for v_x to be less than v_z, e.g., in media that exhibit vertical fractures (Berryman, 2007).

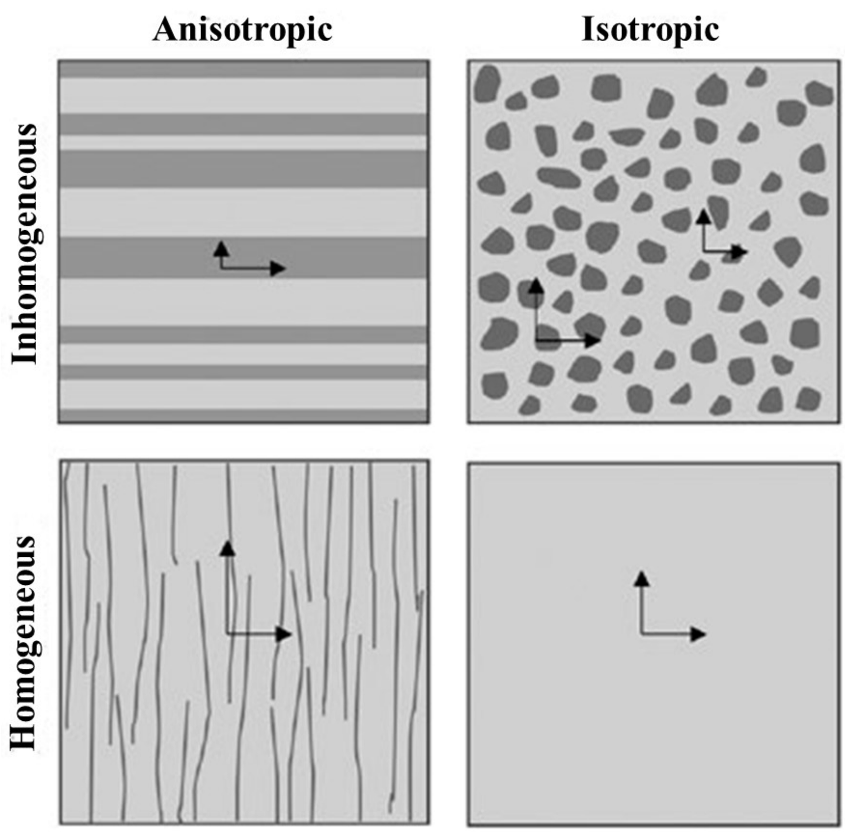

Figure 1.1: Sketches to illustrate the terms: isotropic–physical properties are the same in all directions; homogeneous–physical properties are the same at all locations; anisotropic–physical properties depend on direction; and inhomogeneous–physical properties depend on location. Length of black arrow is proportional to velocity, as measured in direction arrow is pointing. (Adapted from Lynn, 2018)

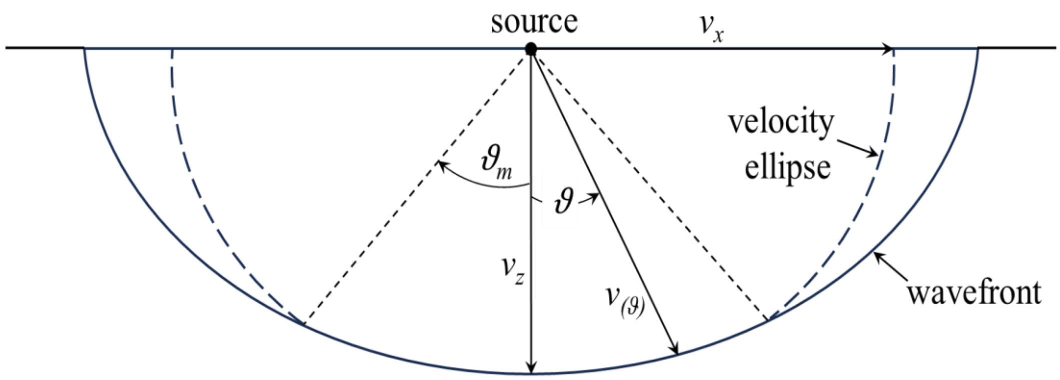

Figure 1.2: Wavefront geometry in an anisotropic medium. The solid curve is the wavefront at an instant in time. The velocity at any non-vertical angle, ϑ, is $v_{(\vartheta)}$. The vertical velocity, when $\vartheta = 0$, is v_z, and the horizontal velocity is v_x. In an anisotropic medium, $v_x > v_z$. When $v_x = v_z$, the medium is isotropic and the wavefront is a semi-circle. (Adapted from Vander Stoep, 1966)

1.2.4 *abχ* model

The velocity model for an anisotropic medium, with a vertical axis of symmetry, can be represented by three parameters a, b, and χ (Rogister and Slawinski, 2005). Since I use VSP first-arrival times, the model considers only quasi-*p* velocities (Slawinski et al., 2004). I refer to such a model as the *abχ* model in this thesis. The model describes the propagation of a signal in the vertical plane containing the source and receiver, subject to the following assumptions:

i) vertical inhomogeneity with a linear velocity dependence with depth, and

ii) the anisotropy results from an elliptical velocity dependence on direction, defined by the ellipticity parameter,

$$\chi = \frac{{v_x}^2 - {v_z}^2}{2{v_z}^2}, \tag{1.1}$$

where v_x and v_z are the magnitudes of the horizontal and vertical wavefront velocities, at any depth, respectively. When $v_x = v_z$, $\chi = 0$, and the medium is isotropic.

For such a model, the elliptical velocity dependence of a wavefront is given by

$$v(\vartheta) = \sqrt{{v_x}^2 \sin^2\vartheta + {v_z}^2 \cos^2\vartheta} = v_z\sqrt{(1+2\chi)\sin^2\vartheta + \cos^2\vartheta}\,, \tag{1.2}$$

where ϑ is the phase angle, which is measured between the wavefront normal and the z-axis. We consider an xz-plane where the horizontal axis, x, corresponds to offset and the vertical axis, z, corresponds to depth.

From a source placed at point (0,0), to a receiver at point (x, z), the traveltime is obtained using equation (1.3) as used by Kaderali (2009),

$$t = \frac{1}{2b}\left[\ln\frac{1-\sqrt{1-p^2a^2(1+2\chi)}+pbx}{1+\sqrt{1-p^2a^2(1+2\chi)}-pbx} - \ln\frac{1-\sqrt{1-p^2a^2(1+2\chi)}}{1+\sqrt{1-p^2a^2(1+2\chi)}}\right], \tag{1.3}$$

this is equivalent to (Rogister and Slawinski, 2005)

$$t = \frac{1}{b}\{\tanh^{-1}[\,pbx - \sqrt{1-(1+2\chi)p^2a^2}] + \tanh^{-1}\sqrt{1-(1+2\chi)p^2a^2}\}, \tag{1.4}$$

which is obtained by making the substitution (Slawinski, 2020a)

$$\zeta \coloneqq pbx - \sqrt{1-p^2a^2(1+2\chi)})\,, \tag{1.5}$$

and using the hyperbolic function identity

$$\tanh^{-1}\zeta = \frac{1}{2}\ln\frac{1+\zeta}{1-\zeta}. \tag{1.6}$$

In equations (1.3) and (1.4), the ray parameter, which is a conserved quantity along the ray, is

$$p = \frac{2x}{\sqrt{[x^2+(1+2\chi)z^2][(2a+bz)^2(1+2\chi)+b^2x^2]}}. \tag{1.7}$$

As shown by Slawinski (2020a), the horizontal distance along the x-axis, for a downgoing signal travelling along an elliptical arc, is

$$x = \frac{1}{pb}\left[\sqrt{1-(1+2\chi)p^2a^2} - \sqrt{1-(1+2\chi)p^2(a+bz)^2}\right]. \tag{1.8}$$

In keeping with SI units, the units for a and b are m/s and 1/s, respectively, for speed are m/s, for traveltime are s, and for the ray parameter, p are s/m.

1.2.5 Backus Average

The Backus (1962) average enables us to quantify the response of a wave propagating through a series of parallel Hookean layers whose thicknesses are much smaller than the wavelength. The Backus average can be used to model a finely stratified medium as a single homogeneous medium. As per Backus (1962):

> A horizontally layered inhomogeneous medium, isotropic or transversely isotropic, is considered, whose properties are constant or nearly so when averaged over some vertical height l'. For waves longer than l' the medium

is shown to behave like a homogeneous, or nearly homogeneous, transversely isotropic medium whose density is the average density and whose elastic coefficients are algebraic combinations of averages of algebraic combinations of the elastic coefficients of the original medium. The nearly homogeneous medium is said to be ‘long-wave equivalent' to the original medium.

Essentially, layered media composed of individual anisotropic or isotropic layers are upscaled to a single layer while maintaining the symmetry of the media. As explained by Slawinski (2020b), the density of this resultant single layer or “equivalent medium” is the average density and its elastic coefficients are expressed as averages of the elastic coefficients of the original medium.

As explained by Slawinski (2020b), if each individual isotropic layer is described by the density-scaled elasticity parameters, then the corresponding resultant parameters of the transversely isotropic medium are given by

$$c_{1111}^{\overline{\mathrm{TI}}} = \overline{\left(\frac{c_{1111} - 2c_{2323}}{c_{1111}}\right)}^{2} \overline{\left(\frac{1}{c_{1111}}\right)}^{-1} + \overline{\left(\frac{4(c_{1111} - c_{2323})c_{2323}}{c_{1111}}\right)}, \tag{1.9}$$

$$c_{1122}^{\overline{\mathrm{TI}}} = \overline{\left(\frac{c_{1111} - 2c_{2323}}{c_{1111}}\right)}^{2} \overline{\left(\frac{1}{c_{1111}}\right)}^{-1} + \overline{\left(\frac{2(c_{1111} - c_{2323})c_{2323}}{c_{1111}}\right)}, \tag{1.10}$$

$$c_{1133}^{\overline{\mathrm{TI}}} = \overline{\left(\frac{c_{1111} - 2c_{2323}}{c_{1111}}\right)}^{2} \overline{\left(\frac{1}{c_{1111}}\right)}^{-1}, \tag{1.11}$$

$$c_{1212}^{\overline{\mathrm{TI}}} = \overline{c_{2323}}\,, \tag{1.12}$$

$$c_{2323}^{\overline{\mathrm{TI}}} = \overline{\left(\frac{1}{c_{2323}}\right)}^{-1}, \tag{1.13}$$

$$c_{3333}^{\overline{\mathrm{TI}}} = \overline{\left(\frac{1}{c_{1111}}\right)}^{-1}, \tag{1.14}$$

which are the Backus parameters for isotropic layers. The bar indicates an average. Density-scaled elasticity parameters, c_{1111} and c_{2323}, can be calculated using P-wave and S-wave speeds, v_p and v_s, which can be obtained from compressional and shear sonic logs: $c_{1111} \coloneqq c_{1111}^{*}/\rho = v_p^2$ and $c_{2323} \coloneqq c_{2323}^{*}/\rho = v_s^2$, where the * denotes non-scaled elasticity parameters.

The anisotropy resulting from taking the Backus average is induced from thin layering. If the layers are isotropic, then the Backus average of these layers results in a transversely isotropic medium. In this medium, the horizontal velocity differs from the vertical velocity as a function of the elasticity parameters of the medium. This is distinct from the elliptical anisotropy that is described in Section 1.2.4. In Section 1.2.4, the elliptical anisotropy pertains to an elliptical velocity dependence of a ray in a medium: the horizontal velocity is a scalar multiple of the vertical velocity, as a function of the anisotropy parameter χ.

According to Backus (1962) the average of function $f(x_3)$ of "length" l' is given by,

$$\bar{f}(x_3) = \int_{-\infty}^{\infty} w(\xi - x_3)\, f(\xi)\, \mathrm{d}\xi \,, \tag{1.15}$$

where x_3 is the position coordinate in a Cartesian coordinate system consisting of three perpendicular axes: the *x*- , the *y*- , and the *z*-axis (otherwise referred to as the x_1- , x_2- , and x_3-axis, respectively). ξ is an integrating parameter (or dummy variable) that allows for integration along the x_3-axis. $(\xi - x_3)$ specifies a translation of the weighting function so that it is centered on x_3. $w(x_3)$ is the weighting function with the following properties:

$$w(x_3) \geq 0, \qquad w(\pm\infty) = 0,$$

$$\int_{-\infty}^{\infty} w(x_3)\ \mathrm{d}x_3 = 1, \tag{1.16}$$

$$\int_{-\infty}^{\infty} x_3 w(x_3)\ \mathrm{d}x_3 = 0, \tag{1.17}$$

$$\int_{-\infty}^{\infty} x_3^2 w(x_3)\ \mathrm{d}x_3 = (l')^2. \tag{1.18}$$

Integral (1.16) is the zeroth moment, it is the area under the curve $w(x_3)$ and is unity. The first moment, which is the mean, is given by integral (1.17) and is zero. The second moment is the variance, often written as σ^2. The positive square root σ of the variance is the standard deviation (Thomas, 1986). Here, the variance is $(l')^2$, and the standard deviation is l'.

Equation (1.15) can be viewed as the convolution of two functions f and w to obtain the average f:

$$\bar{f}(x_3) = f(x_3) * w(-x_3).$$

$\bar{f}(x_3)$ is a moving average. It can be computed as a convolution or arithmetically. To perform it as a convolution, the weights and the quantities to be averaged are considered to be components of vectors, and their scalar or dot product evaluated.

The length l' is a controversial parameter (Liner and Fei, 2007). It does not appear in equation (1.15), as it is defined by the properties of the weighting function, $w(x_3)$, in the equation. $w(x_3)$ can be any desired probability-density function, for example, a Gaussian curve (normal distribution) or a boxcar function (uniform distribution), that satisfies the above-mentioned properties. Backus, in his paper, states that $\bar{f}(x_3)$ "is the average of f over a distance roughly l' around the position x_3". This is because l' is arbitrary, i.e., it does not have a specific value. It is dependent on the function that is to be used. If the probability-density function, for example, is Gaussian, then l' is the standard deviation. If it is a boxcar function, then the averaging is performed along the length of the boxcar, and l' is not as meaningful. Figure 1.3 is a pictorial depiction of convolution with a Gaussian weighting function and a boxcar weighting function.

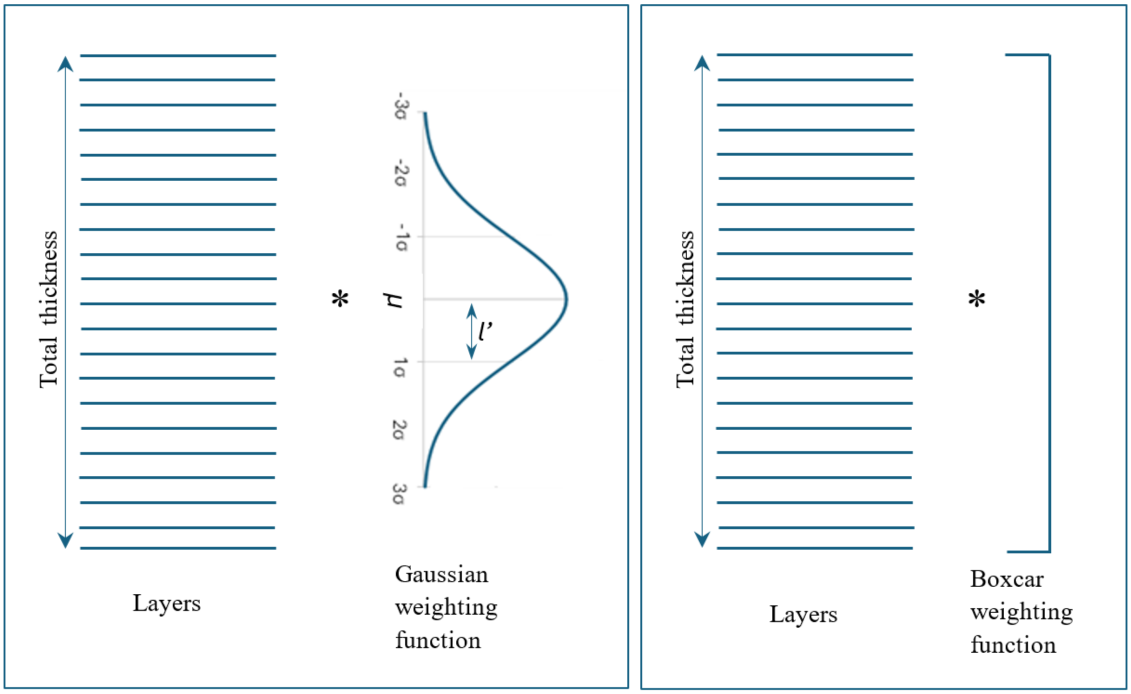

Figure 1.3: Sketch of convolution with a Gaussian weighting function and a boxcar weighting function. The Gaussian weighting function has an averaging window of length l' around the mean, μ, of the function. It is a moving average. For the boxcar function, the averaging is performed along the length of the boxcar.

In Chapter 4 of this thesis, I use the boxcar function as the weighting function. The averaging is performed along the length of the boxcar, and the weights are the thicknesses of the layers. The Backus average of thin layers appears, at the scale of a long wavelength (where the wavelength is considerably larger than the layer thicknesses), as a homogeneous transversely isotropic medium as depicted in Figure 1.4.

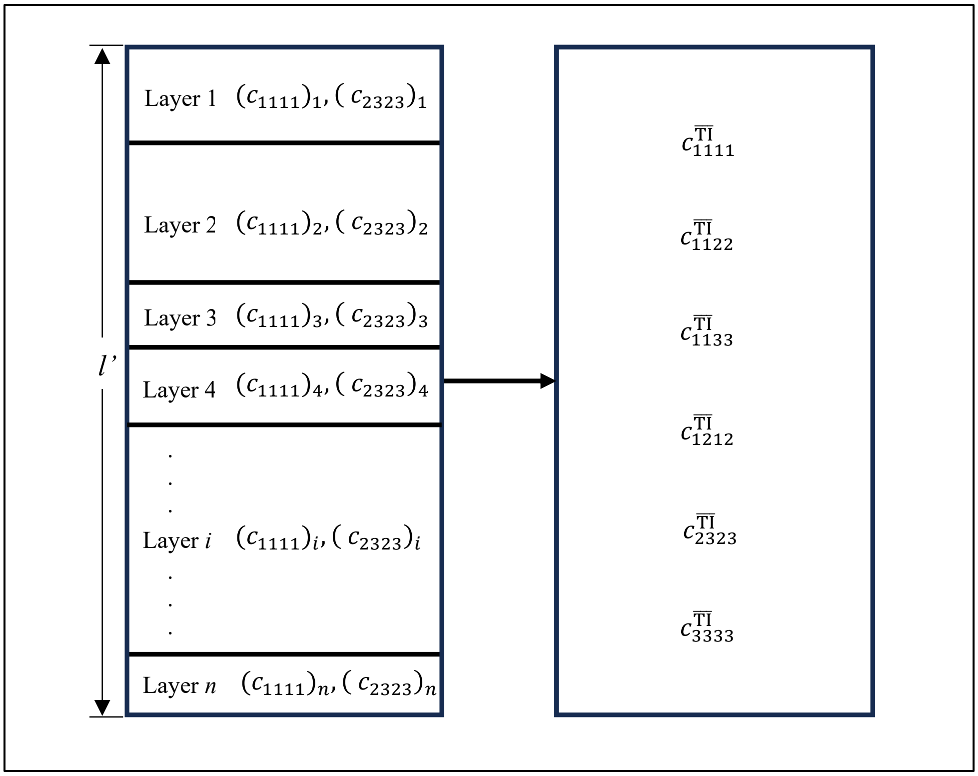

Figure 1.4: Backus Average for horizontal isotropic layers and resultant equivalent transversely isotropic medium. l' is the vertical height of the medium. The elasticity parameters, c_{1111} and c_{2323}, have different values in each layer. The averaged parameters of the equivalent medium are shown on the right as per equations (1.9) - (1.14).

1.2.6 The Nelder-Mead Algorithm

The Nelder-Mead (NM) algorithm (Nelder and Mead, 1965) is a popular numerical direct search method for unconstrained optimization (e.g., Nocedal and Wright; 2006, Baudin, 2010; Wright, 2012). The method is also known as the "downhill simplex method" (Press et al., 2007). The goal is to find parameter values that minimize the value of a function, *f*. The method requires only the values of the function that is to be optimized and does not require any derivatives. It is based on simplices.

A simplex is a matrix consisting of points that are approximations of an optimal point (Baudin, 2010). It is a geometrical shape with an *n*-dimensional collection of points, or vertices, enclosed by faces. For a function with *n* variables, the simplex would consist of *n*+1 vertices. As described by Press et al. (2007), and illustrated in Figure 1.5, when $n = 1$ the simplex is one-dimensional, has 2 points, and is a line; for $n = 2$, it is two-dimensional, has 3 points, and is a triangle; for $n = 3$, it is three-dimensional, has 4 points and is a tetrahedron; i.e., an *n*-dimensional simplex is a polyhedron with *n*+1 vertices.

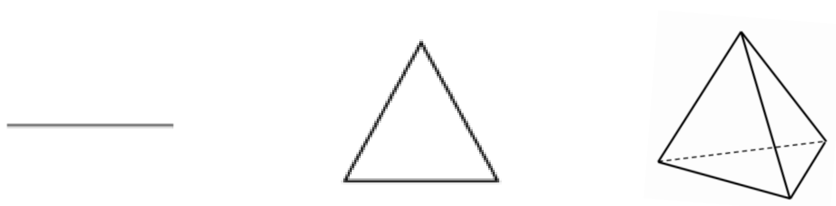

Line
$n = 1$
2 points

Triangle
$n = 2$
3 points

Tetrahedron
$n = 3$
4 points

Figure 1.5: Simplices for a function with *n* variables. The simplices consist of *n*+1 points, or vertices.

The NM method begins with the construction of a starting simplex composed of an initial set of points, with progressive iterations of the simplex towards an optimal solution. For every iteration, the value of the objective function at each vertex of the simplex is evaluated and sorted in terms of best to worst. The ranking is used to determine the simplex that is to be used for the next iteration. The algorithm attempts to replace the worst vertex with a new point, which depends on the worst point and the centre of the remaining vertices.

The simplex is reflected, expanded, or contracted to determine the new point. If this is not successful, then each point moves towards the best point, by shrinking the simplex. The aim is to move each point of the simplex towards the current best point. The new simplex differs by a single vertex or has only one vertex in common with the previous simplex. (Audet and Hare, 2017; Baudin, 2010).

The five ways the Nelder-Mead simplex can change during an iteration are shown in Figure 1.6 for a two-dimensional simplex. With each iteration, the function values at the vertices get smaller and smaller until the minimum point is found. The minimum point is essentially found when all vertices in the simplex have values close to each other. The search is stopped when the minimum point is found, when a desired number of iterations is reached, or when the relative improvement from one iteration to the next is less than some specified tolerance.

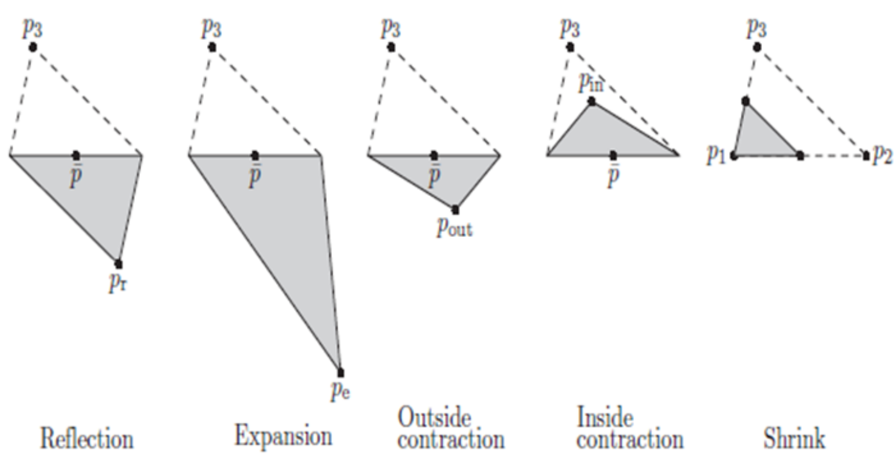

Figure 1.6: The five different ways the Nelder-Mead simplex can change during an iteration, illustrated in two dimensions. The original simplex is depicted by the dashed line, with its worst vertex labelled p_3. The point $\bar{p}$ is the average of the two best vertices. Except in the case of a shrink, the worst vertex of the simplex at iteration k (the point p_3) is replaced at iteration $k + 1$ by one of the reflection, expansion, or contraction points. (Figure and caption from Wright, 2012)

1.2.7 Adaptive Nelder-Mead Algorithm

The above describes the standard Nelder-Mead Algorithm. Described below is an adaptive version, proposed by Gao and Han (2012), that outperforms the standard Nelder-Mead method for large dimensional problems.

In the standard NM method, the scalar parameters for the four possible operations (reflection (α), expansion (β), contraction (γ), and shrink (δ)) are

$$\alpha = 1, \quad \beta = 2, \quad \gamma = 1/2, \quad \delta = 1/2.$$

Gao and Han (2012) choose these parameters adaptively according to the problem dimension n. In particular, they choose for $n \geq 2$,

$$\alpha = 1, \quad \beta = 1 + 2/n, \quad \gamma = 0.75 - 1/2n, \quad \delta = 1 - 1/n.$$

They suggest that choosing $\beta = 1+2/n$ can help prevent the simplex from bad distortion caused by expansion steps in high dimensions; using $\gamma = 0.75 - 1/2n$ instead of 1/2 can alleviate the reduction of the simplex diameter when n is large; and, using $\delta = 1-1/n$ instead of 1/2 prevents the simplex diameter from sharp reduction when n is large. This can make the subsequent expansion or contraction steps reduce the objective function more than the standard NM method. Essentially, the adaptive NM algorithm promotes more iterations by keeping the simplex open for longer, thus avoiding premature convergence. Further details on the method and the algorithm used are provided in Appendix A.

1.3 Data

1.3.1 Geographical Location

The VSP data used in this study were acquired in the Jeanne d'Arc Basin, in the White Rose field, offshore Newfoundland in 2003. Figure 1.7 shows the location of the White Rose field.

Figure 1.7: The Jeanne d'Arc Basin, and the White Rose field, offshore Newfoundland. (From Husky Oil, 2000)

1.3.2 Geologic Setting

The Jeanne d'Arc Basin is an extensional basin with complex geology. As described by Enachescu (1987), McAlpine (1990), and Kaderali et al. (2007), the tectonic history of the area includes three rifting events with significant thermal subsidence. The White Rose region lies in the easternmost part of the Jeanne d'Arc Basin, Figure 1.8.

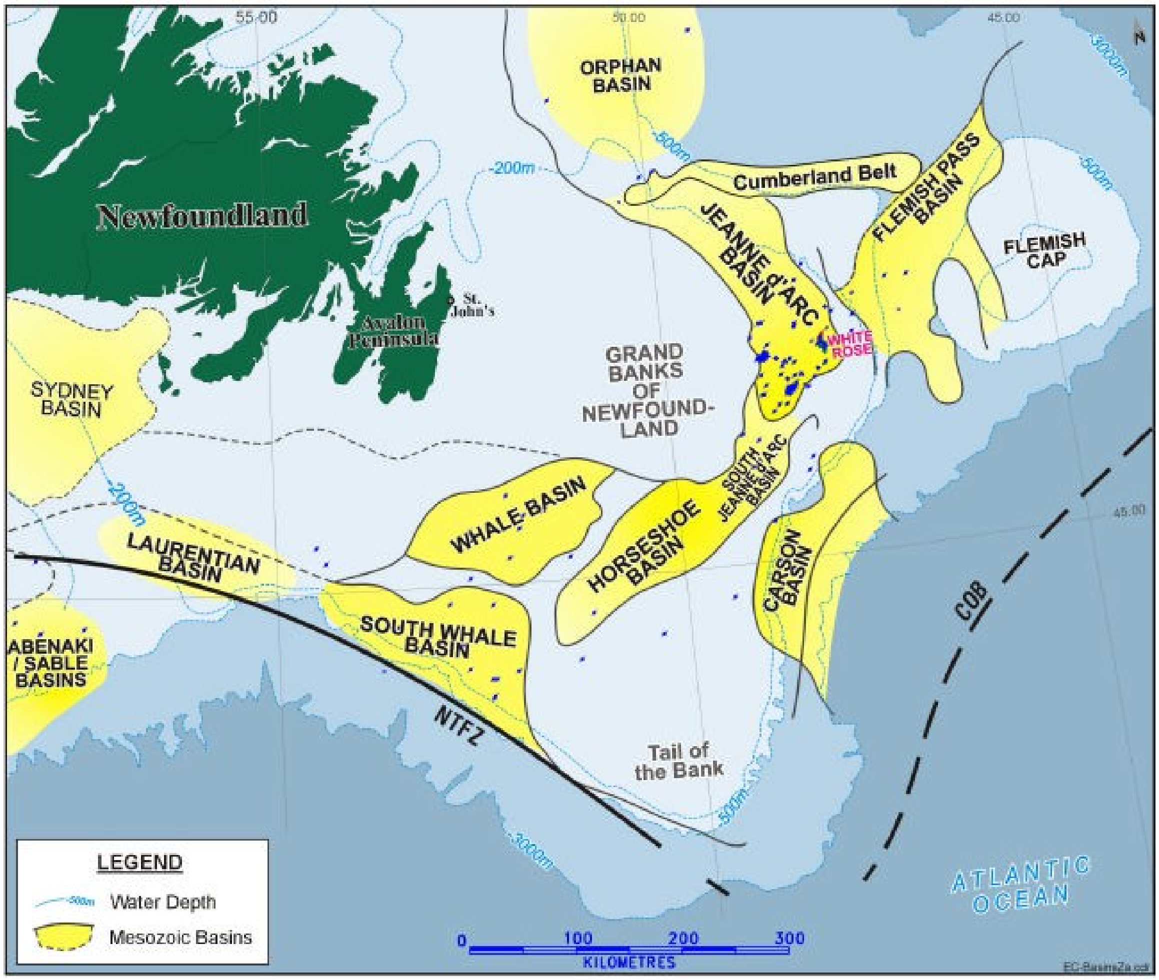

Figure 1.8: Distribution of sedimentary basins offshore Newfoundland. The White Rose region lies in the easternmost part of the Jeanne d'Arc Basin. (From Husky, 2001)

The study zone for this thesis is to 2100 m depth and covers a distance of approximately 4000 m (the farthest offset of the walkaway VSP). Deposition for this zone mainly occurred during the Tertiary period. Except for the top 10 m, which consist of sand

and gravel, the sediments consist of horizontally layered mudstones and shales of the Banquereau Formation (McIver, 1971; Grant et al., 1986; Husky, 2001).

1.3.2.1 Sonic log

A sonic log for compressional (*P*-wave) slowness was recorded from 1383 m to the total depth of the same well that the VSP data were acquired in. Figure 1.9 shows the sonic log to 2100 m. The subsurface to this depth consists mainly of shales, as described above and as observed by gamma ray logs (Zhou and Kaderali, 2006).

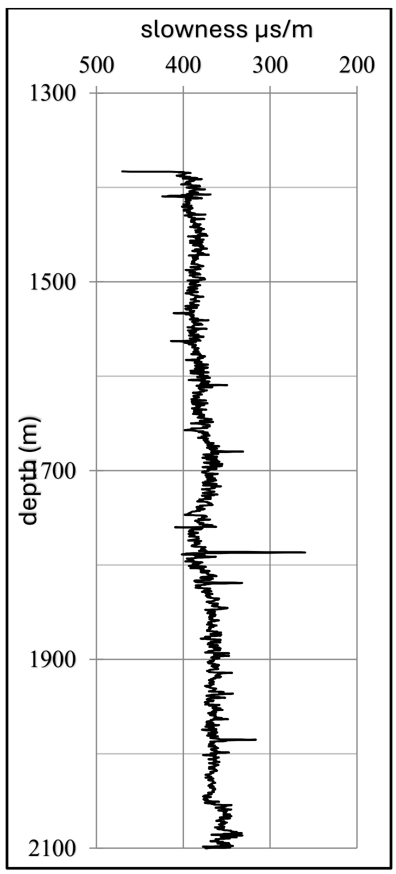

Figure 1.9: Compressional (*P*-wave) sonic log. (Adapted from Zhou and Kaderali, 2006)

1.3.3 Well Configuration

The geometry of the well is shown in Figures 1.10a and 1.10b as a plan view and a cross-sectional view, respectively. The borehole was deviated, with a maximum deviation of 52.3°.

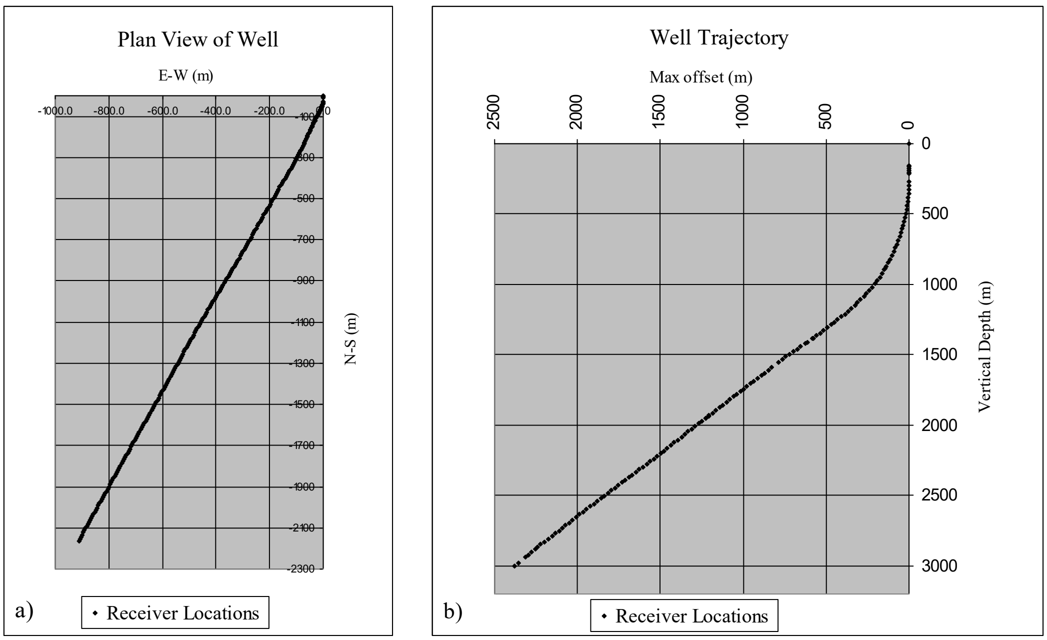

Figure 1.10: a) Plan view of well trajectory, referenced to wellhead at (0, 0), b) Well trajectory, with receiver locations for zero-offset VSP. Sources were placed above the receivers to obtain normal incidence ray paths. (From Kaderali, 2009)

1.3.4 Vertical Seismic Profiling Data

In this section, descriptions of the VSPs and Figures 1.11, 1.13, 1.14, 1.16 and 1.18 are from Kaderali, 2009.

VSP data are acquired with the placement of receivers in a well and sources at the surface (Balch and Lee, 1984; Hardage, 1985). In this case, three types of VSPs with different source-receiver configurations were acquired in the same well: a zero-offset VSP (ZVSP), a walkaround VSP (WAVSP) and a walkaway VSP (WVSP) as illustrated in Figure 1.11. In this study, I use the data from the ZVSP and WVSP.

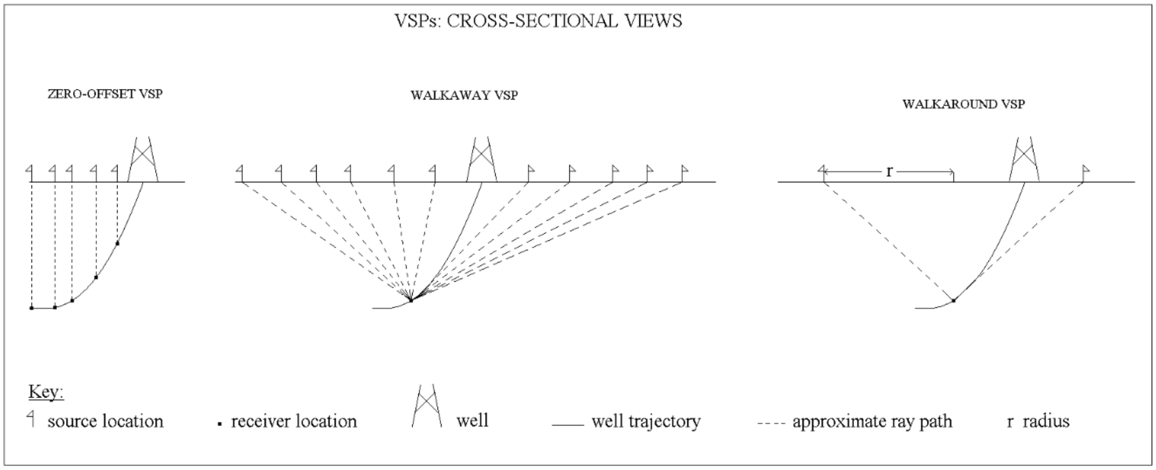

Figure 1.11: Cross-sectional views of the three types of VSPs which were acquired. For the zero-offset VSP, sources were placed above the receivers to obtain normal incidence ray paths. For the walkaway VSP, sources were placed at various offset intervals linearly in a particular direction from the receiver array. In the case of the walkaround VSP, sources were arranged radially around the receiver.

1.3.4.1 Source

For the zero-offset and walkaway VSPs, the source consisted of a four-gun array, composed of two 100 cu in plus two 150 cu in airguns, placed 6.0 m below sea level. For the walkaround VSP, the source consisted of an eight-gun array, composed of four 150 cu in plus four 300 cu in airguns, placed 6.0 m below sea level. Figure 1.12 shows an example of an airgun. When triggered, the airgun releases a specified volume of high-pressure air into the water producing a high-energy pulse (Evans, 1997). A tuned airgun array reduces the oscillations resulting from the repeated collapse and expansion of the air bubble created from the initial explosion and generates a broader frequency spectrum. Energy generated by arrays is concentrated vertically down (and vertically up) (Sheriff, 1991; Caldwell and Dragoset, 2000).

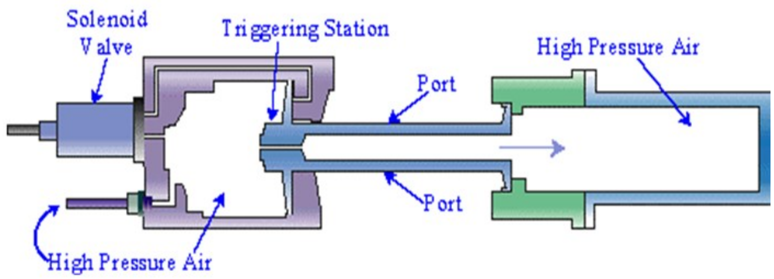

Figure 1.12: The airgun: When triggered, the airgun releases a specified volume of high-pressure air into the water. (Adapted from Sheriff, 1991)

1.3.4.2 Receivers

For the zero-offset and walkaway VSPs, the receivers were configured as a five-level array. Each level was composed of a set of triaxial geophones: three orthogonal gimbal-mounted geophones, one mounted vertically and two mounted horizontally at 90° to each other to measure *x*-, *y*- and *z*-component motions (Gal'perin, 1984; Hardage, 1985). The levels were spaced 15.0 m apart. For the walkaround VSP, the receivers consisted of an eight-level array of three-component geophones, spaced 15.0 m apart. Figure 1.13 depicts the receiver array configurations.

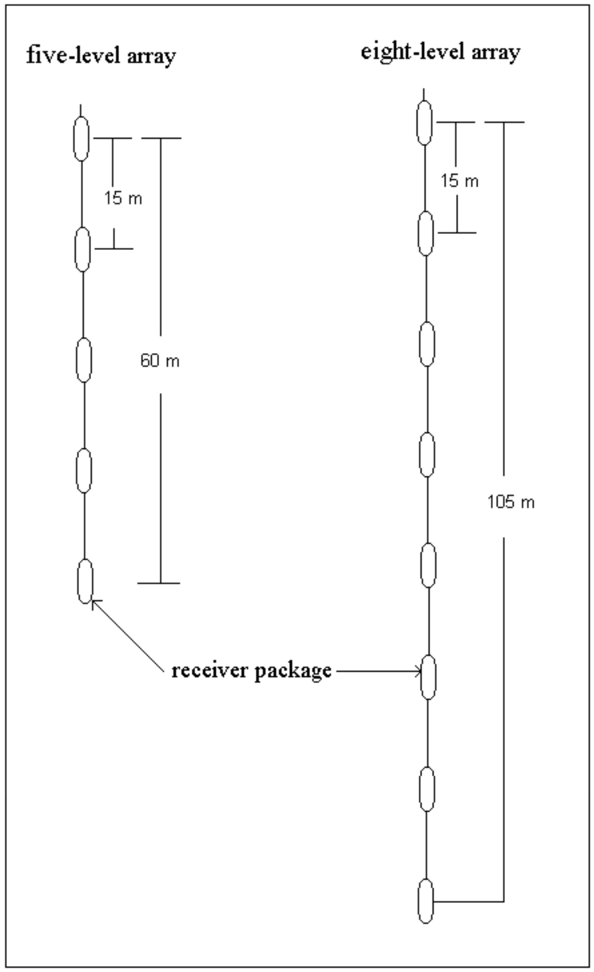

Figure 1.13: Receiver array configurations: five-level array and eight-level array. Receiver packages are composed of three orthogonal geophones.

1.3.4.3 Zero-offset VSP

For a zero-offset vertical seismic profile (ZVSP), sources are placed at the surface, or near-surface, to obtain normal incidence ray paths to receivers placed at various depths in the well, as shown in Figure 1.11. In the case of a deviated well, as described here, a VSP may be referred to as a walkabove VSP (Rector, 2011).

In this case, receivers were placed at 15 m intervals from the bottom of the well to the surface. Sources were positioned above the centre receiver of the five-level array at 6 m below the sea surface. An average of seven shots were recorded at each depth level. The geophone traces within each level were subsequently aligned and stacked to produce a single trace for each depth level. Figure 1.14 shows the *z*-component stack. Traveltimes are obtained by picking the direct (first) arrival.

From the traveltimes, and depths, I computed interval velocities by dividing the depth interval by the traveltime for that interval. Interval velocities were smoothed using an exponential smoother to remove scatter. From the interval velocities three layers can be interpreted with boundaries at 1300 m and 1750 m, see Figure 1.15. This forms the basis of using a 3-layer model, with the boundaries mentioned, for the modelling in this thesis. Layer boundaries interpreted from the ZVSP are the same as indicated by Zhou and Kaderali (2006). Interval velocities and smoothed interval velocities are provided in Appendix B.

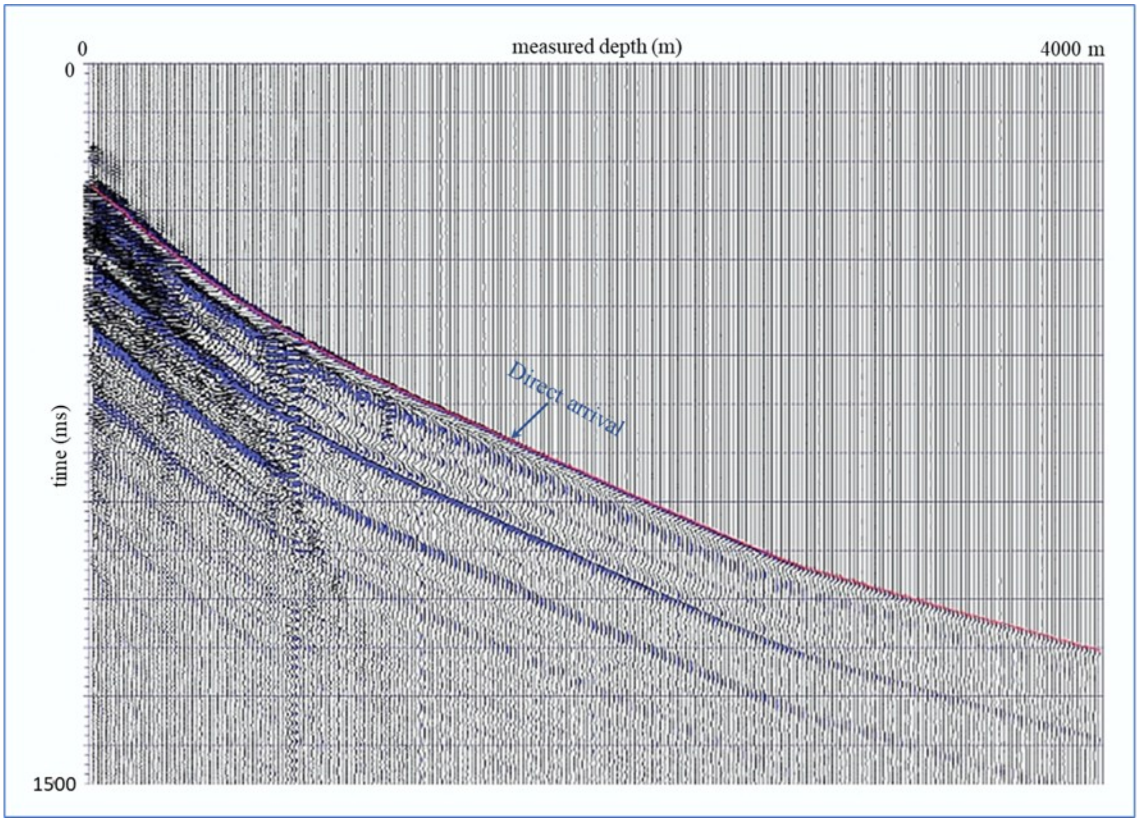

Figure 1.14: Vertical (z-) component stacked data for zero-offset VSP. Direct arrivals are picked (red line) to obtain traveltimes.

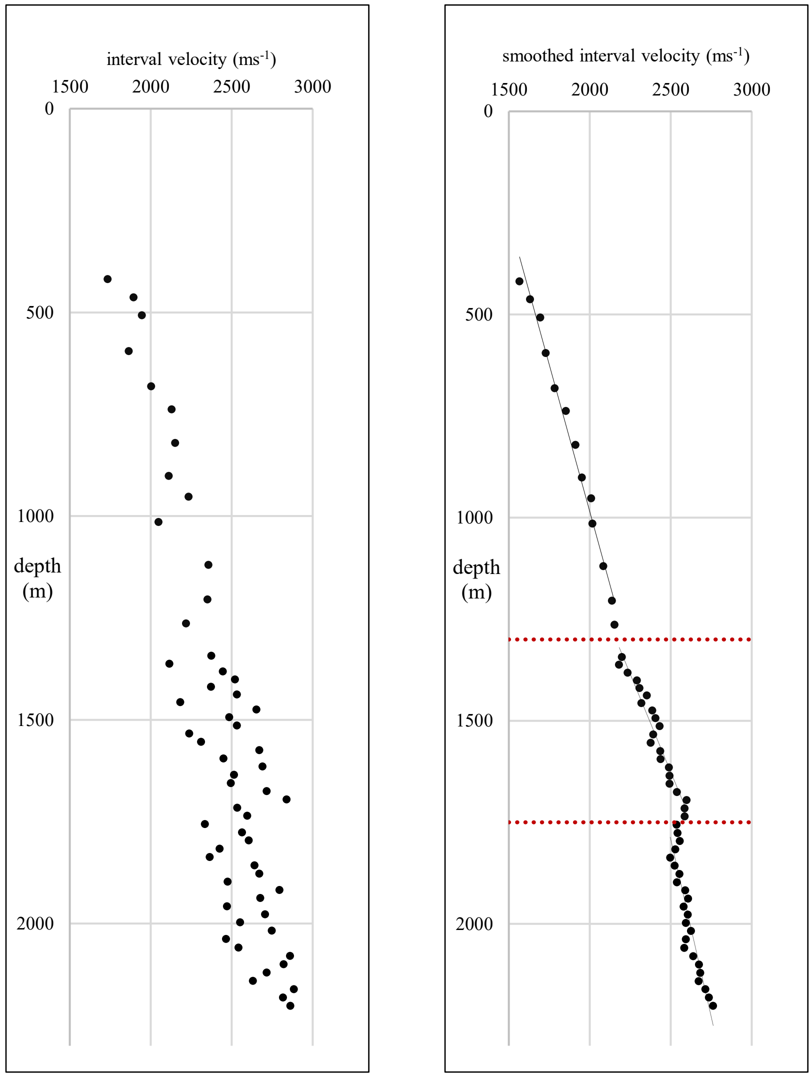

Figure 1.15: ZVSP interval velocities and smoothed interval velocities. Dotted horizontal lines indicate interpreted layer boundaries. The sonic log shown in Figure 1.9 was recorded from 1383 m, which is just below the first layer boundary.

1.3.4.4 Walkaway VSP

For the walkaway VSP (WVSP), as shown in Figure 1.16, 200 sources were placed in a line, at 25 m intervals, above an array of receivers in the well. From the centre of the receiver array, the maximum source-receiver offset was 4000 m for the longside, and 1000 m, for the shortside. The receiver array comprised five geophones over a vertical depth range of 1980 m to 2020 m (mean sea level). The depths for each receiver and the source-receiver spread for both source offset directions, i.e., the longside and the shortside, are provided in Appendix B.

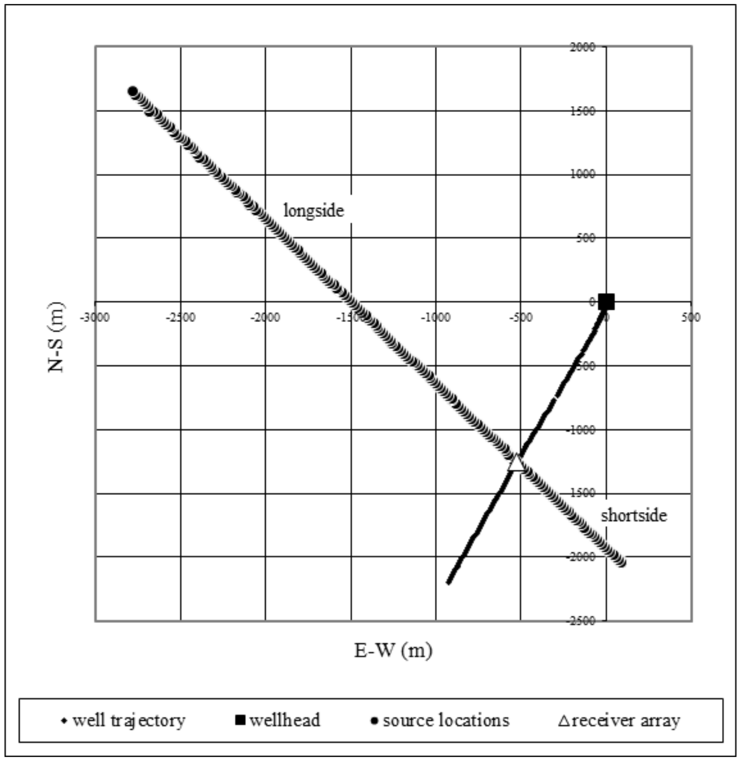

Figure 1.16: Walkaway VSP survey geometry, plan view. The source line consists of 200 source locations with an interval of 25 m, with maximum source-receiver offsets from the centre of the receiver array of 4000 m (longside) and 1000 m (shortside), in opposing directions. (Adapted from Kaderali, 2009)

Figure 1.17 depicts the components recorded by the triaxial geophones placed in the borehole. The recorded WVSP wavefield was rotated to separate it into three components: horizontally (*SH*) and vertically (*SV*) polarized shear, and compressional (*P)* wave energy. Two rotations were performed. The first, to obtain the *SH* component and the second, to obtain the *SV* and *P*-wave components (Hardage, 1985; Hinds et al., 2012).

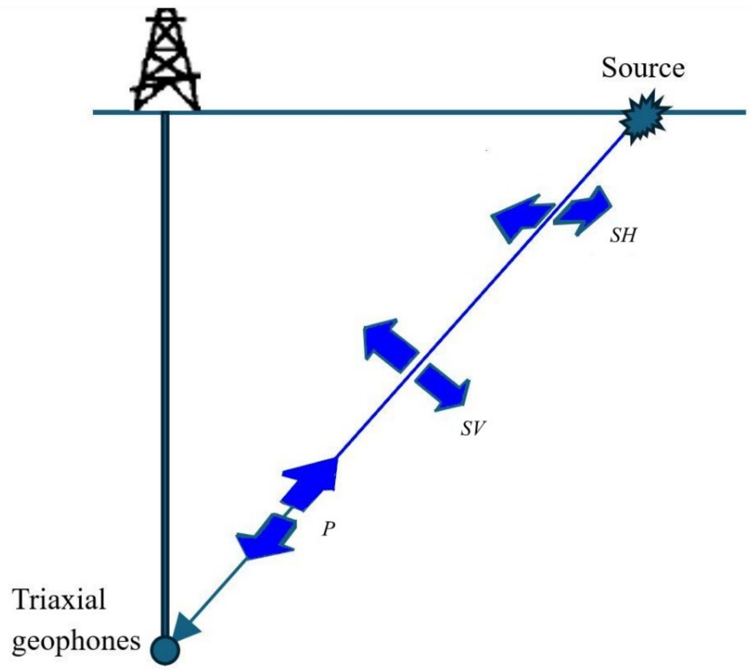

Figure 1.17: Downgoing waves recorded by the triaxial geophones in the borehole: compressional *P*-waves that vibrate in the direction of travel, and shear *SV*- or *SH*-waves that vibrate normal to the direction of travel, either in the plane of the source and receiver, or out of the plane.

The *P*-wave component waveform from which the traveltimes were derived are shown in Figure 1.18 for the five receivers. Sources are at 6.0 m (mean sea level) depth. There are 200 source locations and five receivers for a total of 1000 source-receiver pairs and corresponding traveltimes. I edited the data for erroneous travel times, resulting from various conditions, e.g., poor receiver coupling, casing ringing, tube wave interference, equipment malfunction, equipment mis-calibration, rig noise interference, etc. After editing, 917 traveltimes remain, 754 on the longside and 161 on the shortside. Only the longside traveltimes are used for this study, as the offsets for the shortside are not sufficient to be appreciably affected by the presence of anisotropy. Of these, 59 source-receiver pairs with offsets of less than 300 m were not used in this study, as the traveltimes are often unreliable when the receiver offset is short, for some of the same reasons as indicated above. Thus, 695 traveltimes are used in this study.

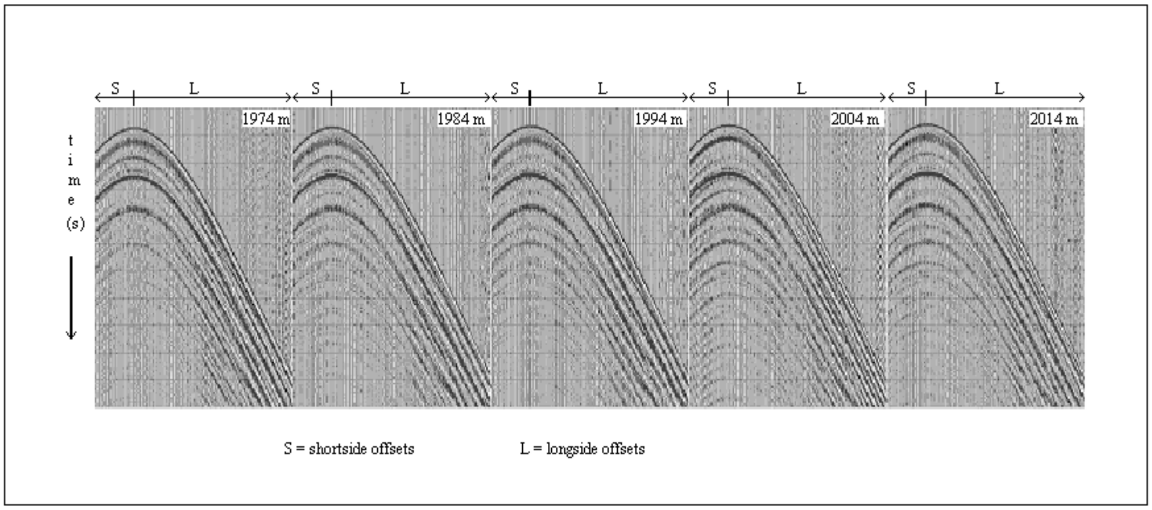

Figure 1.18: Walkaway VSP *P*-wave component waveform in source-receiver plane. (From Kaderali, 2009)

Chapter 2

2 Examination of traveltimes to estimate anisotropy and inhomogeneity parameters, and sensitivity to errors (noise) in the traveltimes

2.1 Collaboration

The research for this chapter was done as a joint project with Theodore Stanoev, from December 2019 to December 2022. A paper[1] on estimation of parameters was submitted to the arXiv repository with Theodore as co-author. Subsequently, we did additional work on the estimation of parameters using the Nelder-Mead simplex method and on the sensitivity of the parameters to noise which is included in this chapter.

Initially, work was performed on both of our computers. In June 2022, under the sponsorship of Dr. Colin Farquharson, we were granted access to Digital Research Alliance of Canada/ACENET supercomputers, namely Beluga and Narval. This increased our computational capacity considerably and enabled a much more extensive and thorough examination in the estimation of the parameters and sensitivity to noise. It enabled us to increase the number of trials significantly and enhanced confidence in our results.

[1] On anisotropy and inhomogeneity
https://doi.org/10.48550/arXiv.2012.03393

Theodore wrote an algorithm in MATLAB for traveltime optimization and determination of model parameters and went over it with me to ensure it was correctly written. He adjusted the raytracing equation for a single layer to accommodate a multilayer setting and devised penalties to constrain model-parameter values to attain values within acceptable ranges.

I did the acquisition, preparation, and conditioning of the VSP and well-log data. I generated synthetic data and noise profiles and provided the data to Theodore. I was responsible for coding in Microsoft Excel. We both ran various optimization trials equally and kept a spreadsheet to keep track. We evaluated and compiled the results together. I have written this chapter independently of Theodore.

Collaboration with Theodore is indicated in the table below as percentages (AK/TS) for each component, where AK denotes the percentage attributed to Ayiaz Kaderali, and TS denotes the percentage attributed to Theodore Stanoev.

Component	**Details**	**Attribution % (AK/TS)**
VSP and well-log data	- Acquisition, preparation, conditioning	100/0
Theory and concepts	- VSP setup for modelling - $ab\chi$ model - Model Parameterizations	90/10 50/50 50/50
Synthetic Data	- Generation of data	100/0
Noise Data	- Addition of noise to data	100/0
Optimization	- Nelder-Mead algorithm	25/75
Implementation	<u>Coding</u> - In Excel - In MATLAB - Verification of Excel programs - Verification of MATLAB programs - Validation of Excel programs - Validation of MATLAB programs	 100/0 0/100 90/10 25/75 100/0 50/50

	Execution of MATLAB programs -On personal computers -On Alliance Canada supercomputers Interpretation - All results interpreted jointly Presentation of results - Generation of figures, tables	 50/50 50/50 50/50 50/50

2.2 Introduction

In this chapter, I consider a multilayered mathematical model to account for measured VSP traveltimes and to estimate the anisotropy and inhomogeneity parameters of the layers. The formulation of analytical equations to do so was developed by Dr. Michael Slawinski. The optimization technique to estimate the parameters, using the Nelder-Mead simplex method, and the application of it to real data is new. The Nelder-Mead algorithm is described in Section 1.2.6.

A traveltime expression for isotropic media derived by Slotnick (1959) considers the velocity of seismic wave propagation in Tertiary basins to be closely approximated by expressing it as a linear function of depth. This expression was modified by Slawinski et al. (2004) where they assume that the velocity increases linearly with depth and introduce an anisotropy term, which is assumed to be the result of elliptical velocity dependence. The expression is suitable for offset distances up to the turning point of a ray. They use least-squares fitting of this traveltime expression to measured traveltimes from a two-offset VSP in the Western Canada Basin and show that there is good agreement between the field data and the modeled data. Furthermore, they show that the elliptical velocity dependence, although small, is significant. Rogister and Slawinski (2005) define a model, the $ab\chi$ model, that describes the velocity of propagation of a signal in a vertical plane and derive a trigonometric expression for the time it takes for a signal to travel along a given ray from a source to a receiver. Kaderali (2009) applies least-squares fitting to multi-offset walkaway VSP data from offshore Newfoundland and provides an analytical expression that is an extension of the analytical expression of Slawinski et al. (2004) that is suitable for all offsets and is equivalent to the expression of Rogister and Slawinski (2005). This is the expression that is expanded to include multilayered mathematical models and used in my thesis. I also use a more extensive VSP data set than used before. Diner and Bayez (2024) obtain a more general solution for a heterogeneous medium, where the horizontal and vertical velocity increase linearly with depth independently and call it the *abcd* model). In essence, they remove the assumption with the $ab\chi$ model that the ratio of the vertical and horizontal velocities, v_x/v_z, is constant with depth, thereby taking into account lateral variations in velocities. As such, a more accurate fit of observed walkaway VSP data may be achieved.

The mathematical model is generated to correspond to the medium, assumed to consist of anisotropic vertically inhomogeneous layers, that the seismic profiling (VSP) data were acquired in. The residual sum of squares (RSS) between measured and modelled traveltimes is minimized to estimate the anisotropy parameter, χ, and inhomogeneity parameters, a and b, of the layers.

To obtain modelled traveltimes between source-receiver pairs, I use the property of the ray parameter being a conserved quantity and, for an initial set of parameters, use analytical equation (1.4) from Section 1.2.4 to calculate traveltimes for each layer and sum them to get the total traveltime, as in equation (2.4) from Section 2.3.1. Using these traveltimes, an optimization is performed to estimate the model parameters.

I use a two-step optimization approach to estimate the model parameters: first, to find raypaths, and second, to calculate traveltimes and the RSS. These steps are repeated to find parameter values of the medium by minimizing the RSS between the model and the data. Moreover, parameters are limited to values that are consistent with this sedimentary basin; where the sediments are predominantly shales and velocities increase with depth, as shown in Chapter 1, Sections 1.3.2 and Figure 1.15. The velocity gradient is kept positive so that velocities increase with depth, and the ellipticity parameter is kept non-negative so that the vertical velocity does not exceed the horizontal velocity at any point. To obtain the model parameters of a multilayer medium, ray theory, with the assumption of elliptical velocity dependence, is used to solve the optimization problem. The traveltime dataset used consists of near- and far-offset sources, giving traveltimes from a long range of offsets, which is necessary to examine anisotropy.

To assess the validity of this approach, I use synthetic traveltime data. I add varied amounts of random noise to the synthetic data and examine the reliability of results under the influence of such noise. I then use the method on a real-data case to get the best estimate of the anisotropy and inhomogeneity parameters and compare the traveltimes using these parameters to the measured traveltimes.

2.3 Theory

2.3.1 Modelled Traveltimes

Rays correspond to curves along which the traveltime is stationary in keeping with Fermat's principle (Cervený, 2001, Robinson and Clark, 2017, Slawinski, 2020a). For a raypath between a given source-receiver pair in horizontally layered media, the ray parameter, p, is constant for the full length of the raypath since it is a conserved quantity (Slawinski, 2020a). In the case of a multilayer model, where each layer is characterized by the values of a, b, and χ, I use this property of the ray parameter, p, to calculate the horizontal distance x travelled in each layer and sum them to obtain the total distance. I keep the velocity gradient, b, positive so that the velocity increases with depth. The direction of the raypath along the x-axis is dependent on the sign of p: for a positive p, the direction is in increasing x, and for a negative p, it is in decreasing x.

In a single layer $ab\chi$ model, where the source is at (0,0) and the receiver at (X, Z), we can write equation (1.8) as

$$X = \frac{1}{pb}\left[\sqrt{1-(1+2\chi)p^2a^2} - \sqrt{1-(1+2\chi)p^2(a+bZ)^2}\right]. \tag{2.1}$$

In a multilayer model with n number of layers, where the source is at (0, 0) and the receiver at (X, Z), for the horizontal distance travelled in each layer, we can write equation (2.1) as

$$X_{j+1} - X_j = \frac{1}{pb_j}\left[\sqrt{1-\left(1+2\chi_j\right)p^2{a_j}^2} - \sqrt{1-(1+2\chi_j)p^2\left(a_j+b_j\left(Z_{j+1}-Z_j\right)\right)^2}\right], \tag{2.2}$$

where j refers to the layer number, and $\left(Z_{j+1}-Z_j\right)$ is the thickness of the layer. To obtain the total horizontal distance travelled from a source at (0,0) and receiver at (X, Z), we sum the distance travelled in each layer,

$$X = X_1 + \sum_{j=1}^{n}\frac{1}{pb_j}\left[\sqrt{1-\left(1+2\chi_j\right)p^2{a_j}^2} - \sqrt{1-(1+2\chi_j)p^2\left(a_j+b_j\left(Z_{j+1}-Z_j\right)\right)^2}\right], \tag{2.3}$$

where X_1 is the source position, n is the number of layers. In any given layer, the traveltime is obtained by equation (1.4). For a multilayer model, we sum the traveltimes for each layer to get the total traveltime,

$$t = \sum_{j=1}^{n}\left(\frac{1}{b_j}\{\tanh^{-1}[\,pb_j(x_{j+1}-x_j)\; - \;\sqrt{1-(1+2\chi)p^2{a_j}^2}] + \tanh^{-1}\sqrt{1-(1+2\chi)p^2{a_j}^2}\}\right), \tag{2.4}$$

where $(x_{j+1} - x_j)$ is the horizontal distance travelled in the *j*th layer.

2.3.2 Optimization

I apply a two-step optimization, in an iterative manner as described below, using the Nelder-Mead (NM) simplex method.

Step 1: For a given set of *a, b, χ* values that a raypath exists between each source-receiver pair is verified. A raypath will exist if the differences within each of the square root terms in equation (2.3) are greater than or equal to zero. If the differences are less than zero a raypath will not exist. The largest *p* value possible corresponds to the *p* value that first results in one of the square root terms being equal to zero. The maximum horizontal distance travelled corresponds to this *p* value and it is considered to be the limiting *p* value. For source-receiver pairs whose horizontal offsets are less than the maximum horizontal distance, a raypath exists. I numerically solve, in Excel or Matlab, for the *p* value that traces a ray to the receiver at (*X, Z*) for each source. For pairs whose offsets are greater than this distance, a raypath does not exist, i.e., a ray is untraceable. In this case, an arbitrary *p* value (1/2 the limiting *p* value) is assigned to enable traveltime calculations in Step 2, and a unit penalty is applied to the RSS, as described in Appendix A.3. This ensures that the given set of *a, b, χ* values are not considered further by the NM algorithm.

Step 2: Once the *p* values have been determined for each source-receiver pair for the given set of *a, b, χ* values, equation (2.4) is used to compute traveltimes for the source-receiver pairs. These traveltimes are compared to the measured traveltimes and the RSS is computed.

At each iteration of the NM algorithm, Steps 1 and 2 are performed to obtain RSS values for the set of a, b, χ values. The algorithm then adjusts the a, b, χ values, as discussed in Sections 1.2.5 and 1.2.6, to reduce the RSS. As the a, b, χ values are adjusted, steps 1 and 2 are repeated to obtain corresponding RSS values. The iterations continue until the RSS is brought to a minimum.

In our case, we have a set of measured traveltimes that is composed of several receivers at various depths and sources with increasing offsets at a fixed depth of 6 m below mean sea level. Thus, we have multiple source-receiver pairs and a set of a, b, χ values to be estimated by minimizing RSS as described above. The residuals are defined as

$$R_i \coloneqq T_i - t_i(\boldsymbol{S}),$$

where for the ith traveltime, T_i is the measured traveltime, t_i is the modelled traveltime, $\boldsymbol{S}$ is the (3N x 1) vector of the set of $(a_1, \ldots, a_N, b_1, \ldots, b_N, \chi_1, \ldots, \chi_N)$ values to be estimated, and N is the number of layers. For any given set of $\boldsymbol{S}$ and measured traveltimes, T, the RSS is obtained by squaring the residuals and taking their sum,

$$\mathrm{RSS} = \sum_{i=1}^{M} R_i^2,$$

where M is the number of traveltimes.

The parameters obtained for the model depend on the initial values. To be more confident of the optimization results being close to or at a global minimum, and to obtain a set of results that is repeatable, I use a multi-start approach which allows for a broad sampling with a wide range of initial values: in this case 10,000 simplices. Each simplex is composed of $3N+1$ vertices and each vertex has a set of a, b, χ values, consisting of $3N$ parameters. For example, for a 3-layer case, $N=3$, the simplex is composed of 10 vertices and each vertex has 9 parameters.

With multi-start, the optimization is performed numerous times with randomly chosen initial-model parameter values for the initial simplices. Thus, the dependence of results on the initial model is diminished. At the end of the multi-start process, we have a final RSS for each of the 10,000 simplices. The set of a, b, χ values with the least RSS from these is considered to be the best or optimal set.

The multi-start approach ensures that there are a sufficient number of starting points for the NM algorithm to find an optimal solution since the NM method can terminate before finding an optimal solution. Using a multi-start approach and ensuring broad sampling, a, b, χ values with the minimum RSS can be treated as close to or at a global minimum.

I use a set of values from the ranges shown in Table A1 for the initial model. The ranges in Table A1 were arrived at by examination of the ZVSP, and values expected for the anisotropy parameter. To ensure that a, b, χ values arrived at using the NM algorithm are within the ranges shown in Table A1 and to ensure that the NM algorithm does not terminate prematurely, penalties are invoked when executing the algorithm. Details are provided in Appendix A.

2.4 Application

2.4.1 Synthetic Data

To check the validity and robustness of the approach, I generate synthetic traveltime data to mimic real data and apply the method to it before applying it to real data. To examine the effects of noise, varied amounts of random noise are added to the synthetic data, and the reliability of results examined under the influence of such noise.

The same acquisition geometry, as described in Section 1.3.4.4 for the walkaway VSP measured data, is kept to obtain synthetic traveltimes. The measured traveltimes are used to estimate arbitrary, but realistic values for a, b, χ in each layer. The a, b, χ values are adjusted to ensure that a p value exists for every source-receiver pair, i.e., the ray is traceable between source-receiver pairs, and the p value determined, as described in Step 1 of Section 2.3.2, for each source-receiver pair. These p values and the adjusted set of a, b, χ values are then used in equation (2.4) to compute traveltimes.

We now have a set of traveltimes for a known set of a, b, χ values, that I refer to as synthetic traveltimes. Synthetic traveltimes are provided in Appendix C. I now proceed with the optimization process, as described in Section 2.3.2, where instead of measured traveltimes I use the synthetic traveltimes to find an optimal set of a, b, χ values that minimize the difference to the modelled traveltimes, and compare this to the known set of a, b, χ values.

I compute synthetic traveltimes, as described above, for a 4-layer model to 5300 m offsets, and use them to find an optimal set of a, b, χ values fitted to

a) a 4-layer model with source-receiver offsets to 5300 m,

b) a 4-layer model with source-receiver offsets to 4000 m, and

c) a 3-layer model with source-receiver offsets to 4000 m.

Source-receiver offsets to 5300 m are used for a), as this is well beyond the offset for the measured traveltimes, and 4000 m offsets for b) and c) as this is the offset to which the measured data were acquired.

Figure 2.1 compares the synthetic traveltimes to the measured traveltimes for Receiver 1. Plots for Receivers 2-5 are similar and are provided in Appendix C. The synthetic traveltimes mimic the measured traveltimes very well. For offsets greater than measured offsets the synthetic data are extrapolated in 25 m intervals.

The values of the optimal a, b, χ set obtained for the 4-layer model to 5300 m offsets are comparable to the known values, see Table 2.1. With offsets reduced to 4000 m, the optimal values are still close, see Table 2.2. Since b is the gradient for a, it varies depending on the value of a and is compensatory to a. A small change in a results in a large change in b, b is thus more difficult to recover than a.

Table 2.1: 4-layer model *a, b,* χ values for source-receiver offsets to 5300 m. Layer boundaries are at 450 m between Layers 1 and 2, 1300 m between Layers 2 and 3, and 1750 m between Layers 3 and 4.

	Used for synthetic traveltimes			Optimal values		
Layer	*a* (ms^{-1})	*b* (s^{-1})	*X*	*a* (ms^{-1})	*b* (s^{-1})	χ
1	1279	0.776	0.0000	1292	0.697	0.0000
2	1748	1.023	0.0195	1760	1.003	0.0191
3	2966	0.219	0.0585	2965	0.219	0.0591
4	2597	0.760	0.0921	2597	0.760	0.0921
	Horizontal distance, X: 5322 m			Horizontal distance, X: 5321 m		

Table 2.2: 4-layer model *a, b,* χ values for source-receiver offsets to 4000 m. Layer boundaries are at 450 m between Layers 1 and 2, 1300 m between Layers 2 and 3, and 1750 m between Layers 3 and 4.

	Used for synthetic traveltimes			Optimal values		
Layer	*a* (ms^{-1})	*b* (s^{-1})	*X*	*a* (ms^{-1})	*b* (s^{-1})	χ
1	1279	0.776	0.0000	1200	1.242	0.0000
2	1748	1.023	0.0195	1701	1.101	0.0213
3	2966	0.219	0.0585	2977	0.218	0.0546
4	2597	0.760	0.0921	2597	0.759	0.0921
	Horizontal distance, X: 5322 m			Horizontal distance, X: 5332 m		

Optimal *a, b,* χ values for the 3-layer model fitted to the synthetic traveltimes, are shown in Table 2.3. The values are close to the known values, particularly for the bottom two layers which are of the same thickness for the 4-layer and 3-layer models. The top two layers of the 4-layer model are combined as a single layer for the 3-layer model. Parameter *a* is applicable at the top of a layer. The values of *a* at the top of Layer 1 are comparable: 1279 m/s for the 4-layer model and 1207 m/s for the 3-layer model. The values for *b* and χ

are applicable to the layer. Considering that in the 3-layer case, the layers are combined, the values then are also comparable.

Table 2.3: *a, b,* χ values for a 4-layer model used for computing synthetic traveltimes fitted to a 3-layer model to offsets of 4000 m. Layer boundaries for the 4-layer model are at 450 m between Layers 1 and 2, 1300 m between Layers 2 and 3, and 1750 m between Layers 3 and 4. For the 3-layer model, Layers 1 and 2 are merged.

	Used for synthetic traveltimes			Optimal values		
Layer	a (ms^{-1})	b (s^{-1})	χ	a (ms^{-1})	b (s^{-1})	χ
1	1279	0.776	0.0000	1207	1.125	0.0156
2	1748	1.023	0.0195			
3	2966	0.219	0.0585	2989	0.215	0.0508
4	2597	0.760	0.0921	2597	0.760	0.0921
	Horizontal distance, X: 5322 m			Horizontal distance, X: 5348 m		

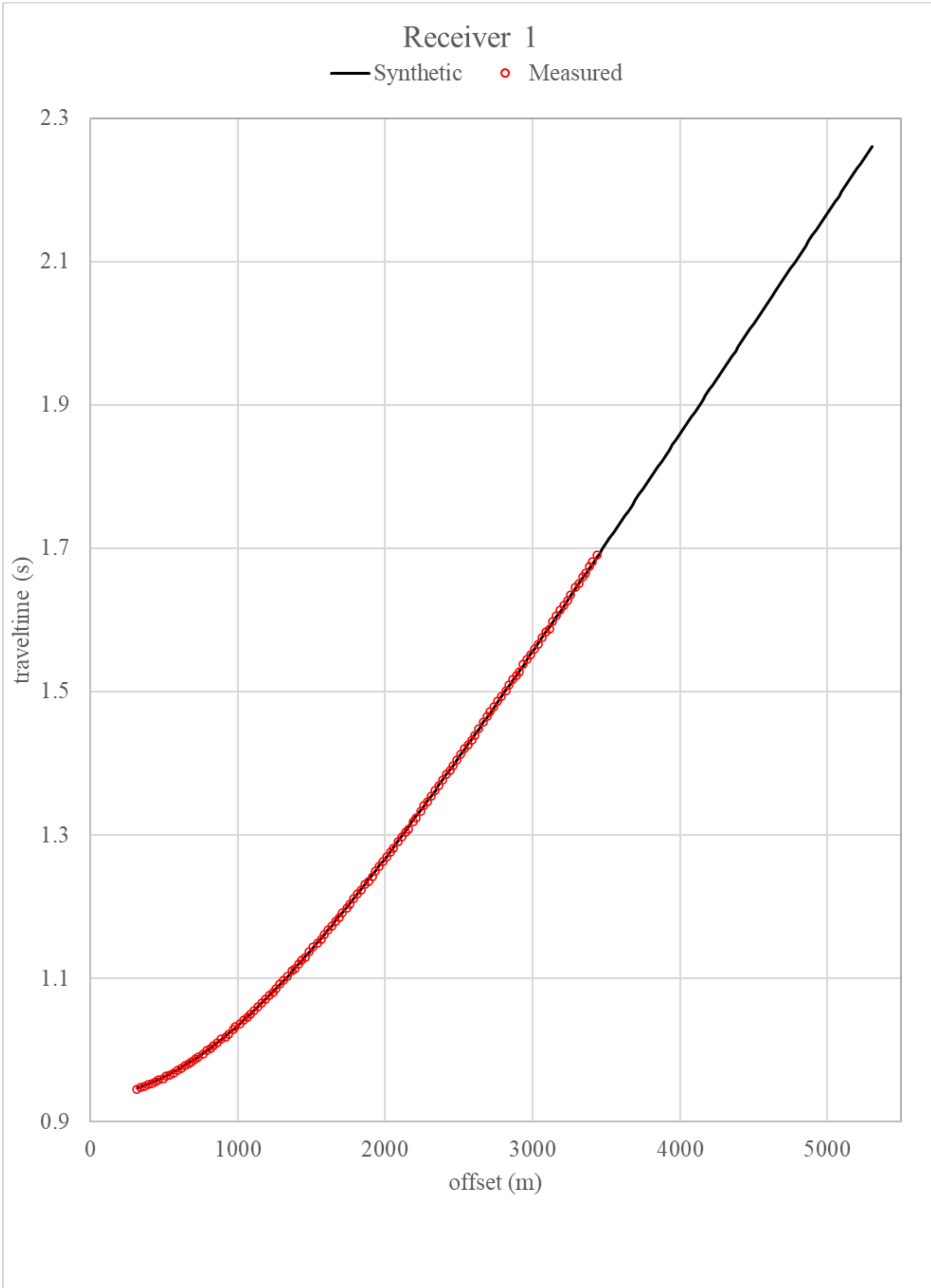

Figure 2.1: Comparison of synthetic traveltimes (black line) to measured traveltimes (red circles) for Receiver 1. The red circles overlie the black dots. For offsets greater than measured offsets the synthetic traveltimes are extrapolated in 25 m intervals.

Figures 2.2 to 2.4 compare the synthetic traveltimes to the modelled traveltimes for Receiver 1, i.e., the traveltimes computed after finding the optimal a, b, χ values, for a) to c) above, respectively. Plots for Receivers 2-5 are similar and are provided in Appendix C. The modelled traveltimes overlie the synthetic traveltimes confirming that the optimal set of a, b, χ values is a good estimate of the real parameters for all three cases, a) to c).

Reducing the offsets in estimating the a, b, χ values or reducing both the offsets and the number of layers does not significantly deteriorate the estimates, and reasonable values are attained. These results validate the approach. A further confirmation is that the maximum horizontal distances for traceable rays, calculated with the optimal parameters, for each of the three models, 5322 m, 5332 m and 5348 m, respectively, are similar to the maximum offset for the synthetic traveltimes, 5322 m.

Thus far, the synthetic data have been noise-free and estimation of the parameters is as expected and encouraging. Section 2.4.3 looks at the addition of noise to the synthetic data and the effect this has on the estimations.

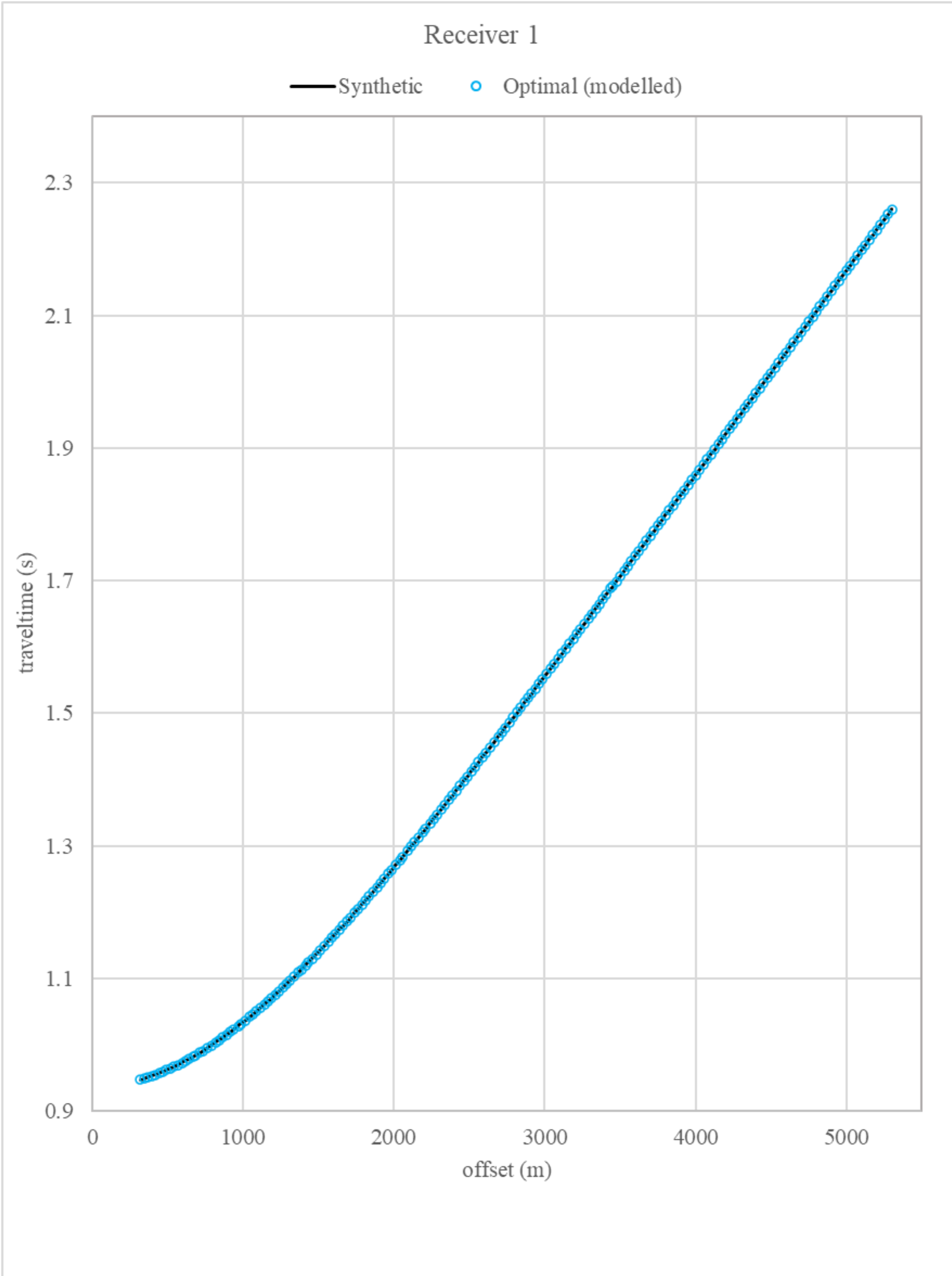

Figure 2.2: Comparison of synthetic (black line) to modelled (blue circles) traveltimes for Receiver 1, for a 4-layer model to source-receiver offsets of 5300 m.

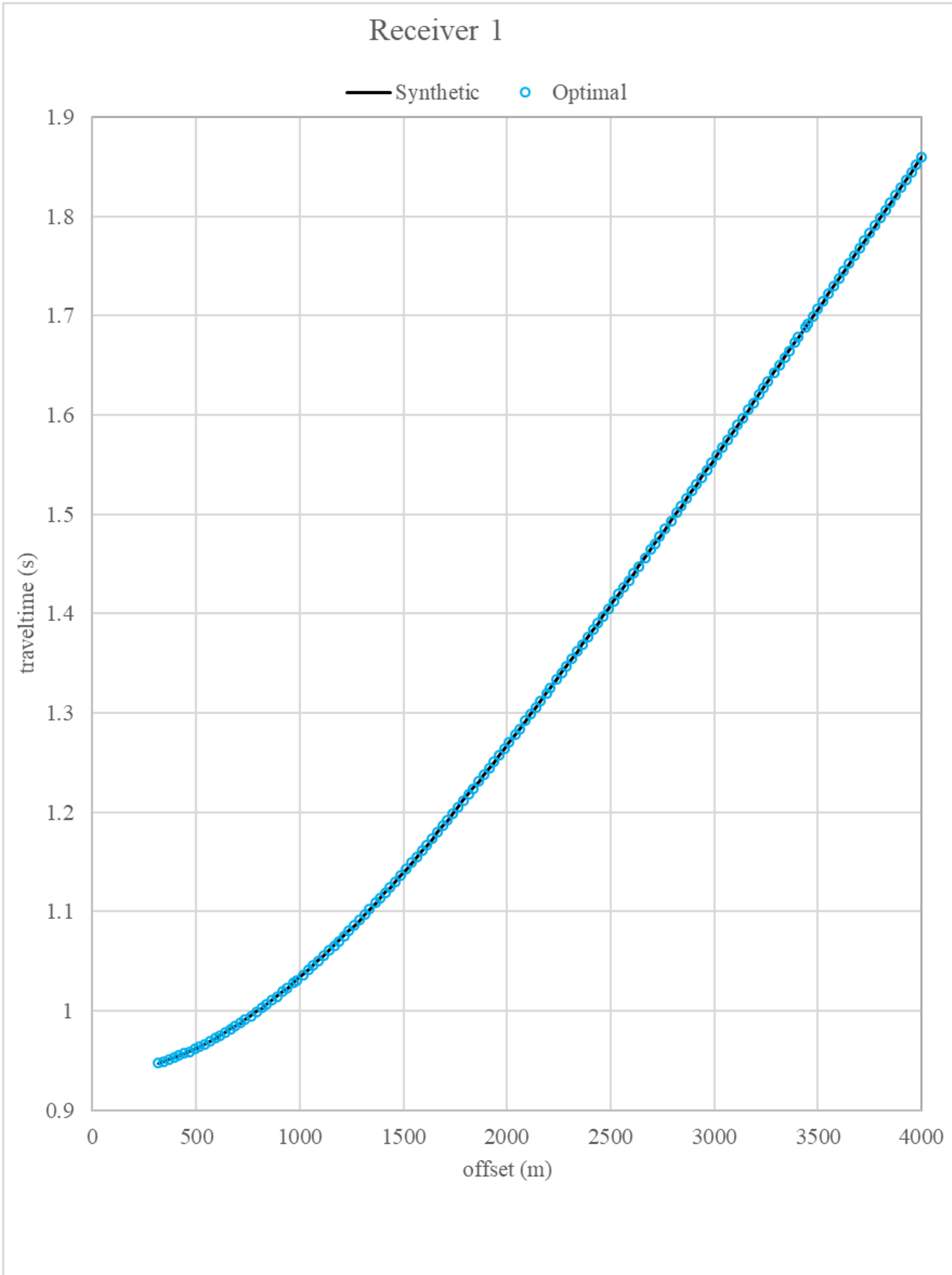

Figure 2.3: Comparison of synthetic (black line) to modelled (blue circles) traveltimes for Receiver 1, for a 4-layer model to source-receiver offsets of 4000 m.

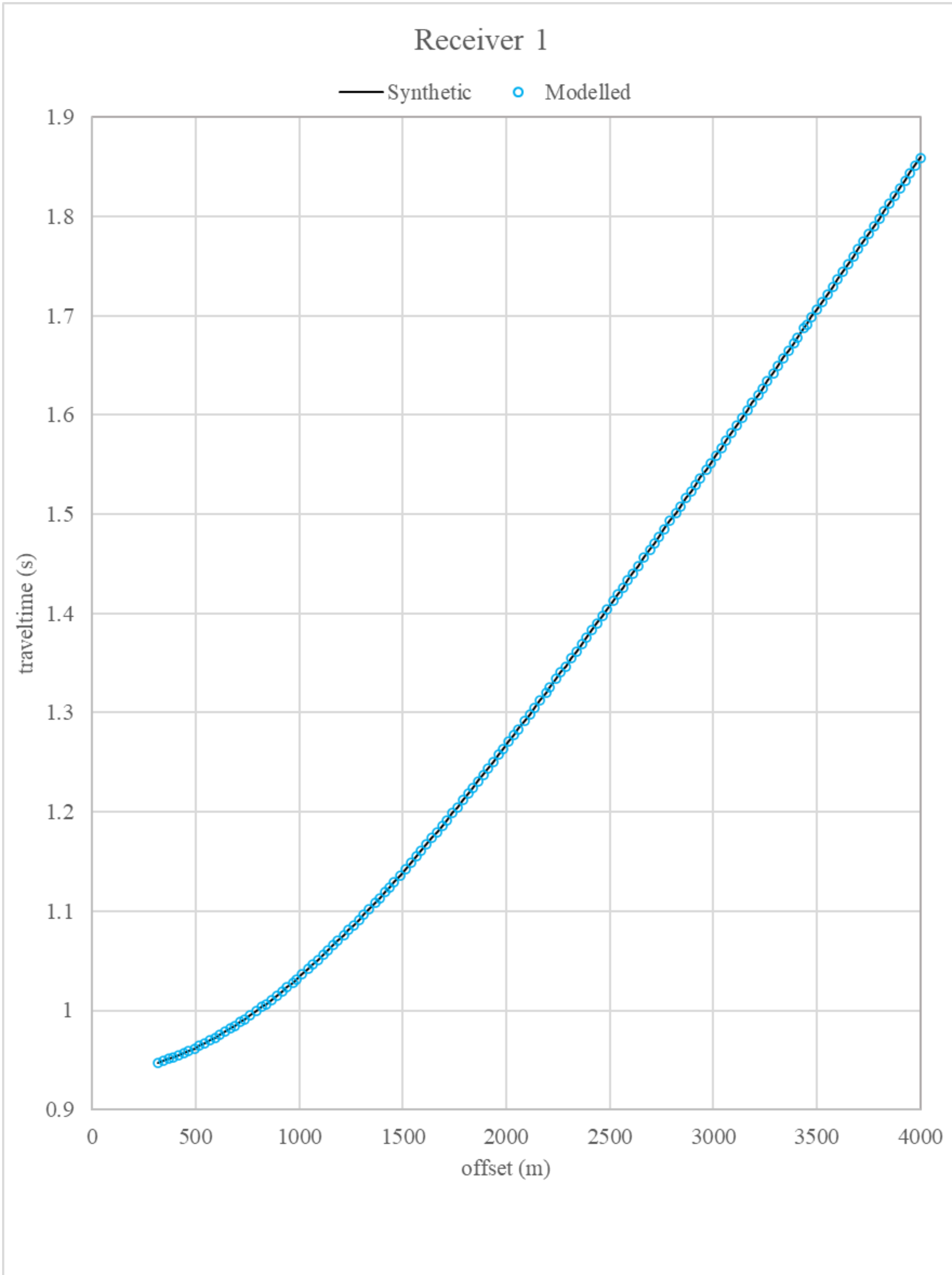

Figure 2.4: Comparison of synthetic (black line) to modelled (blue circles) traveltimes for Receiver 1, for a 3-layer model to source-receiver offsets of 4000 m.

2.4.2 Standard versus Adaptive Nelder-Mead Algorithm

In this study, results for the search for optimal *a, b,* χ parameters are presented for the adaptive Nelder-Mead (NM) algorithm. The adaptive NM algorithm, as mentioned in Section 1.1.6 and Appendix A, provides superior results than the standard NM. Figure 2.5 shows the results for 10,000 simplexes, with different starting points, using the standard NM for the 3-layer model fitted to synthetic traveltimes. Figure 2.6 shows the results for the adaptive NM for the same starting simplexes.

In this example, we fit a 3-layer model to synthetic traveltimes derived from a 4-layer model where the first two layers of the 4-layer model are equivalent to the first layer of the 3-layer model. Thus, there is no red line representing the true value for displays of *a, b,* χ parameters in Layer 1.

For the adaptive NM, Figure 2.6, values for the parameters are less scattered and tend to concentrate closer to the known values or true values as compared to the standard NM, Figure 2.5. A further comparison is also provided in Chapter 3.

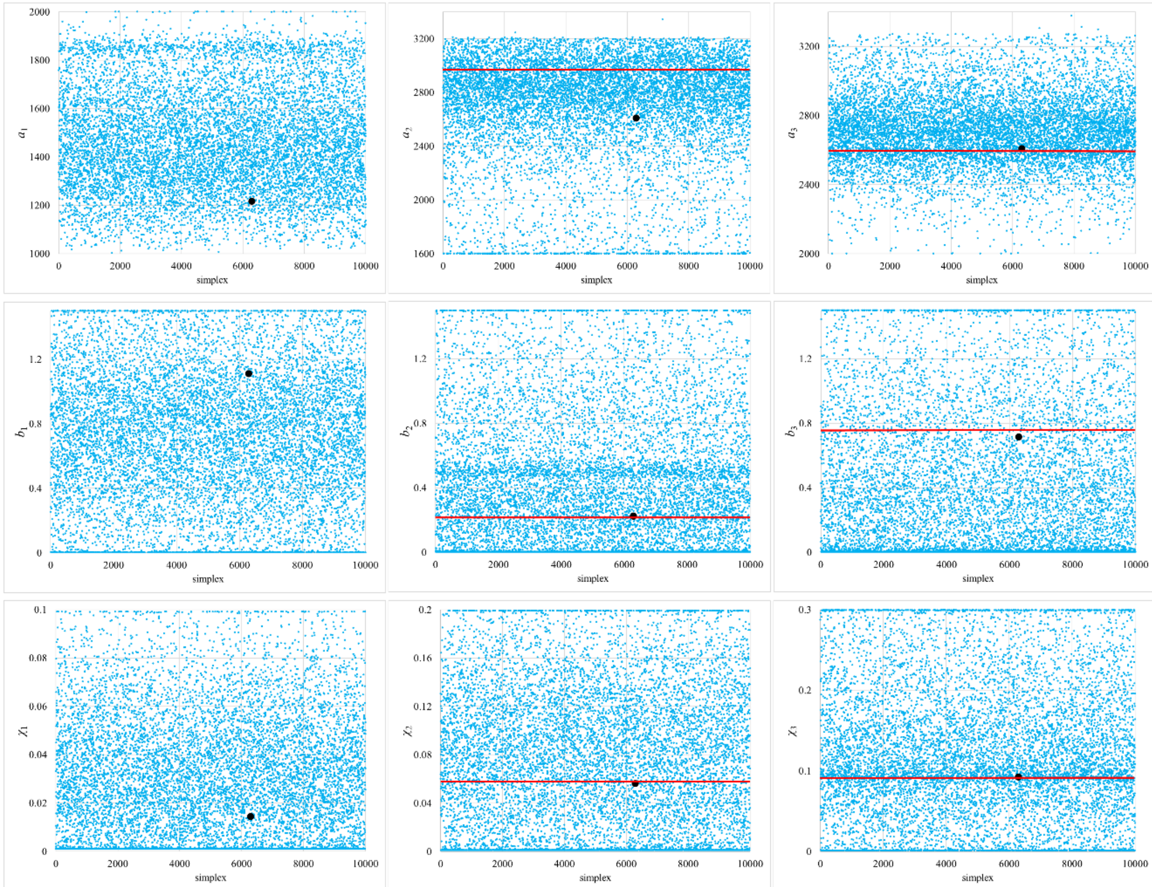

Figure 2.5. Standard Nelder-Mead algorithm. Results of the search for *a, b, χ* values for a 3-layer model fitted to synthetic traveltimes from a 4-layer model are shown as blue dots, the value with the minimum RSS is shown as a black dot, the red line shows where the true value is. Layer 1 does not have a red line as it is fitted to the traveltimes of the first two layers of the 4-layer model. Results are displayed from left to right for layer 1 to layer 3, and from top to bottom for *a, b, χ* values for the layer. Units for *a* are ms^{-1}, for *b* are s^{-1}, and *χ* is unitless.

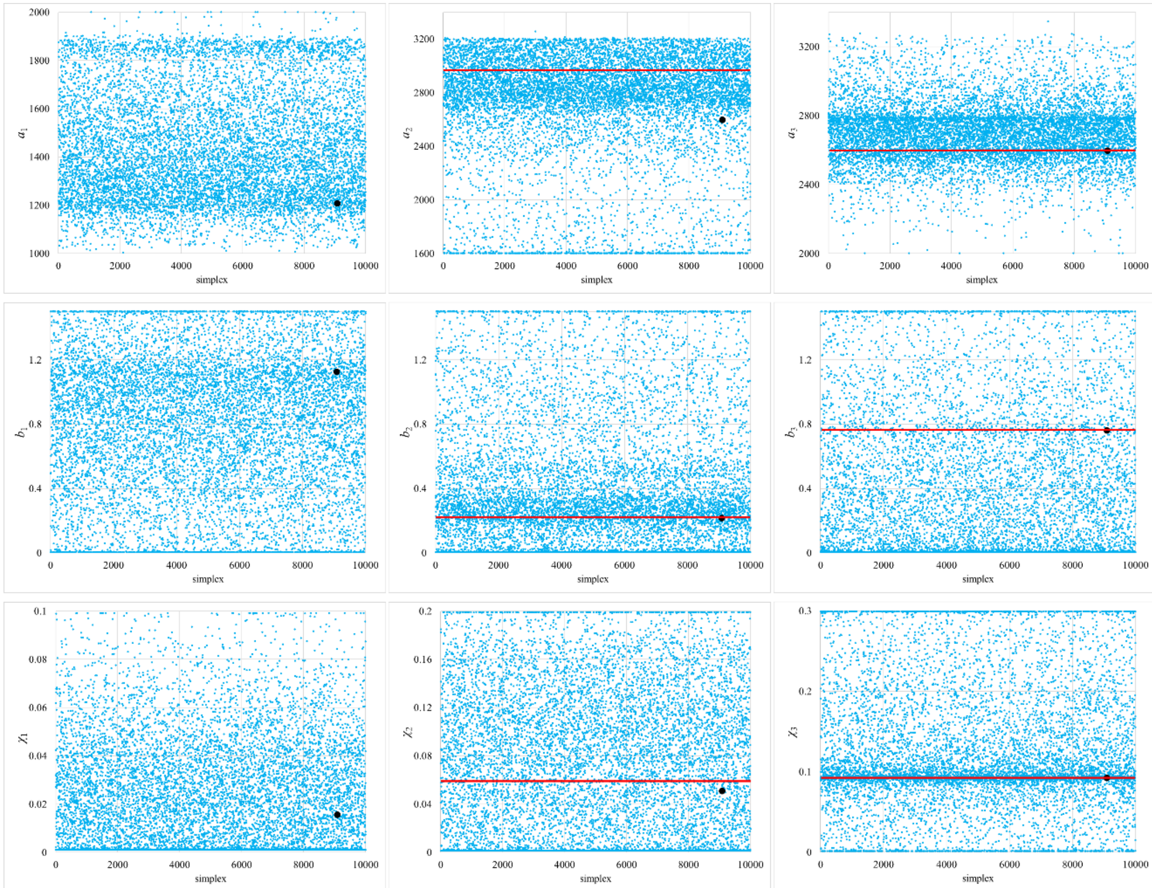

Figure 2.6. Adaptive Nelder-Mead algorithm. Results of the search for *a, b,* χ values for a 3-layer model fitted to synthetic traveltimes are shown as blue dots, the value with the minimum RSS is shown as a black dot, the red line shows where the true value is. Layer 1 does not have a red line as it is fitted to the traveltimes of the first two layers of the the 4-layer model. Results are displayed from left to right for layer 1 to layer 3, and from top to bottom for *a, b,* χ values for the layer. Units for *a* are ms^{-1}, for *b* are s^{-1}, and χ is unitless.

2.4.3 Noise

Since measured data are subject to noise, varied amounts of random noise were added to the synthetic data to examine the reliability of results under the influence of such noise. I generated three noise profiles, as a percentage of the traveltimes, using Excel. The profiles differ in that they were generated using different random seeds. The profiles were generated to a maximum noise level of 0.1% of the traveltimes, which limited the noise to a maximum of ±2 ms, which is the range of scatter for most of the real data, as will be discussed in Section 2.4.5. The maximum noise for the profiles was subsequently scaled to obtain a range of magnitudes: 0.1%, 0.01%, 0.001%, and 0.0001% for each profile. Figure 2.7 shows the noise profile, at the maximum noise magnitude of 0.1%, for Receiver 1. Displays for the full suite of noise profiles and noise values are provided in Appendix C.

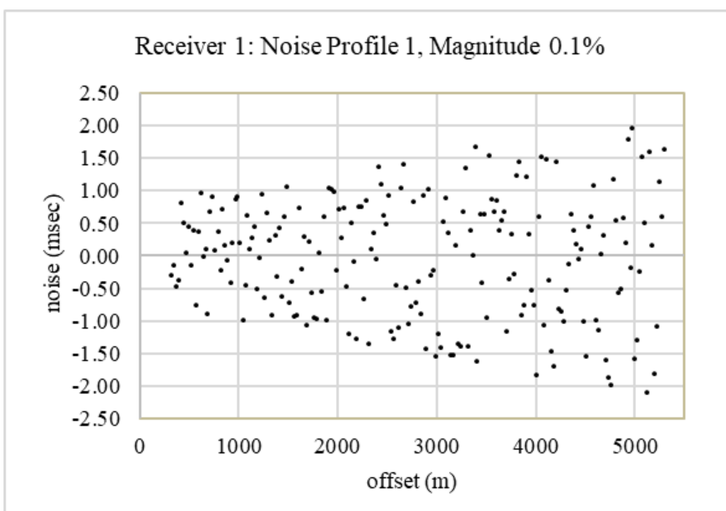

Figure 2.7: Noise Profile 1 at magnitude 0.1% for Receiver 1.

The noise was added to the synthetic traveltimes and sets of optimal values found as in Section 2.4.1 for

a) a 4-layer model with source-receiver offsets to 4000 m, and

b) a 3-layer model with source-receiver offsets to 4000 m.

Tables 2.4 and 2.5 show the optimal *a, b*, χ values attained for a) and b) above, respectively, with added noise of magnitudes 0.0001%, 0.001%, 0.01%, 0.1%, for noise Profile 1. The same for Profiles 2 to 3 are provided in Appendix C.

Table 2.4: Optimal *a, b*, χ values, 4-layer model, source-receiver offsets to 4000 m, synthetic data with added noise of magnitude 0.1%, 0.01%, 0.001%, 0.0001% for noise Profile 1.

	Used for synthetic traveltimes	Optimal values with no noise added	Noise magnitude			
			0.0001%	0.001%	0.01%	0.1%
			Optimal values with Profile 1 noise added to synthetic traveltimes:			
RSS		6.41×10^{-11}	4.69×10^{-10}	4.52×10^{-08}	4.53×10^{-06}	4.54×10^{-04}
a_1	1279	1200	1225	1219	1308	1463
a_2	1748	1701	1815	1946	2104	1524
a_3	2966	2977	2925	2879	2865	2755
a_4	2597	2597	2596	2601	2654	2786
b_1	0.776	1.242	0.981	0.901	0.433	0.751
b_2	1.023	1.101	0.911	0.671	0.297	1.259
b_3	0.219	0.218	0.227	0.236	0.260	0.374
b_4	0.760	0.759	0.762	0.743	0.532	0.001
χ_1	0.0000	0.0000	0.0000	0.0000	0.0000	0.0000
χ_2	0.0195	0.0213	0.0110	0.0014	0.0012	0.0010
χ_3	0.0585	0.0546	0.0728	0.0892	0.0915	0.1202
χ_4	0.0921	0.0921	0.0921	0.0921	0.0918	0.0894
X	5322	5332	5264	5196	5036	4518

For all of the noise profiles, Profile 1 to 3, added to the traveltimes, the RSS value deteriorates progressively as the percentage of added noise increases compared to the case where no noise is added. In the no-noise case, the RSS is of magnitude 10^{-11}. As the noise is increased, by an order of magnitude each time, i.e., from 0.0001% to 0.001% to 0.01% to 0.1%, the RSS increases from 10^{-10} to 10^{-08} to 10^{-06} to 10^{-04}, correspondingly.

Table 2.5: Optimal *a, b,* χ values, 3-layer model, source-receiver offsets to 4000 m, synthetic data with added noise of magnitude 0.1%, 0.01%, 0.001%, 0.0001% for noise profile 1.

	Used for synthetic traveltimes	Optimal values with no noise added	Noise magnitude			
			0.0001%	0.001%	0.01%	0.10%
			Optimal values with Profile 1 noise added			
RSS		6.58×10^{-11}	5.31×10^{-10}	4.55×10^{-08}	4.54×10^{-06}	4.54×10^{-04}
a_1	1279	1207	1208	1213	1256	1332
a_2	1748					
a_3	2966	2989	2988	2975	2883	2779
a_4	2597	2597	2597	2601	2647	2786
b_1	0.776	1.125	1.125	1.117	1.044	0.904
b_2	1.023					
b_3	0.219	0.215	0.216	0.221	0.265	0.362
b_4	0.760	0.760	0.759	0.741	0.558	0.001
χ_1	0.0000	0.0156	0.0155	0.0144	0.0070	0.0010
χ_2	0.0195					
χ_3	0.0585	0.0508	0.0510	0.0552	0.0840	0.1123
χ_4	0.0921	0.0921	0.0921	0.0921	0.0918	0.0889
X	5322	5348	5345	5300	5001	4564

2.4.4 Noise Threshold

The noise threshold is arrived at by comparing the optimal *a, b*, χ values obtained with the addition of increasing amounts of noise to the no-noise case. We consider the noise threshold to be between 0.001% and 0.01% of noise added. Table 2.4 shows the optimal *a, b*, χ values obtained with the addition of the various magnitudes of noise, for noise Profile 1, for the 4-layer model with source offsets to 4000 m. The same for Profiles 2 to 3 are provided in Appendix C.

In general, as the amount of noise increases, the parameter estimations progressively worsen. The addition of 0.1% of noise, which is the largest amount of noise added, gives the worst estimates for all profiles of noise added. The addition of 0.0001% has the least overall effect. The maximum horizontal distances for traceable rays also worsen with increasing noise. The horizontal distance travelled is given by equation (2.2). As the estimated *a, b*, χ values worsen with the addition of noise, this correspondingly adversely affects the horizontal distance travelled. For noise levels of 0.01% and 0.1% the maximum horizontal distances for traceable rays are significantly shorter than the no-noise case of 5332 m. For example, for noise Profile 1 with a noise level of 0.01% added to the traveltimes, the maximum horizontal distance is 5036 m, which at a source interval of 25 m, is 11.8 source stations shorter than the no-noise case. For the 0.001% noise level, the maximum horizontal distances for all three noise profiles are within about 5 source stations, whereas with noise levels 0.01% and greater, they are all greater than 5 source stations. We thus consider the threshold to lie between 0.001% and 0.01%. The corresponding RSS magnitudes are 10^{-08} and 10^{-06} respectively.

The best estimate of the parameters occurs for the deepest layer regardless of the noise level. We further observe that the estimated values of parameter *a,* which is the vertical velocity at the top of the layer, and *b*, which is the gradient or rate of change of *a* in the layer*,* for the shallowest layer are not as close to the no-noise case as compared to the deeper layers, for all levels of noise and for all three noise profiles. These values also vary more than for the deeper layers. The value of *b* is compensatory to the value of *a*, in that when *a* is large *b* is small and when *a* is small *b* is large. The shallowest layer, in this case, does not have anisotropy, i.e., χ is set to zero, which is the same condition as for the no-noise tests in Section 2.4.1, Tables 2.1 to 2.3. The number of parameters available for optimization and fitting to the traveltimes in the shallowest layer is thus reduced and this is manifested in the behaviour of these two parameters.

In fitting the 3-layer model, with offsets to 4000 m, to the synthetic traveltimes, the same observations are held as above. The threshold can be considered to lie between 0.001% and 0.01%, for similar reasons as above. In this case, the first two layers are merged into a single layer, as a result, all three layers have anisotropy, i.e., $\chi \neq 0$ for any layer. The estimated values of *a* and *b* are more consistent and vary less in the first layer. Reducing the number of layers, from three to four, does not significantly deteriorate the estimates, and the values obtained are comparable to the no-noise case. The best estimates of the parameters are obtained for the deepest layer and are very similar to those obtained for the 4-layer model.

2.4.5 Crossplots

Crossplots of parameters are useful to examine trends between parameters. Crossplots of parameter *b* versus *a*, for the no-noise case, and noise of magnitudes 0.001% and 0.01% from Profile 1, are shown in Figures 2.8, 2.9 and 2.10 for *a* and *b* values estimated in Layers 1 to 3, respectively. In all three layers, points have a large scatter. Linear trends, as a broad band of concentrated points, are observed between *b* versus *a.* As *a* increases, *b* decreases. The value of *b*, which is the rate of change of *a*, is compensatory to the value of *a*, i.e., if *a* is large *b* is small and if *a* is small *b* is large.

Distribution of points on the crossplots are colour coded, as percentiles of the RSS to the minimum RSS, to aid analyses. Since a 3-layer model is fitted to traveltimes derived from a 4-layer model, where the first two layers of the 4-layer model are equivalent to the first layer of the 3-layer model, there is no large red dot representing the true values of the parameters in Layer 1. Crossplots for the three noise profiles and all magnitudes of noise added are provided in Appendix C.

Figure 2.8 is a plot of *b* versus *a*, for Layer 1, for three conditions: no noise, noise of magnitude 0.001%, and 0.01%. In all three, the percentile bands, shown in increments of 5% up to 25%, appear as progressively increasing linear narrow bands within the broad band of concentrated points. By noting the position of the large black dot, which is the best estimate of the parameters, on each of the displays, the plots confirm the choice of the noise threshold. The position of the black dot is almost the same as in the no-noise case for the 0.001% noise magnitude, whereas it is farther for the 0.01% noise magnitude.

Figure 2.9 is a plot of b versus a, for Layer 2 for the same noise conditions as above. Here, the 5% percentile bands are concentrated closer to the best estimate of the parameters. The separation between the large red dot, representing the true values, and the black dot, representing the estimated parameters, is small and very similar between the no-noise and 0.001% noise magnitude, whereas, for the 0.01% noise magnitude, there is a distinct separation, again confirming that the noise threshold lies between 0.001% and 0.01% noise magnitudes.

For Layer 3, Figure 2.10, there is a very narrow linear trend observable. For a small range of a values, there are a large number of possible corresponding b values. Here again, the separation between the red dot and the black dot is small and very similar between the no-noise and 0.001% noise magnitude, whereas, for the 0.01% noise magnitude, there is a much larger separation, confirming that the noise threshold lies between 0.001% and 0.01% noise magnitudes.

Crossplots of parameter a versus χ, for the no-noise case, and noise of magnitudes 0.001% and 0.01% from Profile 1, are shown in Figures 2.11, 2.12 and 2.13. The full suite of crossplots for all noise profiles and noise magnitudes is provided in Appendix C. Similar trends, as above, can be interpreted from the crossplots. At and beyond the noise magnitude of 0.01%, in most cases, the separation between the red and black dot is noticeably larger as compared to the noise at magnitude 0.001%, exemplifying the choice of the noise threshold.

The linear trends, and therefore, the trade-offs between *a* and *b*, are consistent for individual layers. The trade-offs are different for different layers since each individual layer has its own material properties, i.e., each individual layer has its own set of *a* and *b* values. The same can be said for the linear trends and trade-offs between *a* and χ.

Figures 2.14, 2.15, and 2.16 are crossplots of parameter χ versus *b*, for the no-noise case, and noise of magnitudes 0.001% and 0.01% from Profile 1. The full suite of crossplots for all noise profiles and noise magnitudes is provided in Appendix C. The linear trends and trade-offs are similar to that of χ versus *a,* Figures 2.11, 2.12, and 2.13.

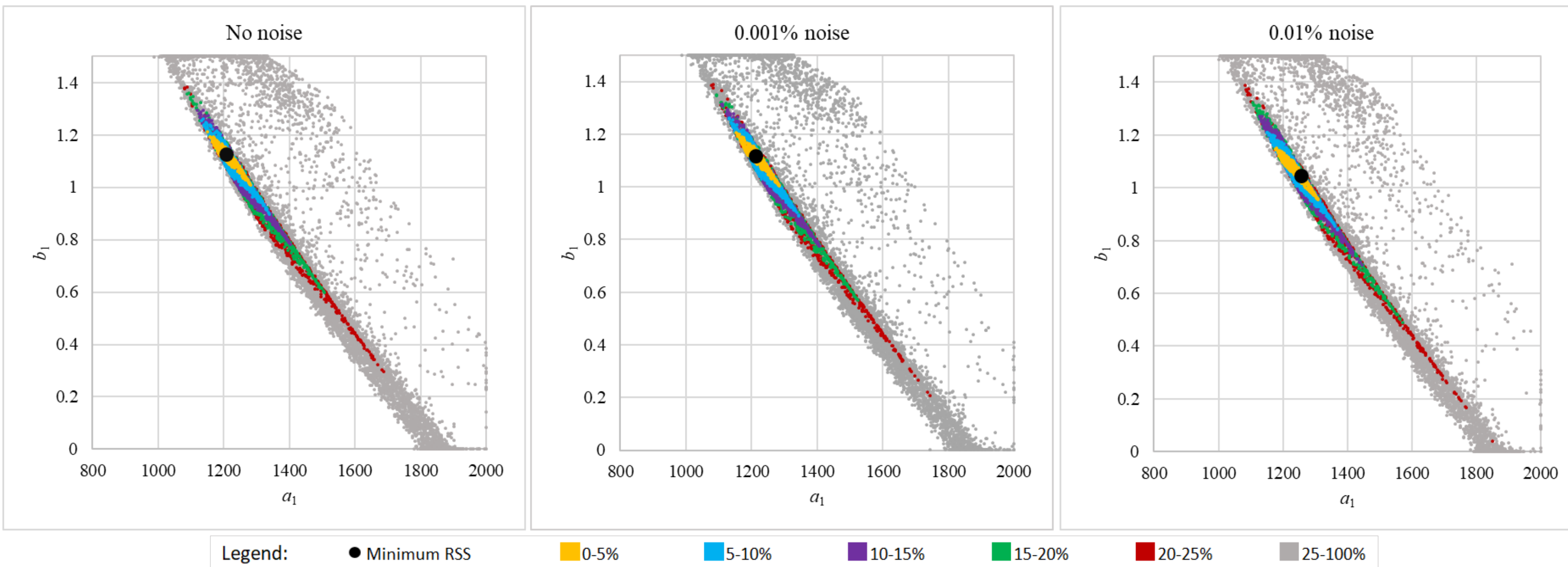

Figure 2.8: Cross-plot of parameters, b vs. a, for Layer 1, for noise added as per Profile 1, with noise at magnitudes 0, 0.001%, 0.01%, from left to right. The noise threshold lies between 0.001% noise and 0.01% noise. The colours indicate the distribution of the parameters w.r.t. the percentile of the RSS to the minimum RSS.

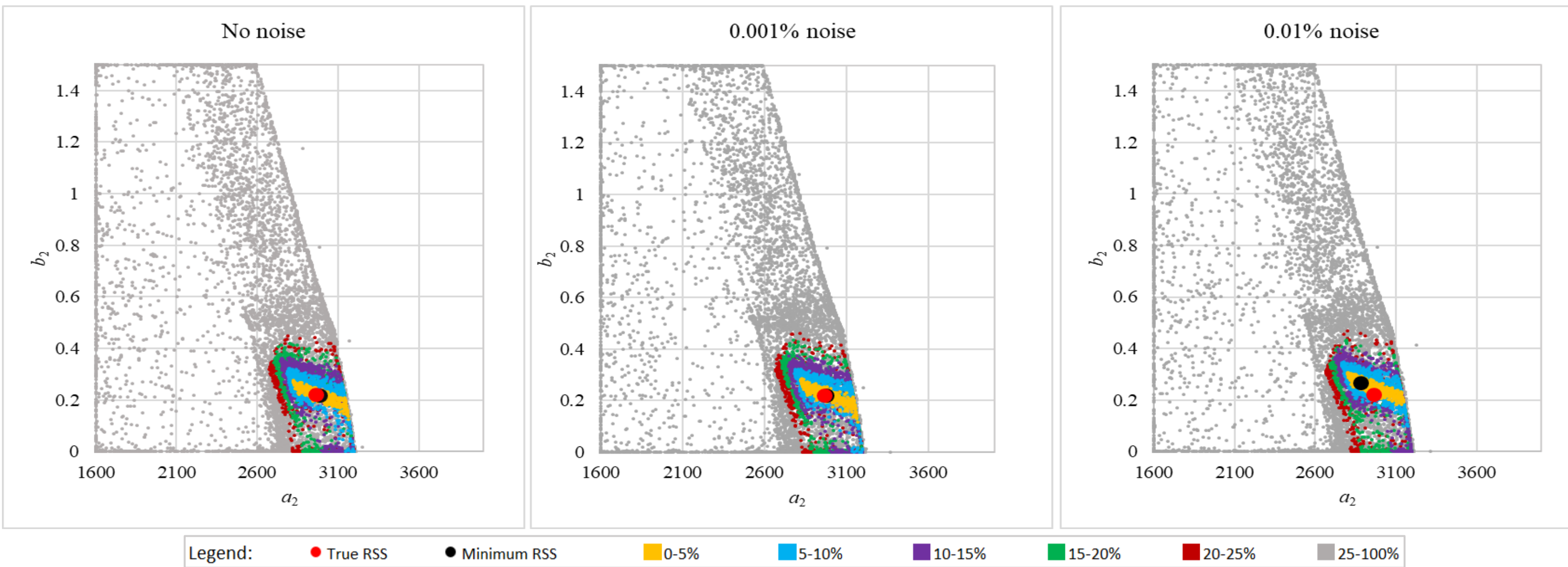

Figure 2.9: Cross-plot of parameters, b vs. a, for Layer 2, for noise added as per Profile 1, with noise at magnitudes 0, 0.001%, 0.01%, from left to right. The noise threshold lies between 0.001% noise and 0.01% noise. The colours indicate the distribution of the parameters w.r.t. the percentile of the RSS to the minimum RSS.

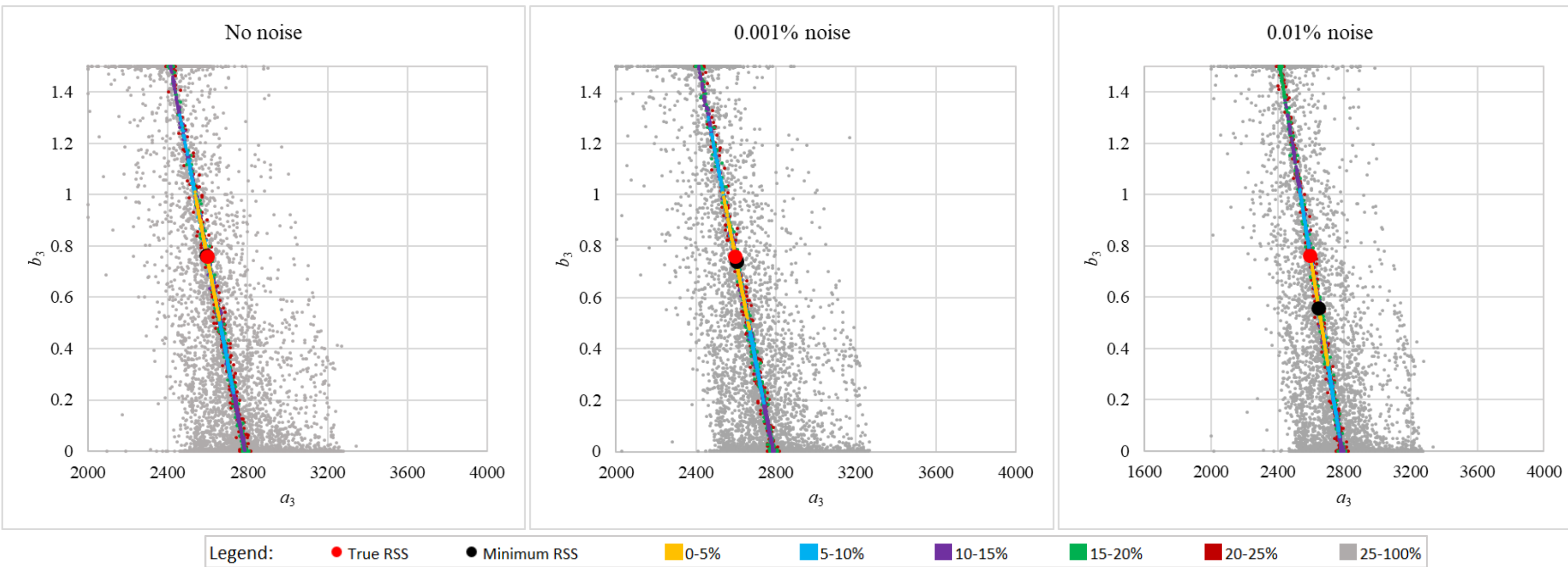

Figure 2.10: Cross-plot of parameters, b vs. a, for Layer 3, for noise added as per Profile 1, with noise at magnitudes 0, 0.001%, 0.01%, from left to right. The noise threshold lies between 0.001% noise and 0.01% noise. The colours indicate the distribution of the parameters w.r.t. the percentile of the RSS to the minimum RSS.

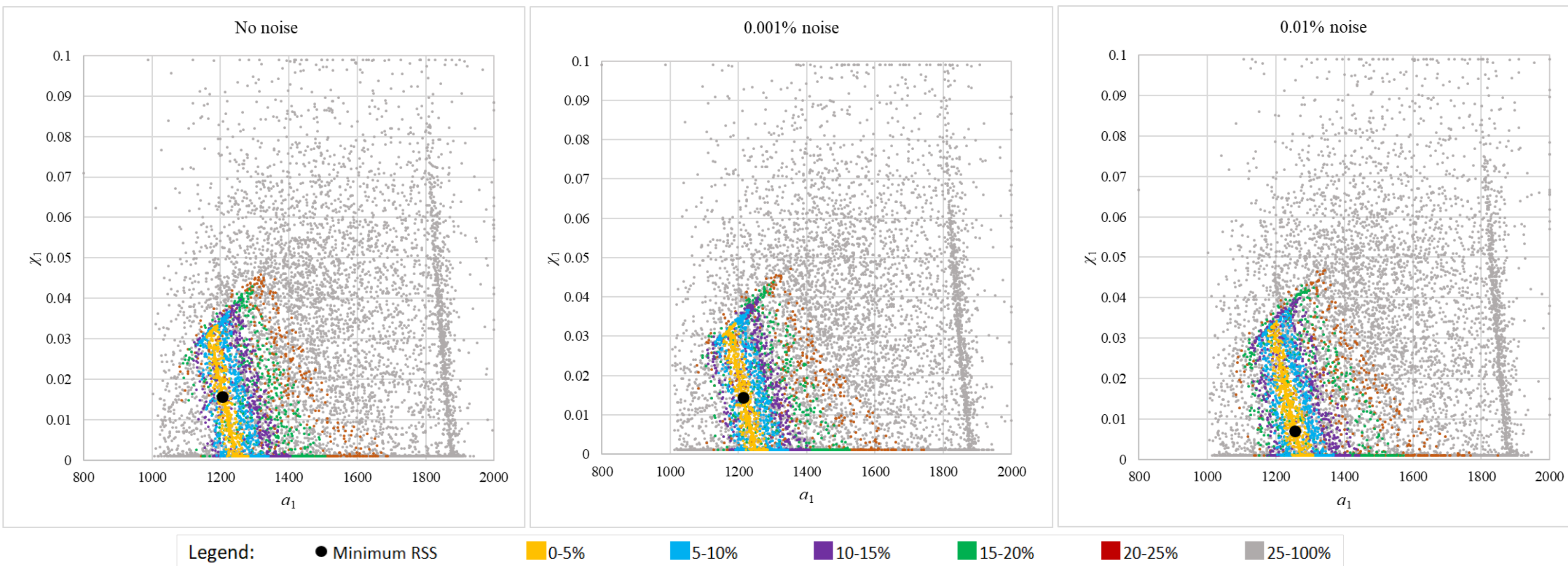

Figure 2.11: Cross-plot of parameters, χ vs. a, for Layer 1, for noise added as per Profile 1 with noise at magnitudes 0, 0.001%, and 0.01%, from left to right. The noise threshold lies between 0.001% noise and 0.01% noise. The colours indicate the distribution of the parameters w.r.t. the percentile of the RSS to the minimum RSS.

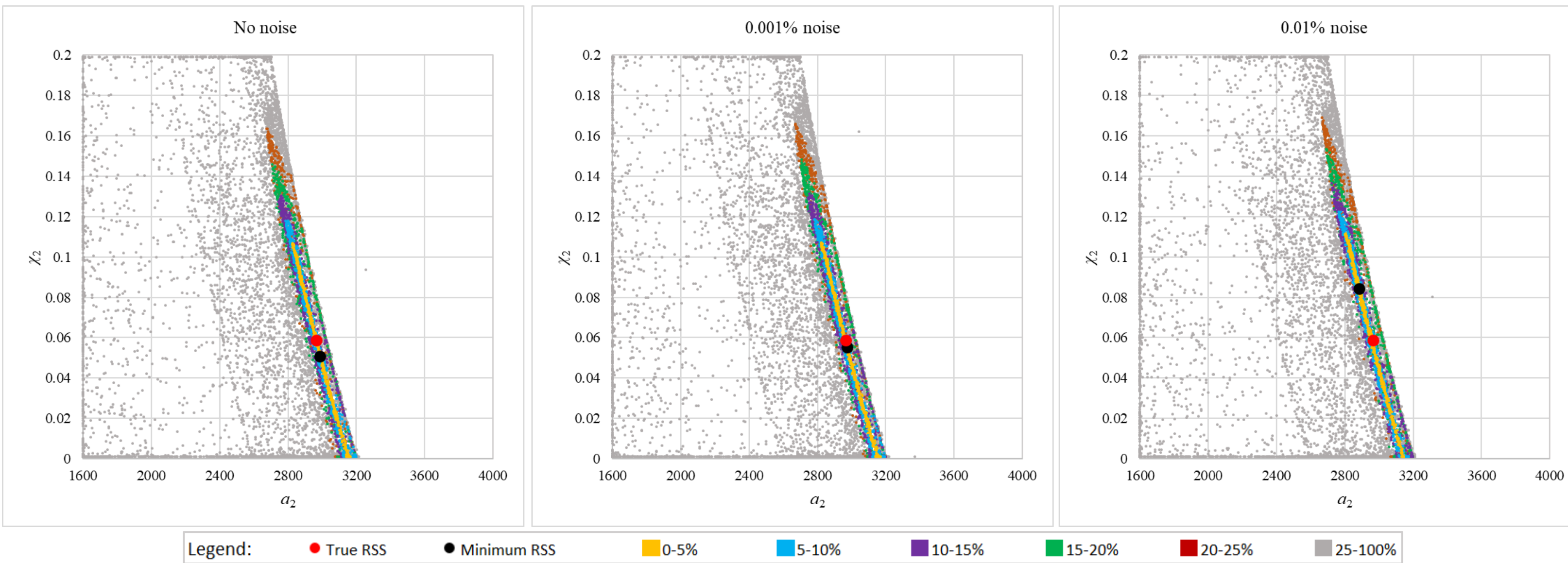

Figure 2.12: Cross-plot of parameters, χ vs. a, for Layer 2, for noise added as per Profile 1 with noise at magnitudes 0, 0.001%, and 0.01%, from left to right. The noise threshold lies between 0.001% noise and 0.01% noise. The colours indicate the distribution of the parameters w.r.t. the percentile of the RSS to the minimum RSS.

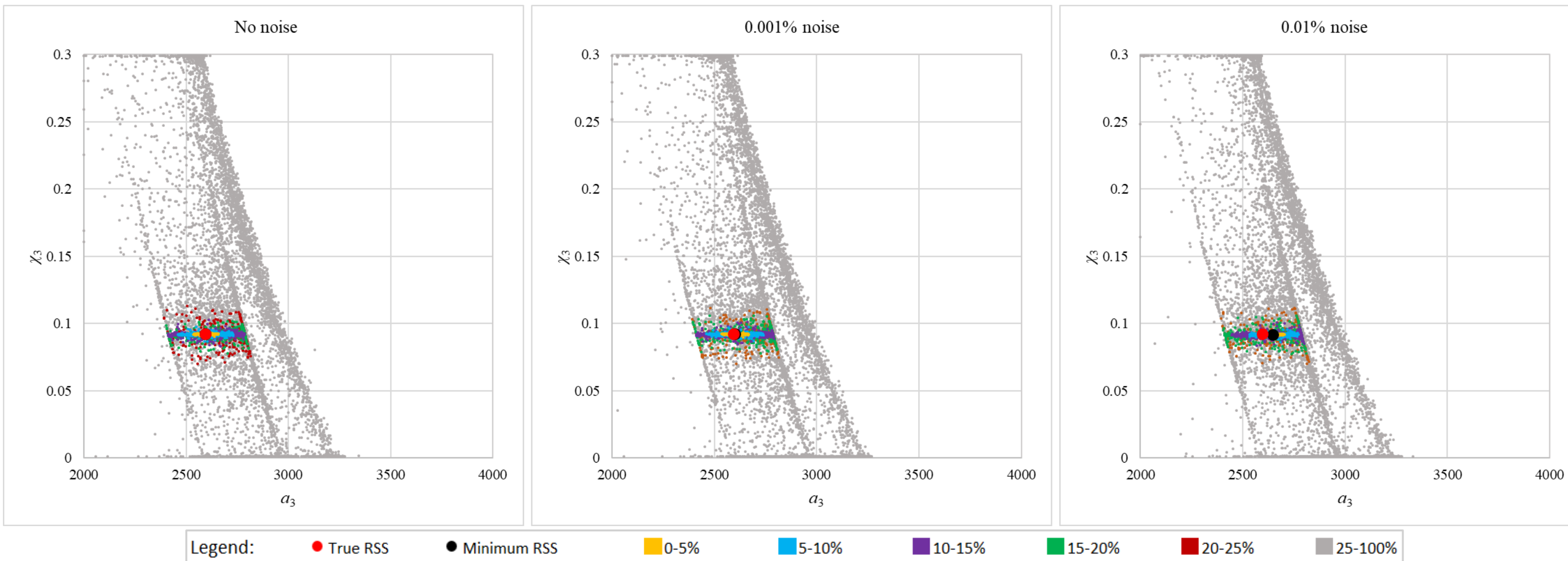

Figure 2.13: Cross-plot of parameters, χ vs. a, for Layer 2, for noise added as per Profile 1 with noise at magnitudes 0, 0.001%, and 0.01%, from left to right. The noise threshold lies between 0.001% noise and 0.01% noise. The colours indicate the distribution of the parameters w.r.t. the percentile of the RSS to the minimum RSS.

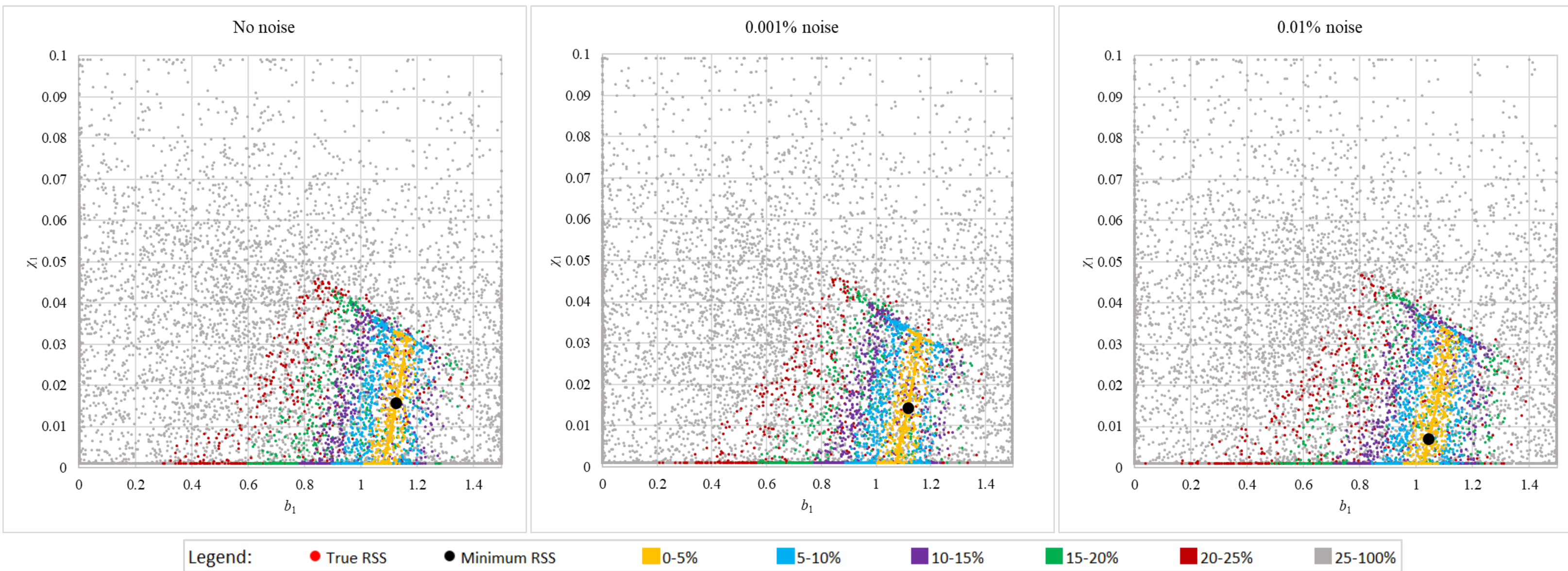

Figure 2.14: Cross-plot of parameters, χ vs. b, for Layer 1, for noise added as per Profile 1 with noise at magnitudes 0, 0.001%, and 0.01%, from left to right. The noise threshold lies between 0.001% noise and 0.01% noise. The colours indicate the distribution of the parameters w.r.t. the percentile of the RSS to the minimum RSS.

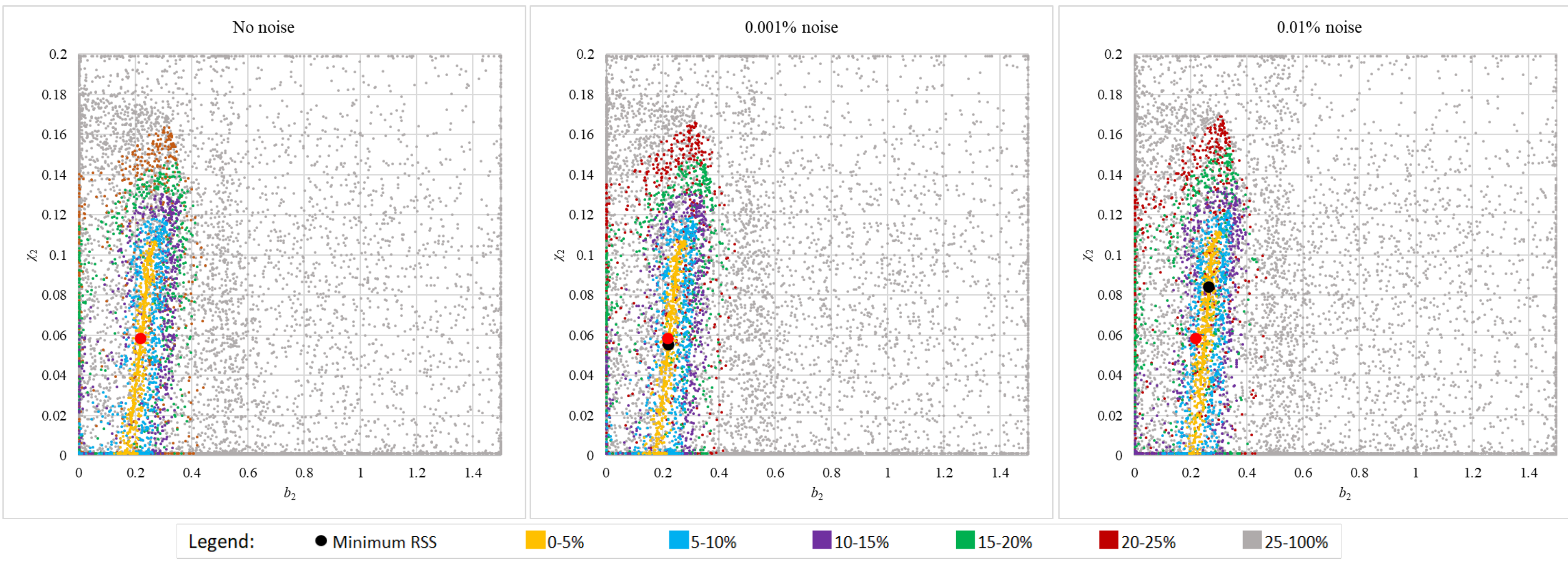

Figure 2.15: Cross-plot of parameters, χ vs. b, for Layer 2, for noise added as per Profile 1 with noise at magnitudes 0, 0.001%, and 0.01%, from left to right. The noise threshold lies between 0.001% noise and 0.01% noise. The colours indicate the distribution of the parameters w.r.t. the percentile of the RSS to the minimum RSS.

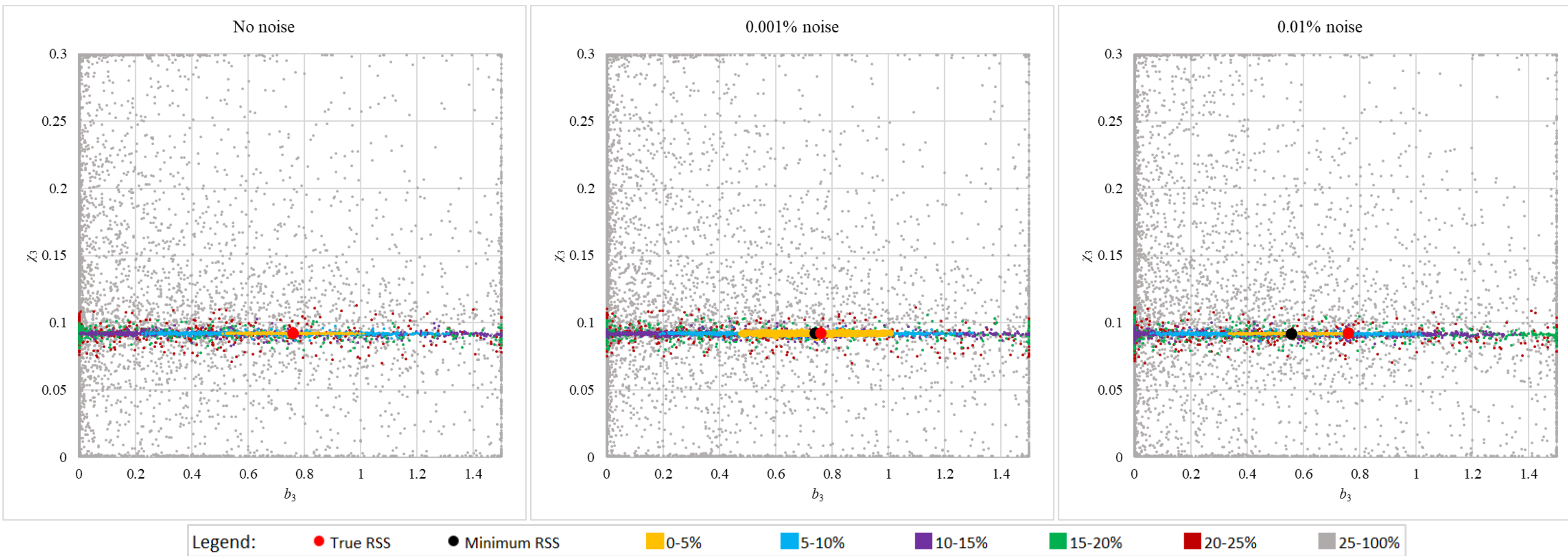

Figure 2.16: Cross-plot of parameters, χ vs. b, for Layer 3, for noise added as per Profile 1 with noise at magnitudes 0, 0.001%, and 0.01%, from left to right. The noise threshold lies between 0.001% noise and 0.01% noise. The colours indicate the distribution of the parameters w.r.t. the percentile of the RSS to the minimum RSS.

2.4.6 Real Data

Having estimated parameters with synthetic data, I now use the measured traveltimes to obtain the optimal parameters. Table 2.6 shows the results. Figure 2.17a compares traveltimes computed using these values to the measured traveltimes. Figure 2.17b is an alternate representation as a plot of the difference between the two. The traveltimes as shown in Figure 2.17a overlay, and the difference plot, Figure 2.17b, shows the computed traveltimes to be mostly within ±2 ms of the measured traveltimes. The values for the parameters thus seem reasonable and acceptable. However, a closer look is required to analyze the results.

Table 2.6: Optimal a, b, χ values for measured traveltimes fitted to a 3-layer model. Layer boundaries for the model are at 1300 m between Layers 1 and 2, and 1750 m between Layers 2 and 3.

	Optimal values		
RSS	$5.64\text{x}10^{-04}$ (s^2)		
Layer	a (ms^{-1})	b (s^{-1})	χ
1	1152	1.238	0.0010
2	3124	0.012	0.0010
3	2597	0.005	0.2164
	Horizontal distance, X: 18735 m		

For Layer 1, the value of a is 1152 ms^{-1}, b is 1.238 s^{-1}, and χ is 0.001. A value of χ this small renders it to be effectively zero. Recall the ellipticity parameter equation (1.1) from Section 1.2.4:

$$\chi = \frac{v_x{}^2 - v_z{}^2}{2v_z{}^2},$$

where v_x is the horizontal velocity and v_z is the vertical velocity, i.e., *a*. Using this equation, with the estimated values of *a, b*, and χ for this layer, v_x is calculated to be 1153 ms^{-1}, which is 1 ms^{-1} different than v_z. The effect of χ is negligible, thus, I consider χ to be effectively zero. So, Layer 1 is inhomogeneous and isotropic. It is the thickest layer with a thickness of 1294 m. The velocity at the bottom of the layer, calculated using the equation for linear velocity, $v = a + bz$, reaches 2754 ms^{-1} which is acceptable at this depth as it is within the range of velocities expected for shales (Telford et al., 1990) and is close to the velocity as logged, Figure 1.9.

For Layer 2, which is 450 m thick, the value for *b* is 0.012 s^{-1}, which is very small, so the velocity varies very little within this layer, The velocity at the top of this layer is 3124 ms^{-1} and calculated to be 3145 ms^{-1} at the bottom, the difference between the velocities is only 21 ms^{-1}, which is 0.67% of the velocity at the top of the layer. χ in this layer is 0.001, and is thus effectively zero, which can be shown in the same manner as above for Layer 1. So, Layer 2 can be considered to be homogeneous and isotropic, which is possible, but not as expected. With such a large overburden and in a predominantly shale environment, there should be at least some degree of anisotropy exhibited in Layer2.

Layer 3, which is the thinnest layer, with a thickness of 230 m, has a *b* value that is even smaller than above, and thus, the velocity is nearly constant within this layer, The velocity at the top of this layer is 2597 ms^{-1} and calculated to be 2606 ms^{-1} at the bottom, a difference of 9 ms^{-1}, which is 0.35% of the velocity at the top of the layer. It has a large χ value, 0.216. The layer can thus be considered to be homogeneous and anisotropic. All of the anisotropy is attributed to Layer 3, with χ having a large value. The horizontal velocity, calculated from the χ value, is 19.7% higher than the vertical velocity. This is possible, but unlikely despite compaction due to the large overburden. The maximum traceable offset is 18735 m. Since Layers 1 and 2 are inhomogeneous, this enables rays to be oblique in these layers and allows the offset to extend well beyond the 4000 m of the acquired data. The RSS is in the order of magnitude 10^{-04}, which is the same as for noise level 0.1%, which is beyond the threshold of noise as described in Section 2.4.4. Although the estimated parameters may be acceptable, the RSS value tends to indicate that the estimated parameters are prone to be spurious, possibly because of the noise content in the real data. This is discussed further in Section 2.5.

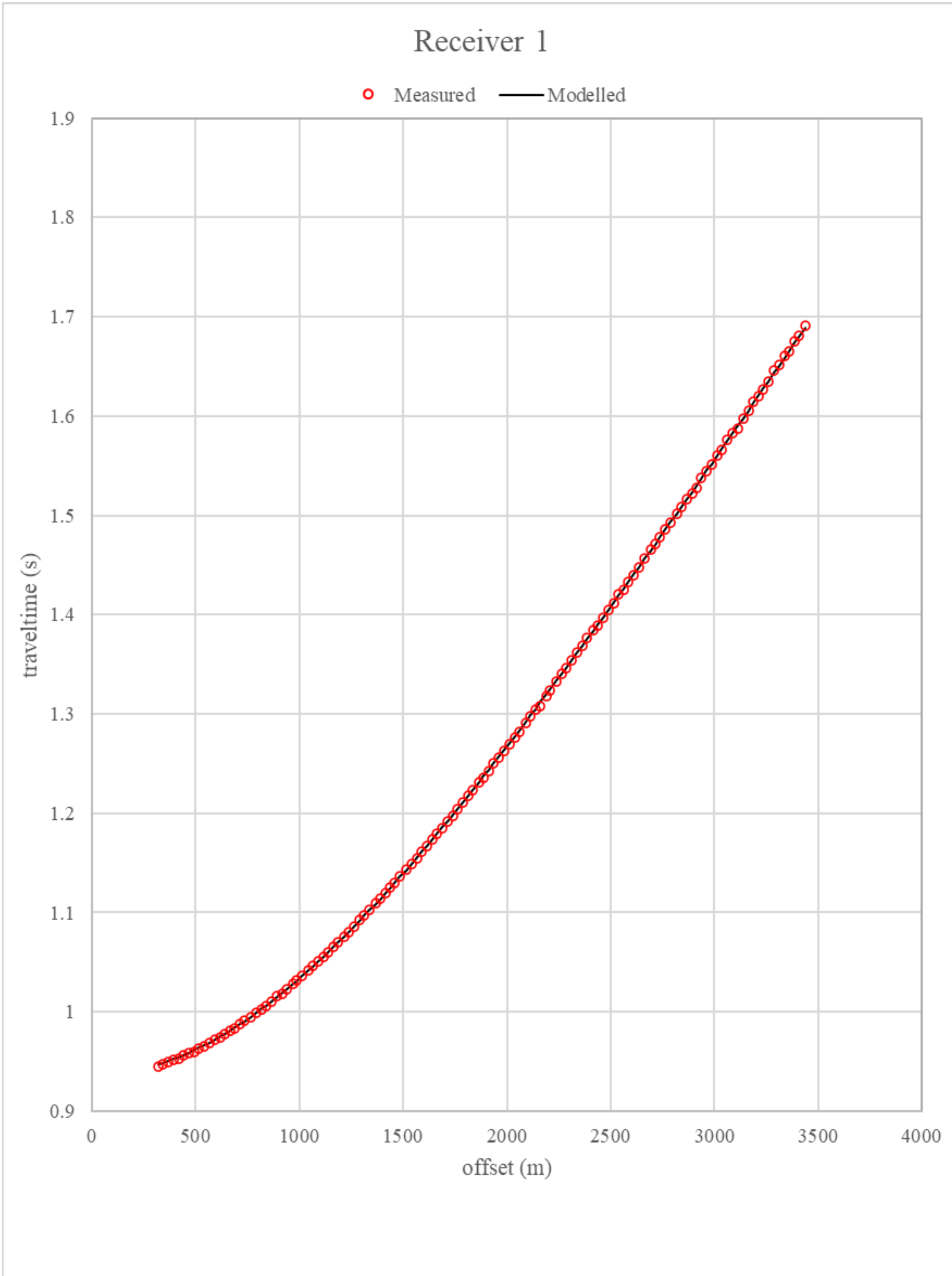

Figure 2.17: a) Comparison of modelled (black line) to measured (red circles) traveltimes for Receiver 1.

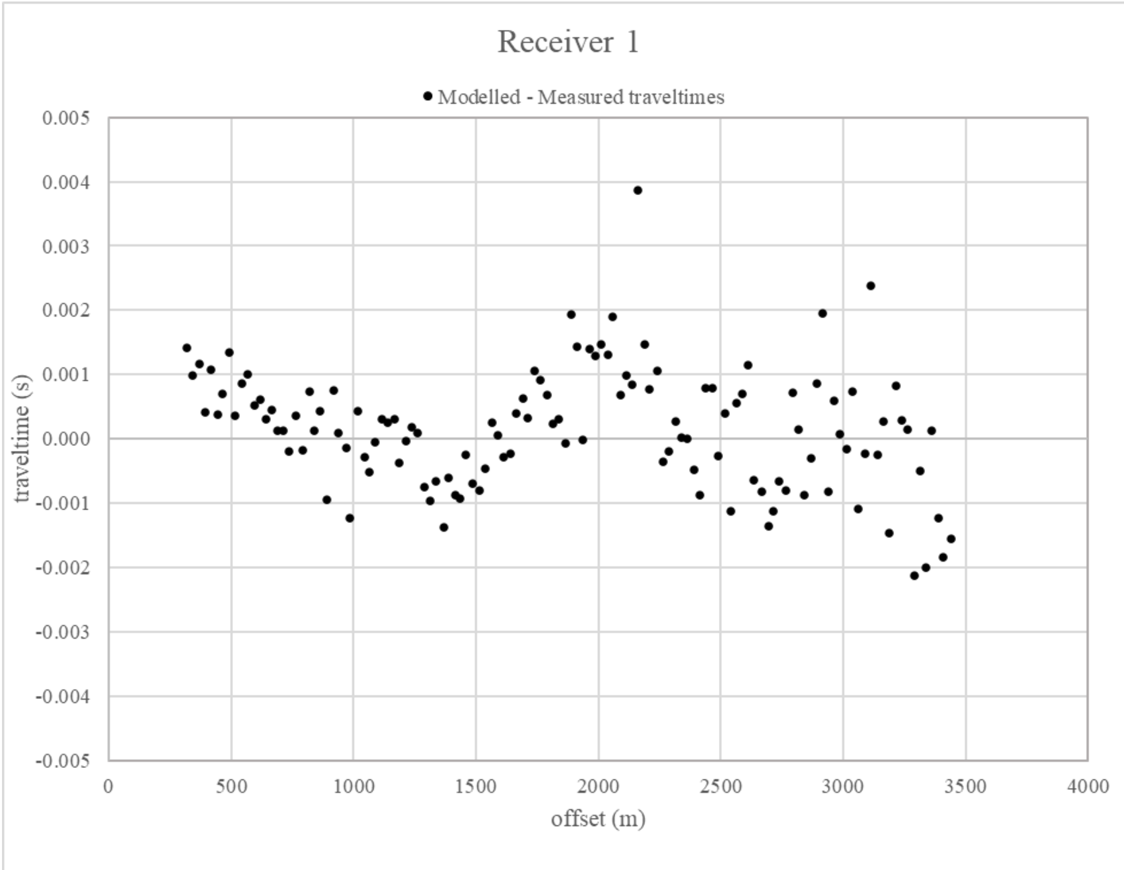

Figure 2.17: b) Comparison of modelled to measured traveltimes for Receiver 1. Black dots represent the difference obtained by subtracting measured traveltimes from modelled traveltimes.

2.5 Discussion

The objective of this study was to see if only traveltimes from a walkaway VSP data set can be used, with minimal constraints, to estimate the anisotropy parameter, χ, and inhomogeneity parameters, a and b, of layers of the earth. The only constraints were that the vertical velocity increases with depth and estimated values of a, b, χ are within specified ranges.

With synthetic data, the parameter estimations are very close to the known values, up to a certain level of noise. This confirms that the analytical equations formulated by Dr. Slawinski are useable, and the optimization technique using the Nelder-Mead algorithm works to find the optimal a, b, χ values. With real data, the estimates for a, b, χ values, however, do not appear to be entirely physically meaningful.

To understand the effect of noise, I added random noise to the data and found that even a small amount of noise affects the estimates. The random noise added is uncorrelated between receivers, and since it was found from the addition of this noise that the data are sensitive to it, other more sophisticated forms of noise, such as correlated noise between receivers arising from the propagation of the wavefield or systematic noise arising, for example, from the acquisition hardware are not considered.

The RSS for the real data associated with the estimated a, b, χ values is in the order of magnitude 10^{-04}, which is the same as for noise level 0.1%, which is beyond the threshold of noise as mentioned in Sections 2.4.4 and 2.4.5. It would seem then that the RSS for the real data indicates that the estimated parameters are affected by the noise content in the real data. However, the real data traveltimes show very little scattering, Figures 2.17a and 2.17b. In Figure 2.17b, which shows the difference between the modelled and measured traveltimes, an overall narrow band of scattered points is observed. The narrow band of scatter indicates that the noise content in the real data is low and there must be another reason for the magnitude of the RSS.

The seabed is at a depth of 131 m. With sources placed at 6 m below sea level, this means that there is a water layer that is 126 m thick between the sources and the top of the borehole. The traveltimes used to obtain the results shown in Table 2.6 were not corrected for this water layer. To check if this affects the outcome, traveltimes were corrected to a datum set at the seabed with a water velocity of 1525 ms^{-1}. Table 2.7 shows the results with the water layer and with the water layer stripped. As can be seen, all of the anisotropy is still attributed to Layer 3, i.e., the outcome is the same as not stripping the water layer.

Table 2.7: Optimal *a, b,* χ values with water layer and with water layer stripped.

	Optimal values (with water layer)			Optimal values (with water layer stripped)		
RSS	5.64×10^{-04} (s^2)			5.64×10^{-04} (s^2)		
Layer	a (ms^{-1})	b (s^{-1})	χ	a (ms^{-1})	b (s^{-1})	X
1	1152	1.238	0.0010	1168	1.422	0.0010
2	3124	0.012	0.0010	3125	0.001	0.0010
3	2597	0.005	0.2164	2604	0.006	0.2108
	Horizontal distance, X: 18734 m			Horizontal distance, X: 18734 m		

In Figure 2.17b, the points, instead of being random and centered around zero, form a cyclical pattern. The cyclical pattern can be attributed to the inadequacy of the model to simulate the measured traveltimes and is indicative of under-sampling.

There are several possible reasons for the under-sampling inherent in the data. The primary reason may be that since the receivers are only in the bottom layer, the data set may not fully represent the anisotropy in all three layers. The walkaway VSP traveltimes measured may not have sufficient information regarding anisotropy in the layers above, especially if the portions of the raypaths in the layers above are not oblique enough to be affected by the presence of anisotropy. The real data thus yield a result with the anisotropy parameter, χ, only in the bottom layer. To have complete information on the anisotropy in the layers above, receivers would have to be placed in these layers, and traveltimes with sufficiently oblique raypaths received.

Other possible contributing factors may be: the number of layers and, consequently, the number of parameters to model the subsurface may be insufficient, since I limit the number of parameters to nine, i.e., three layers with three parameters in each layer, whereas in reality, each layer is a macro-layer, with layers within having varied properties. Increasing the number of layers, and hence, the number of parameters, however, increases significantly the number of parameter combinations that are possible and increases the computational capacity required; the analytical equations used assume linear inhomogeneity and elliptical velocity dependence in the layers, which may not necessarily be the case here; a horizontally layered medium with no lateral heterogeneity is assumed, this too may not be the case; the traveltimes may be subject to scattering effects as well as dispersion and attenuation that are not accounted for. A single walkaway VSP data set is used, additional data sets may provide further information and insight.

Estimating anisotropy and inhomogeneity parameters is a complex problem. It is possible that the traveltimes alone, although they seem well behaved, are not sufficient to find the true solution, i.e., the best solution, in this case, may not be the true solution, and other information is required to find the true solution. This is a known problem with any inversion, due to the non-uniqueness of the solutions. It does not mean that the technique does not work, only that in essence, and in this instance, the model may be oversimplified.

2.6 Conclusions

The anisotropy parameter, χ, and inhomogeneity parameters, a and b, of layers of the earth can be estimated by the use of a mathematical model. In an ideal case, such as with synthetic walkaway VSP data, the estimated parameters are close to the known or true values. This serves to confirm that the analytical equations formulated, and the optimization technique, the Nelder-Mead algorithm, work well for this purpose.

Although, in an ideal case, the estimation of the parameters is good, even a small amount of noise affects the estimations.

With real data, the estimation of the parameters is dependent on a number of factors, the main one being the amount of information inherent in the data. In this case, since the walkaway VSP traveltimes were from receivers that were only in the bottom layer, they may not have contained sufficient information to construct a model to adequately represent the anisotropy in all layers. Furthermore, the number of layers (3), and hence, the number of parameters (9), to construct the model may too be insufficient. Thus, the best solution found may not be the true solution being sought.

The technique works, however, in this case, the model may be oversimplified due to the nature of the data and in the number of layers used to model the data because of computational limitations.

Chapter 3

3 Application of Bayesian Information Criterion in the selection of an appropriate model

3.1 Collaboration

A paper[2] with additional co-authors: T. Danek, B. Gierlach, M. A. Slawinski, and T. Stanoev, was submitted to the arXiv repository and was subsequently accepted for publication in Geophysical Prospecting (Danek et al., 2023). However, we requested it to be replaced with a modified paper. In the paper submitted, anisotropy was shown to be in the middle layer of a three-layer model. Being familiar with the data and the geology of the area, I felt that it was better to place anisotropy in the third layer, so that the geology was better represented.

Theodore Stanoev, and I, decided to replicate the experiment to verify the results. We found that the placement of anisotropy in the middle layer was as a consequence of incorrectly configured data, which had inadvertently been biased to the shallowest of the five receivers. Except for the traveltime for the shallowest source-receiver pairs, the traveltime for other pairs were incorrectly assigned resulting in the appearance of anisotropy in the middle of the three layers. The reworking was done with detailed scrutiny and took many months. I ensured the data were correctly configured and Theodore verified

[2] Selecting Velocity Models using Bayesian Information Criterion (https://doi.org/10.48550/arXiv.2012.12812)

the configuration. Subsequently, he wrote an algorithm in MATLAB for traveltime optimization and determination of model parameters and went over it with me to ensure it was correctly written. To reduce computation time, we ran the MATLAB code for various model parameterizations on both of our computers. Under the sponsorship of Dr. Colin Farquharson, we were granted access to Digital Research Alliance of Canada/ACENET supercomputers. The use of supercomputers increased our computational capacity and enabled a much more extensive and thorough examination in the estimation of parameters. It enhanced confidence in our results as we were able to increase the number of trials significantly. We evaluated and compiled the results together. We revised the paper and resubmitted it for publication in Geophysical Prospecting. Described here is the work that was performed jointly with Theodore, with the data correctly configured.

Collaboration with Theodore is indicated in the table below as percentages (AK/TS) for each component, where AK denotes the percentage attributed to Ayiaz Kaderali, and TS denotes the percentage attributed to Theodore Stanoev.

Component	**Details**	**Attribution % (AK/TS)**
VSP and well log data	- Acquisition, preparation, conditioning	100/0
Theory and concepts	- VSP setup for modelling - $ab\chi$ model - Bayesian Information Criterion - Model Parameterizations	90/10 50/50 50/50 50/50
Optimization	- Nelder-Mead algorithm	25/75
Implementation	<u>Coding</u> - In Excel - In MATLAB - Verification of Excel programs - Verification of MATLAB programs	 100/0 0/100 90/10 25/75

	- Validation of Excel programs - Validation of MATLAB programs <u>Execution of MATLAB programs</u> -On personal computers -On Alliance Canada supercomputers <u>Interpretation</u> - All results interpreted jointly <u>Presentation of results</u> - Generation of figures, tables	100/0 50/50 50/50 50/50 50/50 50/50

3.2 Introduction

The Bayesian Information Criterion (BIC) is presented, in this chapter, as a means for selecting the best representative model from a number of models. Each model is comprised of three layers with varied parameters. The models are generated to correspond to the multilayered medium, assumed to consist of anisotropic vertically inhomogeneous layers, in which the seismic profiling (VSP) data were acquired.

As explained by Priestly (1982), and Burnham and Anderson (2002), the Akaike Information Criterion (Akaike, 1974), abbreviated as AIC, is a very general statistical method for evaluating how well a model fits the data it was generated from; it was modified by Akaike (1978, 1979) and by Shwarz (1978) to obtain the BIC. BIC ranks models in terms of their fit to the data and has a penalty for the number of parameters. As the number of parameters increases, so does the penalty. Thereby, complex models are penalized and simpler models favoured, reducing the risk of overfitting. BIC is usually used to select the best model from a very large or infinite number of models with the minimum number of parameters.

BIC is widely used in various disciplines for model selection: for example, statistics finance, engineering, economics, medicine, biological sciences and social sciences. As far as I am aware, there is very limited application of BIC in geophysics using VSP data. The following are some recent publications. Danek and Slawinski (2012) introduce the use of BIC to test model parametrizations and to justify the anisotropy parameter. They use a two-offset VSP in the Western Canada Sedimentary Basin for a single-layer model, whereas I use a multi-offset VSP and a three-layer model, as well as a different optimization technique. Gierlach and Danek (2018) use BIC on synthetic data to choose an optimal model for two cases: a three-layer model with the middle layer being anisotropic and a five-layer model with the fourth layer being anisotropic, whereas I use real data with models that do not restrict anisotropy to any particular layer. Gierlach et al. (2019), use BIC in the same manner, and with the same VSP data set, as presented in this thesis, except that the best model found was with anisotropy in the middle layer as compared to the bottom layer. This paper was subsequently revised, by Danek et al. (2023), as it was found that the placement of anisotropy in the middle layer was due to incorrectly configured data. Zareba et al. (2023) use BIC in a different context than above. They use it as a tool for the estimation of the optimal number of clusters in applying machine learning on a walkaway VSP data set from Northern Poland.

I use BIC in a more specific situation than others, in that the number of models is restricted to three-layer models with a range of six to nine parameters. For the optimization, two steps are applied, as described in Section 2.3.2, first, to find the raypaths, and second, to calculate traveltimes and the residual sum of squares (RSS). The steps are repeated to find parameter values of the medium by minimizing the misfit, using the RSS, between the model and the data.

In order to reduce the number of parameterizations from a large number of models, eight traveltime parameterizations are selected to be considered in BIC, as described below.

3.3 Theory

3.3.1 Bayesian Information Criterion

The Bayesian Information Criterion (BIC) is a statistical method to compare models applicable to a data set. It provides a relative-fit index as a comparative evaluation for a series of models. The model with the lowest index is considered to be the best as it is the model with the fewest number of parameters that fits the data. There are two basic components in the computation for the BIC value: the deviance of the best guess, and a penalty term.

The value for BIC according to Priestley (1982) can be obtained by the following equation

$$\mathrm{BIC} = M \ln \hat{\sigma}^2 + k \ln M, \tag{3.1}$$

where $\hat{\sigma}^2$ is obtained by taking the mean of squared differences between the measured and modelled traveltimes, i.e., the residual sum of squares (RSS) divided by the number of data points, k is the number of model parameters, and M is the number of data points, which, in this case, is the number of traveltimes. The minimum value for BIC can be obtained by minimizing the error variance, $\hat{\sigma}^2$. The penalty term, $k \ln M$, is the product of the number of parameters, k, and the natural log of the sample size, M; it is a measure of model complexity, in that it represents the effective number of parameters in the model that is the best fit. As the number of parameters being estimated, k, increases, the penalty term gets larger. Likewise, as the sample size, M, increases the penalty parameter also increases. Since the model with the lowest index is considered to be the best by BIC, it effectively tends to select the model with the fewest possible parameters over complex models.

I use BIC in this study to see if it would justify the inclusion of anisotropy and which layer or layers it would point to as the best three-layer model from eight models ranging in the number of parameters from six to nine. A three-layer model was chosen as this was the number of layers determined from the VSP data, as shown in Figure 3.1 below, and in Figure 1.15 in Section 1.3.4.3.

3.4 Methodology

3.4.1 Ray Optimization

Layer interfaces of the model used are based on VSP measurements, as described in Section 1.3.4.3. Each layer is characterized by the values of a, b, χ. The optimization requires setting the number of parameters *a priori.* In this case, we have a three-layer model that permits up to nine parameters, i.e., a maximum of three parameters, a, b, χ , per layer. This gives eight traveltime parameterizations to be considered in BIC as shown in Table 3.1.

Table 3.1: Possible model parameterizations for three layers; a, b, χ combinations and classification. All layers have inhomogeneity parameters, a and b. Inclusion of χ renders the layer as anisotropic otherwise layers are isotropic. Isotropic layers are denoted by " –", anisotropic by χ_n, where n is the layer number.

	Number of parameters, k							
Layer, n	6	7			8			9
1	–	χ_1	–	–	χ_1	χ_1	–	χ_1
2	–	–	χ_2	–	χ_2	–	χ_2	χ_2
3	–	–	–	χ_3	–	χ_3	χ_3	χ_3

In each layer, the traveltime along a ray is given by equation (1.4) in Section 1.2.4. I apply a two-step optimization, as described in Section 2.3.2, using the Nelder-Mead simplex and summarized below.

Step 1: For a set of the a, b, χ values, find the raypaths for each source-receiver pair. To do so, numerically solve for the ray parameter value that traces a ray to the receiver for each source.

Step 2: Compute traveltimes for the raypaths, compare them to the measured traveltimes, and compute the RSS.

At each iteration of the NM algorithm, Steps 1 and 2 are repeated to obtain RSS values for the set of a, b, χ values. The algorithm then adjusts the a, b, χ values, repeating Steps 1 and 2 accordingly, until the RSS is brought to a minimum.

3.4.2 Models

Layer interfaces for the models used in the optimizations were determined using the zero-offset VSP (ZVSP) data. Figure 3.1. shows a plot of smoothed interval velocities from the ZVSP, the same as shown in Figure 1.15 in Section 1.3.4.3. I infer from the plot a three-layer model from the three distinct velocity gradients that are visible. The interfaces at 1300 m and 1750 m are used in all computations.

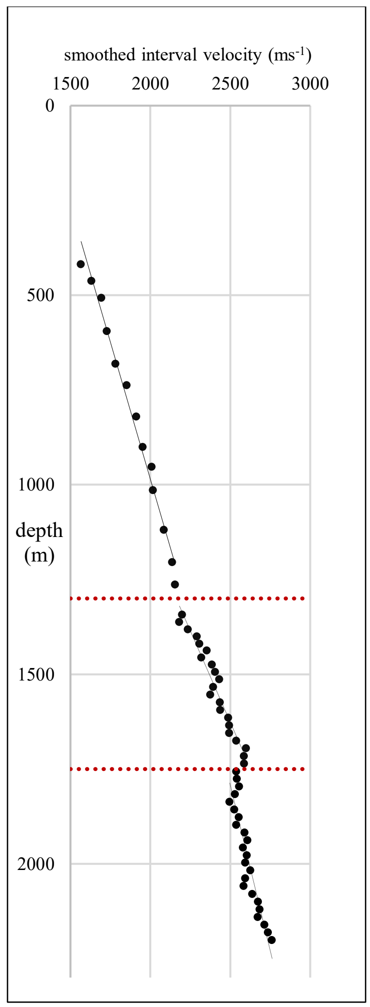

Figure 3.1: ZVSP smoothed interval velocities. Dotted horizontal lines indicate interpreted layer boundaries.

As explained by Burnham and Anderson (2002), models provide an approximation to reality. The larger the data set, and assuming the data are good, the greater the chance of finding the "true" or "best" model that is a good estimate and is representative of reality. They indicate that one of the aspects of BIC is that if such a model is within the test set, the probability of choosing it tends to unity while $n \rightarrow \infty$. In practical applications, however, with relatively low number of data points, it is important to limit the set of tested models to avoid spurious solutions.

I limit the choice of models to three layers based on ZVSP data, as indicated in Figure 3.1. This results in eight models of different parameterizations, as shown in Table 3.1. The simplest model is inhomogeneous, but isotropic, and consists of six parameters a_i, b_i, where i = 1, 2, 3. The most complicated model is inhomogeneous and anisotropic and consists of nine parameters a_i, b_i, and χ_i, where i = 1, 2, 3. In between these two extremes, are three seven-parameter models and three eight-parameter models. For each model in Table 3.1, I calculate the Bayesian Information Criterion value using expression (3.1).

3.5 Results and Discussion

Table 3.2 shows the values of a, b, and χ, that give the least Residual Sum of Squares (RSS) for the eight model parameterizations in Table 3.1, for both the Standard Nelder-Mead and Adaptive Nelder-Mead algorithms. BIC values are calculated using equation (3.1) and are included in Table 3.2. For example, the BIC value for the 6-parameter model with the adaptive NM is -9031:

$$BIC = \; M \ln \hat{\sigma}^2 + k \; ln \; M = 695 \; ln\left(\frac{1.49261 \; x \; 10^{-3}}{695}\right) + \; 6 \; ln(695) \; = \; -9031,$$

where M is the number of traveltimes, $\hat{\sigma}^2$ = RSS/M, and k is the number of model parameters.

Table 3.2: Values of *a, b*, χ, and BIC, corresponding to the least Residual Sum of Squares (RSS). Model parameterizations are as shown in Table 3.1. Subscripts indicate the layer number.

Standard NM											
Model parameters	RSS (s^2)	a_1 (ms^{-1})	a_2 (ms^{-1})	a_3 (ms^{-1})	b_1 (s^{-1})	b_2 (s^{-1})	b_3 (s^{-1})	χ_1	χ_2	χ_3	BIC
6	1.49264E-03	999	3175	3112	1.499	0.004	0.001	-	-	-	-9031
7	6.95942E-04	1005	3164	2954	1.499	0.006	0.001	0.0280	-	-	-9555
7	6.91974E-04	1031	2933	2954	1.499	0.003	0.001	-	0.0799	-	-9559
7	5.61293E-04	1139	3129	2601	1.265	0.001	0.001	-	-	0.2144	-9704
8	5.62094E-04	1136	3126	2602	1.271	0.008	0.021	-	0.0010	0.2106	-9697
8	6.92888E-04	1030	2941	2946	1.499	0.013	0.034	0.0014	0.0763	-	-9552
8	5.63401E-04	1144	3126	2603	1.253	0.017	0.001	0.0010	-	0.2132	-9695
9	5.64744E-04	1164	3127	2579	1.214	0.002	0.030	0.0010	0.0014	0.2237	-9687

Adaptive NM											
Model parameters	RSS (s^2)	a_1 (ms^{-1})	a_2 (ms^{-1})	a_3 (ms^{-1})	b_1 (s^{-1})	b_2 (s^{-1})	b_3 (s^{-1})	χ_1	χ_2	χ_3	BIC
6	1.49261E-03	999	3176	3112	1.499	0.001	0.001	-	-	-	-9031
7	6.95920E-04	1004	3165	2955	1.499	0.001	0.001	0.0279	-	-	-9555
7	6.91970E-04	1031	2933	2953	1.499	0.001	0.001	-	0.0799	-	-9559
7	5.61293E-04	1139	3129	2601	1.265	0.001	0.001	-	-	0.2143	-9704
8	5.61959E-04	1141	3126	2601	1.260	0.001	0.001	-	0.0010	0.2142	-9697
8	6.92164E-04	1030	2943	2954	1.499	0.001	0.001	0.0012	0.0761	-	-9552
8	5.63384E-04	1144	3130	2602	1.252	0.002	0.001	0.0010	-	0.2135	-9695
9	5.64100E-04	1152	3124	2597	1.238	0.012	0.005	0.0010	0.0010	0.2164	-9688

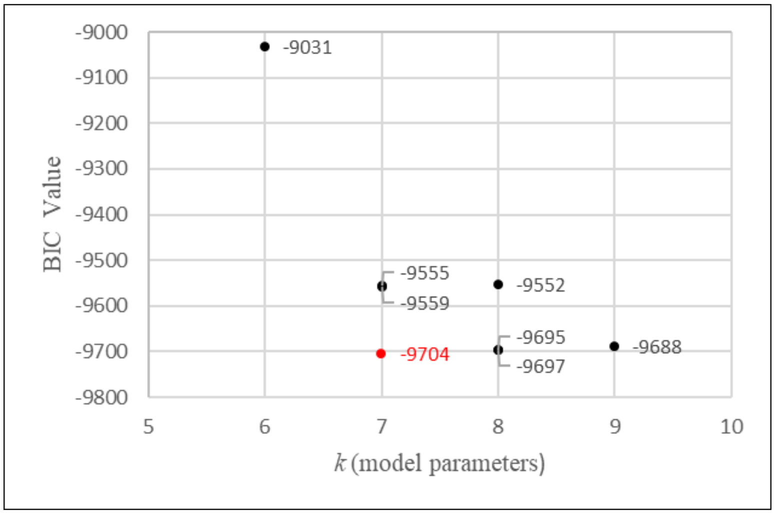

Figure 3.2: BIC values for nine three-layer models. The BIC values are shown beside the points. The model that has the lowest BIC value (-9704) occurs when the number of model parameters, *k*, is seven; when anisotropy is present in the third layer and the overlying two layers are isotropic.

Figure 3.2 is a display of the BIC values for the models as per Table 3.2. BIC values for the seven-parameter model with χ in the first layer, -9555, and in the second layer, -9559, are very close and are not discernable. The same is true for the two eight-parameter models with χ in the third layer, -9697 and -9695. Thus, only six points are visible instead of eight.

Table 3.3: Ranking of models by BIC.

Ranking	Model parameters	BIC value	RSS (s^2)	χ_1	χ_2	χ_3
1	7	-9704	5.61E-04	-	-	0.2143
2	8	-9697	5.62E-04	-	0.0010	0.2142
3	8	-9695	5.63E-04	0.0010	-	0.2135
4	9	-9688	5.64E-04	0.0010	0.0010	0.2164
5	7	-9559	6.92E-04	-	0.0799	-
6	7	-9555	6.96E-04	0.0279	-	-
7	8	-9552	6.92E-04	0.0012	0.0761	-
8	6	-9031	1.49E-03	-	-	-

As seen in Figure 3.2, and by ranking the BIC values, Table 3.3, the model with the lowest BIC value, -9704, is the seven-parameter model, with χ in the third layer. The lowest BIC value corresponds to the lowest RSS value. The worst model is the six-parameter model, i.e., the isotropic model.

The model with the lowest BIC index is considered to be the best as it is the model with the fewest number of parameters that fits the data, in this case, seven. Increasing or decreasing the number of parameters increases BIC, see Table 3.3. This indicates that there is no benefit in increasing parameters, as corroborated by the RSS values in Table 3.3, and it is not justified. Conversely, when the number of parameters is decreased to six, i.e., to the isotropic model, the BIC index gets significantly larger, -9031, and we observe a poorer fit.

All the models with anisotropy rank better than the isotropic model, which justifies the introduction of anisotropy in the models. Geological information for the area, as described in Section 1.3.2, indicates that the subsurface is mainly composed of shale, it is thus expected that models with some degree of anisotropy would rank better than the isotropic model. Models with anisotropy in the third layer rank better than other models. When χ is present in the third layer, values of χ in the first layer and second layer are negligible and their anisotropy is effectively zero. The first layer may be isotropic by virtue of its position, in that being the shallowest, it may be unconsolidated and is not subject to significant compaction due to overburden. Compaction increases with overburden as a function of depth resulting in preferential alignment of particles and, hence, in anisotropy.

The deepest layer is subjected to the most significant compaction due to overburden and, thus, exhibits the greatest amount of anisotropy. For example, the nine-parameter model places anisotropy in the third layer with a high χ value.

Comparisons of measured traveltimes, used in the optimization, and calculated traveltimes for receivers 1 to 5, for the best resulting model from BIC, are shown in Figure 3.3. Calculated traveltimes are based on equations (1.4) and (1.7) in Section 1.2.4. As can be seen, the results are consistent and the fit between the curves is very good. Figure 3.4 includes the shortside and longside for comparison. Again, the fit is very good, even at offsets not used in the optimization.

Figures 3.5 and 3.6 show two-dimensional anisotropy ellipses at the top of the third layer, for different parameterizations. When b is negligible, the layer can be considered to be homogeneous, and the shape of the anisotropy ellipse remains the same with depth. Table 3.4 shows the values of χ, and corresponding horizontal and vertical velocities (v_x and v_z), used to generate the ellipses in the third layer for the various models. Note that the shapes of these ellipses are nearly identical, for the seven-, eight-, and nine-parameter models. This is due to the ellipticity parameter, which is a measure of anisotropy, being very similar for all three models.

Table 3.4: Values of χ , and corresponding horizontal and vertical velocities (v_x and v_z), in the third layer for the six-, seven-, eight- and nine-parameter models, k = 6, 7, 8 and 9.

k	χ	v_x (ms^{-1})	v_z (ms^{-1})
6	0	3112	3112
7	0.2144	3109	2601
8	0.2106	3102	2602
	0.2132	3108	2603
9	0.2237	3103	2579

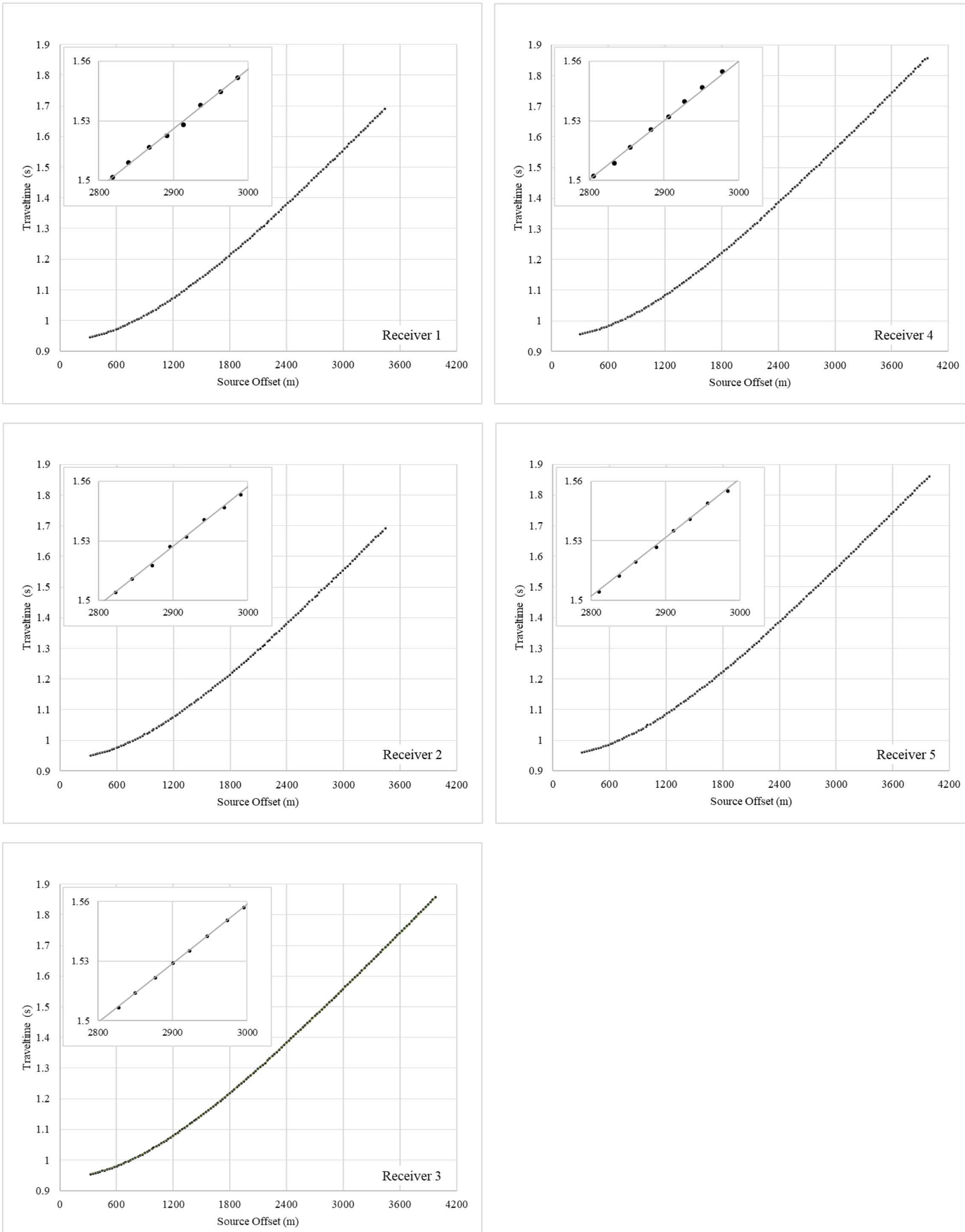

Figure 3.3: Comparison of measured (black dots) and calculated (grey line) traveltimes for receivers 1 to 5 for the seven-parameter model. The inset shows a closer view of the fit.

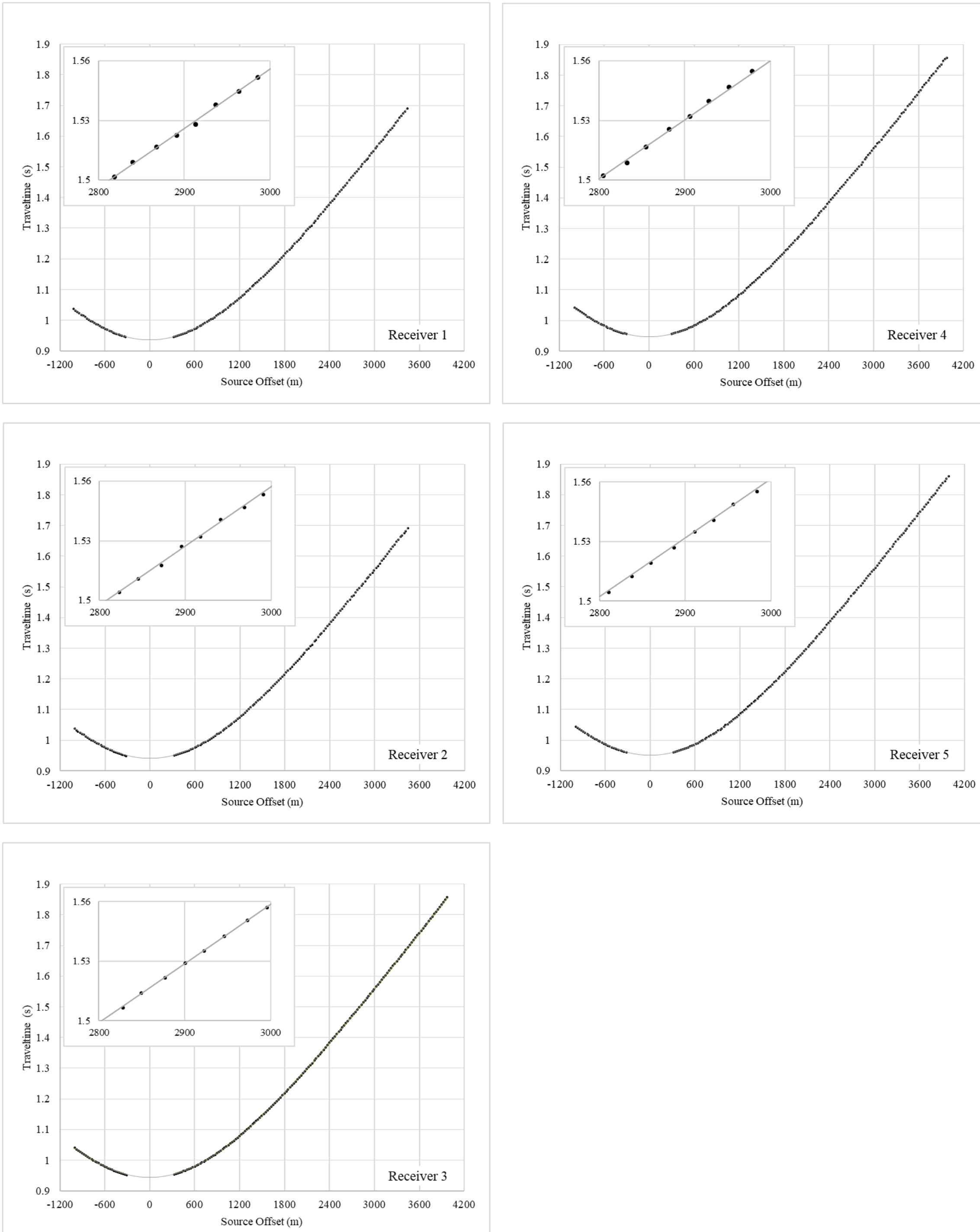

Figure 3.4: Comparison of measured (black dots) and calculated (grey line) traveltimes for receivers 1 to 5 for the seven-parameter model for shortside and longside. The inset shows a closer view of the fit.

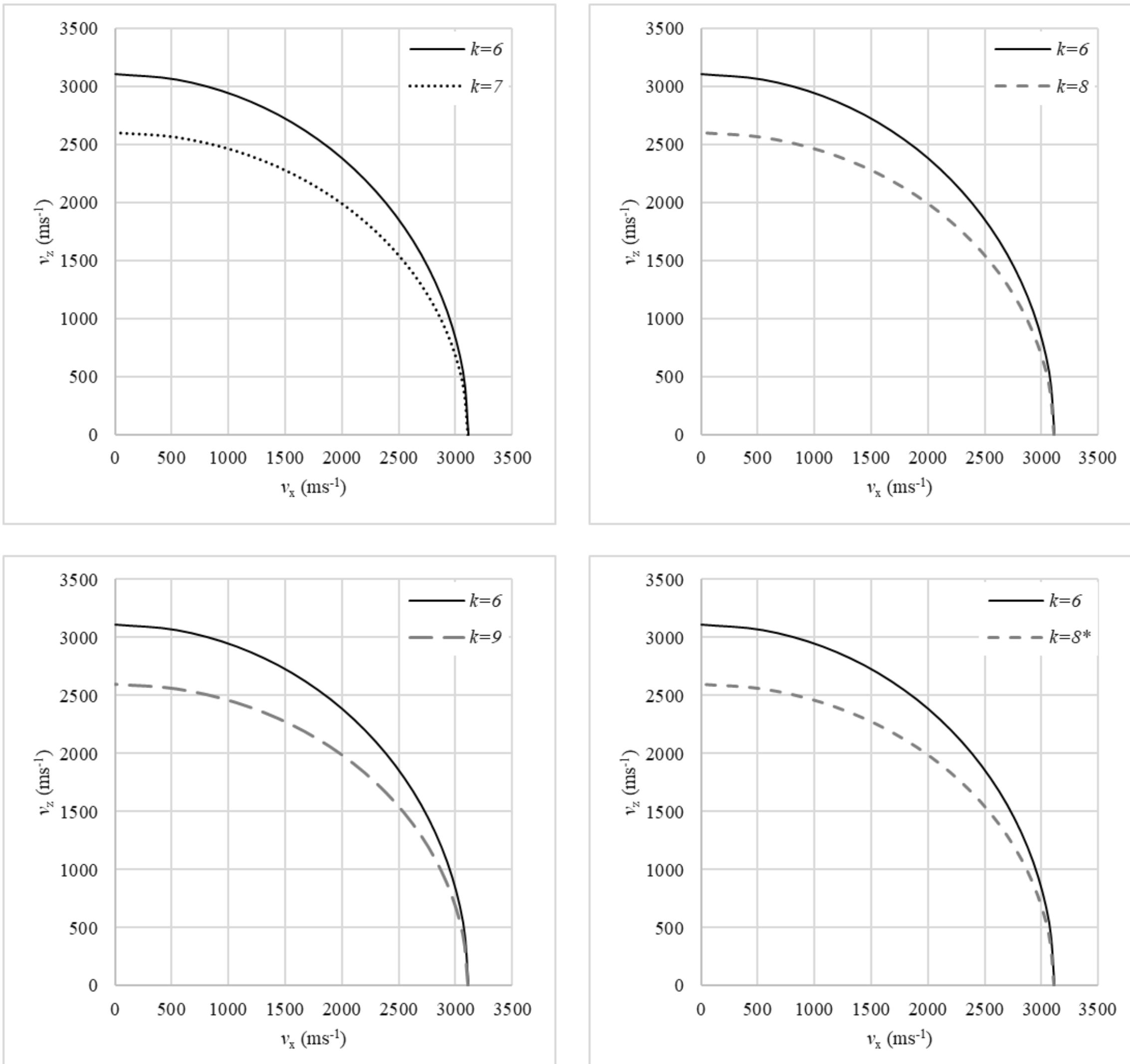

Figure 3.5: First quadrant of velocity ellipses in the third layer; generated from the values in Table 3.4. The isotropic model has six model parameters, i.e., $k = 6$, and is shown as the black solid curve. The anisotropic models where $k = 7$, 8, or 9 are shown as grey dotted or dashed curves. For $k = 8$, χ is in the first and third layers, for $k = 8^*$, χ is in the second and third layers.

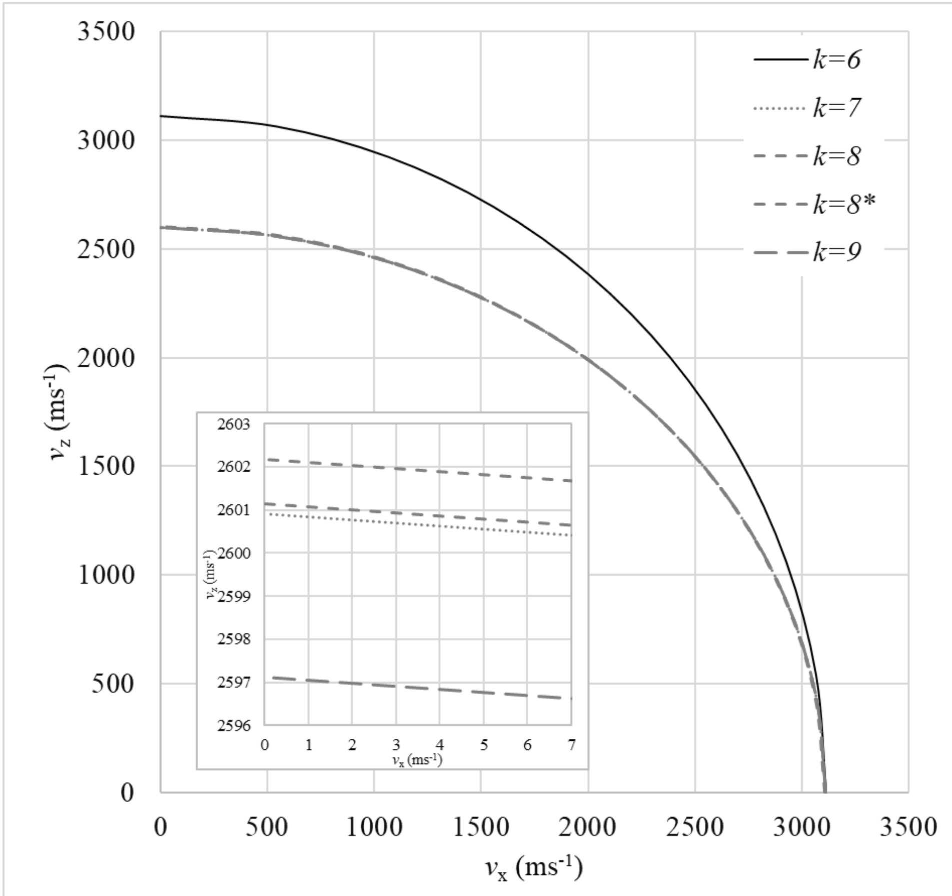

Figure 3.6: Overlay of velocity ellipses shown in Figure 3.5, to illustrate the similarity between the anisotropic models where k = 7, 8, or 9. For k = 8, χ is in the first and third layers, for k = 8*, χ is in the second and third layers and has the lower velocity, v_z, of the two.

To examine relations between parameters, crossplots of parameter values were generated, Figures 3.7 to 3.10. Since all the results from the optimizations may not necessarily be solutions, in some cases, they may be values at termination points, and we seek a, b and χ parameters that exhibit a low RSS, I look at values in the vicinity of the minimum RSS. The figures show the top 25% of the results with respect to the residual sum of squares to identify scatter points, and possible trends, that are close to the best solution. Crossplots for the best resulting model from BIC are compared to the model with the maximum number of parameters, k = 9. This model allows for inhomogeneity and anisotropy in every layer, i.e., each layer has a b χ, whereas the best resulting model has χ only in the third layer.

Figures 3.7, 3.8, and 3.9 are plots of a versus b for the first, second, and third layers, respectively. Figure 3.10 is a plot of a versus χ for the third layer. In all cases, as the number of parameters increases, i.e., increasing k from 7 to 9, values that are within the top 25% of the results have a greater spread. Linear trends can be observed between a versus b as well as a versus χ on the crossplots.

The parameter pairs of interest are a versus b in the first layer, i.e., the relation between the vertical velocity at the top of the layer and the increase of the vertical velocity with depth, and a versus χ in the third layer, i.e., vertical velocity and the ellipticity parameter. Other pairs are not of interest because the lowest RSS occurs when the second and third layers are homogeneous, i.e., b tends to zero, and when the first and second layers are isotropic, i.e., χ is or tends to zero. Crossplots for the eight-parameter models with χ in the first and third layers, and in the second and third layers are included in Appendix D.

Table 3.5: Correlation coefficients (R) and coefficient of determinations (R^2) for the best resulting model from BIC, k =7, compared to the model with the maximum number of parameters, k = 9. Correlation values correspond to Figures 3.7 and 3.10.

Layer	Crossplot parameters	Model			
		k = 7		k = 9	
		R	R^2	R	R^2
1	a vs. b	-0.9994	0.9988	-0.9980	0.9960
3	a vs. χ	-0.7729	0.5973	-0.5689	0.3236

Table 3.5 shows the correlation coefficient, R, and coefficient of determination, R^2, for the linear relationship between a versus b and a versus χ, of the k =7 and the k = 9 models. To interpret the values, I use the guidelines from Ratner (2009), where R is a measure of the strength of the linear relationship between two variables, whereas R^2 measures the amount of variation in the data that is explained by the regression model. For the relationship between a and b, the values of R and R^2 are close to -1 and 1, respectively, which is the case for both models. This indicates a strong linear relationship between these two parameters, as can be seen in Figure 3.7, and that the regression models have a good fit with the data, i.e., the models explain the variation in the data well. For the relationship between a and χ, the seven-parameter model shows a stronger relationship than the nine-parameter model. For the seven-parameter model, the relationship can be considered as strong whereas it is moderate for the nine-parameter model. As the number of model parameters increases, anisotropy is introduced in more layers; hence, there are a greater number of combinations of a, b and χ that are possible that will fit the data, which manifests in the crossplot as a greater spread of points, see Figure 3.10.

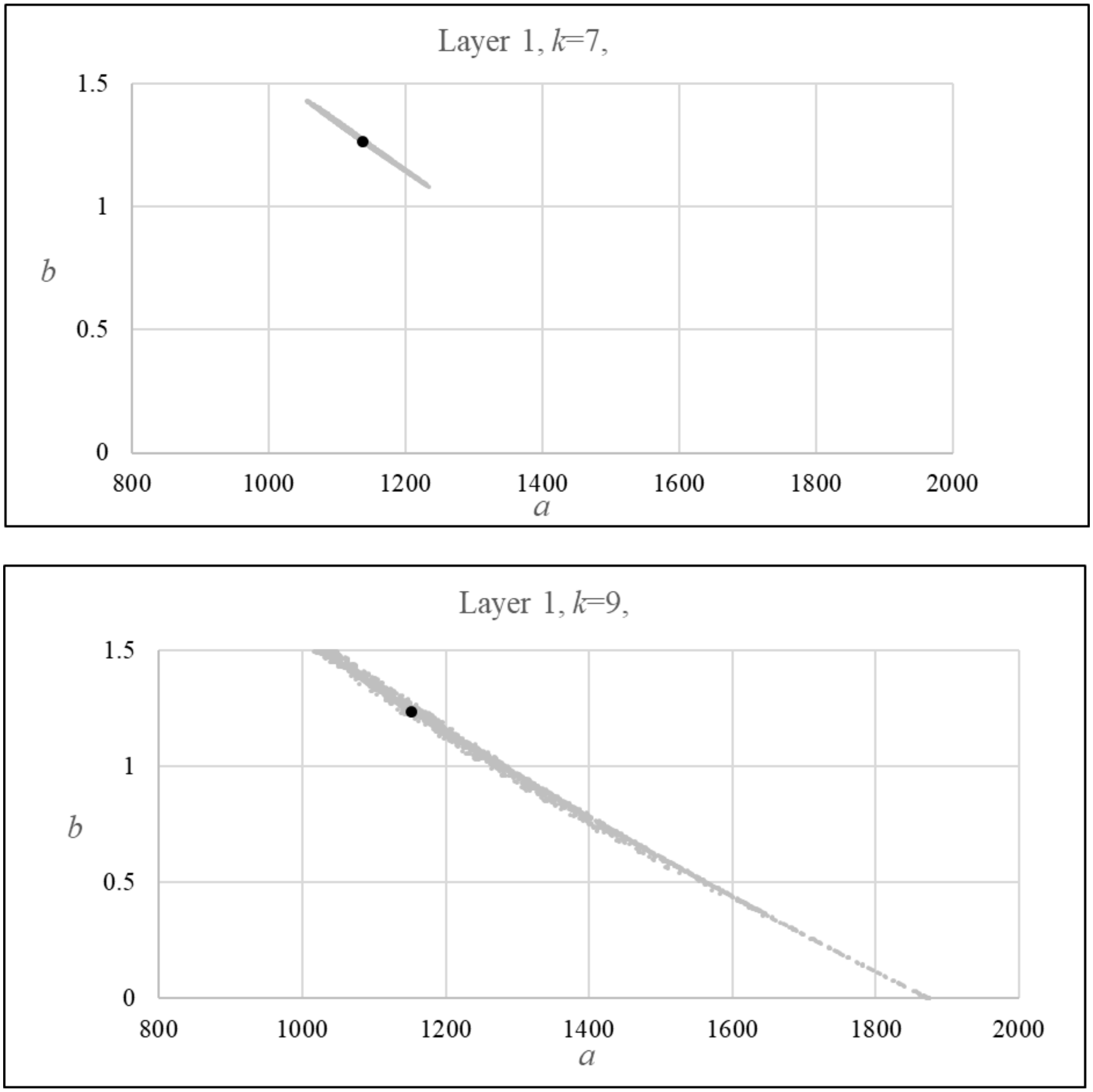

Figure 3.7: Crossplots of parameters *a* (ms^{-1}) versus *b* (s^{-1}) for the seven-parameter model, *k* = 7, and nine-parameter model, *k* = 9, for the first layer. *a* is the speed at the top of the layer. The results shown are the top 25% with respect to the residual sum of squares. The dimensions of the display correspond to the nine-parameter model for comparison. The black dot is where the parameters give the least RSS value.

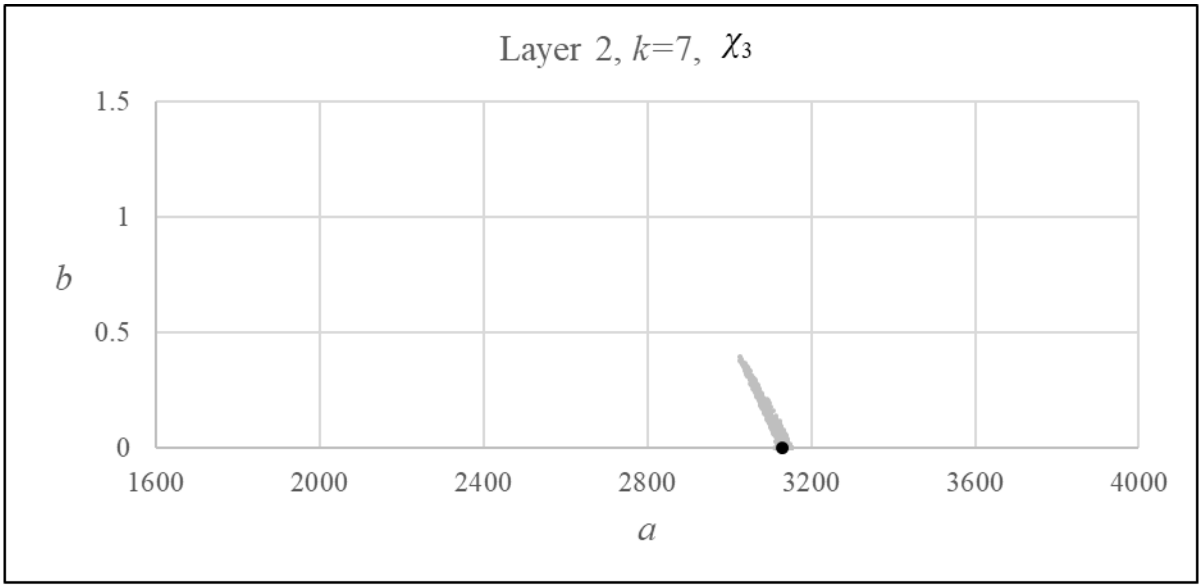

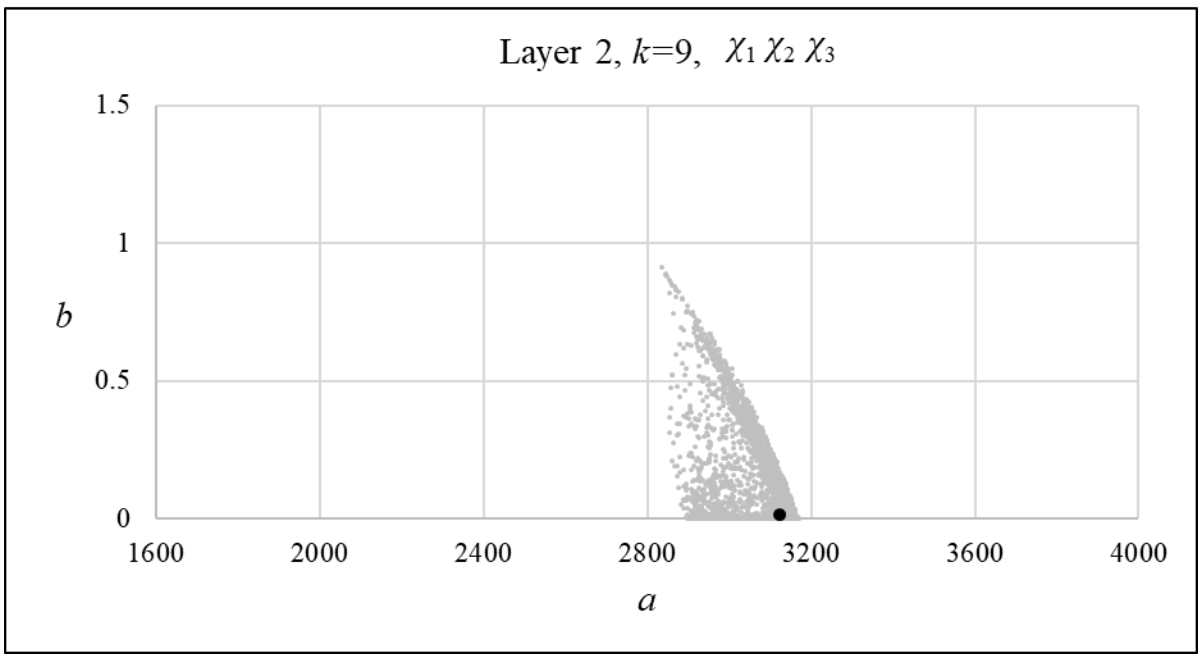

Figure 3.8: Crossplots of parameters *a* (ms^{-1}) versus *b* (s^{-1}) for the seven-parameter model, *k* = 7, and nine-parameter model, *k* = 9, for the second layer. Note: Formatting of the figures is the same as Figure 3.7.

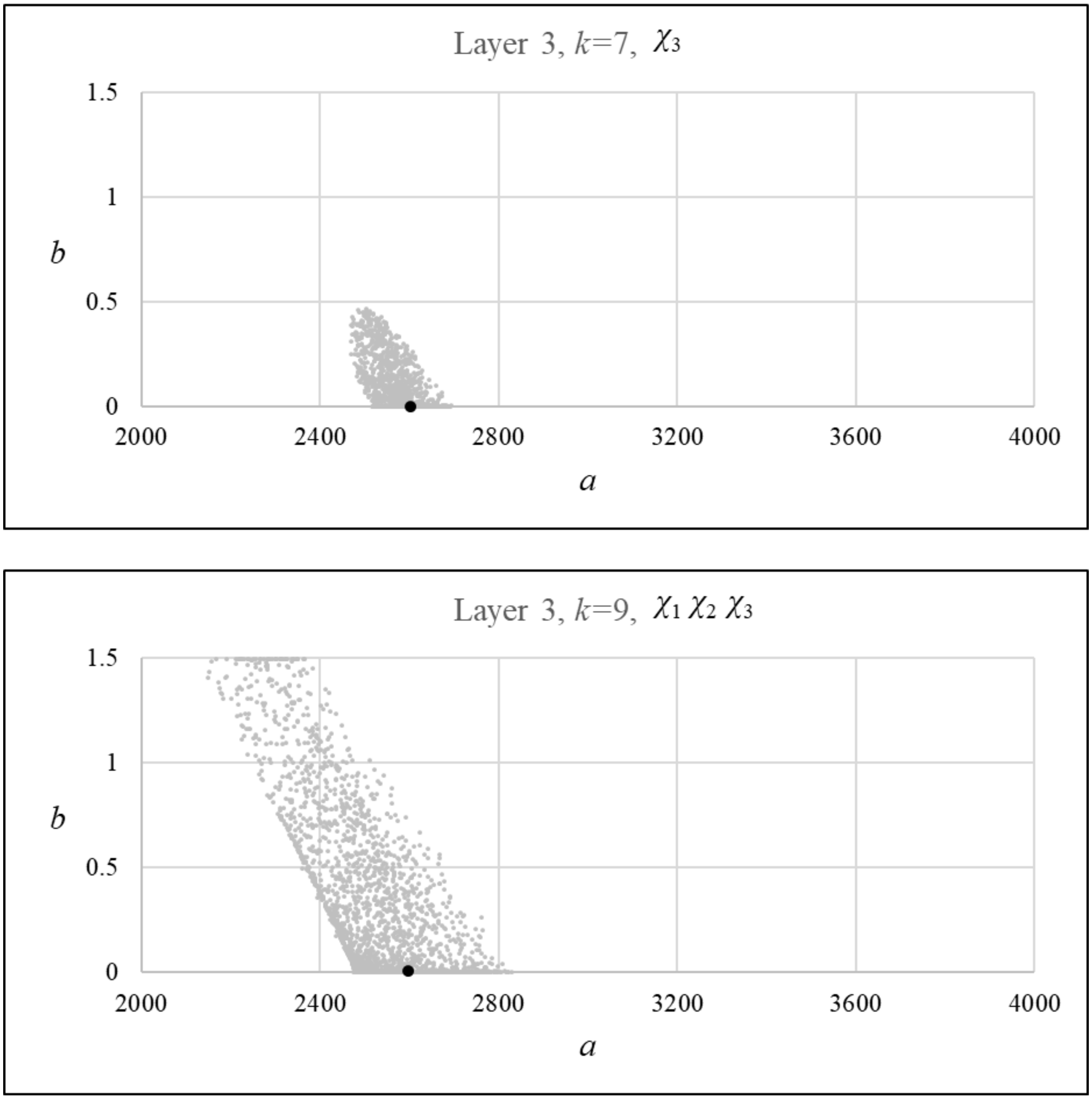

Figure 3.9: Crossplots of parameters a (ms^{-1}) versus b (s^{-1}) for the seven-parameter model, k = 7, and nine-parameter model, k = 9, for the third layer. Note: Formatting of the figures is the same as in Figure 3.7.

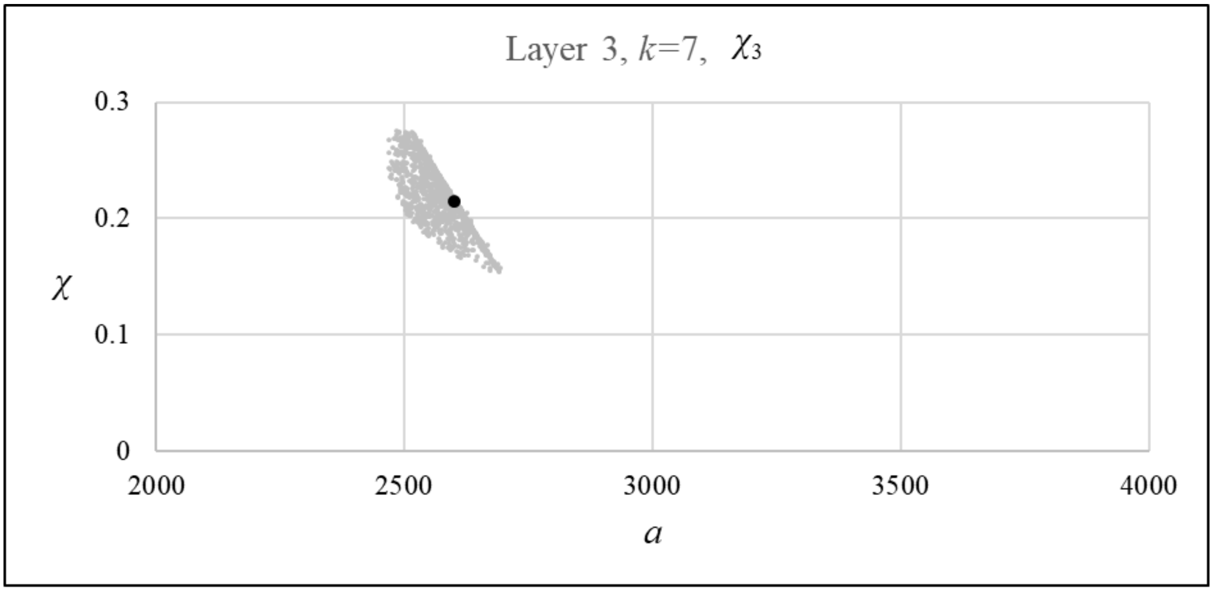

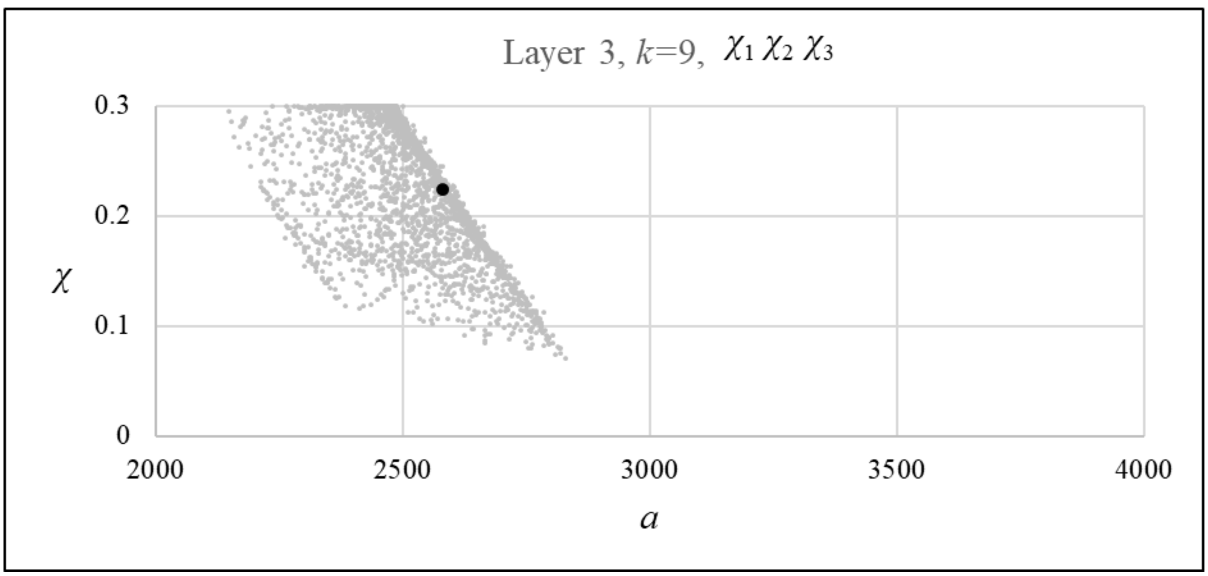

Figure 3.10: Crossplots of parameters a (ms^{-1}) versus χ for the seven-parameter model, k = 7, and nine-parameter model, k = 9, for the third layer. Note: Formatting of the figures is the same as in Figure 3.7.

3.6 Conclusions

From the eight models considered, according to BIC, the model that best fits the data and has the fewest number of parameters is the seven-parameter model, with χ in the third layer.

All the models with anisotropy rank better than the isotropic model. This justifies the introduction of anisotropy in the models. Models with anisotropy in the third layer rank better than other models, indicating that anisotropy is mainly in the third layer. This is consistent with the result in Chapter 2 where the estimated parameters using the real data indicates anisotropy to be only in the third layer.

The shapes of anisotropy ellipses at the top of the third layer are nearly identical, for models with χ in the third layer. The ellipticity parameter, which is a measure of anisotropy, is very similar for these models. The consistency of this result further supports the placement of anisotropy in the third layer.

The fit of the traveltimes obtained for the best BIC model is good, even at offsets not used in the optimization.

Crossplots of parameter values have a greater spread when the number of model parameters is increased from 7 to 9, especially for values that are within the top 25% of the results. Linear trends are also observed. For a versus b there is a strong linear relationship for both models and the regression models in each case have a good fit with the parameter values. b is the rate of change of a, it is compensatory to the value of a, i.e., as a increases b decreases, and conversely, as a decreases b increases. The strong linear relationship implies that the value of b is predictable given a value for a and vice versa.

For the relationship between a and χ, the seven-parameter model shows a stronger relationship than the nine-parameter model. As the number of model parameters increases, anisotropy is introduced in more layers; hence, there are a greater number of combinations of a, b and χ that are possible that will fit the traveltime data. Thus, the spread for the nine-parameter model is greater and the fit of the regression model is not as good.

BIC enables a means to pick the best model from a set of models that fit the data and indicates the placement of anisotropy in the third layer. It provides the most empirically adequate model even though a more complex model may be a better fit to the data. It provides a satisfactory model to account for measurements and ensures that the model complexity does not surpass the accuracy of the data.

Chapter 4

Modification of the Backus average with offset weightings for a more accurate prediction of traveltimes

4.1 Collaboration

The study for this chapter was done in conjunction with Dr. David R. Dalton, under the supervision of Dr. Michael Slawinski. Deviation of ray paths from normal incidence and effects on Backus averages were considered theoretically and empirically. A paper[3] on a modified Backus average was submitted to the arXiv repository with Dr. Dalton as co-author.

For numerical solutions, computations were performed by Dr. Dalton in Wolfram Mathematica 10.0. I computed elasticity parameters and Fermat traveltimes in a layered medium and an equivalent medium, for both synthetic and real data, in Microsoft Excel (Version 2311). This study only appears in this thesis.

4.2 Introduction

The Backus average, Backus (1962), can be used to model a finely stratified medium as a single homogeneous medium. According to its original formulation, the "standard Backus

---

[1] On Backus average for oblique incidence
https://doi.org/10.48550/arXiv.1601.02966

average” is obtained for parallel layers by taking an average along the line perpendicular to these layers, as shown in Section 1.2.5, Figure 1.4. The Backus average can be estimated from signals that are propagating through horizontal layers obliquely instead of vertically. To do so, adjustments are required. These adjustments which are achieved by applying a weighted average, are the essence of this study.

As mentioned by Liner and Fei (2007), the progressive development of the Backus averaging has been active for a long time, since around the 1950s (Postma, 1955), with the foundational paper by Backus appearing in 1962. Subsequently, further developments have occurred, as described by Kumar (2013), Schoenberg and Muir (1989), Schoenberg and Douma (1988), Liner and Fei, (2006), and many others.

There is a considerable amount of literature on Backus averaging. Schoenberg and Douma (1988) and Schoenberg and Muir (1989) model fractures in a Backus equivalent medium. Sams and Williamson (1994) look at Backus averaging to correct for differences between traveltimes from sonic to seismic frequencies. Liner and Fei (2007) propose a dimensionless number they call the Backus number, B, to determine the averaging length that is “correct” for a given frequency and purpose. Tiwary et al. (2009) examine three different methods for upscaling elastic-wave velocities: simple averaging, Backus averaging, and the pair correlation function method. Danek and Slawinski (2016) use a repetitive shale-sandstone model to examine Backus averaging by perturbing the model with random errors and analysing the effect of these perturbations on the parameters of the transversely isotropic medium and their effect on the relation between layer thicknesses and wavelengths. Bos et al. (2017) examine assumptions and approximations of the Backus formulation and extend it to generally anisotropic layers. Dalton et al. (2019) look at the applicability of the Backus average to guided-wave-dispersion modelling and consider the application of the Backus average to quasi-Rayleigh and Love wave dispersion curves measured across a stack of horizontal layers, and find there is good agreement only for thin layers or low frequencies. Maalouf et al. (2020) examine the effect of spatial averaging that is inherent to borehole acoustic tools on the Backus Average.

While there is much literature on Backus averaging, as far as I am aware, no work has been reported in the available literature that specifically considers non-vertical raypaths in computing the Backus average. The nearest article is by Lindsay and van Koughnet (2001), where they consider both vertical and non-vertical raypaths and use Backus averaging to upscale log measurements to seismic wavelengths for the purpose of generating 1-D offset synthetic seismograms. To correct for non-vertical raypaths, they adjust the size of the Backus averaging operator based on the seismic bandwidth, average velocity, depth and source-receiver offset. This modulation of the operator is performed at each depth sample and at each offset (which, as described by them, can be a very computer-intensive and time-consuming process). Whereas, I apply a weighting that considers the distance travelled in each layer, with the weight corresponding to the source-receiver offset for the purpose of correcting traveltimes.

In this chapter, the validity of the Backus average, whose weights are layer thicknesses, is shown to be limited to waves whose incidence is nearly vertical. The accuracy of this average decreases when the propagation of a wave is non-vertical, e.g., with an increase in source-receiver offsets. However, if the weighting is adjusted by the distance travelled by a signal in each layer, a modified average can be obtained that results in a more accurate prediction of traveltimes through these layers. The Backus average is adapted in this study to obtain more accurate traveltimes for obliquely propagating waves by applying a weighting that considers the distance travelled in each layer, with the weight corresponding to the source-receiver offset. I present here real data that are used to verify and demonstrate that such an adjustment produces a better Backus average.

4.3 Theory

According to Backus (1962), the propagation of "long seismic waves" in an elastic medium, whose axis of symmetry is vertical, and which is finely layered, horizontally stratified, and isotropic or transversely isotropic, can be averaged so that the medium can be replaced by an equivalent, but less "wildly varying" medium. The same may be applied to a Hookean solid, comprised of a series of parallel layers whose thicknesses are much smaller than the wavelength of the propagating seismic wave (Slawinski, 2020b).

As described in Section 1.2.5, and as per Backus (1962), the average of function $f(x_3)$ of "length" l' is given by the equation,

$$\overline{f}(x_3) = \int_{-\infty}^{\infty} w(\xi - x_3) f(\xi)\, \mathrm{d}\xi, \tag{4.1}$$

where $w(x_3)$ is a weighting function, x_3 is along the direction perpendicular to the layering in a Cartesian co-ordinate system. As explained in Section 1.2.5, l' does not appear in equation (4.1), as it is defined by the properties of the weighting function, $w(x_3)$, in the equation. I use a boxcar as the weighting function for the examples in this chapter. The averaging is performed along the length of the boxcar, and the weights are the thicknesses of the layers. Layered media comprised of individual isotropic or anisotropic layers are, thus, upscaled by the Backus average to a single layer. The symmetry of the media is maintained for all layer symmetries except for isotropic layers which result in a transversely isotropic "equivalent medium" (Slawinski, 2020b). As shown by Backus (1962) and further explained by Slawinski (2020b), if each individual layer is described by the density-scaled elasticity parameters c_{1111} and c_{2323}, the corresponding resultant parameters of the single layer or transversely isotropic equivalent medium are given by equations 4.2 to 4.7 (same as equations 1.9 to 1.14, in Section 1.2.4), which are algebraic calculations of averages of the elastic coefficients of the original medium:

$$c_{1111}^{\overline{\mathrm{TI}}} = \overline{\left(\frac{c_{1111} - 2c_{2323}}{c_{1111}}\right)}^{2} \overline{\left(\frac{1}{c_{1111}}\right)}^{-1} + \overline{\left(\frac{4(c_{1111} - c_{2323})c_{2323}}{c_{1111}}\right)}, \tag{4.2}$$

$$c_{1122}^{\overline{\mathrm{TI}}} = \overline{\left(\frac{c_{1111} - 2c_{2323}}{c_{1111}}\right)}^{2} \overline{\left(\frac{1}{c_{1111}}\right)}^{-1} + \overline{\left(\frac{2(c_{1111} - c_{2323})c_{2323}}{c_{1111}}\right)}, \tag{4.3}$$

$$c_{1133}^{\overline{\mathrm{TI}}} = \overline{\left(\frac{c_{1111} - 2c_{2323}}{c_{1111}}\right)}^{2} \overline{\left(\frac{1}{c_{1111}}\right)}^{-1}, \tag{4.4}$$

$$c_{1212}^{\overline{\mathrm{TI}}} = \overline{c_{2323}}\,, \tag{4.5}$$

$$c_{2323}^{\overline{\mathrm{TI}}} = \overline{\left(\frac{1}{c_{2323}}\right)}^{-1}, \tag{4.6}$$

$$c_{3333}^{\overline{\mathrm{TI}}} = \overline{\left(\frac{1}{c_{1111}}\right)}^{-1}, \tag{4.7}$$

where the bar indicates an average.

The Backus (1962) formulation is reviewed by Slawinski (2020b) and Bos et al. (2017), where formulations for generally anisotropic, monoclinic, and orthotropic thin layers are also derived. Bos et al. (2017) examine assumptions and approximations underlying the Backus (1962) formulation, which is derived by expressing rapidly varying stresses and strains in terms of products of algebraic combinations of rapidly varying elasticity parameters with slowly varying stresses and strains. The only mathematical approximation in the formulation is that the average of a product of a rapidly varying function and a slowly varying function is approximately equal to the product of the averages of the two functions.

4.3.1 Ten-layer synthetic model

To demonstrate the averaging described above, I present a ten-layer case, similar to Brisco (2014) and Slawinski (2020b), as illustrated in Figure 4.1, with elasticity parameters as listed in Table 4.1. The stack is made up of ten isotropic horizontal layers, each with a thickness of 100 metres. The Fermat traveltime through each layer, for vertical incidence, is simply the thickness of the layer divided by the velocity of the layer. For example, for layer 1 the Fermat traveltime is 100 m/3250 ms^{-1} = 30.77 ms. Fermat times for the layers are shown in Table 4.1. The Fermat traveltime through the entire stack is 229.46 ms, it is obtained by summing the traveltimes for each layer.

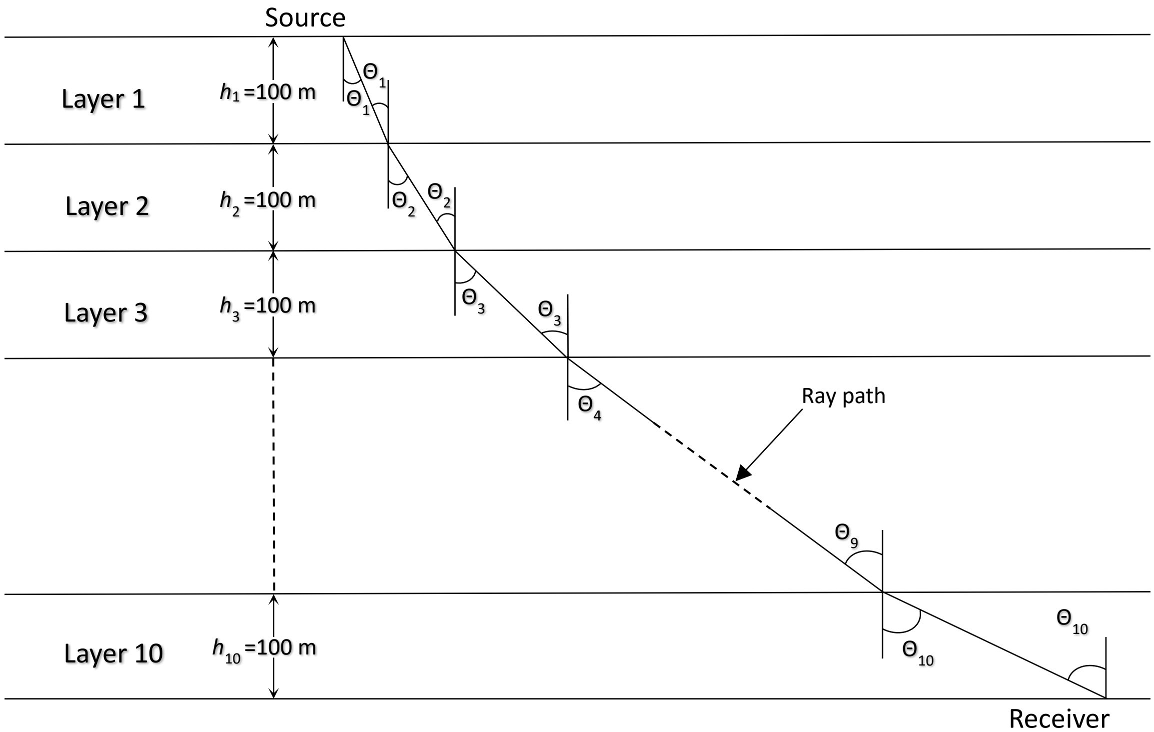

Figure 4.1: Stack of ten, 100 m thick, isotropic horizontal layers. Θ_n denotes the refraction and incidence angles in layers $n = 1\ldots10$. Θ_1 is the "take-off angle". h_n ($n = 1\ldots10$), is the height (or thickness) of each layer.

To calculate the standard Backus parameters equations (4.2) to (4.7) are used; then, the equivalent density-scaled elasticity parameters for the ten layers, or the equivalent medium, as calculated in Appendix E, are

$$c_{1111}^{\overline{\mathrm{TI}}} = 18.84,\ c_{1133}^{\overline{\mathrm{TI}}} = 10.96,\ c_{1212}^{\overline{\mathrm{TI}}} = 3.99,\ c_{2323}^{\overline{\mathrm{TI}}} = 3.38 \text{ and } c_{3333}^{\overline{\mathrm{TI}}} = 18.43,$$

with units of $10^6\ \mathrm{m^2s^{-2}}$.

Table 4.1: P-wave velocities, v_p, S-wave velocities, v_s, density-scaled elasticity parameters, c_{1111}, c_{2323}, and Fermat traveltimes for a stack of ten, 100 m thick, isotropic layers. The Fermat traveltime to the bottom of the stack is 229.46 ms, obtained by summing the traveltimes for each layer. (Modified from Slawinski, 2020b)

Layer	v_P ($\mathrm{kms^{-1}}$)	v_S ($\mathrm{kms^{-1}}$)	c_{1111} ($10^6\ \mathrm{m^2s^{-2}}$)	c_{2323} ($10^6\ \mathrm{m^2s^{-2}}$)	Fermat traveltime (10^{-3} s)
1	3.25	1.42	10.56	2.02	30.77
2	4.53	2.11	20.52	4.45	22.08
3	5.58	1.70	31.14	2.89	17.92
4	3.85	1.62	14.82	2.62	25.97
5	5.67	1.71	32.15	2.92	17.64
6	4.00	1.60	16.00	2.56	25.00
7	4.05	2.52	16.40	6.35	24.69
8	4.25	2.08	18.06	4.33	23.53
9	5.61	2.83	31.47	8.01	17.83
10	4.16	1.94	17.31	3.76	24.04
				Traveltime sum	229.46

The thickness-weighted arithmetic average equation, the derivation of which is shown in Appendix E, can also be used to obtain the result above.

$$\bar{f}(Z/2) = \frac{1}{Z}\sum_{i=1}^{n} h_i f_i \,, \tag{4.8}$$

where $Z = \sum h_i$, is the total height, and $Z/2$ is the mid-point. For layers of equal thickness, i.e., h_i is constant over all layers, this becomes

$$\bar{f}(Z/2) = \frac{1}{n}\sum_{i=1}^{n} f_i \,. \tag{4.9}$$

As an example, let us consider one of the equivalent medium parameters. Recall equation (4.5), $c_{1212}^{\overline{\mathrm{TI}}} = \overline{c_{2323}}$. Since, in this case, the layers are of equal thickness, it becomes

$$c_{1212}^{\overline{\mathrm{TI}}} = \frac{1}{n}\sum_{i=1}^{n}(c_{2323})_i\,, \tag{4.10}$$

where n is the number of layers.

If the layers are of different thicknesses, the equation is

$$c_{1212}^{\overline{\mathrm{TI}}} = \frac{\sum_{i=1}^{n} h_i (c_{2323})_i}{\sum_{j=1}^{n} h_j}\,, \tag{4.11}$$

where h_i is the thickness of the ith layer. In terms of weighting, considering that the thickness, or height, h_i, of each layer is 100 m, then each layer, in this case, can be considered to have an equal weighting of 0.1 for vertical incidence.

The vertical *P*-wave traveltime through the equivalent transversely isotropic medium, with the Backus Parameters as calculated above for a medium with 10 layers, each of constant thickness of 100 m, is 232.91 ms (calculations are shown in Appendix E). This is 3.45 ms higher than the Fermat traveltime of 229.46 ms from above. As expected, since the equivalent medium parameters are averaged, they give a less accurate traveltime than the Fermat traveltime of 229.46 ms.

Instead of weighting by the thickness of each layer, the traveltime in each layer can be used for the weighting. The traveltime for each layer is different depending on the velocity in that layer even though each layer is of the same thickness. In equation (4.11), instead of thickness in the *i*th layer, h_i can represent the traveltime in the *i*th layer. Using the traveltime for weighting, the *P*-wave traveltime, for vertical incidence, through the equivalent transversely isotropic medium is 239.77 ms, as shown in Appendix E. This is higher by 10.31 ms compared to the Fermat traveltime of 229.46 ms. Weighting by traveltime gives a less accurate result than using the thickness as weighting.

4.3.2 Slanted travel path: Fixed takeoff angle of 30°

Table 4.2 shows the *P*-wave speeds, angles of incidence, horizontal distances, and Fermat traveltimes for a signal travelling through a stack of ten isotropic layers for a *P*-wave signal whose takeoff angle, with respect to the vertical, is 30° or $\pi/6$. Starting at the top of Layer 1, given the takeoff angle and *P*-wave speed for each layer, Snell's Law is applied to obtain the subsequent angles of incidence, angles of refraction, the horizontal distance and Fermat traveltime for each layer. Figure 4.1 is a sketch of the scenario. Summing the values for the horizontal distances and Fermat traveltimes, the signal is seen to arrive at the bottom of the stack with a Fermat traveltime of 330.52 ms at a horizontal distance of 1072.53 m.

For the equivalent medium with a thickness of 1000 m and Backus parameters as calculated in Section 4.3.1, the ray angle, Θ, is 47.00° for a horizontal distance of 1072.53 m, is given by $\tan^{-1}$(horizontal distance/thickness). Deriving the ray velocity, *V*, from the ray angle as described in Appendix E, a traveltime of 343.82 ms is obtained. This is 13.30 ms higher than the Fermat traveltime.

Table 4.2: *P*-wave velocities, v_p, angles of incidence, Θ, horizontal distances, x, and Fermat traveltimes for a signal travelling through a stack of ten isotropic layers with a takeoff angle of 30°. The bottom of the stack is reached at a horizontal distance of 1072.53 m, with a Fermat traveltime of 330.52 ms.

Layer	v_p (kms^{-1})	Θ (deg)	x (m)	Fermat traveltime (10^{-3} s)
1	3.25	30.00	57.74	35.53
2	4.53	44.18	97.18	30.78
3	5.58	59.14	167.38	34.94
4	3.85	36.32	73.51	32.24
5	5.67	60.73	178.40	36.07
6	4.00	37.98	78.07	31.72
7	4.05	38.54	79.66	31.57
8	4.25	40.83	86.42	31.10
9	5.61	59.66	170.88	35.29
10	4.16	39.79	83.29	31.28
		Sums	1072.53	330.52

The Backus average can be weighted by the distance travelled in each layer. The averaging weight, w_i , for each layer is obtained by dividing the distance travelled in a particular layer by the total distance travelled, i.e., $w_i = d_i/\sum_{j=1}^{10} d_j$. In this case, in the example shown in Section 4.3.1, in equation (4.11), h_i, the vertical thickness of the *i*th layer, is replaced by d_i which is the distance travelled in the *i*th layer to get equation (4.12):

$$c_{1212}^{\overline{\mathrm{TI}}} = \frac{\sum_{i=1}^{n} d_i (c_{2323})_i}{\sum_{j=1}^{n} d_j} . \tag{4.12}$$

The distance-weighted equivalent elasticity parameters, or slant-distance-weighted Backus average medium elasticity parameters, as calculated in Appendix E, are:

$c_{1111}^{\overline{\mathrm{TI}}} = 20.13$, $c_{1133}^{\overline{\mathrm{TI}}} = 12.06$, $c_{1212}^{\overline{\mathrm{TI}}} = 4.10$, $c_{2323}^{\overline{\mathrm{TI}}} = 3.45$ and $c_{3333}^{\overline{\mathrm{TI}}} = 19.76$, with units of 10^6 m^{2}s^{-2}.

The distance, d_i , travelled by the P-wave in each layer and the corresponding averaging weights are shown in Table 4.3. The traveltime is computed to be 332.36 ms. Compared to the Fermat traveltime of 330.52 ms, this is higher by only 1.84 ms. It is an order of magnitude more accurate than the traveltime of 343.82 ms obtained using the standard Backus average, where the average is considered in a nearly vertical line.

Table 4.3: Distances, d_i , in metres, travelled by the P-wave in each layer, and the corresponding averaging weights, for a takeoff angle of 30°.

Layer	d_i	w_i
1	115.47	0.0773
2	139.44	0.0934
3	194.98	0.1305
4	124.11	0.0831
5	204.52	0.1369
6	126.87	0.0849
7	127.85	0.0856
8	132.17	0.0885
9	197.99	0.1326
10	130.14	0.0871

4.3.3 Extreme slanted travel path

Considering a horizontal distance of 7000 m, which can be regarded as an extreme distance, using the same ten-layer model as in the previous sections, the takeoff angle is 34.97° giving a ray angle in the equivalent medium of 81.87°, which is an extremely slanted travel path compared to the earlier example where the ray angle was 47.00°.

The slant-distance-weighted Backus average medium elasticity parameters, as shown in Appendix E, work out to be:

$$c_{1111}^{\overline{\mathrm{TI}}} = 27.73,\ c_{1133}^{\overline{\mathrm{TI}}} = 21.04,\ c_{1212}^{\overline{\mathrm{TI}}} = 3.52,\ c_{2323}^{\overline{\mathrm{TI}}} = 3.16 \ \text{ and } \ c_{3333}^{\overline{\mathrm{TI}}} = 28.08,$$

with units of $10^6\ \mathrm{m^2 s^{-2}}$.

The distance, d_i , travelled by the *P*-wave in each layer and the corresponding averaging weights are shown in Table 4.4. The Fermat traveltime is 1364.97 ms. The thickness-weighted Backus average medium has the same elasticity parameters as in the previous section and yields a corresponding traveltime of 1631.27 ms, which is higher by 266.30 ms.

The corresponding traveltime, using the slant-distance-weighted Backus average medium elasticity parameters, shown above, is 1343.10 ms which compared to the Fermat time is lower by 21.87 ms. Once again, the slant-distance-weighting performs better than the thickness weighting.

Table 4.4: Extremely slanted travel path. Distances, di, in metres, travelled by the P-wave in each layer, and the corresponding averaging weights, for a horizontal distance set at 7000 m.

Layer	d_i	w_i
1	122.03	0.0167
2	166.22	0.0228
3	560.13	0.0767
4	136.19	0.0186
5	5056.39	0.6921
6	141.07	0.0193
7	142.86	0.0196
8	151.03	0.0207
9	683.03	0.0935
10	147.14	0.0201

4.4 Example using real data

To illustrate further and to verify that, indeed, a better Backus average is obtained if the average is modified by applying a weighting that is adjusted by the distance travelled by a signal in each layer, I present a real data example. The real data are from the same offshore Newfoundland well as described in Section 1.3. The data consist of a sonic log, with 15631 samples, from a depth range of 1383 m to 2978 m, a length of 1595 m. The compressional sonic log is shown in Figure 1.9, Section 1.3.2.1. Each sample can be considered to represent a single layer. Table 4.5 gives layer thicknesses, P-wave speeds, and S-wave speeds for the first ten and last ten layers. c_{1111} and c_{2323}, which are the layer density-scaled elasticity parameters, are obtained by taking the squares of the P-wave velocities and S-wave velocities, respectively.

The Fermat traveltime through these layers, for vertical incidence, obtained by summing the traveltimes for each layer is 510.2 ms. The equivalent density-scaled elasticity parameters, obtained by taking the standard Backus average weighted by layer thickness of these layers, as in equation (4.12), are:

$$c_{1111}^{\overline{\mathrm{TI}}} = 10.75,\ c_{1133}^{\overline{\mathrm{TI}}} = 4.10\,,\ c_{1212}^{\overline{\mathrm{TI}}} = 3.29\,,\ c_{2323}^{\overline{\mathrm{TI}}} = 2.42 \quad \text{and} \quad c_{3333}^{\overline{\mathrm{TI}}} = 9.46,$$

with units of $10^6\ \mathrm{m^2 s^{-2}}$. The *P*-wave traveltime through the equivalent transversely isotropic medium with these parameters is 518.5 ms. Compared to the Fermat traveltime of 510.2 ms, it is higher by 8.3 ms.

Considering a takeoff angle of 18.3° and weighting the average by the distance travelled in each layer, as in equation (4.12), the equivalent elasticity parameters are:

$$c_{1111}^{\overline{\mathrm{TI}}} = 11.05\,,\ c_{1133}^{\overline{\mathrm{TI}}} = 4.14,\ c_{1212}^{\overline{\mathrm{TI}}} = 3.41\,,\ c_{2323}^{\overline{\mathrm{TI}}} = 2.49 \quad \text{and} \quad c_{3333}^{\overline{\mathrm{TI}}} = 9.67.$$

The Fermat traveltime is 581.2 ms, the thickness-weighted Backus average medium traveltime is 597.6 ms, which compared to the Fermat traveltime is higher by 16.4 ms. The slant-weighted Backus average medium traveltime is 591.1 ms, which is higher by 9.9 ms compared to the Fermat traveltime. As seen, the slant-distance weighting gives a better traveltime than the thickness weighting.

Table 4.5: Layer thicknesses, h, P-wave, v_p, and S-wave, v_s, velocities for the first ten and last ten layers.

Layer	h (m)	v_p (ms^{-1})	v_s (ms^{-1})	Fermat traveltime (s)
1	0.097	2131.23	1017.06	0.046
2	0.097	2165.30	1019.65	0.045
3	0.097	2230.32	1029.47	0.043
4	0.097	2320.83	1039.11	0.042
5	0.097	2409.92	1050.14	0.040
6	0.097	2463.18	1067.63	0.039
7	0.097	2496.51	1081.11	0.039
8	0.097	2505.24	1088.57	0.039
9	0.097	2486.60	1093.83	0.039
10	0.097	2465.52	1098.30	0.039
.	.	.	.	.
.	.	.	.	.
.	.	.	.	.
15622	0.106	3824.09	2200.10	0.028
15623	0.106	3823.88	2200.03	0.028
15624	0.106	3823.43	2199.99	0.028
15625	0.106	3823.07	2199.95	0.028
15626	0.106	3823.03	2199.91	0.028
15627	0.106	3823.03	2199.87	0.028
15628	0.106	3823.03	2199.84	0.028
15629	0.106	3823.03	2199.82	0.028
15630	0.106	3823.03	2199.81	0.028
15631	0.106	3823.03	2199.81	0.028

4.5 Discussion

The objective of this chapter is to modify the Backus average to account for non-vertical raypaths through a multi-layered medium. The approach is to take the original formulation and modify it by applying weightings based on the distance travelled in the layers for a particular offset or take-off angle, i.e., for that particular raypath. The Backus average considers anisotropy due to thin layering and an effective medium is computed, with new elasticity coefficients, in this case, for each raypath being considered.

I use well log data for the Backus averaging. The well log data are sampled at approximately 0.1 m intervals giving rise to very thin layers compared to seismic wavelengths. The well log data are from the same well in which the VSP data were acquired and used in Chapters 2 and 3. Since the well logs were available, I took the opportunity to investigate Backus averaging. However, the two approaches to indicate anisotropy are different. With the WVSP I use traveltimes, from sources at various offsets to receivers at a depth range of 1980 m to 2020 m, to estimate the ellipticity parameter, χ, as an indication of the anisotropy. For the Backus average, in this chapter, I use the sonic log and layer-induced anisotropy from thin layering and correct for non-vertical traveltimes, I do not quantify anisotropy. The two measurements are different, and the anisotropy is not directly comparable.

The Backus average as originally formulated assumes vertical or near-vertical incidence, i.e., it is obtained by considering an average along a line perpendicular, or nearly perpendicular, to parallel layers. Where the travel path of a signal may be slanted or oblique, such an average does not result in accurate traveltimes.

Today, as compared to when the Backus average was formulated in 1962, it is much more common to have deviated wells, conduct cross-well tomography experiments, and acquire seismic data with large source-receiver offsets, all of which give rise to oblique ray paths. Thus, in applications where averages are sought, it is increasingly necessary to find techniques that can provide better estimates. One way to obtain a better Backus average is to apply weighting that takes into account the distance travelled in each layer, especially when the ray path is oblique. For oblique ray paths, since the distance travelled in each layer is a function of Snell's law, the weights need to be modified by the distance travelled in each layer as a function of offset. As shown, doing so results in significantly more accurate traveltimes.

The modified equivalent medium is defined by its elasticity parameters, which are functions of the obliqueness of rays within each layer. This gives rise to an interesting situation. It means that the equivalent-medium parameters are different for the *qP* waves, for the *qSV* waves and for the *qSH* waves, where *q* denotes quasi. At first glance, this may seem odd. However, since we are considering a Hookean solid, which is a mathematical entity and not the physical world, such a consideration is not necessarily contradictory.

In every case, except for the slant-distance weighted equivalent medium for the extreme oblique model, the traveltime in the equivalent medium is greater than its Fermat counterpart through the sequence of layers. This may be as a consequence of averaging, since averaging causes a loss of fidelity, i.e., a loss in detail.

A fundamental question may be whether the Fermat traveltime is an appropriate criterion to consider the accuracy of the Backus average. Let us consider a stack of thin layers that contains a layer with a wave speed such that waves propagate much faster in it than in all others. As per Fermat's principle, the distance travelled by a signal within this layer is much greater than in any other layer. This can be expressed by the ratio of the distance travelled in a given layer divided by its thickness. Such an effect is not accommodated by the standard Backus average, since it is offset-dependent and the average is not, but it is accommodated by the modified Backus average. For long-wavelength signals, such a property of a single layer may be negligible. Such issues may be better addressed by considering a full-waveform forward model, and, perhaps, even a laboratory experimental set-up.

As can be seen in Table 4.2, layer 5 has the largest v_p compared to the other layers. The ray angle with respect to the vertical in this layer approaches the critical angle of 90°, as the takeoff angle approaches the maximum takeoff angle. The distance travelled in this layer is much greater than the distance travelled in other layers as shown in Tables 4.3 and 4.4.

The discrepancy between the traveltimes in the layered and equivalent media increases with the source-receiver offset. Making the propagation speed a function of the wavelength would not accommodate the traveltime discrepancy due to offset. Although the modified Backus average enables a better estimation, in the limit, for a wave propagating horizontally through a stack of horizontal layers it is not valid, because of its underlying assumption of a load on the top and bottom only, i.e., it assumes normal stress.

4.6 Conclusions

As shown, the accuracy and validity of the standard Backus average is limited to waves whose incidence is vertical, or nearly vertical. This is because its weights are based on layer thicknesses. When the obliqueness of the ray path increases, the accuracy of the average decreases.

Adjusting the standard Backus average, with a weighted average that considers the distance travelled in each layer by a signal, a modified Backus average can be obtained that is more accurate. Applying such a modified Backus average, where the weights correspond to the source-receiver offsets, provides a means for obtaining more accurate traveltimes for obliquely propagating waves.

Seismic data are often calibrated with sonic logs. Because of the difference in frequencies between the two, well logs need to be upscaled to seismic frequencies. The upscaling is often done by applying Backus averaging. For deviated wells and well trajectories that may be tortuous, i.e., with twists and turns, ray paths may be non-vertical. It is thus useful to have a modified Backus average that accounts for non-vertical ray paths and provides more accurate traveltimes.

Chapter 5

Conclusions and future work

The research in Chapter 2 aims to estimate anisotropy and inhomogeneity parameters from traveltimes using a new optimization approach with minimal constraints. With synthetic data, the parameters are successfully estimated. However, it is found that the noise threshold is quite low, at a level between 0.001% and 0.01% of the traveltimes.

Results using the real data show the first layer, which is the thickest layer, to be inhomogeneous and isotropic, the second layer to be homogeneous and isotropic, and the anisotropy to exist only in the third layer with χ, the anisotropy parameter, at a value of 0.216, a, which is the vertical velocity, at 2597 ms, and the gradient, b, effectively zero. In a predominantly shale environment, such as here, where only the first few metres are composed of unconsolidated material, the rest being shales, it would be expected that anisotropy would be detected in all three layers due to the intrinsic anisotropy property of shales.

Although the data are sensitive to noise, the noise threshold is low and can affect the results, examination of the real data shows that it has little noise content. Traveltimes computed from estimated parameters using the real data compared to measured traveltimes show a cyclical pattern indicative of under-sampling, which may be why anisotropy is only detected in the third layer. The main reason that may cause this is that the receivers for the walkaway VSP are only in the third layer, and the data set may thus not fully represent the anisotropy in all three layers. To have complete information on the anisotropy present in the medium, receivers would have to be placed in all layers. Future work may entail, if possible, obtaining a walkaway VSP data set with receivers in all layers.

Another factor that may improve the estimation, using the real data, of the anisotropy in the medium would be to more accurately represent the Earth. This could be done by increasing the number of layers to more than three, and hence, increasing the number of parameters to represent the medium. In this study, I limit the number of parameters to nine, i.e., three layers with three parameters in each layer. The number of layers in the models is restricted to a few layers based on macro-layering interpreted from the ZVSP data. Each macro-layer has layers within with varied properties and could be split into more layers. Doing so may provide a better fit to the data, and be more physically representative of the subsurface, thus providing a better estimate of the parameters. However, increasing the number of layers, and hence, the number of parameters, increases significantly the number of parameter combinations that are possible and increases the computational capacity required. It may also require a better search algorithm than used in this study. Increasing the number of layers was not possible for this study due to the limited computational capacity and time constraints but may be a consideration for future work.

The estimation of parameters from traveltime data is a complex problem. Being able to estimate reasonable parameters is useful and has practical value. It allows, for example, better design of seismic acquisition, improved processing of seismic data and, hence, better seismic imaging. The adaptive Nelder-Mead algorithm, as the search engine, was found to be computationally intense, especially with the use of a multi-start approach. In future work, a better algorithm could be sought out and tried that may be more suited for this purpose. Further analysis of the effects of noise, errors in the data, and propagation of errors could also be undertaken.

In Chapter 3, the focus is on the use of the Bayesian Information Criterion (BIC) for the selection of a model that best represents the data, with the fewest number of parameters. Eight models are put forward. This objective was successfully achieved with BIC. BIC values show the best model to be the seven-parameter model, with anisotropy in the third layer. This agrees with and confirms the outcome in Chapter 2, in terms of the inclusion and placement of anisotropy. A more sophisticated model is not required for this data set. With more parameters, the improvement of the solution is not sufficient to justify additional parameters.

The greatest value of BIC, especially in this context, is when the data set is very large, or there are a large number of possible models that could fit the data. BIC effectively narrows the choice and provides a way to avoid overfitting. It is an efficient and cost-effective approach for large data sets with multiple possible models. Future work could be to use models that have a larger number of parameters and model layers, which was not done in this study due to computational limitations and time constraints.

The fourth chapter provides a way to attain more accurate traveltimes when using the Backus average in situations where ray paths are non-vertical. A weighting is applied that takes into consideration the distance travelled in each layer. Weightings are modified based on the offsets. This results in significantly more accurate traveltimes, especially for large offsets.

With the 30° take-off angle, i.e., an offset of 1073 m, the difference between the standard Backus average, where the average is considered for normal incidence, and the Fermat time is 13.30 ms. Applying the modified Backus average results in a traveltime difference of only 1.84 ms. With the extremely slanted travel path, where the offset is 7000 m, the difference between the standard Backus average and the Fermat time is 266.30 ms, whereas with the modified Backus average it is 21.87 ms. In both cases, the weighted average gives a better traveltime, markedly so in the extreme case.

With the real data, the difference between the standard Backus average and the Fermat time is 16.4 ms, whereas with the modified Backus average it is 9.9 ms. Again, the distance-weighted average gives a better result.

The modified Backus average has implications in many aspects of seismic and engineering applications, anywhere where data are upscaled. For example, in seismic data calibration; reservoir modelling - where such data are used to populate reservoir simulation models; seismic data processing and imaging. There is immense practical value in obtaining accurate traveltimes where a complex real Earth is simplified to an effective medium using the Backus average. A future study could look at disciplines that would benefit the most. Future studies could also be more sophisticated, for example, using many more layers and varied parameters, using full-waveform forward modelling, and even verifying results in a laboratory set-up under various conditions.

Mathematical models used to represent the medium in which the VSP data were acquired, synthetic data generated using such models, and complementing this with real data, are invaluable in providing insights into the understanding of the nature of the problem at hand, and the application of the theory before application to real data. Although the availability of real data is scarce, it is important to have some to test and validate the theoretical aspects of any study. It is also desirable to use a diversity of data, i.e., of different lithologies, and geology, to broaden the scope, and thereby, have a more comprehensive understanding of the nature of the Earth. With the advent of Artificial Intelligence (AI), in the future, as AI applications become more available, all of the above could be done with the aid of AI, perhaps much more efficiently and more in-depth.

Bibliography

H. Akaike. A new look at the statistical model identification. *IEEE Transactions on Automatic Control*, 19, 716–723, 1974.

H. Akaike. A Bayesian analysis of the minimum AIC procedure. *Annals of the Institute of Statistical Mathematics*, 30, 9–14, 1978.

H. Akaike. A Bayesian extension of the minimum AIC procedure of autoregressive model fitting. *Biometrika*, 66, 237–242, 1979.

M. Al-Chalabi, and P. L. Rosenkranz. Velocity–depth and time–depth relationships for a decompacted uplifted unit. *Geophysical Prospecting*, 50, 661-664, 2002.

C. Audet, and W. Hare. *Derivative-Free and Blackbox Optimization*. Springer, 2017.

G. E. Backus. Long-wave elastic anisotropy produced by horizontal layering. *Journal of Geophysical Research*, 67(11), 4427–4440, 1962.

A. H. Balch, and M. W. Lee. *Vertical seismic profiling: techniques, applications, and case histories.* International Human Resources Development Corporation, 1984.

M. Baudin. *Nelder-Mead User's Manual*. Scilab, 2010.

J. G. Berryman. Seismic waves in rocks with fluids and fractures. *Geophysical Journal International*, 171(2), 954–974, 2007.

L. Bos, D. R. Dalton, M. A. Slawinski, and T. Stanoev. On Backus average for generally anisotropic layers. *Journal of Elasticity*, 127(2),179–196, 2017.

C. Brisco. Anisotropy vs. inhomogeneity: Algorithm formulation, coding and modelling. *Honours Thesis, Memorial University of Newfoundland*, 2014.

J. R. Brown, and M.A. Slawinski. *On Foundations of Seismology.* World Scientific, 2017.

K. P. Burnham, and D. R. Anderson. *Model Selection and Multimodel Inference*. Springer, Second Edition, 2002.

J. Caldwell, and W. Dragoset. A brief overview of seismic air-gun arrays. *The Leading Edge (Tulsa, Okla.)*, 19(8), 898–902, 2000.

V. Červený. *Seismic ray theory*. Cambridge University Press. 2001.

C. Chapman. *Fundamentals of Seismic Wave Propagation*. Cambridge University Press, 2004

A. R. Conn, K. Scheinberg, and L. N. Vicente. *Introduction to Derivative-Free Optimization.* SIAM. 2009.

D. R. Dalton, T. B. Meehan, and Slawinski, M. A. On Backus average in modelling guided waves. *Journal of Applied Geophysics*, 170, 103815, 2019.

D. R. Dalton, and A. Kaderali. On Backus average for oblique incidence. *arXiv*,1601.02966 [physics.geo-ph], 2020.

T. Danek, and M. A. Slawinski. Bayesian inversion of VSP traveltimes for linear inhomogeneity and elliptical anisotropy. *Geophysics*, 77(6), R239–R243, 2012.

T. Danek, and M. A. Slawinski. Backus average under random perturbations of layered media. *SIAM Journal on Applied Mathematics*, 76(4), 1239–1249, 2016.

T. Danek, B. Gierlach, A. Kaderali, M. A. Slawinski, and T. Stanoev. Selecting velocity models using Bayesian Information Criterion. *Geophysical Prospecting*, 71, 811–815, 2023.

Ç. Diner, and A. Beyaz. Analytical solutions of ray-tracing equations in generalized elliptical anisotropy. *Geophysics*, 89(6), C267–C276, 2024.

M. E. Enachescu. Integrated Geophysical Study of Newfoundland Continental Margin (East Coast Canada). *Geophysics*, 52(3), 425–426, 1986.

B. J. Evans. *A handbook for seismic data acquisition in exploration.* Society of Exploration Geophysicists, 1997.

E. I. Gal'perin. *Polarization Method of Seismic Exploration* (1st ed., Vol. 1). Springer Netherlands, 1983.

F. Gao, and L. Han. Implementing the Nelder-Mead simplex algorithm with adaptive parameters. *Computational Optimization and Applications,* 51, 259–277, 2012.

B. Gierlach, and T. Danek. Inversion of velocity parameters in multilayered elliptical anisotropy medium - synthetic data example. *E3S Web of Conferences*, 66, 1017, 2018.

B. Gierlach, T. Danek, and A. Kaderali. VSP data inversion for vertical velocity gradient and elliptical anisotropy model. *E3S Web of Conferences*, 133, 1008, 2019.

A. C. Grant, K. D. McAlpine, and J. A. Wade. Offshore geology and petroleum potential of Eastern Canada. *Energy Exploration & Exploitation*, 4(1), 5–52, 1986.

B. A. Hardage. *Vertical seismic profiling* (2nd enl. ed.). Geophysical Press, 1985.

R. C. Hinds, N. L. Anderson, R. D. Kuzmiski, and B. A. Hardage. *VSP interpretive processing: theory and practice* (Vol. 3). Society of Exploration Geophysicists, 1996.

Husky Oil Operations Limited. White Rose Oilfield development application. *Centre for Newfoundland Studies*. Husky Oil, 2000.

Husky Oil Operations Limited. White Rose Oilfield development application. Vol 2. *Centre for Newfoundland Studies*. Husky Oil, 2001.

B. E. Hornby, L. M. Schwartz, and J. A. Hudson. Anisotropic effective-medium modeling of the elastic properties of shales. *Geophysics*, 59(10), 1570–1582, 1994.

A. Kaderali. Investigating anisotropy and inhomogeneity using tomographic inversion of VSP traveltimes: Validation of analytic expressions for linearly inhomogeneous elliptically anisotropic models. *Master's thesis, Memorial University of Newfoundland*, 2009.

A. Kaderali, M. Jones, and J. Howlett. White rose seismic with well data constraints: A case history. *The Leading Edge*, 26(6),742–754, 2007.

D. Kumar. Applying Backus averaging for deriving seismic anisotropy of a long-wavelength equivalent medium from well-log data. *Journal of Geophysics and Engineering*, 10(5), 055001, 2013.

R. Lindsay, and R. van Koughnet. Sequential Backus averaging: upscaling well logs to seismic wavelengths. *The Leading Edge (Tulsa, Okla.)*, 20(2), 188, 190–191, 2001.

C. L. Liner, and T. W. Fei. Layer-induced seismic anisotropy from full wave sonic logs; theory, application, and validation. *Geophysics*, 71(6), D183–D190, 2006.

C. Liner, and T. Fei. The Backus number. *The Leading Edge (Tulsa, Okla.)*, 26(4), 420–426, 2007.

S. Ling, J. Sanny, and W. Moebs. *University physics Volume 1*. OpenStax, 2016.

H. B. Lynn. The fabric, or internal structure, of rocks; the patterns of anisotropy; Part 1. *AAPG Explorer*, 39(2), 20–21, 23, 2018.

E. Maalouf, C. Torres-Verdín, and J. Li. Application of Backus average to simulate acoustic logs in thinly bedded formations. *Geophysics*, 85(3), D93–D104, 2020.

K. D. McAlpine. Mesozoic stratigraphy, sedimentary evolution, and petroleum potential of the Jeanne D'Arc Basin, Grand Banks of Newfoundland. *Geological Survey of Canada,* Vol. 89-17, 1990.

N. L. McIver. Cenozoic and Mesozoic Stratigraphy of the Nova Scotia Shelf. *Canadian Journal of Earth Sciences*, 9(1), 54–70, 1972.

J. A. Nelder, and R. Mead. A Simplex Method for Function Minimization. *The Computer Journal*, 4, 308–313, 1965.

J. Nocedal, and S. J. Wright. *Numerical optimization* (Second Edition) Springer series in operations research. Springer, 2006.

G. W. Postma. Wave propagation in a stratified medium. *Geophysics*, 20(4), 780–806, 1955.

W. H. Press, S. A. Teukolsky, W. T. Vetterling and B. P. Flannery. *Numerical Recipes, The Art of Scientific Computing*. Cambridge University Press, Third Edition. 2007.

M. B. Priestley. *Spectral Analysis and Time Series*. Academic Press, 1982.

B. Ratner. The correlation coefficient: Its values range between +1 / −1, or do they? *Journal of Targeting, Measurement and Analysis for Marketing*, 17(2), 139–142, 2009.

J. W. Rector, and M-D. Mangriotis. Vertical Seismic Profiling. In *Encyclopedia of Solid Earth Geophysics* (pp. 1507–1509). Springer Netherlands, 2011.

E. A. Robinson, and D. Clark. *Basic Geophysics*. SEG Society of Exploration Geophysicists, 2017.

Y. Rogister, and M. A. Slawinski. Analytic solution of ray-tracing equations for a linearly inhomogeneous and elliptically anisotropic velocity model. *Geophysics*, 70(5), D37–D41, 2005.

M. S. Sams, and P. R. Williamson. Backus averaging, scattering and drift. *Geophysical Prospecting*, 42(6), 541–564, 1994.

C. M. Sayers. Seismic anisotropy of shales. *Geophysical Prospecting*, 53(5), 667–676, 2005.

M. E. Schoenberg, and J. Douma. Elastic wave propagation in media with parallel fractures and aligned cracks. *Geophysical Prospecting*, 36(6), 571–590, 1988.

M. E. Schoenberg, and F. Muir. A calculus for finely layered anisotropic media. *Geophysics*, 54(5), 581–589, 1989.

G. Schwarz. Estimating the dimension of a model. *Annals of Statistics*, 6, 461–464, 1978.

R. E. Sheriff. *Encyclopedic dictionary of exploration geophysics* (3rd ed.). Society of Exploration Geophysicists, 1991.

M. A. Slawinski. *Seismic waves and rays in elastic media* (Vol. 34). Pergamon, 2003.

M. A. Slawinski. *Waves and rays in elastic continua* (Fourth Edition). World Scientific, 2020a.

M. A. Slawinski. *Waves and rays in seismology answers to unasked questions* (Third Edition). World Scientific, 2020b.

M. A. Slawinski, C. J. Wheaton, and M. Powojowski. VSP traveltime inversion for linear inhomogeneity and elliptical anisotropy. *Geophysics*, 69(2), 373–377, 2004.

M. M. Slotnick. *Lessons in Seismic Computing: A memorial to the author*. Society of Exploration Geophysicists, 1959.

W. M. Telford, L. P. Geldart, and R.E. Sheriff. *Applied Geophysics (2nd Edition)*. Cambridge University Press, 1990.

J. B. Thomas. *Introduction to Probability*. Springer New York, 1986.

L. Thomsen. Weak elastic anisotropy. *Geophysics*, 51(10), 1954–1966.

D. K. Tiwary, I. O. Bayuk, A. A. Vikhorev, and E. M. Chesnokov. Comparison of seismic upscaling methods; from sonic to seismic. *Geophysics*, 74(2), WA3–WA14, 2009.

I. Tsvankin, J. Gaiser, V. Grechka, M. van der Baan, and L. Thomsen. Seismic anisotropy in exploration and reservoir characterization; an overview. *Geophysics*, 75(5), 75A15 75A29, 2010.

L. F. Uhrig, and F. A. Van Melle. Velocity anisotropy in stratified media. *Geophysics*, 20(4), 774–779, 1955.

D. M. Vander Stoep. Velocity anisotropy measurements in wells. *Geophysics*, 31(5), 900–916, 1966.

K. W. Winkler, and W. F. Murphy. Acoustic velocity and attenuation in porous rocks. In T. J. Ahrens, ed., *Rock physics & phase relations*, 20–34: AGU, 1995.

M. H. Wright. Nelder, Mead, and the Other Simplex Method. *Documenta Mathematica · Extra Volume*, ISMP 271–276, 2012.

M. Zareba, H. Dlugosz, T. Danek, and E. Weglinska. Big-Data-Driven Machine Learning for Enhancing Spatiotemporal Air Pollution Pattern Analysis. *Atmosphere,* 14(4), 760, 2023.

R. Zhou, and A. Kaderali. Anisotropy evaluation using an array walk-away VSP. *Offshore Technology Conference*, 2006.

APPENDICES

APPENDIX A: The Nelder-Mead Algorithm

The description of the method and the algorithm are adapted from Conn et al. (2009) and Gao and Han (2012).

A.1 Description of the method

Every iteration is based on a simplex of n +1 vertices $Y = \{y^1, y^2, . . . , y^{n+1}\}$ ordered by increasing values of the function that is to be minimized, f, where n is the number of vertices of the simplex/parameters to optimize. For an iteration that is a reflection, an expansion, or a contraction (inside or outside the simplex) the worst vertex y^{n+1} is replaced by a point in the line that connects y^{n+1} and y^c,

$$y = y^c + m(y^c - y^{n+1}),\ m \in \mathbb{R},$$

where $y^c = \sum_{i=1}^{n} \frac{y^i}{n}$ is the centroid of the best n +1 vertices. The value of m indicates the type of iteration. For instance, if m = α we have a reflection, m = β an expansion, m = γ an outside contraction, and m = −γ an inside contraction, as shown in Figure A1. For implementing the standard Nelder-Mead algorithm we use, α = 1, β =2, γ = ½, δ = ½, which is consistent with Gao and Han (2012).

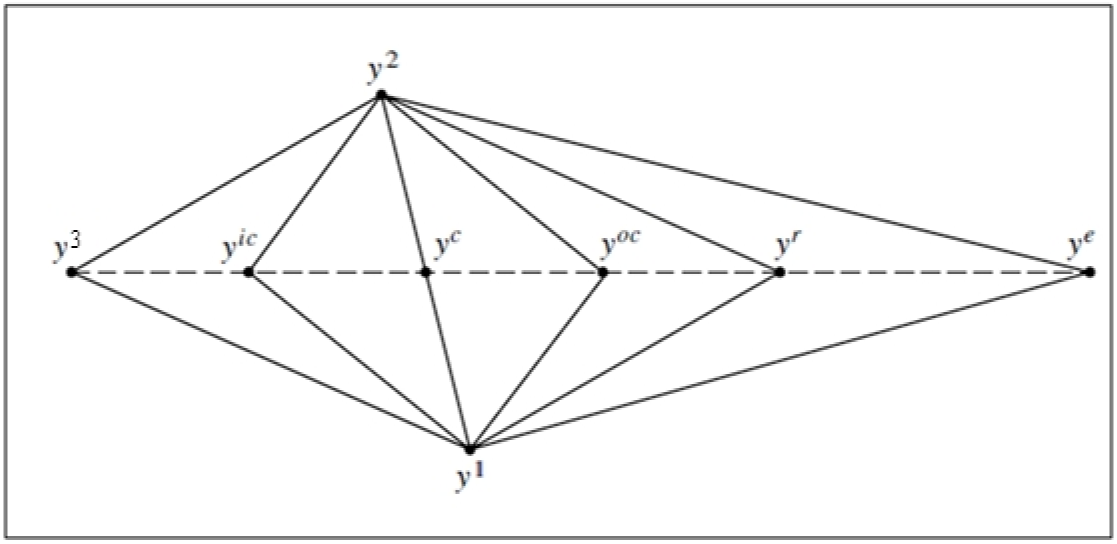

Figure A.1: Reflection (y^r), expansion (y^e), outside contraction (y^{oc}), and inside contraction (y^{ic}) of a simplex. (Adapted from Conn et al., 2009)

When a shrink is performed all the vertices in Y are thrown away except the best one y^1. Then n new vertices are computed by shrinking the simplex at y^1, i.e., by computing, for instance, $y^1 + \delta\,(y^i - y^1)$, $i = 2, \ldots, n+1$. See Figure A2. Note that the "shape" of the resulting simplices can change by being stretched or contracted, unless a shrink occurs.

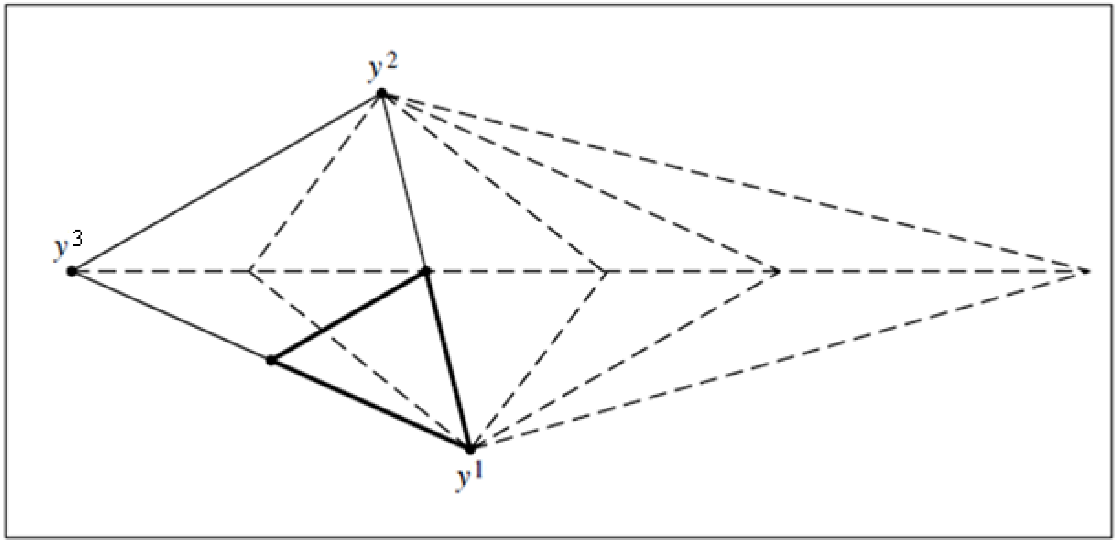

Figure A.2: Shrink of a simplex. (From Conn et al., 2009)

A.2 Algorithm

Initialization step: Choose an initial simplex of vertices $Y_1 = \{y_1^1, y_1^2, \ldots, y_1^{n+1}\}$. Evaluate f at the points in Y_1.

For $k = 1, 2, 3, \ldots$

1. Set $Y = Y_k$.

2. Order: Order the n+1 vertices of $Y = \{y^1, y^2, \ldots, y^{n+1}\}$ so that

$$f^1 = f(y^1) \le f^2 = f(y^2) \le \cdots \le f^{n+1} = f(y^{n+1}).$$

3. Reflect: Reflect the worst vertex y^{n+1} over the centroid $y^c = \sum_{i=1}^{n} \frac{y^i}{n}$ of the remaining n vertices:

$$y^r = y^c + \alpha(y^c - y^{n+1}).$$

Evaluate $f^r = f(y^r)$. If $f^1 \le f^r < f^n$, then replace y^{n+1} by the reflected point y^r and terminate the iteration: $Y_{k+1} = \{y^1, y^2, \ldots, y^n, y^r\}$.

4. Expand: If $f^r < f^1$, then calculate the expansion point

$$y^e = y^c + \beta\,(y^r - y^c)$$

and evaluate $f^e = f(y^e)$. If $f^e \leq f^r$, replace y^{n+1} by the expansion point y^e and terminate the iteration: $Y_{k+1} = \{y^1, y^2, \ldots, y^n, y^e\}$. Otherwise, replace y^{n+1} by the reflected point y^r and terminate the iteration: $Y_{k+1} = \{y^1, y^2, \ldots, y^n, y^r\}$.

5. Contract: If $f^r \geq f^n$, then a contraction is performed between the best of y^r and y^{n+1}.

(a) Outside contraction: If $f^r < f^{n+1}$, perform an outside contraction

$$y^{oc} = y^c + \gamma(y^r - y^c)$$

and evaluate $f^{oc} = f(y^{oc})$. If $f^{oc} \leq f^r$, then replace y^{n+1} by the outside contraction point y^{oc} and terminate the iteration: $Y_{k+1} = \{y^1, y^2, \ldots, y^n, y^{oc}\}$. Otherwise, perform a shrink.

(b) Inside contraction: If $f^r \geq f^{n+1}$, perform an inside contraction

$$y^{ic} = y^c - \gamma(y^r - y^c)$$

and evaluate $f^{ic} = f(y^{ic})$. If $f^{ic} < f^{n+1}$, then replace y^{n+1} by the inside contraction point y^{ic} and terminate the iteration: $Y_{k+1} = \{y^1, y^2, \ldots, y^n, y^{ic}\}$. Otherwise, perform a shrink.

6. Shrink: Evaluate f at the n points $y^1 + \delta(y^i - y^1)$, $i = 2, \ldots, n+1$, and replace $y^2, \ldots, y^{n+1}$ by these points, terminating the iteration.

The stopping criterion of the run is when the diameter of the simplex becomes smaller than a chosen tolerance $\Delta tol > 0$. In our case, the diameter of the simplex is the difference between the best and worst value of the vertices. The tolerance selected is machine precision, which is

2.2204e^{-16} (https://www.mathworks.com/help/matlab/ref/eps.html),

or if the number of iterations reaches 13,500 for the standard NM and 25,000 for the adaptive NM. The run is also stopped when the absolute difference of the diameter between the current and previous iteration is less than the machine precision.

The following number of function evaluations are performed per iteration:

1 if the iteration is a reflection,

2 if the iteration is an expansion or contraction,

n+2 if the iteration is a shrink.

A.3 Penalties

Penalties are applied when a, b, χ parameter values found during execution of the algorithm are outside the ranges shown in Table A.1. For a parameter, the parameter penalty, PP, is given by

$$\mathrm{PP} = e^{(l-x)}(l > x) + e^{(x-u)}(x > u),$$

where x is the parameter, l is the lower bound, and u is the upper bound.

When a parameter value is less than its lower bound, the first inequality is 1 and the second is 0; a penalty is applied. For example, if $a_1 = 799$, which is less than its lower bound,

$$\mathrm{PP} = e^{(800-799)}(800 > 799) + e^{(799-2000)}(799 > 2000)$$

$$= e^{(1)}(1) + e^{(-1201)}(0) = e^{(1)} \approx 2.7.$$

When the value is within its range, both inequalities are 0; no penalty is applied. For example, if $a_1 = 1000$, it is within its lower and upper bounds, and

$$\text{PP} = e^{(800-1000)}(800 > 1000) + e^{(1000-2000)}(1000 > 2000)$$

$$= e^{(-200)}(0) + e^{(-1000)}(0) = 0.$$

When the value is greater than its upper bound, the first inequality is 0 and the second is 1; a penalty is applied. For example, if $a_1 = 2001$, it is greater than its upper bound,

$$\text{PP} = e^{(800-2001)}(800 > 2001) + e^{(2001-2000)}(2001 > 2000)$$

$$= e^{(-1201)}(0) + e^{(1)}(1) = e^{(1)} \approx 2.7.$$

In the examples above, which are for illustration, the values of the ranges in Table A1 are rounded.

Table A.1: Ranges/bounds for a_i, b_i, χ_i parameters for the three-layer model, where i indicates the layer number. The ranges were chosen based on the VSP data.

i	a_i	b_i	χ_i
1	800.001 – 1999.999	0.001 – 1.499	0.001 – 0.099
2	1600.001 – 3999.999	0.001 – 1.499	0.001 – 0.199
3	2000.001 – 3999.999	0.001 – 1.499	0.001 – 0.299

A penalty is also applied for untraceable rays between source receiver pairs. A ray is untraceable when the critical angle is reached. For any untraceable ray, we apply a unit value (1), sum all untraceable rays, and apply this as a bulk penalty. We refer to this as the Offset Penalty (OP). Furthermore, we take ½ the limiting p value to calculate the traveltime, so that the RSS can be calculated, and the NM algorithm can continue.

The sum of PP and the sum of OP are added to the RSS for a total RSS. The NM algorithm minimizes this total RSS.

A.4 Example MATLAB program

The program consists of a main body and five sub-functions. The main body of the program performs the following tasks:

- reads in VSP traveltimes (INPUT_DATA.txt),
- generates random start-up values and stores in a text file (SIMPLEX_STARTUP_VALUES.txt),
- performs the optimization in parallel,
- stores outputs in a text file (FINAL_OUTPUT_VALUES.txt).

To perform these tasks, five sub-functions are included in the code. These functions serve to execute the NM algorithm through the following steps: calculate the functions for the NM, perform ray tracing through the medium layers, calculate traveltimes along the rays, and calculate parameter penalties. Comments are included to describe lines in the code.

The MATLAB code, in this example, is prepared for execution as it appears. The only inputs required are the traveltimes associated with source and receiver positions and their offsets, see “INPUT_DATA.txt”. Along with the code a sample of the files generated are included. The file named “SIMPLEX_STARTUP_VALUES.txt” contains the start-up simplices to be used as input for the NM algorithm. The file named “FINAL_OUTPUT_VALUES.txt” contains the best a, b, χ values for the simplices at the termination of the program.

Consistent with the algorithm description above, we use the following notation:

Reflection: α; expansion: β; outside contraction: γ; inside contraction: -γ; shrink: δ.

We set the coefficients as follows:

Standard NM { α, β, γ, δ } = {1, 2, 1/2, 1/2},

Adaptive NM { α, β, γ, δ } = {1, 1+2/n, 0.75 - 1/(2n), 1-1/n }.

In this example, we use real traveltimes with a maximum source offset of up to 4000 m. We use a three-layer model to find the best a, b, χ values by reducing the residual sum of squares (RSS). We set the number of parameters to optimize as $n = 9$, i.e., a, b, χ parameters in each of the three layers. We perform a multi-start using four parallel “workers” with four simplices of 10 vertices each, giving a total of 40 vertices in this case. We set the ranges, or bounds, for each of the parameters as shown in Table A.1, with penalties being invoked when the parameters lie outside the bounds.

Input/Output Files

1. INPUT_DATA.txt

This file has traveltimes and source offsets for each receiver. Input to MATLAB is a [695x4] matrix, where each row corresponds to the index in the following table formatted as follows: Column {1,2,3,4} = {Index, Source Offset (m), Traveltime (s), Receiver Depth (m)}.

Table A.2: Traveltimes and source offsets for each receiver.

Index	Source Offset (m)	Traveltime (s)	Receiver Depth (m)	Index	Source Offset (m)	Traveltime (s)	Receiver Depth (m)	Index	Source Offset (m)	Traveltime (s)	Receiver Depth (m)
1	317.805	0.945562	1979.923	26	938.114	1.022636	1979.923	51	1565.130	1.154933	1979.923
2	343.415	0.947720	1979.923	27	967.871	1.028093	1979.923	52	1588.644	1.160874	1979.923
3	369.719	0.949464	1979.923	28	984.094	1.032088	1979.923	53	1612.475	1.167062	1979.923
4	393.092	0.952038	1979.923	29	1014.404	1.035925	1979.923	54	1638.883	1.173549	1979.923
5	417.457	0.953379	1979.923	30	1043.220	1.041995	1979.923	55	1663.079	1.178955	1979.923
6	443.392	0.956346	1979.923	31	1065.184	1.046384	1979.923	56	1689.771	1.185425	1979.923
7	465.151	0.958015	1979.923	32	1088.895	1.050471	1979.923	57	1711.871	1.191324	1979.923
8	493.184	0.960078	1979.923	33	1115.015	1.055210	1979.923	58	1739.048	1.197521	1979.923
9	515.711	0.963346	1979.923	34	1140.098	1.060235	1979.923	59	1763.081	1.203817	1979.923
10	541.511	0.965572	1979.923	35	1165.295	1.065256	1979.923	60	1789.370	1.210837	1979.923
11	566.218	0.968150	1979.923	36	1187.085	1.070389	1979.923	61	1814.387	1.217784	1979.923
12	594.084	0.971846	1979.923	37	1214.352	1.075694	1979.923	62	1836.461	1.223474	1979.923
13	616.525	0.974437	1979.923	38	1238.248	1.080502	1979.923	63	1863.985	1.231080	1979.923
14	640.390	0.977709	1979.923	39	1262.578	1.085769	1979.923	64	1888.688	1.235614	1979.923
15	666.096	0.980848	1979.923	40	1288.093	1.092119	1979.923	65	1912.386	1.242405	1979.923
16	686.674	0.983892	1979.923	41	1312.260	1.097591	1979.923	66	1936.696	1.250340	1979.923
17	714.131	0.987625	1979.923	42	1337.566	1.102887	1979.923	67	1962.993	1.255989	1979.923
18	734.065	0.990735	1979.923	43	1366.579	1.110075	1979.923	68	1986.236	1.262363	1979.923
19	763.765	0.994462	1979.923	44	1386.806	1.113877	1979.923	69	2011.513	1.269025	1979.923
20	790.341	0.998943	1979.923	45	1413.235	1.120171	1979.923	70	2038.012	1.276389	1979.923
21	818.537	1.002359	1979.923	46	1434.249	1.125078	1979.923	71	2058.654	1.281452	1979.923
22	838.613	1.006107	1979.923	47	1457.820	1.129865	1979.923	72	2089.406	1.291095	1979.923
23	864.183	1.009904	1979.923	48	1485.368	1.136798	1979.923	73	2113.127	1.297340	1979.923
24	889.644	1.015459	1979.923	49	1513.211	1.143508	1979.923	74	2137.010	1.304095	1979.923
25	916.870	1.018333	1979.923	50	1539.303	1.149417	1979.923	75	2162.001	1.308005	1979.923

76	2190.353	1.318307	1979.923	121	3312.831	1.651273	1979.923	166	1292.784	1.096443	1989.809
77	2208.538	1.324103	1979.923	122	3338.804	1.660710	1979.923	167	1316.929	1.101800	1989.809
78	2240.131	1.332692	1979.923	123	3361.215	1.665429	1979.923	168	1342.261	1.107092	1989.809
79	2262.848	1.340505	1979.923	124	3387.640	1.674863	1979.923	169	1371.339	1.113786	1989.809
80	2285.069	1.346629	1979.923	125	3405.836	1.681033	1979.923	170	1391.577	1.118027	1989.809
81	2313.522	1.354231	1979.923	126	3438.279	1.690683	1979.923	171	1418.030	1.124079	1989.809
82	2338.818	1.361689	1979.923	127	321.033	0.949649	1989.809	172	1439.032	1.129362	1989.809
83	2364.031	1.368898	1979.923	128	346.827	0.952137	1989.809	173	1462.608	1.134666	1989.809
84	2387.757	1.376166	1979.923	129	373.160	0.953549	1989.809	174	1490.113	1.140644	1989.809
85	2414.140	1.384134	1979.923	130	396.718	0.955886	1989.809	175	1517.949	1.147233	1989.809
86	2438.493	1.389482	1979.923	131	421.107	0.957665	1989.809	176	1544.086	1.153155	1989.809
87	2462.794	1.396500	1979.923	132	447.157	0.960745	1989.809	177	1569.900	1.158895	1989.809
88	2487.398	1.404673	1979.923	133	469.001	0.962260	1989.809	178	1593.404	1.164270	1989.809
89	2515.010	1.412021	1979.923	134	497.013	0.964153	1989.809	179	1617.242	1.170602	1989.809
90	2538.668	1.420411	1979.923	135	519.641	0.967471	1989.809	180	1643.658	1.177444	1989.809
91	2561.908	1.425506	1979.923	136	545.499	0.969745	1989.809	181	1667.848	1.182653	1989.809
92	2586.946	1.432678	1979.923	137	570.228	0.972201	1989.809	182	1694.537	1.189136	1989.809
93	2611.466	1.439409	1979.923	138	598.156	0.975986	1989.809	183	1716.647	1.194793	1989.809
94	2634.472	1.447930	1979.923	139	620.641	0.978617	1989.809	184	1743.842	1.201199	1989.809
95	2664.740	1.457009	1979.923	140	644.580	0.981874	1989.809	185	1767.872	1.207696	1989.809
96	2693.145	1.465913	1979.923	141	670.325	0.985060	1989.809	186	1794.159	1.214073	1989.809
97	2713.475	1.471688	1979.923	142	691.031	0.988157	1989.809	187	1819.208	1.220868	1989.809
98	2737.504	1.478316	1979.923	143	718.482	0.991753	1989.809	188	1841.269	1.226550	1989.809
99	2763.498	1.486156	1979.923	144	738.482	0.994879	1989.809	189	1868.805	1.233862	1989.809
100	2790.900	1.492776	1979.923	145	768.171	0.998693	1989.809	190	1893.512	1.240130	1989.809
101	2818.515	1.501544	1979.923	146	794.790	1.002989	1989.809	191	1917.232	1.246604	1989.809
102	2840.130	1.509010	1979.923	147	822.941	1.006748	1989.809	192	1941.535	1.253548	1989.809
103	2867.558	1.516612	1979.923	148	843.036	1.010184	1989.809	193	1967.839	1.259847	1989.809
104	2891.097	1.522475	1979.923	149	868.614	1.013894	1989.809	194	1991.090	1.265565	1989.809
105	2913.083	1.527969	1979.923	150	894.119	1.019595	1989.809	195	2016.374	1.273312	1989.809
106	2936.480	1.537739	1979.923	151	921.307	1.022321	1989.809	196	2042.866	1.280025	1989.809
107	2963.685	1.544497	1979.923	152	942.569	1.027050	1989.809	197	2063.524	1.285407	1989.809
108	2985.984	1.551710	1979.923	153	972.347	1.032722	1989.809	198	2094.281	1.294071	1989.809
109	3013.154	1.560112	1979.923	154	988.598	1.036735	1989.809	199	2117.996	1.299952	1989.809
110	3037.280	1.566471	1979.923	155	1018.913	1.040235	1989.809	200	2141.883	1.307700	1989.809
111	3062.143	1.575806	1979.923	156	1047.728	1.045885	1989.809	201	2166.886	1.310301	1989.809
112	3087.867	1.582710	1979.923	157	1069.727	1.050348	1989.809	202	2195.224	1.323274	1989.809
113	3113.355	1.587800	1979.923	158	1093.448	1.054671	1989.809	203	2213.413	1.327841	1989.809
114	3137.870	1.597852	1979.923	159	1119.573	1.059151	1989.809	204	2245.016	1.336037	1989.809
115	3163.910	1.605218	1979.923	160	1144.664	1.064439	1989.809	205	2267.713	1.343859	1989.809
116	3187.722	1.614170	1979.923	161	1169.907	1.069724	1989.809	206	2289.923	1.348996	1989.809
117	3214.578	1.620041	1979.923	162	1191.722	1.074964	1989.809	207	2318.389	1.357301	1989.809
118	3236.351	1.627195	1979.923	163	1219.006	1.080203	1989.809	208	2343.698	1.365345	1989.809
119	3259.675	1.634435	1979.923	164	1242.914	1.084769	1989.809	209	2368.914	1.372069	1989.809
120	3288.287	1.645422	1979.923	165	1267.262	1.090486	1989.809	210	2392.644	1.379635	1989.809

211	2419.031	1.386817	1989.809	256	400.611	0.960273	1999.699	301	1522.751	1.151295	1999.699
212	2443.401	1.392626	1989.809	257	425.009	0.961745	1999.699	302	1548.932	1.156979	1999.699
213	2467.697	1.400358	1989.809	258	451.156	0.964632	1999.699	303	1574.732	1.162905	1999.699
214	2492.313	1.408040	1989.809	259	473.074	0.966243	1999.699	304	1598.225	1.168160	1999.699
215	2519.922	1.415364	1989.809	260	501.052	0.968510	1999.699	305	1622.070	1.174337	1999.699
216	2543.581	1.422726	1989.809	261	523.771	0.971570	1999.699	306	1648.491	1.180674	1999.699
217	2566.833	1.429279	1989.809	262	549.677	0.973782	1999.699	307	1672.676	1.186362	1999.699
218	2591.883	1.436051	1989.809	263	574.419	0.976722	1999.699	308	1699.359	1.192925	1999.699
219	2616.403	1.443447	1989.809	264	602.401	0.980039	1999.699	309	1721.478	1.198836	1999.699
220	2639.425	1.451370	1989.809	265	624.922	0.982692	1999.699	310	1748.692	1.204910	1999.699
221	2669.654	1.459092	1989.809	266	648.928	0.985882	1999.699	311	1772.717	1.211548	1999.699
222	2698.020	1.468384	1989.809	267	674.706	0.988900	1999.699	312	1799.002	1.217934	1999.699
223	2718.334	1.472716	1989.809	268	695.534	0.992308	1999.699	313	1824.082	1.224612	1999.699
224	2742.351	1.481698	1989.809	269	722.973	0.995547	1999.699	314	1846.130	1.230545	1999.699
225	2768.347	1.489435	1989.809	270	743.035	0.998774	1999.699	315	1873.676	1.237567	1999.699
226	2795.751	1.496836	1989.809	271	772.708	1.002640	1999.699	316	1898.386	1.244110	1999.699
227	2823.373	1.504003	1989.809	272	799.365	1.007501	1999.699	317	1922.128	1.250350	1999.699
228	2845.001	1.510775	1989.809	273	827.466	1.010404	1999.699	318	1946.425	1.256844	1999.699
229	2872.444	1.517430	1989.809	274	847.578	1.014153	1999.699	319	1972.733	1.263463	1999.699
230	2895.995	1.527097	1989.809	275	873.161	1.017853	1999.699	320	1995.992	1.269489	1999.699
231	2917.992	1.531993	1989.809	276	898.705	1.023541	1999.699	321	2021.284	1.276605	1999.699
232	2941.398	1.540569	1989.809	277	925.852	1.026076	1999.699	322	2047.768	1.283477	1999.699
233	2968.622	1.546735	1989.809	278	947.130	1.030365	1999.699	323	2068.441	1.289092	1999.699
234	2990.918	1.553385	1989.809	279	976.925	1.036107	1999.699	324	2099.202	1.297742	1999.699
235	3018.090	1.561528	1989.809	280	993.203	1.040563	1999.699	325	2122.910	1.304563	1999.699
236	3042.218	1.568398	1989.809	281	1023.519	1.044037	1999.699	326	2146.801	1.310749	1999.699
237	3067.084	1.576207	1989.809	282	1052.331	1.049905	1999.699	327	2171.815	1.314782	1999.699
238	3092.811	1.585550	1989.809	283	1074.363	1.054403	1999.699	328	2200.140	1.325703	1999.699
239	3118.302	1.590731	1989.809	284	1098.092	1.058814	1999.699	329	2218.331	1.331626	1999.699
240	3142.820	1.600101	1989.809	285	1124.219	1.063483	1999.699	330	2249.944	1.339540	1999.699
241	3168.861	1.608303	1989.809	286	1149.317	1.068660	1999.699	331	2272.620	1.346336	1999.699
242	3192.675	1.615857	1989.809	287	1174.603	1.073632	1999.699	332	2294.818	1.352489	1999.699
243	3219.534	1.622663	1989.809	288	1196.443	1.078861	1999.699	333	2323.298	1.360202	1999.699
244	3241.315	1.631572	1989.809	289	1223.741	1.084101	1999.699	334	2348.619	1.368284	1999.699
245	3264.630	1.638071	1989.809	290	1247.658	1.088584	1999.699	335	2373.838	1.375471	1999.699
246	3293.246	1.647669	1989.809	291	1272.022	1.094326	1999.699	336	2397.572	1.382493	1999.699
247	3317.799	1.653441	1989.809	292	1297.550	1.100294	1999.699	337	2423.962	1.389803	1999.699
248	3343.766	1.662421	1989.809	293	1321.672	1.105547	1999.699	338	2448.348	1.396371	1999.699
249	3366.177	1.667257	1989.809	294	1347.028	1.110953	1999.699	339	2472.638	1.403782	1999.699
250	3392.607	1.675520	1989.809	295	1376.170	1.117626	1999.699	340	2497.266	1.411481	1999.699
251	3410.802	1.681964	1989.809	296	1396.418	1.121891	1999.699	341	2524.872	1.418757	1999.699
252	3443.246	1.691929	1989.809	297	1422.895	1.128178	1999.699	342	2548.532	1.425434	1999.699
253	324.600	0.953662	1999.699	298	1443.884	1.132653	1999.699	343	2571.795	1.432337	1999.699
254	350.549	0.955781	1999.699	299	1467.463	1.138044	1999.699	344	2596.858	1.439589	1999.699
255	376.889	0.957374	1999.699	300	1494.924	1.144481	1999.699	345	2621.377	1.446632	1999.699

346	2644.413	1.453807	1999.699	391	3773.125	1.794582	1999.699	436	1201.324	1.083181	2009.758
347	2674.605	1.462258	1999.699	392	3797.180	1.802597	1999.699	437	1228.635	1.088640	2009.758
348	2702.929	1.470753	1999.699	393	3823.886	1.810145	1999.699	438	1252.559	1.092830	2009.758
349	2723.228	1.476894	1999.699	394	3847.157	1.817675	1999.699	439	1276.939	1.098534	2009.758
350	2747.233	1.483652	1999.699	395	3873.904	1.825487	1999.699	440	1302.470	1.104879	2009.758
351	2773.232	1.491746	1999.699	396	3899.011	1.833940	1999.699	441	1326.568	1.109972	2009.758
352	2800.637	1.498916	1999.699	397	3924.745	1.841541	1999.699	442	1351.947	1.115153	2009.758
353	2828.265	1.506587	1999.699	398	3947.236	1.849245	1999.699	443	1381.150	1.121642	2009.758
354	2849.906	1.514083	1999.699	399	3974.137	1.857089	1999.699	444	1401.407	1.126247	2009.758
355	2877.363	1.521606	1999.699	400	303.261	0.956100	2009.758	445	1427.905	1.132330	2009.758
356	2900.926	1.528903	1999.699	401	328.581	0.957547	2009.758	446	1448.880	1.136977	2009.758
357	2922.933	1.535242	1999.699	402	354.657	0.959877	2009.758	447	1472.461	1.142246	2009.758
358	2946.349	1.542711	1999.699	403	380.983	0.961524	2009.758	448	1499.879	1.148672	2009.758
359	2973.590	1.550466	1999.699	404	404.849	0.964467	2009.758	449	1527.695	1.155408	2009.758
360	2995.885	1.557133	1999.699	405	429.240	0.965664	2009.758	450	1553.918	1.161119	2009.758
361	3023.058	1.565767	1999.699	406	455.469	0.968875	2009.758	451	1579.704	1.167420	2009.758
362	3047.187	1.573079	1999.699	407	477.448	0.970314	2009.758	452	1603.186	1.172206	2009.758
363	3072.056	1.580030	1999.699	408	505.381	0.972350	2009.758	453	1627.036	1.178204	2009.758
364	3097.786	1.588145	1999.699	409	528.180	0.975954	2009.758	454	1653.462	1.184507	2009.758
365	3123.280	1.595589	1999.699	410	554.124	0.977649	2009.758	455	1677.641	1.190805	2009.758
366	3147.799	1.603017	1999.699	411	578.871	0.980507	2009.758	456	1704.318	1.197292	2009.758
367	3173.841	1.610568	1999.699	412	606.897	0.984222	2009.758	457	1726.445	1.203018	2009.758
368	3197.658	1.618286	1999.699	413	629.448	0.987011	2009.758	458	1753.676	1.209147	2009.758
369	3224.520	1.625947	1999.699	414	653.514	0.990246	2009.758	459	1777.695	1.215748	2009.758
370	3246.308	1.633840	1999.699	415	679.317	0.993458	2009.758	460	1803.977	1.221607	2009.758
371	3269.615	1.641181	1999.699	416	700.261	0.996693	2009.758	461	1829.087	1.228617	2009.758
372	3298.234	1.648665	1999.699	417	727.683	1.000173	2009.758	462	1851.122	1.234195	2009.758
373	3322.795	1.656675	1999.699	418	747.801	1.003167	2009.758	463	1878.678	1.241198	2009.758
374	3348.757	1.664216	1999.699	419	777.454	1.006854	2009.758	464	1903.390	1.247676	2009.758
375	3371.168	1.670785	1999.699	420	804.143	1.011369	2009.758	465	1927.153	1.254113	2009.758
376	3397.601	1.678696	1999.699	421	832.193	1.015020	2009.758	466	1951.442	1.260869	2009.758
377	3415.795	1.685196	1999.699	422	852.318	1.018689	2009.758	467	1977.755	1.267338	2009.758
378	3448.241	1.694415	1999.699	423	877.902	1.022437	2009.758	468	2001.021	1.273069	2009.758
379	3472.837	1.701577	1999.699	424	903.481	1.027936	2009.758	469	2026.319	1.280433	2009.758
380	3498.606	1.710192	1999.699	425	930.585	1.030703	2009.758	470	2052.794	1.287490	2009.758
381	3522.813	1.717371	1999.699	426	951.877	1.035000	2009.758	471	2073.482	1.293358	2009.758
382	3549.675	1.725993	1999.699	427	981.685	1.040677	2009.758	472	2104.247	1.301024	2009.758
383	3572.790	1.733222	1999.699	428	997.988	1.045077	2009.758	473	2127.948	1.308343	2009.758
384	3596.293	1.739830	1999.699	429	1028.302	1.048441	2009.758	474	2151.842	1.314503	2009.758
385	3624.682	1.748377	1999.699	430	1057.108	1.054518	2009.758	475	2176.867	1.318469	2009.758
386	3649.510	1.756174	1999.699	431	1079.172	1.058712	2009.758	476	2205.177	1.329099	2009.758
387	3674.382	1.763768	1999.699	432	1102.905	1.063161	2009.758	477	2223.370	1.334982	2009.758
388	3696.833	1.770490	1999.699	433	1129.033	1.067551	2009.758	478	2254.993	1.342631	2009.758
389	3725.141	1.779702	1999.699	434	1154.135	1.072604	2009.758	479	2277.647	1.350118	2009.758
390	3748.488	1.786963	1999.699	435	1179.462	1.077918	2009.758	480	2299.834	1.357171	2009.758

481	2328.326	1.364622	2009.758	526	3453.340	1.698745	2009.758	571	882.753	1.026294	2019.927
482	2353.659	1.371613	2009.758	527	3477.933	1.705403	2009.758	572	908.363	1.031885	2019.927
483	2378.880	1.379627	2009.758	528	3503.704	1.711605	2009.758	573	935.422	1.034363	2019.927
484	2402.618	1.386764	2009.758	529	3527.909	1.720754	2009.758	574	956.725	1.038713	2019.927
485	2429.010	1.393956	2009.758	530	3554.773	1.729231	2009.758	575	986.543	1.044700	2019.927
486	2453.412	1.400834	2009.758	531	3577.890	1.735458	2009.758	576	1002.868	1.049014	2019.927
487	2477.697	1.407589	2009.758	532	3601.391	1.744448	2009.758	577	1033.179	1.052495	2019.927
488	2502.335	1.415158	2009.758	533	3629.788	1.751149	2009.758	578	1061.975	1.058421	2019.927
489	2529.938	1.422226	2009.758	534	3654.610	1.760526	2009.758	579	1084.068	1.062677	2019.927
490	2553.598	1.429520	2009.758	535	3679.484	1.768197	2009.758	580	1107.805	1.066960	2019.927
491	2576.873	1.436827	2009.758	536	3701.937	1.775120	2009.758	581	1133.931	1.071377	2019.927
492	2601.946	1.443173	2009.758	537	3730.246	1.782591	2009.758	582	1159.036	1.076518	2019.927
493	2626.465	1.450736	2009.758	538	3753.592	1.790948	2009.758	583	1184.402	1.081816	2019.927
494	2649.516	1.458285	2009.758	539	3778.230	1.798312	2009.758	584	1206.284	1.087232	2019.927
495	2679.669	1.465704	2009.758	540	3802.290	1.804984	2009.758	585	1233.606	1.092486	2019.927
496	2707.953	1.474176	2009.758	541	3828.996	1.813300	2009.758	586	1257.536	1.096881	2019.927
497	2728.236	1.480744	2009.758	542	3852.268	1.823626	2009.758	587	1281.929	1.102535	2019.927
498	2752.229	1.487699	2009.758	543	3879.018	1.828743	2009.758	588	1307.463	1.108661	2019.927
499	2778.230	1.494594	2009.758	544	3904.126	1.835432	2009.758	589	1331.536	1.113833	2019.927
500	2805.637	1.502098	2009.758	545	3929.863	1.845600	2009.758	590	1356.935	1.119047	2019.927
501	2833.270	1.508771	2009.758	546	3952.356	1.852445	2009.758	591	1386.199	1.125490	2019.927
502	2854.923	1.516733	2009.758	547	3979.256	1.857067	2009.758	592	1406.463	1.130003	2019.927
503	2882.394	1.525492	2009.758	548	307.433	0.960111	2019.927	593	1432.981	1.136112	2019.927
504	2905.969	1.531940	2009.758	549	332.872	0.961630	2019.927	594	1453.941	1.141041	2019.927
505	2927.986	1.539600	2009.758	550	359.049	0.963944	2019.927	595	1477.524	1.145902	2019.927
506	2951.411	1.546765	2009.758	551	385.343	0.965418	2019.927	596	1504.896	1.152406	2019.927
507	2978.669	1.554718	2009.758	552	409.334	0.968447	2019.927	597	1532.702	1.159518	2019.927
508	3000.961	1.561351	2009.758	553	433.705	0.969921	2019.927	598	1558.966	1.164752	2019.927
509	3028.136	1.568134	2009.758	554	460.001	0.972838	2019.927	599	1584.736	1.170728	2019.927
510	3052.265	1.577714	2009.758	555	482.029	0.974457	2019.927	600	1608.206	1.176191	2019.927
511	3077.138	1.582686	2009.758	556	509.907	0.976609	2019.927	601	1632.059	1.182031	2019.927
512	3102.869	1.590615	2009.758	557	532.777	0.979967	2019.927	602	1658.491	1.188399	2019.927
513	3128.367	1.599738	2009.758	558	558.748	0.981933	2019.927	603	1682.662	1.193896	2019.927
514	3152.887	1.606000	2009.758	559	583.493	0.985107	2019.927	604	1709.332	1.200831	2019.927
515	3178.930	1.613464	2009.758	560	611.554	0.988531	2019.927	605	1731.466	1.206627	2019.927
516	3202.748	1.619519	2009.758	561	634.129	0.991086	2019.927	606	1758.713	1.212206	2019.927
517	3229.613	1.630294	2009.758	562	658.248	0.994422	2019.927	607	1782.727	1.218930	2019.927
518	3251.407	1.636149	2009.758	563	684.072	0.997434	2019.927	608	1809.004	1.224991	2019.927
519	3274.706	1.643357	2009.758	564	705.124	1.000876	2019.927	609	1834.144	1.232119	2019.927
520	3303.329	1.649475	2009.758	565	732.526	1.004018	2019.927	610	1856.165	1.237956	2019.927
521	3327.898	1.657560	2009.758	566	752.696	1.007432	2019.927	611	1883.729	1.244659	2019.927
522	3353.854	1.664552	2009.758	567	782.323	1.011254	2019.927	612	1908.443	1.250987	2019.927
523	3376.264	1.675352	2009.758	568	809.041	1.015565	2019.927	613	1932.226	1.257720	2019.927
524	3402.702	1.680203	2009.758	569	837.034	1.019073	2019.927	614	1956.508	1.264184	2019.927
525	3420.895	1.687718	2009.758	570	857.170	1.022852	2019.927	615	1982.824	1.270513	2019.927

616	2006.097	1.276609	2019.927	643	2684.768	1.469199	2019.927	670	3358.978	1.669892	2019.927
617	2031.400	1.283866	2019.927	644	2713.012	1.477709	2019.927	671	3381.389	1.674585	2019.927
618	2057.867	1.290939	2019.927	645	2733.279	1.482503	2019.927	672	3407.830	1.683330	2019.927
619	2078.568	1.296333	2019.927	646	2757.260	1.489196	2019.927	673	3426.021	1.689103	2019.927
620	2109.336	1.305118	2019.927	647	2783.262	1.497292	2019.927	674	3458.467	1.699251	2019.927
621	2133.030	1.311261	2019.927	648	2810.670	1.504319	2019.927	675	3483.057	1.707174	2019.927
622	2156.926	1.317697	2019.927	649	2838.309	1.512353	2019.927	676	3508.829	1.714270	2019.927
623	2181.962	1.322426	2019.927	650	2859.972	1.519220	2019.927	677	3533.031	1.721476	2019.927
624	2210.257	1.332953	2019.927	651	2887.458	1.526834	2019.927	678	3559.898	1.730402	2019.927
625	2228.452	1.338401	2019.927	652	2911.043	1.534916	2019.927	679	3583.016	1.738836	2019.927
626	2260.084	1.346712	2019.927	653	2933.070	1.540726	2019.927	680	3606.516	1.744451	2019.927
627	2282.716	1.353271	2019.927	654	2956.504	1.548725	2019.927	681	3634.919	1.752517	2019.927
628	2304.890	1.359676	2019.927	655	2983.778	1.555046	2019.927	682	3659.735	1.760693	2019.927
629	2333.394	1.367060	2019.927	656	3006.069	1.562470	2019.927	683	3684.612	1.767779	2019.927
630	2358.739	1.375573	2019.927	657	3033.245	1.570417	2019.927	684	3707.066	1.774926	2019.927
631	2383.962	1.382318	2019.927	658	3057.374	1.578054	2019.927	685	3735.376	1.785556	2019.927
632	2407.702	1.389120	2019.927	659	3082.250	1.585655	2019.927	686	3758.721	1.792247	2019.927
633	2434.097	1.396500	2019.927	660	3107.982	1.593522	2019.927	687	3783.360	1.799150	2019.927
634	2458.515	1.403233	2019.927	661	3133.483	1.600080	2019.927	688	3807.424	1.805479	2019.927
635	2482.793	1.410509	2019.927	662	3158.005	1.608654	2019.927	689	3834.131	1.814840	2019.927
636	2507.442	1.418106	2019.927	663	3184.048	1.615445	2019.927	690	3857.404	1.823009	2019.927
637	2535.041	1.425056	2019.927	664	3207.868	1.623756	2019.927	691	3884.155	1.829612	2019.927
638	2558.701	1.432211	2019.927	665	3234.734	1.630595	2019.927	692	3909.264	1.837849	2019.927
639	2581.986	1.439055	2019.927	666	3256.536	1.639147	2019.927	693	3935.005	1.845303	2019.927
640	2607.071	1.445480	2019.927	667	3279.827	1.646444	2019.927	694	3957.499	1.852544	2019.927
641	2631.588	1.452599	2019.927	668	3308.451	1.654579	2019.927	695	3984.399	1.860716	2019.927
642	2654.653	1.459835	2019.927	669	3333.029	1.662212	2019.927				

2. SIMPLEX_STARTUP_VALUES.txt

Program generated random start-up values, i.e., the start-up simplices used as input for the NM algorithm, are stored in this text file. The formatting is as follows:

Column {1,2,3,4,5,6,7,8,9,10,11,12,13,14,15,16} = {Simplex Index (SI), Vertex Index (VI), Residual Sum of Squares (RSS), Parameter Penalty (PP), Offset Penalty(OP), Total Penalty (TP), a_1, a_2, a_3, b_1, b_2, b_3, χ_1, χ_2, χ_3, Maximum Offset (MO)}. For display purposes values with decimals are shown to a reduced number of decimal places in Table A3.

Table A.3: Simplex startup values.

SI	VI	RSS (s^2)	PP	OP	TP	a_1 (ms^{-1})	a_2 (ms^{-1})	a_3 (ms^{-1})	b_1	b_2	b_3	χ_1	χ_2	χ_3	MO (m)
1	1	115.940	0	218	333.940	1323.194	3914.922	3165.370	0.822	1.314	0.752	0.038	0.138	0.014	2669.979
1	2	67.473	0	117	184.473	831.112	2800.020	2051.103	1.049	0.649	0.759	0.018	0.146	0.075	3171.638
1	3	49.805	0	74	123.805	1459.595	3734.847	3324.404	0.369	0.929	0.329	0.078	0.174	0.282	3351.929
1	4	28.787	0	0	28.787	1322.387	2419.873	2775.047	0.281	0.436	0.008	0.047	0.189	0.167	16663.141
1	5	57.906	0	146	203.906	1304.442	2961.146	2994.148	0.167	0.923	0.627	0.026	0.170	0.108	3003.486
1	6	67.640	0	251	318.640	1196.402	2626.110	2829.812	0.412	1.430	0.845	0.069	0.128	0.004	2489.767
1	7	148.646	0	257	405.646	1045.579	2648.194	2701.744	0.016	0.672	1.314	0.097	0.016	0.077	2487.556
1	8	25.580	0	0	25.580	1543.125	3463.741	3101.956	0.944	0.311	1.016	0.025	0.124	0.077	4880.466
1	9	70.237	0	292	362.237	1159.586	2885.450	3945.820	0.443	0.638	1.263	0.078	0.071	0.052	2314.097
1	10	64.230	0	136	200.230	1120.193	3888.980	2225.553	0.282	0.667	1.388	0.076	0.034	0.104	3078.854
2	1	52.207	0	115	167.207	1545.360	2906.099	2626.517	0.144	0.761	1.411	0.013	0.178	0.061	3167.521
2	2	41.707	0	0	41.707	1434.970	1797.029	2083.596	0.426	0.789	1.223	0.083	0.164	0.020	3924.106
2	3	138.816	0	0	138.816	961.497	2479.222	3476.799	0.323	0.065	0.198	0.046	0.105	0.030	3995.337
2	4	2.295	0	0	2.295	1416.294	3642.041	3315.024	0.429	0.247	0.520	0.013	0.093	0.149	5338.436
2	5	68.592	0	111	179.592	1021.328	2575.060	2429.272	0.707	0.675	0.313	0.054	0.098	0.022	3188.391
2	6	112.916	0	237	349.916	1742.402	1665.287	2833.507	0.824	1.062	1.300	0.030	0.053	0.280	2587.283
2	7	119.708	0	109	228.708	1824.770	2193.226	3287.684	1.267	1.166	1.188	0.018	0.081	0.062	3231.932
2	8	59.535	0	78	137.535	1393.084	1761.147	3322.962	1.482	1.165	0.524	0.009	0.087	0.139	3382.495
2	9	82.615	0	134	216.615	1815.873	3985.244	2340.955	0.074	0.754	0.854	0.020	0.004	0.125	3086.373
2	10	75.651	0	242	317.651	895.575	3929.392	3763.304	0.349	1.434	1.207	0.043	0.178	0.088	2532.368

3	1	115.227	0	170	285.227	1406.295	3520.619	3556.016	0.965	0.498	1.249	0.064	0.007	0.097	2923.951
3	2	181.348	0	198	379.348	878.345	3044.361	2267.909	0.243	0.722	0.309	0.010	0.075	0.064	2763.569
3	3	111.319	0	127	238.319	1313.747	3435.903	3737.833	1.304	1.122	1.096	0.071	0.020	0.085	3138.360
3	4	99.453	0	359	458.453	915.838	2006.142	3497.555	0.327	1.286	1.205	0.011	0.040	0.036	1982.462
3	5	6.984	0	0	6.984	952.593	2303.256	3597.171	1.112	0.622	0.066	0.018	0.188	0.206	7029.438
3	6	17.154	0	0	17.154	1516.094	2857.760	3086.690	0.979	1.272	0.162	0.071	0.075	0.193	6201.859
3	7	4.642	0	1	5.642	1071.215	2455.899	2441.676	1.198	0.667	0.653	0.088	0.145	0.094	3918.566
3	8	278.438	0	78	356.438	928.336	1709.630	3836.916	0.048	1.073	0.332	0.097	0.026	0.263	3387.445
3	9	32.234	0	0	32.234	1064.368	3959.567	3184.169	0.345	0.014	1.320	0.065	0.051	0.116	17947.952
3	10	41.277	0	77	118.277	1219.792	2659.252	2692.476	1.057	0.039	1.079	0.048	0.175	0.183	3391.605
4	1	67.240	0	256	323.240	1361.345	2809.601	2527.558	0.132	1.410	1.069	0.010	0.180	0.157	2463.580
4	2	105.952	0	342	447.952	1042.092	2376.500	3827.830	0.047	0.154	1.154	0.056	0.058	0.098	2058.728
4	3	33.417	0	54	87.417	1568.488	2223.388	2839.471	0.536	0.993	0.496	0.019	0.192	0.278	3548.388
4	4	4.807	0	3	7.807	1379.684	2528.536	3080.383	0.884	0.425	0.343	0.051	0.133	0.254	3971.772
4	5	21.923	0	33	54.923	1406.284	3596.840	3216.884	0.079	0.302	0.939	0.061	0.101	0.252	3711.928
4	6	52.264	0	126	178.264	1264.271	3368.192	3652.499	0.099	0.583	0.622	0.083	0.076	0.285	3144.534
4	7	90.783	0	223	313.783	1752.364	2510.106	3247.126	0.066	1.388	1.404	0.033	0.068	0.002	2657.776
4	8	47.674	0	102	149.674	1496.005	1631.243	2353.425	0.593	0.855	0.963	0.098	0.189	0.148	3262.024
4	9	65.217	0	166	231.217	994.759	3513.771	3182.515	1.002	1.374	0.581	0.099	0.138	0.280	2895.311
4	10	79.610	0	198	277.610	1640.902	2246.534	2978.532	0.298	1.053	1.282	0.082	0.107	0.041	2787.843

3. FINAL_OUTPUT_VALUES.txt.

The best a, b, χ values for the simplices at the termination of the program are output to this file. Formatting is as follows:

Column {1,2,3,4,5,6,,8,9,10,11,12,13,14,15,16} = {Simplex Index (SI), Vertex Index (VI), Residual Sum of Squares (RSS), Parameter Penalty (PP), Offset Penalty (OP), Total Penalty (TP), $a_1, a_2, a_3, b_1, b_2, b_3, \chi_1, \chi_2, \chi_3$, Maximum Offset for this set of a, b, χ (MO), Iterations to Termination (IT), Time to Termination (TM), Total Time (TT)}. For display purposes values with decimals are shown to a reduced number of decimal places in Table A.4.

Table A.4: Final output values.

SI	VI	RSS (s^2)	PP	OP	TP	a_1 (ms^{-1})	a_2 (ms^{-1})	a_3 (ms^{-1})	b_1	b_2	b_3	χ_1	χ_2	χ_3	MO (m)	IT	TM (s)	TT (s)
1	1	0.000726	0	0	0.000726	1283.703	2836.944	2396.662	1	0	1.5	0	0.1	0.1	12417.886	3054	2158.349	3214.147
2	1	0.000668	0	0	0.000668	1660.981	2892.466	2373.362	0.4	0	0.8	0	0.1	0.2	57685.956	4375	2867.83	3214.147
3	1	0.000648	0	0	0.000648	1877.577	2801.852	2482.964	0	0.4	0.1	0	0.1	0.3	4880.728	5036	3124.176	3214.147
4	1	0.000862	0	0	0.000862	1849.397	2914.907	2543.361	0	0.2	1	0	0.1	0.1	5374.326	3931	2727.299	3214.147

```
%%%%%%%%%%%%%%%%%%%%%%%%%%%%%%%%%%%%%%%%%%%%%%%%%%
% EXAMPLE OF MAIN MATLAB PROGRAM OF NELDER-MEAD OPTIMIZATION
APPLIED TO:
%
% VSP TRAVELTIMES USING:
% > THREE-LAYER TRAVELTIME MODEL
% > ADAPTIVE SCALING CONSTANTS
% > MACHINE-PRECISION/ITERATIONS TERMINATION CONDITIONS
% > PARALLEL COMPUTING
%
% GENERATES RANDOM STARTUP VALUES, SAVES TO
'INPUTS_abchi_NM_example.txt'
% SAVES OUTPUTS TO 'OUTPUTS_abchi_NM_example.txt'
%
% OUTPUTS EVERY 1000 ITERATIONS TO THE COMMAND WINDOW
%
%%%%%%%%%%%%%%%%%%%%%%%%%%
clear all         % clear all variables
clc               % clear command window
close all         % close all figures
format compact    % compact command window outputs
format longG      % number formatting
rng(2)            % random seed

% -- file names
infileTxt =  'SIMPLEX_STARTUP_VALUES.txt';
outfileTxt = 'FINAL_OUTPUT_VALUES.txt';

% -- number of initial simplices used in parallel
n_parallel = 4;        % number of simplices to use in multistart
n_parallel_workers = 4; % number of parallel workers to run at same time

% -- read input traveltimes
dataIn = readmatrix('INPUT_DATA.txt');

% -- designate variables
SrcX = dataIn(:,2);     % input sources
tt = dataIn(:,3);       % input traveltimes
RcvrZ = dataIn(:,4);    % input receiver depths

% -- set interface depths
z = [6;1300;1750];      % three-layer model

% -- specify number of model parameters to optimize
n = 9;                  % three parameters per layer
np1 = n + 1;            % number of vertices in simplex
numY = n_parallel*np1;  % number of total vertices
```

```
% -- initialize anonymous functions for maximum offset
% % -- Indexing:
% y1: a1
% y2: a2
% y3: a3
% y4: b1
% y5: b2
% y6: b3
% y7: chi1
% y8: chi2
% y9: chi3
maxOff = @(p,y) ... % final horizontal coordinate given ray parameter, p, and abchi values, y
   (sqrt(1-p.^2.*y(1).^2.*(1+2.*y(7))) - sqrt(1-p.^2.*(y(1) + y(4).*(z(2)-
z(1))).^2.*(1+2.*y(7))))./(p.*y(4)) + ...
   (sqrt(1-p.^2.*y(2).^2.*(1+2.*y(8))) - sqrt(1-p.^2.*(y(2) + y(5).*(z(3)-
z(2))).^2.*(1+2.*y(8))))./(p.*y(5)) + ...
   (sqrt(1-p.^2.*y(3).^2.*(1+2.*y(9))) - sqrt(1-p.^2.*(y(3) + y(6).*(RcvrZ(1)-
z(3))).^2.*(1+2.*y(9))))./(p.*y(6));
pmaxi = @(y) [ ...  % maximum ray parameter value given y in each above square root
      1/sqrt(y(1)^2*(1+2*y(7))); ...
      1/sqrt(y(2)^2*(1+2*y(8))); ...
      1/sqrt(y(3)^2*(1+2*y(9))); ...
      1/sqrt((y(1)+y(4)*(z(2)-z(1)))^2*(1+2*y(7))); ...
      1/sqrt((y(2)+y(5)*(z(3)-z(2)))^2*(1+2*y(8))); ...
      1/sqrt((y(3)+y(6)*(RcvrZ(1)-z(3)))^2*(1+2*y(9)))] - eps;

% % -- generate initial abchi parameters from specified bounds
du = 1e-3;
a1min =  800+du; a1max =  2000-du;
a2min = 1600+du; a2max =  4000-du;
a3min = 2000+du; a3max =  4000-du;
b1min =    0+du; b1max =   1.5-du;
b2min =    0+du; b2max =   1.5-du;
b3min =    0+du; b3max =   1.5-du;
chi1min =  0+du; chi1max = 0.1-du;
chi2min =  0+du; chi2max = 0.2-du;
chi3min =  0+du; chi3max = 0.3-du;
minBounds = [a1min,a2min,a3min,b1min,b2min,b3min,chi1min,chi2min,chi3min];
maxBounds = [a1max,a2max,a3max,b1max,b2max,b3max,chi1max,chi2max,chi3max];

YCatIn = (maxBounds-minBounds).*rand(numY,n)+minBounds;

% % -- calculate function values for initial abchi parameters
fIn = zeros(numY,1);           % allocate memory for input function values
fileID = fopen(infileTxt,'w');  % open file
sID = 1;                    % simplex indexing
vID = 1;                    % vertex indexing
for ii = 1:numY
```

```
   % calculate RSS and penalties
   [RSSOut,ypenOut,offpenOut] = tRSS_stats_3lyr(SrcX,RcvrZ,tt,YCatIn(ii,:),z);
   % sum into function value
   fIn(ii) = sum([RSSOut,ypenOut,offpenOut]);
%     fprintf(fileID,...          % print to file
%         '%5i %3i %19.14f %5i %5.3g %19.14f %17.9f %17.9f %17.9f %14.9f %14.9f %14.9f
%14.9f %14.9f %14.9f %13.4f\n',...
%
sID,vID,RSSOut,ypenOut,offpenOut,fIn(ii),YCatIn(ii,:),maxOff(min(pmaxi(YCatIn(ii,:))),YCatI
n(ii,:)));
   fprintf(fileID,...          % print to file
      '%1i %4i %12.6f %3i %5i %12.6f %10.3f %10.3f %10.3f %7.3f %7.3f %7.3f %7.3f %7.3f
%7.3f %11.3f\n',...

sID,vID,RSSOut,ypenOut,offpenOut,fIn(ii),YCatIn(ii,:),maxOff(min(pmaxi(YCatIn(ii,:))),YCatI
n(ii,:)));

   if vID == np1               % indexing
      vID = 0;
      sID = sID + 1;
   end
   vID = vID + 1;
end
fclose(fileID);

% -- specify Nelder-Mead optimization algorithm as function to evaluate
% -- used for parallel computing
toEvalFunc = @NMalgorithm_3lyr;

% -- initialize startup values for parallel optimization
funcsIn = cell(n_parallel,1);   % allocate memory for function to evaluate
arguments = cell(n_parallel,6); % allocate memory for input data
for sID = 1:n_parallel

   funcsIn{sID} = toEvalFunc;  % specify function to evaluate
   % input function values
   arguments{sID,1} = fIn((np1*(sID-1)+1):(np1*sID),:);
   % input abchi values
   arguments{sID,2} = YCatIn((np1*(sID-1)+1):(np1*sID),:);
   arguments{sID,3} = SrcX;       % input sources
   arguments{sID,4} = RcvrZ;      % input receivers
   arguments{sID,5} = tt;         % input traveltimes
   arguments{sID,6} = z;          % input interface depths

end

% -- allocate memory for optimization outputs
infoOut = cell(n_parallel,1);   % number of iterations and computation time
```

```
fOut = cell(n_parallel,1);      % output function values
YOut = cell(n_parallel,1);      % output abchi values

% -- perform optimization with parallel computing
tic                                  % begin timer for total time
q = parallel.pool.DataQueue;            % call parallel pool
parpool('local',n_parallel_workers)     % specify number of workers
parfor sID = 1:n_parallel              % run optimizations in parallel
   [infoOut{sID,1},fOut{sID,1},YOut{sID,1}] = funcsIn{sID}(arguments{sID,:});
end
partocOut = toc                        % record total time

% -- output optimization results to text files
fileID = fopen(outfileTxt,'w');         % open output text file
for sID = 1:n_parallel
   infoOut1 = infoOut{sID,1};          % collect optimization info
   fCat = fOut{sID,1};                % collect function values
   Y = YOut{sID,1};                   % collect abchi values
   infoOut1 = infoOut1(1,:);          % first vertex iterations and time
   f1 = fCat(1);                     % first vertex function value
   y1 = Y(1,:);                      % first vertex abchi values
   % calculate RSS and penalties
   [RSSOut,ypenOut,offpenOut] = tRSS_stats_3lyr(SrcX,RcvrZ,tt,y1,z);
   % print to output text file
%     fprintf(fileID,...
%        '%5i %3i %19.14f %5i %5.3g %19.14f %17.9f %17.9f %17.9f %14.9f %14.9f %14.9f
%14.9f %14.9f %14.9f %13.4f %7i %12.4f %11.4f\n',...
%
sID,1,RSSOut,ypenOut,offpenOut,f1,y1,maxOff(min(pmaxi(y1)),y1),infoOut1(1),infoOut1(2),pa
rtocOut);
   fprintf(fileID,...
      '%1i %3i %10.6f %3i %3i %10.6f %10.3f %10.3f %10.3f %7.3f %7.3f %7.3f %7.3f %7.3f
%7.3f %11.3f %6i %9.3f %9.3f\n',...

sID,1,RSSOut,ypenOut,offpenOut,f1,y1,maxOff(min(pmaxi(y1)),y1),infoOut1(1),infoOut1(2),pa
rtocOut);
end
fclose(fileID);

% -- shut down parallel pools
poolobj = gcp('nocreate')
delete(poolobj);
```

```
%%%%%%%%%%%%%%%%%%%%%%%%%%%%
%
% EXAMPLE OF NELDER-MEAD ALGORITHM:
%
% INPUTS:
% > f:        INITIAL FUNCTION VALUES
% > Y:        INITIAL ABCHI PARAMETER VALUES
% > SrcX:     SOURCE OFFSETSS
% > RcvrZ:    RECEIVER DEPTHS
% > tt:       TRAVELTIMES
% > z:        INTERFACE DEPTHS
%
% OUTPUTS:
% > infoOut:  NUMBER OF ITERATIONS AND DURATION
% > fOut:     OUTPUTTED FUNCTION VALUES
% > YOut:     OUTPUTTED ABCHI VALUES
%%%%%%%%%%%%%%%%%%%%%%%%%%%%
function [infoOut,fOut,YOut] = NMalgorithm_3lyr(f,Y,SrcX,RcvrZ,tt,z)

  % -- specify number of parameters to optimize
  np1 = length(f);           % n+1 vertices in simplex
  n = np1-1;                 % n parameters to optimize

  % -- specify scaling parameters:
  % standard Nelder-Mead simplex;
  % reflection; expansion; contraction; shrink;
  % alpha = 1; beta = 2; gamma = 0.5; delta = 0.5;
  % adaptive Nelder-Mead simplex (Gao and Han, 2010);
  alpha = 1; beta = 1+2/n; gamma = 0.75 - 1/(2*n); delta = 1-1/n;


  % -- initialize Nelder-Mead settings
  tol = abs(f(1)-f(np1));        % size of simplex
  tol_prev = 1;                  % initialze previous size of simplex
  iter = 1;                      % iteration variable
  reportID = 0;                  % used to identify NM step
  tic                            % begin counter
  % -- begin Nelder-Mead optimization
  while tol > eps % while loop that runs while tolerance is greater than machine precision

    % -- Order n+1 vertices in ascending order
    [fSort,fSortID] = sort(abs(f));    % sort function values
    YSort = Y(fSortID,:);              % index abchi by sorting

    % -- specify Nelder-Mead step based on reportID
    if iter > 1

      % -- progress identification chart
```

```
        if reportID == 1
            NMstep = 'reflection';
        elseif reportID == 21
            NMstep = 'expansion';
        elseif reportID == 22
            NMstep = 'reflection';
        elseif reportID == 31
            NMstep = 'outside contraction';
        elseif reportID == 32
            NMstep = 'inside contraction';
        elseif reportID == 4
            NMstep = 'shrink';
        else
            % -- algorithm error
            NMstep = 'error';
            return
        end
    end

    % -- reset reportID
    reportID = 0;

    % -- print report to command window
    if iter == 1
        tic
        fprintf("iter: %i | tol: %0.8g\n",iter,abs(fSort(1)-fSort(np1)));
        vpa([fSort YSort],16)
    elseif mod(iter,1000) == 0
        timeOut = toc;
        fprintf("iter: %i | %s | tol: %0.8g | time: %i | time/iter: %0.4f\n",iter,NMstep,abs(fSort(1)-
fSort(np1)),round(timeOut),timeOut/iter);
        vpa([fSort YSort],16)

    end

    % -- calculate centroid
    yc = (sum(YSort(1:n,:))./n)';       % average of first n vertices
    ynp1 = YSort(np1,:)';               % n+1 vertex

    % -- calculate reflect
    yr = yc + alpha.*(yc - ynp1);
    [RSSOut,ypenOut,offpenOut] = tRSS_stats_3lyr(SrcX,RcvrZ,tt,yr,z);
    fr = sum([RSSOut;ypenOut;offpenOut]);

    % -- Nelder-Mead if structure to determine step
    if fSort(1) <= fr && fr < fSort(n)

        % -- accept reflected point
```

```
    YSort(np1,:) = yr;
    reportID = 1;

elseif fr < fSort(1)

    % -- calculate expansion point
    ye = yc + beta.*(yr - yc);
    [RSSOut,ypenOut,offpenOut] = tRSS_stats_3lyr(SrcX,RcvrZ,tt,ye,z);
    fe = sum([RSSOut;ypenOut;offpenOut]);

    if fe <= fr

        % -- accept expansion point
        YSort(np1,:) = ye;
        reportID = 21;

    else

        % -- accept reflected point
        YSort(np1,:) = yr;
        reportID = 22;

    end

elseif fr >= fSort(n)

    if fSort(n) <= fr && fr < fSort(np1)
        % -- calculate outside contraction point
        yoc = yc + gamma.*(yr - yc);
        [RSSOut,ypenOut,offpenOut] = tRSS_stats_3lyr(SrcX,RcvrZ,tt,yoc,z);
        foc = sum([RSSOut;ypenOut;offpenOut]);

        if foc <= fr

            % -- accept outside contraction point
            YSort(np1,:) = yoc;
            reportID = 31;

        end

    else

        % -- calculate inside contraction point
        yic = yc - gamma.*(yr - yc);
        [RSSOut,ypenOut,offpenOut] = tRSS_stats_3lyr(SrcX,RcvrZ,tt,yic,z);
        fic = sum([RSSOut;ypenOut;offpenOut]);

        if fic <= fSort(np1)
```

```
        % -- accept inside contraction point
        YSort(np1,:) = yic;
        reportID = 32;

      end

    end
  end

  if YSort == Y(fSortID,:)
    % if simplex has not been updated, trigger shrink
    % -- accept shrink
    for ii = 2:np1
      YSort(ii,:) =  YSort(1,:) + delta.*(YSort(ii,:) - YSort(1,:));
    end
    reportID = 4;

  end

  % -- prepare abchi values for update
  Y = YSort;
  f = fSort;

  if reportID == 0
    % if reportID has not been changed, error somehow...
    % -- algorithm fail safe
    fprintf("reportID == 0\n >> return\n")
    return
  elseif reportID == 4
    % shrink has been triggered
    % -- update vertices 2 to n+1 with shrink
    for ii = 2:np1
      yi = transpose(Y(ii,:));
      [RSSOut,ypenOut,offpenOut] = tRSS_stats_3lyr(SrcX,RcvrZ,tt,yi,z);
      f(ii,1) = sum([RSSOut;ypenOut;offpenOut]);
    end

  else
    % reflect, expand, or contract has been triggered
    % -- update n+1 vertex
    ynp1 = transpose(Y(np1,:));
    [RSSOut,ypenOut,offpenOut] = tRSS_stats_3lyr(SrcX,RcvrZ,tt,ynp1,z);
    f(np1,1) = sum([RSSOut;ypenOut;offpenOut]);

  end

  % -- calculate tolerance values for termination conditions
  fSort = sort(abs(f));
```

```
        tol = abs(fSort(1)-fSort(np1));

        % -- termination condition: relative improvement
        if abs(tol-tol_prev) < eps
            fprintf("\niter: %i\n",iter);
            fprintf("tol: %0.20f\n",tol);
            fprintf("tol_prev: %0.20f\n",tol_prev);
            fprintf("abs(tol-tol_prev): %0.20f\n",abs(tol-tol_prev));
            break
        end

        % -- termination condition: iterations
        if iter > 25000
            fprintf("iter > 25000\n");
            break
        end

        % -- update for next iteration
        tol_prev = tol;
        iter = iter + 1;


    end

    % -- final sorting and update before exit Nelder-Mead optimization
    [fOut,fSortID] = sort(abs(f));
    YOut = Y(fSortID,:);
    infoOut(1) = iter;      % output number of iterations
    tocOut = toc;
    infoOut(2) = tocOut;    % output duration

end
```

```
%%%%%%%%%%%%%%%%%%%%%%%%%%%%
%
% EXAMPLE OF OPTIMIZATION STATS FUNCTION USED IN NELDER-MEAD
OPTIMIZATION:
%
% INPUTS:
% > SrcX:      SOURCE OFFSETS
% > RcvrZ:     RECEIVER DEPTHS
% > ttmeas:    TRAVELTIMES
% > y:         ABCHI VALUES
% > z:         INTERFACE DEPTHS
%
% OUTPUTS:
% > RSS:       RESIDUAL SUM OF SQUARES
% > ypen:      ABCHI PARAMETER PENALTIES
% > offPen:    OFFSET PENALTIES
%%%%%%%%%%%%%%%%%%%%%%%%%%%%
function [RSS,ypen,offPen] = tRSS_stats_3lyr(SrcX,RcvrZ,tt,y,z)

  % -- maximum ray parameter value
  pmaxi = [ ... % maximum ray parameter value in each square root
    1/sqrt(y(1)^2*(1+2*y(7))); ...
    1/sqrt(y(2)^2*(1+2*y(8))); ...
    1/sqrt(y(3)^2*(1+2*y(9))); ...
    1/sqrt((y(1)+y(4)*(z(2)-z(1)))^2*(1+2*y(7))); ...
    1/sqrt((y(2)+y(5)*(z(3)-z(2)))^2*(1+2*y(8))); ...
    1/sqrt((y(3)+y(6)*(RcvrZ(1)-z(3)))^2*(1+2*y(9)))] - eps;
  pmax = min(pmaxi); % minimum of the possible maximum ray parameter values

  % -- ray tracing for each source offset
  x0x1x2IntTemp = zeros(size(SrcX,1),6);  % initialize memory for each horizontal intercept
  for offSetID = 1:size(SrcX,1)

    if real(p_fun_3lyr(-pmax,y,z,SrcX(offSetID),RcvrZ(offSetID))) < 0
      % since SrcX > 0 and RcvrZ at x=0, ray is traced to the left
      % maximum horizontal offset must be traceable to beyond x=0

      % -- calculate ray parameter if traceable
      rayParam_fzero = fzero(@(p) real(p_fun_3lyr(p,y,z,SrcX(offSetID),RcvrZ(offSetID))),[-
pmax eps]);
      exitflag = 1;

    else
      % Since NM is unconstrained, we can only penalize by increasing
      % function values. In this case, the ray cannot be traced from
      % source to reciever without breaking model. Thus, we assign a
      % generic ray parameter and flag offsetID as not traceable
      rayParam_fzero = -pmax/2;
```

```
            exitflag = -6;

        end

        % -- calculate x intercepts based on ray parameter value
        p = rayParam_fzero;
        x1Int = SrcX(offSetID) + ... % ray tracing expression (layer 1)
            (sqrt(1-p.^2.*y(1).^2.*(1+2.*y(7))) - sqrt(1-p.^2.*(y(1) + y(4).*(z(2)-
z(1))).^2.*(1+2.*y(7))))./(p.*y(4));
        x2Int = x1Int + ... % ray tracing expression (layer 2)
            (sqrt(1-p.^2.*y(2).^2.*(1+2.*y(8))) - sqrt(1-p.^2.*(y(2) + y(5).*(z(3)-
z(2))).^2.*(1+2.*y(8))))./(p.*y(5));
        xFinal = x2Int + ... % ray tracing expression (layer 3)
            (sqrt(1-p.^2.*y(3).^2.*(1+2.*y(9))) - sqrt(1-p.^2.*(y(3) + y(6).*(RcvrZ(offSetID)-
z(3))).^2.*(1+2.*y(9))))./(p.*y(6));
        % assign source, xints, final x, ray parameter, and exit flag
        x0x1x2IntTemp(offSetID,1:6) = [SrcX(offSetID) x1Int x2Int real(xFinal) rayParam_fzero
exitflag];

    end

    % -- calculate traveltimes given xintercepts
    ttOut = real(tCalculate_3lyr(y,x0x1x2IntTemp));

    if sum(isreal(ttOut)) == 0
        % -- fail safe to ensure real traveltimes
        fprintf("sum(isreal(ttOut)) == 0\n");
        return

    end

    % -- calculate RSS
    RSS = sum((tt-ttOut).^2);

    % -- calculate parameter penalties
    ypen = ypen_3lyr(y);

    % -- calculate offset penalty
    offPen = sum(logical(x0x1x2IntTemp(:,6)<1));

end
```

```
%%%%%%%%%%%%%%%%%%%%%%%%%%%%
%
% EXAMPLE OF RAY PARAMETER FUNCTION USED IN NELDER-MEAD
OPTIMIZATION:
%
% INPUTS:
% > p:        RAY PARAMETER
% > y:        ABCHI VALUES
% > z:        INTERFACE DEPTHS
% > SrcXID:   SPECIFIED SOURCE OFFSET
% > RcvrZID:  SPECIFIED RECEIVER DEPTH
%
% OUTPUTS:
% > p_fun_Out:  DISTANCE BETWEEN MODEL AND INPUT SOURCE OFFSET
%%%%%%%%%%%%%%%%%%%%%%%%%%%%
function p_fun_Out = p_fun_3lyr(p,y,z,SrcXID,RcvrZID)

   % Since ray parameter is constant along a ray, we trace along the arc
   % of an ellipse in each layer that is connected across all three
   % layers. Given a set of abchi values, we calculate the horizontal
   % distance travelled for a specified p value. Since SrcXID > 0 and ray
   % is traced to the left, a solution is if the sum below equals zero

   p_fun_Out = SrcXID + (...
           (sqrt(1-p.^2.*y(1).^2.*(1+2.*y(7))) - sqrt(1-p.^2.*(y(1) + y(4).*(z(2)-
z(1))).^2.*(1+2.*y(7))))./(p.*y(4)) + ...
           (sqrt(1-p.^2.*y(2).^2.*(1+2.*y(8))) - sqrt(1-p.^2.*(y(2) + y(5).*(z(3)-
z(2))).^2.*(1+2.*y(8))))./(p.*y(5)) + ...
           (sqrt(1-p.^2.*y(3).^2.*(1+2.*y(9))) - sqrt(1-p.^2.*(y(3) + y(6).*(RcvrZID-
z(3))).^2.*(1+2.*y(9))))./(p.*y(6)));
end

%%%%%%%%%%%%%%%%%%%%%%%%%%%%
%
% EXAMPLE OF TRAVELTIME FUNCTION USED IN NELDER-MEAD OPTIMIZATION:
%
% INPUTS:
% > y:        ABCHI VALUES
% > xInts:    RAY TRACING INFORMATION
%
% OUTPUTS:
% > tOut:     OUTPUT TRAVELTIMES
%%%%%%%%%%%%%%%%%%%%%%%%%%%%
function tOut = tCalculate_3lyr(y,xInts)

   % -- initialize x intercept values
   SrcX = xInts(:,1);
   x1 = xInts(:,2);
```

```
   x2 = xInts(:,3);
   x3 = xInts(:,4);
   p = xInts(:,5);

   % -- allocate memory and perform traveltime calculations
   % sum of traveltime expressions in each layer for a given ray tracing
   ttOut = zeros(size(SrcX,1),1);
   for ii = 1:size(ttOut,1)
      ttOut(ii) = ...
         (1/y(4)).*(atanh(p(ii).*y(4).*(x1(ii)-SrcX(ii))-sqrt(1-
(1+2.*y(7)).*p(ii).^(2).*y(1).^2))+atanh(sqrt(1-(1+2.*y(7)).*p(ii).^(2).*y(1).^2))) + ...
         (1/y(5)).*(atanh(p(ii).*y(5).*(x2(ii)-x1(ii))  -sqrt(1-
(1+2.*y(8)).*p(ii).^(2).*y(2).^2))+atanh(sqrt(1-(1+2.*y(8)).*p(ii).^(2).*y(2).^2))) + ...
         (1/y(6)).*(atanh(p(ii).*y(6).*(x3(ii)-x2(ii))  -sqrt(1-
(1+2.*y(9)).*p(ii).^(2).*y(3).^2))+atanh(sqrt(1-(1+2.*y(9)).*p(ii).^(2).*y(3).^2)));
   end

   % -- pass traveltimes to output
   tOut = ttOut;

end

%%%%%%%%%%%%%%%%%%%%%%%%%%%
%
% EXAMPLE OF PARAMETER PENALTY FUNCTION USED IN NELDER-MEAD
OPTIMIZATION:
%
% INPUTS:
% > y:        ABCHI VALUES
%
% OUTPUTS:
% > pen_Out:    OUTPUTTED PARAMETER PENALTIES
%
%%%%%%%%%%%%%%%%%%%%%%%%%%%
function pen_Out = ypen_3lyr(y)

   % -- each parameter penalized beyond the lower/upper bounds specified
   % a1:    800+du / 2000-du
   % a2:   1600+du / 4000-du
   % a3:   2000+du / 4000-du
   % b1-3:    0+du /  1.5-du
   % chi1:    0+du /  0.1-du
   % chi2:    0+du /  0.2-du
   % chi3:    0+du /  0.3-du

   % if abchi values are within the bounds, the penalty equals zero.
   % Otherwise, the penalties increase exponentially
```

```
    du = 1e-3;
    pen_Out = ...
        (exp(-(y(1)-(800+du))).*((800+du)>y(1)) + exp(y(1)-(2000-du)).*(y(1)>(2000-du))) + ...
        (exp(-(y(2)-(1600+du))).*((1600+du)>y(2)) + exp(y(2)-(4000-du)).*(y(2)>(4000-du))) + ...
        (exp(-(y(3)-(2000+du))).*((2000+du)>y(3)) + exp(y(3)-(4000-du)).*(y(3)>(4000-du))) + ...
        (exp(-(y(4)-(du))).*((du)>y(4)) + exp(y(4)-(1.5-du)).*(y(4)>(1.5-du))) + ...
        (exp(-(y(5)-(du))).*((du)>y(5)) + exp(y(5)-(1.5-du)).*(y(5)>(1.5-du))) + ...
        (exp(-(y(6)-(du))).*((du)>y(6)) + exp(y(6)-(1.5-du)).*(y(6)>(1.5-du))) + ...
        (exp(-(y(7)-(du))).*((du)>y(7)) + exp(y(7)-(0.1-du)).*(y(7)>(0.1-du))) + ...
        (exp(-(y(8)-(du))).*((du)>y(8)) + exp(y(8)-(0.2-du)).*(y(8)>(0.2-du))) + ...
        (exp(-(y(9)-(du))).*((du)>y(9)) + exp(y(9)-(0.3-du)).*(y(9)>(0.3-du)));

end

%%%%%%%%%%%%%%%%%%%%%%%%%%%%%%%%%%%%%%%%%%%%%%%%%%%%%%%%%%
```

APPENDIX B: VSP DATA

B.1 ZVSP interval velocities

To obtain exponentially smoothed interval velocities we use

$$(v_{smt})_i = \alpha(v_{int})_i + (1-\alpha)((v_{smt})_{i-1},$$

where v_{smt} is the smoothed velocity, v_{int} is the interval velocity, $\alpha = 0.2$ is the smoothing factor, $0 \leq \alpha \leq 1$, and $i = 2,3,4 \ldots n$ for n interval velocity values.

For Tables B.1 to B.4, depths are referenced from mean sea level (MSL). Source depth is 6.0 m. Sea-floor is at 130.8 m depth.

Table B.1: Smoothed interval velocities.

Depth (MSL) (m)	Traveltime (ms)	Interval velocity (ms^{-1})	Smoothed interval velocity (ms^{-1})
130.8	85.8	1524.0	1524.0
418.6	251.7	1735.2	1566.2
463.1	275.1	1894.9	1632.0
507.4	297.9	1945.9	1694.8
595.1	344.9	1865.7	1729.0
681.5	388.1	2003.3	1783.8
738.1	414.6	2130.8	1853.2
820.9	453.1	2151.0	1912.8
901.3	491.2	2112.3	1952.7
953.0	514.4	2235.1	2009.2
1014.7	544.4	2050.0	2017.3
1119.9	589.0	2357.9	2085.4
1205.0	625.2	2350.7	2138.5
1264.0	651.8	2220.0	2154.8
1343.4	685.2	2375.4	2198.9
1362.8	694.4	2116.2	2182.4
1381.9	702.3	2445.6	2235.0
1400.9	709.8	2521.2	2292.2
1419.6	717.6	2373.0	2308.4
1438.1	725.0	2533.2	2353.4
1456.6	733.4	2183.8	2319.4
1475.2	740.4	2654.7	2386.5
1494.2	748.1	2486.0	2406.4
1513.9	755.9	2533.3	2431.8
1534.1	764.9	2239.7	2393.4
1554.6	773.7	2312.1	2377.1
1574.9	781.3	2670.8	2435.9
1595.1	789.6	2450.0	2438.7
1615.2	797.1	2691.1	2489.2
1635.4	805.1	2514.7	2494.3
1655.5	813.2	2495.2	2494.4
1675.6	820.6	2717.5	2539.1
1695.9	827.7	2841.1	2599.5
1716.1	835.7	2534.5	2586.5
1736.2	843.4	2596.9	2588.6
1756.4	852.1	2335.0	2537.8
1776.4	859.8	2565.8	2543.4
1796.6	867.6	2606.4	2556.0
1816.9	875.9	2427.1	2530.2
1837.1	884.5	2365.1	2497.2
1857.3	892.2	2641.7	2526.1
1877.6	899.8	2670.7	2555.0
1897.8	907.9	2475.5	2539.1
1917.8	915.0	2796.6	2590.6
1938.0	922.6	2676.6	2607.8
1958.1	930.7	2471.5	2580.5
1977.9	938.0	2706.5	2605.7
1997.7	945.8	2552.3	2595.0
2017.9	953.1	2749.5	2625.9
2038.5	961.5	2466.8	2594.1
2059.2	969.6	2542.6	2583.8
2079.8	976.9	2861.5	2639.4
2100.3	984.1	2821.1	2675.7
2120.8	991.7	2718.0	2684.2
2141.2	999.4	2632.5	2673.8
2161.5	1006.4	2884.6	2716.0
2181.8	1013.6	2818.8	2736.6
2202.0	1020.7	2863.2	2761.9

B.2 WVSP traveltimes

Receiver and source depths are referenced from mean sea level (MSL). Source depths are 6.0 m. Source offsets are denoted positive on the longside and negative on the shortside.

Table B.2: Receiver depths and source spreads for walkaway-VSP. (Modified from Kaderali, 2009)

Receiver No.	Depth (m)	Longside		Shortside	
		Far offset (m)	Near offset (m)	Near offset (m)	Far offset (m)
1	1979.92	3964.13	74.74	-76.92	-1014.08
2	1989.81	3969.12	66.31	-66.46	-1008.35
3	1999.70	3974.14	56.20	-61.00	-1002.71
4	2009.76	3979.26	46.36	-50.09	-997.09
5	2019.93	3984.40	37.13	-39.17	-991.55

B.2.1 Longside

Table B.3: Walkaway-VSP longside traveltimes. (Modified from Kaderali, 2009)

Receiver Depth: 1979.923 m								
Source No.	Source offset (m)	Traveltime (s)	Source No.	Source offset (m)	Traveltime (s)	Source No.	Source offset (m)	Traveltime (s)
1	74.741	0.935336	47	1165.295	1.065256	93	2313.522	1.354231
2	84.530	0.935707	48	1187.085	1.070389	94	2338.818	1.361689
3	93.234	0.935612	49	1214.352	1.075694	95	2364.031	1.368898
4	112.705	0.936244	50	1238.248	1.080502	96	2387.757	1.376166
5	130.648	0.936110	51	1262.578	1.085769	97	2414.140	1.384134
6	152.613	0.937377	52	1288.093	1.092119	98	2438.493	1.389482
7	176.332	0.938209	53	1312.260	1.097591	99	2462.794	1.396500
8	200.664	0.939183	54	1337.566	1.102887	100	2487.398	1.404673
9	222.033	0.940566	55	1366.579	1.110075	101	2515.010	1.412021
10	244.406	0.941458	56	1386.806	1.113877	102	2538.668	1.420411
11	270.447	0.942481	57	1413.235	1.120171	103	2561.908	1.425506
12	293.032	0.944033	58	1434.249	1.125078	104	2586.946	1.432678
13	317.805	0.945562	59	1457.820	1.129865	105	2611.466	1.439409
14	343.415	0.947720	60	1485.368	1.136798	106	2634.472	1.447930
15	369.719	0.949464	61	1513.211	1.143508	107	2664.740	1.457009

16	393.092	0.952038	62	1539.303	1.149417	108	2693.145	1.465913
17	417.457	0.953379	63	1565.130	1.154933	109	2713.475	1.471688
18	443.392	0.956346	64	1588.644	1.160874	110	2737.504	1.478316
19	465.151	0.958015	65	1612.475	1.167062	111	2763.498	1.486156
20	493.184	0.960078	66	1638.883	1.173549	112	2790.900	1.492776
21	515.711	0.963346	67	1663.079	1.178955	113	2818.515	1.501544
22	541.511	0.965572	68	1689.771	1.185425	114	2840.130	1.509010
23	566.218	0.968150	69	1711.871	1.191324	115	2867.558	1.516612
24	594.084	0.971846	70	1739.048	1.197521	116	2891.097	1.522475
25	616.525	0.974437	71	1763.081	1.203817	117	2913.083	1.527969
26	640.390	0.977709	72	1789.370	1.210837	118	2936.480	1.537739
27	666.096	0.980848	73	1814.387	1.217784	119	2963.685	1.544497
28	686.674	0.983892	74	1836.461	1.223474	120	2985.984	1.551710
29	714.131	0.987625	75	1863.985	1.231080	121	3013.154	1.560112
30	734.065	0.990735	76	1888.688	1.235614	122	3037.280	1.566471
31	763.765	0.994462	77	1912.386	1.242405	123	3062.143	1.575806
32	790.341	0.998943	78	1936.696	1.250340	124	3087.867	1.582710
33	818.537	1.002359	79	1962.993	1.255989	125	3113.355	1.587800
34	838.613	1.006107	80	1986.236	1.262363	126	3137.870	1.597852
35	864.183	1.009904	81	2011.513	1.269025	127	3163.910	1.605218
36	889.644	1.015459	82	2038.012	1.276389	128	3187.722	1.614170
37	916.870	1.018333	83	2058.654	1.281452	129	3214.578	1.620041
38	938.114	1.022636	84	2089.406	1.291095	130	3236.351	1.627195
39	967.871	1.028093	85	2113.127	1.297340	131	3259.675	1.634435
40	984.094	1.032088	86	2137.010	1.304095	132	3288.287	1.645422
41	1014.404	1.035925	87	2162.001	1.308005	133	3312.831	1.651273
42	1043.220	1.041995	88	2190.353	1.318307	134	3338.804	1.660710
43	1065.184	1.046384	89	2208.538	1.324103	135	3361.215	1.665429
44	1088.895	1.050471	90	2240.131	1.332692	136	3387.640	1.674863
45	1115.015	1.055210	91	2262.848	1.340505	137	3405.836	1.681033
46	1140.098	1.060235	92	2285.069	1.346629	138	3438.279	1.690683
Receiver Depth: 1989.809 m								
Source No.	Source offset (m)	Traveltime (s)	Source No.	Source offset (m)	Traveltime (s)	Source No.	Source offset (m)	Traveltime (s)
1	66.310	0.939227	47	1169.907	1.069724	93	2318.389	1.357301
2	78.328	0.939527	48	1191.722	1.074964	94	2343.698	1.365345
3	89.803	0.939563	49	1219.006	1.080203	95	2368.914	1.372069
4	111.608	0.940394	50	1242.914	1.084769	96	2392.644	1.379635
5	130.642	0.940091	51	1267.262	1.090486	97	2419.031	1.386817

6	153.154	0.941688	52	1292.784	1.096443	98	2443.401	1.392626
7	177.687	0.942350	53	1316.929	1.101800	99	2467.697	1.400358
8	202.354	0.943109	54	1342.261	1.107092	100	2492.313	1.408040
9	224.320	0.944924	55	1371.339	1.113786	101	2519.922	1.415364
10	247.111	0.945205	56	1391.577	1.118027	102	2543.581	1.422726
11	273.339	0.946366	57	1418.030	1.124079	103	2566.833	1.429279
12	296.045	0.947988	58	1439.032	1.129362	104	2591.883	1.436051
13	321.033	0.949649	59	1462.608	1.134666	105	2616.403	1.443447
14	346.827	0.952137	60	1490.113	1.140644	106	2639.425	1.451370
15	373.160	0.953549	61	1517.949	1.147233	107	2669.654	1.459092
16	396.718	0.955886	62	1544.086	1.153155	108	2698.020	1.468384
17	421.107	0.957665	63	1569.900	1.158895	109	2718.334	1.472716
18	447.157	0.960745	64	1593.404	1.164270	110	2742.351	1.481698
19	469.001	0.962260	65	1617.242	1.170602	111	2768.347	1.489435
20	497.013	0.964153	66	1643.658	1.177444	112	2795.751	1.496836
21	519.641	0.967471	67	1667.848	1.182653	113	2823.373	1.504003
22	545.499	0.969745	68	1694.537	1.189136	114	2845.001	1.510775
23	570.228	0.972201	69	1716.647	1.194793	115	2872.444	1.517430
24	598.156	0.975986	70	1743.842	1.201199	116	2895.995	1.527097
25	620.641	0.978617	71	1767.872	1.207696	117	2917.992	1.531993
26	644.580	0.981874	72	1794.159	1.214073	118	2941.398	1.540569
27	670.325	0.985060	73	1819.208	1.220868	119	2968.622	1.546735
28	691.031	0.988157	74	1841.269	1.226550	120	2990.918	1.553385
29	718.482	0.991753	75	1868.805	1.233862	121	3018.090	1.561528
30	738.482	0.994879	76	1893.512	1.240130	122	3042.218	1.568398
31	768.171	0.998693	77	1917.232	1.246604	123	3067.084	1.576207
32	794.790	1.002989	78	1941.535	1.253548	124	3092.811	1.585550
33	822.941	1.006748	79	1967.839	1.259847	125	3118.302	1.590731
34	843.036	1.010184	80	1991.090	1.265565	126	3142.820	1.600101
35	868.614	1.013894	81	2016.374	1.273312	127	3168.861	1.608303
36	894.119	1.019595	82	2042.866	1.280025	128	3192.675	1.615857
37	921.307	1.022321	83	2063.524	1.285407	129	3219.534	1.622663
38	942.569	1.027050	84	2094.281	1.294071	130	3241.315	1.631572
39	972.347	1.032722	85	2117.996	1.299952	131	3264.630	1.638071
40	988.598	1.036735	86	2141.883	1.307700	132	3293.246	1.647669
41	1018.913	1.040235	87	2166.886	1.310301	133	3317.799	1.653441
42	1047.728	1.045885	88	2195.224	1.323274	134	3343.766	1.662421
43	1069.727	1.050348	89	2213.413	1.327841	135	3366.177	1.667257
44	1093.448	1.054671	90	2245.016	1.336037	136	3392.607	1.675520

45	1119.573	1.059151	91	2267.713	1.343859	137	3410.802	1.681964
46	1144.664	1.064439	92	2289.923	1.348996	138	3443.246	1.691929
Receiver Depth: 1999.699 m								
Source No.	Source offset (m)	Traveltime (s)	Source No.	Source offset (m)	Traveltime (s)	Source No.	Source offset (m)	Traveltime (s)
1	58.722	0.942353	54	1347.028	1.110953	107	2674.605	1.462258
2	73.252	0.942618	55	1376.170	1.117626	108	2702.929	1.470753
3	87.620	0.942868	56	1396.418	1.121891	109	2723.228	1.476894
4	111.582	0.943735	57	1422.895	1.128178	110	2747.233	1.483652
5	131.554	0.943171	58	1443.884	1.132653	111	2773.232	1.491746
6	154.473	0.945169	59	1467.463	1.138044	112	2800.637	1.498916
7	179.703	0.945881	60	1494.924	1.144481	113	2828.265	1.506587
8	204.619	0.946732	61	1522.751	1.151295	114	2849.906	1.514083
9	227.115	0.948627	62	1548.932	1.156979	115	2877.363	1.521606
10	250.268	0.949125	63	1574.732	1.162905	116	2900.926	1.528903
11	276.636	0.950368	64	1598.225	1.168160	117	2922.933	1.535242
12	299.430	0.952101	65	1622.070	1.174337	118	2946.349	1.542711
13	324.600	0.953662	66	1648.491	1.180674	119	2973.590	1.550466
14	350.549	0.955781	67	1672.676	1.186362	120	2995.885	1.557133
15	376.889	0.957374	68	1699.359	1.192925	121	3023.058	1.565767
16	400.611	0.960273	69	1721.478	1.198836	122	3047.187	1.573079
17	425.009	0.961745	70	1748.692	1.204910	123	3072.056	1.580030
18	451.156	0.964632	71	1772.717	1.211548	124	3097.786	1.588145
19	473.074	0.966243	72	1799.002	1.217934	125	3123.280	1.595589
20	501.052	0.968510	73	1824.082	1.224612	126	3147.799	1.603017
21	523.771	0.971570	74	1846.130	1.230545	127	3173.841	1.610568
22	549.677	0.973782	75	1873.676	1.237567	128	3197.658	1.618286
23	574.419	0.976722	76	1898.386	1.244110	129	3224.520	1.625947
24	602.401	0.980039	77	1922.128	1.250350	130	3246.308	1.633840
25	624.922	0.982692	78	1946.425	1.256844	131	3269.615	1.641181
26	648.928	0.985882	79	1972.733	1.263463	132	3298.234	1.648665
27	674.706	0.988900	80	1995.992	1.269489	133	3322.795	1.656675
28	695.534	0.992308	81	2021.284	1.276605	134	3348.757	1.664216
29	722.973	0.995547	82	2047.768	1.283477	135	3371.168	1.670785
30	743.035	0.998774	83	2068.441	1.289092	136	3397.601	1.678696
31	772.708	1.002640	84	2099.202	1.297742	137	3415.795	1.685196
32	799.365	1.007501	85	2122.910	1.304563	138	3448.241	1.694415
33	827.466	1.010404	86	2146.801	1.310749	139	3472.837	1.701577
34	847.578	1.014153	87	2171.815	1.314782	140	3498.606	1.710192

35	873.161	1.017853	88	2200.140	1.325703	141	3522.813	1.717371
36	898.705	1.023541	89	2218.331	1.331626	142	3549.675	1.725993
37	925.852	1.026076	90	2249.944	1.339540	143	3572.790	1.733222
38	947.130	1.030365	91	2272.620	1.346336	144	3596.293	1.739830
39	976.925	1.036107	92	2294.818	1.352489	145	3624.682	1.748377
40	993.203	1.040563	93	2323.298	1.360202	146	3649.510	1.756174
41	1023.519	1.044037	94	2348.619	1.368284	147	3674.382	1.763768
42	1052.331	1.049905	95	2373.838	1.375471	148	3696.833	1.770490
43	1074.363	1.054403	96	2397.572	1.382493	149	3725.141	1.779702
44	1098.092	1.058814	97	2423.962	1.389803	150	3748.488	1.786963
45	1124.219	1.063483	98	2448.348	1.396371	151	3773.125	1.794582
46	1149.317	1.068660	99	2472.638	1.403782	152	3797.180	1.802597
47	1174.603	1.073632	100	2497.266	1.411481	153	3823.886	1.810145
48	1196.443	1.078861	101	2524.872	1.418757	154	3847.157	1.817675
49	1223.741	1.084101	102	2548.532	1.425434	155	3873.904	1.825487
50	1247.658	1.088584	103	2571.795	1.432337	156	3899.011	1.833940
51	1272.022	1.094326	104	2596.858	1.439589	157	3924.745	1.841541
52	1297.550	1.100294	105	2621.377	1.446632	158	3947.236	1.849245
53	1321.672	1.105547	106	2644.413	1.453807	159	3974.137	1.857089
Receiver Depth: 2009.758 m								
Source No.	Source offset (m)	Traveltime (s)	Source No.	Source offset (m)	Traveltime (s)	Source No.	Source offset (m)	Traveltime (s)
1	52.469	0.946447	54	1351.947	1.115153	107	2679.669	1.465704
2	69.671	0.946954	55	1381.150	1.121642	108	2707.953	1.474176
3	86.893	0.947101	56	1401.407	1.126247	109	2728.236	1.480744
4	112.734	0.947711	57	1427.905	1.132330	110	2752.229	1.487699
5	52.469	0.946447	58	1448.880	1.136977	111	2778.230	1.494594
6	69.671	0.946954	59	1472.461	1.142246	112	2805.637	1.502098
7	86.893	0.947101	60	1499.879	1.148672	113	2833.270	1.508771
8	112.734	0.947711	61	1527.695	1.155408	114	2854.923	1.516733
9	133.464	0.947722	62	1553.918	1.161119	115	2882.394	1.525492
10	156.651	0.949129	63	1579.704	1.167420	116	2905.969	1.531940
11	182.453	0.949659	64	1603.186	1.172206	117	2927.986	1.539600
12	207.535	0.950746	65	1627.036	1.178204	118	2951.411	1.546765
13	230.490	0.952851	66	1653.462	1.184507	119	2978.669	1.554718
14	253.949	0.953203	67	1677.641	1.190805	120	3000.961	1.561351
15	280.412	0.954468	68	1704.318	1.197292	121	3028.136	1.568134
16	303.261	0.956100	69	1726.445	1.203018	122	3052.265	1.577714
17	328.581	0.957547	70	1753.676	1.209147	123	3077.138	1.582686

18	354.657	0.959877	71	1777.695	1.215748	124	3102.869	1.590615
19	380.983	0.961524	72	1803.977	1.221607	125	3128.367	1.599738
20	404.849	0.964467	73	1829.087	1.228617	126	3152.887	1.606000
21	429.240	0.965664	74	1851.122	1.234195	127	3178.930	1.613464
22	455.469	0.968875	75	1878.678	1.241198	128	3202.748	1.619519
23	477.448	0.970314	76	1903.390	1.247676	129	3229.613	1.630294
24	505.381	0.972350	77	1927.153	1.254113	130	3251.407	1.636149
25	528.180	0.975954	78	1951.442	1.260869	131	3274.706	1.643357
26	554.124	0.977649	79	1977.755	1.267338	132	3303.329	1.649475
27	578.871	0.980507	80	2001.021	1.273069	133	3327.898	1.657560
28	606.897	0.984222	81	2026.319	1.280433	134	3353.854	1.664552
29	629.448	0.987011	82	2052.794	1.287490	135	3376.264	1.675352
30	653.514	0.990246	83	2073.482	1.293358	136	3402.702	1.680203
31	679.317	0.993458	84	2104.247	1.301024	137	3420.895	1.687718
32	700.261	0.996693	85	2127.948	1.308343	138	3453.340	1.698745
33	727.683	1.000173	86	2151.842	1.314503	139	3477.933	1.705403
34	747.801	1.003167	87	2176.867	1.318469	140	3503.704	1.711605
35	777.454	1.006854	88	2205.177	1.329099	141	3527.909	1.720754
36	804.143	1.011369	89	2223.370	1.334982	142	3554.773	1.729231
37	832.193	1.015020	90	2254.993	1.342631	143	3577.890	1.735458
38	852.318	1.018689	91	2277.647	1.350118	144	3601.391	1.744448
39	877.902	1.022437	92	2299.834	1.357171	145	3629.788	1.751149
40	903.481	1.027936	93	2328.326	1.364622	146	3654.610	1.760526
41	930.585	1.030703	94	2353.659	1.371613	147	3679.484	1.768197
42	951.877	1.035000	95	2378.880	1.379627	148	3701.937	1.775120
43	981.685	1.040677	96	2402.618	1.386764	149	3730.246	1.782591
44	997.988	1.045077	97	2429.010	1.393956	150	3753.592	1.790948
45	1028.302	1.048441	98	2453.412	1.400834	151	3778.230	1.798312
46	1057.108	1.054518	99	2477.697	1.407589	152	3802.290	1.804984
47	1079.172	1.058712	100	2502.335	1.415158	153	3828.996	1.813300
48	1102.905	1.063161	101	2529.938	1.422226	154	3852.268	1.823626
49	1129.033	1.067551	102	2553.598	1.429520	155	3879.018	1.828743
50	1154.135	1.072604	103	2576.873	1.436827	156	3904.126	1.835432
51	1179.462	1.077918	104	2601.946	1.443173	157	3929.863	1.845600
52	1201.324	1.083181	105	2626.465	1.450736	158	3952.356	1.852445
53	1228.635	1.088640	106	2649.516	1.458285	159	3979.256	1.857067
Receiver Depth: 2019.927 m								
Source No.	Source offset (m)	Traveltime (s)	Source No.	Source offset (m)	Traveltime (s)	Source No.	Source offset (m)	Traveltime (s)

1	37.125	0.949931	55	1356.935	1.119047	109	2713.012	1.477709
2	47.917	0.949852	56	1386.199	1.125490	110	2733.279	1.482503
3	67.679	0.950437	57	1406.463	1.130003	111	2757.260	1.489196
4	87.531	0.950647	58	1432.981	1.136112	112	2783.262	1.497292
5	114.917	0.951544	59	1453.941	1.141041	113	2810.670	1.504319
6	136.226	0.951374	60	1477.524	1.145902	114	2838.309	1.512353
7	159.548	0.953025	61	1504.896	1.152406	115	2859.972	1.519220
8	185.804	0.953865	62	1532.702	1.159518	116	2887.458	1.526834
9	210.975	0.954950	63	1558.966	1.164752	117	2911.043	1.534916
10	234.325	0.956605	64	1584.736	1.170728	118	2933.070	1.540726
11	258.040	0.957373	65	1608.206	1.176191	119	2956.504	1.548725
12	284.557	0.958386	66	1632.059	1.182031	120	2983.778	1.555046
13	307.433	0.960111	67	1658.491	1.188399	121	3006.069	1.562470
14	332.872	0.961630	68	1682.662	1.193896	122	3033.245	1.570417
15	359.049	0.963944	69	1709.332	1.200831	123	3057.374	1.578054
16	385.343	0.965418	70	1731.466	1.206627	124	3082.250	1.585655
17	409.334	0.968447	71	1758.713	1.212206	125	3107.982	1.593522
18	433.705	0.969921	72	1782.727	1.218930	126	3133.483	1.600080
19	460.001	0.972838	73	1809.004	1.224991	127	3158.005	1.608654
20	482.029	0.974457	74	1834.144	1.232119	128	3184.048	1.615445
21	509.907	0.976609	75	1856.165	1.237956	129	3207.868	1.623756
22	532.777	0.979967	76	1883.729	1.244659	130	3234.734	1.630595
23	558.748	0.981933	77	1908.443	1.250987	131	3256.536	1.639147
24	583.493	0.985107	78	1932.226	1.257720	132	3279.827	1.646444
25	611.554	0.988531	79	1956.508	1.264184	133	3308.451	1.654579
26	634.129	0.991086	80	1982.824	1.270513	134	3333.029	1.662212
27	658.248	0.994422	81	2006.097	1.276609	135	3358.978	1.669892
28	684.072	0.997434	82	2031.400	1.283866	136	3381.389	1.674585
29	705.124	1.000876	83	2057.867	1.290939	137	3407.830	1.683330
30	732.526	1.004018	84	2078.568	1.296333	138	3426.021	1.689103
31	752.696	1.007432	85	2109.336	1.305118	139	3458.467	1.699251
32	782.323	1.011254	86	2133.030	1.311261	140	3483.057	1.707174
33	809.041	1.015565	87	2156.926	1.317697	141	3508.829	1.714270
34	837.034	1.019073	88	2181.962	1.322426	142	3533.031	1.721476
35	857.170	1.022852	89	2210.257	1.332953	143	3559.898	1.730402
36	882.753	1.026294	90	2228.452	1.338401	144	3583.016	1.738836
37	908.363	1.031885	91	2260.084	1.346712	145	3606.516	1.744451
38	935.422	1.034363	92	2282.716	1.353271	146	3634.919	1.752517
39	956.725	1.038713	93	2304.890	1.359676	147	3659.735	1.760693

40	986.543	1.044700	94	2333.394	1.367060	148	3684.612	1.767779
41	1002.868	1.049014	95	2358.739	1.375573	149	3707.066	1.774926
42	1033.179	1.052495	96	2383.962	1.382318	150	3735.376	1.785556
43	1061.975	1.058421	97	2407.702	1.389120	151	3758.721	1.792247
44	1084.068	1.062677	98	2434.097	1.396500	152	3783.360	1.799150
45	1107.805	1.066960	99	2458.515	1.403233	153	3807.424	1.805479
46	1133.931	1.071377	100	2482.793	1.410509	154	3834.131	1.814840
47	1159.036	1.076518	101	2507.442	1.418106	155	3857.404	1.823009
48	1184.402	1.081816	102	2535.041	1.425056	156	3884.155	1.829612
49	1206.284	1.087232	103	2558.701	1.432211	157	3909.264	1.837849
50	1233.606	1.092486	104	2581.986	1.439055	158	3935.005	1.845303
51	1257.536	1.096881	105	2607.071	1.445480	159	3957.499	1.852544
52	1281.929	1.102535	106	2631.588	1.452599	160	3984.399	1.860716
53	1307.463	1.108661	107	2654.653	1.459835			
54	1331.536	1.113833	108	2684.768	1.469199			

B.2.2 Shortside

Table B.4: Walkaway-VSP shortside traveltimes. (Modified from Kaderali, 2009)

Receiver Depth: 1979.923 m								
Source No.	Source offset (m)	Traveltime (s)	Source No.	Source offset (m)	Traveltime (s)	Source No.	Source offset (m)	Traveltime (s)
1	-76.916	0.935534	15	-373.059	0.949506	29	-716.162	0.987772
2	-82.931	0.935126	16	-394.946	0.951438	30	-740.308	0.991292
3	-94.406	0.935931	17	-418.215	0.953700	31	-765.793	0.994844
4	-119.615	0.936139	18	-444.262	0.955686	32	-788.795	0.998318
5	-136.395	0.936890	19	-469.040	0.958225	33	-816.118	1.002145
6	-151.037	0.937281	20	-489.340	0.960062	34	-841.107	1.005947
7	-182.634	0.937775	21	-515.799	0.963125	35	-864.303	1.010473
8	-201.211	0.938334	22	-538.050	0.966045	36	-889.718	1.014435
9	-225.285	0.940090	23	-568.580	0.968847	37	-915.969	1.018204
10	-246.708	0.941975	24	-591.674	0.971165	38	-941.466	1.023055
11	-275.418	0.943693	25	-617.231	0.975246	39	-966.288	1.027439
12	-297.101	0.944746	26	-642.565	0.977875	40	-989.797	1.031409
13	-324.116	0.946461	27	-663.944	0.980535	41	-1014.078	1.036432
14	-344.072	0.948215	28	-694.514	0.985218			
Receiver Depth: 1989.809 m								

Source No.	Source offset (m)	Traveltime (s)	Source No.	Source offset (m)	Traveltime (s)	Source No.	Source offset (m)	Traveltime (s)
1	-66.459	0.939149	15	-366.440	0.953134	29	-710.170	0.990638
2	-71.966	0.938903	16	-388.454	0.954877	30	-734.346	0.994381
3	-83.743	0.939623	17	-411.844	0.956849	31	-759.852	0.997567
4	-109.503	0.939762	18	-437.891	0.958631	32	-782.892	1.001203
5	-126.875	0.940937	19	-462.703	0.961095	33	-810.244	1.004878
6	-142.494	0.940727	20	-483.059	0.963084	34	-835.240	1.008312
7	-174.105	0.941308	21	-509.525	0.966093	35	-858.483	1.013209
8	-193.088	0.942345	22	-531.796	0.968724	36	-883.891	1.017319
9	-217.478	0.943625	23	-562.487	0.971586	37	-910.130	1.021168
10	-239.050	0.945197	24	-585.598	0.974139	38	-935.676	1.025027
11	-267.858	0.946986	25	-611.188	0.977982	39	-960.508	1.029148
12	-289.835	0.947845	26	-636.545	0.981287	40	-984.043	1.033122
13	-317.048	0.949415	27	-657.899	0.983886	41	-1008.351	1.038840
14	-337.400	0.951426	28	-688.527	0.988177			
Receiver Depth: 1999.699 m								
Source No.	Source offset (m)	Traveltime (s)	Source No.	Source offset (m)	Traveltime (s)	Source No.	Source offset (m)	Traveltime (s)
1	-56.197	0.942147	15	-360.032	0.955795	29	-704.297	0.992892
2	-61.000	0.941890	16	-382.167	0.957363	30	-728.501	0.996141
3	-73.169	0.942483	17	-405.669	0.959313	31	-754.023	0.999276
4	-99.571	0.942953	18	-431.704	0.961216	32	-777.100	1.003557
5	-117.607	0.943475	19	-456.543	0.963431	33	-804.476	1.007059
6	-134.304	0.943874	20	-476.947	0.965518	34	-829.477	1.010589
7	-165.862	0.944430	21	-503.412	0.968550	35	-852.764	1.015012
8	-185.259	0.945197	22	-525.697	0.971431	36	-878.162	1.019032
9	-209.954	0.946459	23	-556.544	0.974146	37	-904.386	1.023126
10	-231.657	0.948256	24	-579.666	0.976420	38	-929.979	1.027610
11	-260.541	0.949642	25	-605.282	0.980150	39	-954.820	1.031448
12	-282.808	0.950759	26	-630.660	0.982786	40	-978.378	1.034722
13	-310.206	0.952081	27	-651.983	0.986067	41	-1002.711	1.040296
14	-330.958	0.953984	28	-682.665	0.990318			
Receiver Depth: 2009.758 m								
Source No.	Source offset (m)	Traveltime (s)	Source No.	Source offset (m)	Traveltime (s)	Source No.	Source offset (m)	Traveltime (s)
1	-46.358	0.946538	15	-353.782	0.959268	29	-698.475	0.995761
2	-50.086	0.945980	16	-376.026	0.960981	30	-722.703	0.999005
3	-62.742	0.946545	17	-399.631	0.962887	31	-748.238	1.002028

4	-89.868	0.947095	18	-425.642	0.964633	32	-771.348	1.005985
5	-108.628	0.947600	19	-450.496	0.966698	33	-798.746	1.009341
6	-126.487	0.948019	20	-470.942	0.969121	34	-823.748	1.012982
7	-157.906	0.948403	21	-497.397	0.971818	35	-847.076	1.017731
8	-177.711	0.949141	22	-519.689	0.974557	36	-872.462	1.021558
9	-202.690	0.950595	23	-550.684	0.977140	37	-898.668	1.025462
10	-224.502	0.952059	24	-573.811	0.979481	38	-924.305	1.029443
11	-253.431	0.953240	25	-599.449	0.983380	39	-949.152	1.033673
12	-275.979	0.954239	26	-624.840	0.985924	40	-972.731	1.037513
13	-303.545	0.955870	27	-646.129	0.988844	41	-997.086	1.042833
14	-324.691	0.957854	28	-676.858	0.993036			
Receiver Depth: 2019.927 m								
Source No.	Source offset (m)	Traveltime (s)	Source No.	Source offset (m)	Traveltime (s)	Source No.	Source offset (m)	Traveltime (s)
1	-39.174	0.949748	15	-370.105	0.963975	29	-717.025	1.001513
2	-52.512	0.950060	16	-393.803	0.966024	30	-742.569	1.004757
3	-80.477	0.950595	17	-419.775	0.967793	31	-765.709	1.008324
4	-100.035	0.951140	18	-444.635	0.970103	32	-793.125	1.011754
5	-119.158	0.951246	19	-465.116	0.971956	33	-818.125	1.015300
6	-150.322	0.951830	20	-491.551	0.974652	34	-841.491	1.019800
7	-170.528	0.952295	21	-513.842	0.977187	35	-866.861	1.023883
8	-195.765	0.953803	22	-544.979	0.980074	36	-893.046	1.027395
9	-217.658	0.955323	23	-568.106	0.982274	37	-918.726	1.031620
10	-246.599	0.956764	24	-593.758	0.986490	38	-943.576	1.035737
11	-269.418	0.957826	25	-619.158	0.988858	39	-967.175	1.039433
12	-297.136	0.959260	26	-640.407	0.991688	40	-991.550	1.044546
13	-318.675	0.960815	27	-671.179	0.995647			
14	-347.762	0.962375	28	-692.777	0.998272			

APPENDIX C: Synthetic Data and Noise

C.1. Synthetic Data

Synthetic traveltimes are computed for a 4-layer model using the expression,

$$t = \sum_{j=1}^{n} \left(\frac{1}{b_j} \{ \tanh^{-1} [\, p b_j (x_{j+1} - x_j) \; - \sqrt{1 - (1 - 2\chi) p^2 {a_j}^2}] + \tanh^{-1} \sqrt{1 - (1 + 2\chi) p^2 {a_j}^2} \} \right),$$

where n is the number of layers and $(x_{j+1} - x_j)$ is the horizontal distance travelled in the jth layer, given by the expression,

$$x_{j+1} - x_j = \frac{1}{p b_j} \left[\sqrt{1 - (1 + 2\chi_j) p^2 {a_j}^2} - \sqrt{1 - (1 + 2\chi_j) p^2 \left(a_j + b_j (z_{j+1} - z_j) \right)^2} \right],$$

where $(z_{j+1} - z_j)$ is the thickness of the layer, p is the ray parameter, and

with the set of the *a, b,* χ values as shown in Table C1.

Table C.1: *a, b,* χ values used to compute synthetic traveltimes, the source is at 6 m depth. Depth of layer-4 is to the receiver, i.e., 1979.923 m, 1989.809 m, 1999.699 m, 2009.758 m, and 2019.927 m, for receivers 1-5 respectively. Depths are referenced from MSL.

Layer	Depth (m)	a (ms^{-1})	b (s^{-1})	χ
1	450	1279.127	0.7761958	0.00000000
2	1300	1747.798	1.0229940	0.01952380
3	1750	2966.244	0.2189034	0.05853239
4	Receiver	2596.646	0.7602582	0.09210773

Noise profiles are computed using the RAND() function in Excel as the seed, limited to $\pm 0.1\%$ of the traveltimes and scaled to the magnitudes as shown in Table C2.

Table C.2: Synthetic traveltimes.

Receiver Depth: 1979.923 m								
Source No.	Source offset (m)	Traveltime (s)	Source No.	Source offset (m)	Traveltime (s)	Source No.	Source offset (m)	Traveltime (s)
1	317.805	0.947417	68	1986.236	1.263938	135	3650.000	1.752552
2	343.415	0.949147	69	2011.513	1.270788	136	3675.000	1.760184
3	369.719	0.951057	70	2038.012	1.278004	137	3700.000	1.767821
4	393.092	0.952869	71	2058.654	1.283648	138	3725.000	1.775460
5	417.457	0.954870	72	2089.406	1.292092	139	3750.000	1.783103
6	443.392	0.957125	73	2113.127	1.298635	140	3775.000	1.790749
7	465.151	0.959116	74	2137.010	1.305247	141	3800.000	1.798399
8	493.184	0.961813	75	2162.001	1.312192	142	3825.000	1.806051
9	515.711	0.964087	76	2190.353	1.320101	143	3850.000	1.813706
10	541.511	0.966806	77	2208.538	1.325191	144	3875.000	1.821363
11	566.218	0.969525	78	2240.131	1.334063	145	3900.000	1.829024
12	594.084	0.972723	79	2262.848	1.340466	146	3925.000	1.836687
13	616.525	0.975399	80	2285.069	1.346746	147	3950.000	1.844352
14	640.390	0.978342	81	2313.522	1.354814	148	3975.000	1.852020
15	666.096	0.981624	82	2338.818	1.362009	149	4000.000	1.859690
16	686.674	0.984332	83	2364.031	1.369201	150	4025.000	1.867363
17	714.131	0.988058	84	2387.757	1.375988	151	4050.000	1.875037
18	734.065	0.990842	85	2414.140	1.383554	152	4075.000	1.882714
19	763.765	0.995112	86	2438.493	1.390557	153	4100.000	1.890392
20	790.341	0.999054	87	2462.794	1.397562	154	4125.000	1.898073
21	818.537	1.003359	88	2487.398	1.404671	155	4150.000	1.905755
22	838.613	1.006500	89	2515.010	1.412668	156	4175.000	1.913440
23	864.183	1.010591	90	2538.668	1.419536	157	4200.000	1.921126
24	889.644	1.014763	91	2561.908	1.426296	158	4225.000	1.928813
25	916.870	1.019332	92	2586.946	1.433594	159	4250.000	1.936503
26	938.114	1.022972	93	2611.466	1.440755	160	4275.000	1.944194
27	967.871	1.028179	94	2634.472	1.447487	161	4300.000	1.951886
28	984.094	1.031071	95	2664.740	1.456361	162	4325.000	1.959580
29	1014.404	1.036572	96	2693.145	1.464707	163	4350.000	1.967275
30	1043.22	1.041918	97	2713.475	1.470690	164	4375.000	1.974971
31	1065.184	1.046066	98	2737.504	1.477773	165	4400.000	1.982669
32	1088.895	1.050616	99	2763.498	1.485448	166	4425.000	1.990368
33	1115.015	1.055711	100	2790.900	1.493552	167	4450.000	1.998068
34	1140.098	1.060684	101	2818.515	1.501733	168	4475.000	2.005770
35	1165.295	1.065757	102	2840.13	1.508145	169	4500.000	2.013472

36	1187.085	1.070206	103	2867.558	1.516293	170	4525.000	2.021176
37	1214.352	1.075852	104	2891.097	1.523296	171	4550.000	2.028880
38	1238.248	1.080870	105	2913.083	1.529845	172	4575.000	2.036586
39	1262.578	1.086045	106	2936.480	1.536822	173	4600.000	2.044292
40	1288.093	1.091543	107	2963.685	1.544945	174	4625.000	2.051999
41	1312.260	1.096814	108	2985.984	1.551611	175	4650.000	2.059707
42	1337.566	1.102400	109	3013.154	1.559743	176	4675.000	2.067416
43	1366.579	1.108885	110	3037.280	1.566971	177	4700.000	2.075126
44	1386.806	1.113455	111	3062.143	1.574429	178	4725.000	2.082836
45	1413.235	1.119488	112	3087.867	1.582153	179	4750.000	2.090547
46	1434.249	1.124332	113	3113.355	1.589814	180	4775.000	2.098258
47	1457.820	1.129814	114	3137.870	1.597190	181	4800.000	2.105971
48	1485.368	1.136286	115	3163.910	1.605032	182	4825.000	2.113683
49	1513.211	1.142895	116	3187.722	1.612210	183	4850.000	2.121397
50	1539.303	1.149149	117	3214.578	1.620312	184	4875.000	2.129111
51	1565.130	1.155396	118	3236.351	1.626886	185	4900.000	2.136825
52	1588.644	1.161131	119	3259.675	1.633934	186	4925.000	2.144540
53	1612.475	1.166988	120	3288.287	1.642587	187	4950.000	2.152255
54	1638.883	1.173530	121	3312.831	1.650016	188	4975.000	2.159970
55	1663.079	1.179570	122	3338.804	1.657884	189	5000.000	2.167686
56	1689.771	1.186283	123	3361.215	1.664677	190	5025.000	2.175402
57	1711.871	1.191880	124	3387.640	1.672692	191	5050.000	2.183119
58	1739.048	1.198808	125	3405.836	1.678215	192	5075.000	2.190835
59	1763.081	1.204977	126	3438.279	1.688068	193	5100.000	2.198552
60	1789.370	1.211768	127	3450.000	1.691629	194	5125.000	2.206270
61	1814.387	1.218272	128	3475.000	1.699230	195	5150.000	2.213987
62	1836.461	1.224043	129	3500.000	1.706835	196	5175.000	2.221705
63	1863.985	1.231279	130	3525.000	1.714444	197	5200.000	2.229422
64	1888.688	1.237812	131	3550.000	1.722057	198	5225.000	2.237140
65	1912.386	1.244112	132	3575.000	1.729675	199	5250.000	2.244858
66	1936.696	1.250606	133	3600.000	1.737297	200	5275.000	2.252576
67	1962.993	1.257667	134	3625.000	1.744922	201	5300.000	2.260294
Receiver Depth: 1989.809 m								
Source No.	Source offset (m)	Traveltime (s)	Source No.	Source offset (m)	Traveltime (s)	Source No.	Source offset (m)	Traveltime (s)
1	321.033	0.951120	68	1991.090	1.267309	135	3675.000	1.761563
2	346.827	0.952867	69	2016.374	1.274149	136	3700.000	1.769196
3	373.160	0.954785	70	2042.866	1.281349	137	3725.000	1.776832
4	396.718	0.956615	71	2063.524	1.286986	138	3750.000	1.784472

5	421.107	0.958622	72	2094.281	1.295417	139	3775.000	1.792115
6	447.157	0.960892	73	2117.996	1.301946	140	3800.000	1.799761
7	469.001	0.962894	74	2141.883	1.308547	141	3825.000	1.807410
8	497.013	0.965592	75	2166.886	1.315483	142	3850.000	1.815062
9	519.641	0.967877	76	2195.224	1.323375	143	3875.000	1.822716
10	545.499	0.970604	77	2213.413	1.328457	144	3900.000	1.830374
11	570.228	0.973326	78	2245.016	1.337318	145	3925.000	1.838034
12	598.156	0.976532	79	2267.713	1.343704	146	3950.000	1.845697
13	620.641	0.979213	80	2289.923	1.349972	147	3975.000	1.853362
14	644.580	0.982165	81	2318.389	1.358030	148	4000.000	1.861030
15	670.325	0.985450	82	2343.698	1.365218	149	4025.000	1.868700
16	691.031	0.988174	83	2368.914	1.372401	150	4050.000	1.876372
17	718.482	0.991897	84	2392.644	1.379178	151	4075.000	1.884047
18	738.482	0.994688	85	2419.031	1.386735	152	4100.000	1.891723
19	768.171	0.998952	86	2443.401	1.393733	153	4125.000	1.899402
20	794.790	1.002896	87	2467.697	1.400726	154	4150.000	1.907082
21	822.941	1.007190	88	2492.313	1.407829	155	4175.000	1.914765
22	843.036	1.010330	89	2519.922	1.415815	156	4200.000	1.922449
23	868.614	1.014416	90	2543.581	1.422674	157	4225.000	1.930135
24	894.119	1.018589	91	2566.833	1.429429	158	4250.000	1.937822
25	921.307	1.023144	92	2591.883	1.436721	159	4275.000	1.945511
26	942.569	1.026780	93	2616.403	1.443874	160	4300.000	1.953202
27	972.347	1.031982	94	2639.425	1.450602	161	4325.000	1.960894
28	988.598	1.034874	95	2669.654	1.459455	162	4350.000	1.968588
29	1018.913	1.040365	96	2698.020	1.467780	163	4375.000	1.976283
30	1047.728	1.045700	97	2718.334	1.473752	164	4400.000	1.983979
31	1069.727	1.049847	98	2742.351	1.480824	165	4425.000	1.991677
32	1093.448	1.054389	99	2768.347	1.488491	166	4450.000	1.999376
33	1119.573	1.059474	100	2795.751	1.496587	167	4475.000	2.007076
34	1144.664	1.064437	101	2823.373	1.504762	168	4500.000	2.014777
35	1169.907	1.069509	102	2845.001	1.511172	169	4525.000	2.022480
36	1191.722	1.073953	103	2872.444	1.519317	170	4550.000	2.030183
37	1219.006	1.079590	104	2895.995	1.526317	171	4575.000	2.037888
38	1242.914	1.084599	105	2917.992	1.532863	172	4600.000	2.045593
39	1267.262	1.089767	106	2941.398	1.539836	173	4625.000	2.053299
40	1292.784	1.095253	107	2968.622	1.547958	174	4650.000	2.061006
41	1316.929	1.100508	108	2990.918	1.554617	175	4675.000	2.068714
42	1342.261	1.106086	109	3018.090	1.562743	176	4700.000	2.076423
43	1371.339	1.112571	110	3042.218	1.569966	177	4725.000	2.084132

44	1391.577	1.117133	111	3067.084	1.577419	178	4750.000	2.091843
45	1418.030	1.123157	112	3092.811	1.585138	179	4775.000	2.099554
46	1439.032	1.127988	113	3118.302	1.592795	180	4800.000	2.107265
47	1462.608	1.133459	114	3142.820	1.600166	181	4825.000	2.114977
48	1490.113	1.139905	115	3168.861	1.608003	182	4850.000	2.122690
49	1517.949	1.146497	116	3192.675	1.615176	183	4875.000	2.130403
50	1544.086	1.152748	117	3219.534	1.623274	184	4900.000	2.138117
51	1569.900	1.158978	118	3241.315	1.629847	185	4925.000	2.145831
52	1593.404	1.164697	119	3264.630	1.636888	186	4950.000	2.153546
53	1617.242	1.170542	120	3293.246	1.645537	187	4975.000	2.161261
54	1643.658	1.177071	121	3317.799	1.652964	188	5000.000	2.168976
55	1667.848	1.183096	122	3343.766	1.660825	189	5025.000	2.176692
56	1694.537	1.189794	123	3366.177	1.667614	190	5050.000	2.184408
57	1716.647	1.195380	124	3392.607	1.675627	191	5075.000	2.192125
58	1743.842	1.202298	125	3410.802	1.681146	192	5100.000	2.199842
59	1767.872	1.208453	126	3443.246	1.690995	193	5125.000	2.207559
60	1794.159	1.215229	127	3475.000	1.700641	194	5150.000	2.215276
61	1819.208	1.221727	128	3500.000	1.708242	195	5175.000	2.222993
62	1841.269	1.227482	129	3525.000	1.715847	196	5200.000	2.230711
63	1868.805	1.234707	130	3550.000	1.723456	197	5225.000	2.238428
64	1893.512	1.241227	131	3575.000	1.731069	198	5250.000	2.246146
65	1917.232	1.247520	132	3600.000	1.738687	199	5275.000	2.253864
66	1941.535	1.253999	133	3625.000	1.746309	200	5300.000	2.261582
67	1967.839	1.261048	134	3650.000	1.753934			
Receiver Depth: 1999.699 m								
Source No.	Source offset (m)	Traveltime (s)	Source No.	Source offset (m)	Traveltime (s)	Source No.	Source offset (m)	Traveltime (s)
1	324.600	0.954837	68	1995.992	1.270683	135	3674.382	1.762733
2	350.549	0.956602	69	2021.284	1.277511	136	3696.833	1.769584
3	376.889	0.958527	70	2047.768	1.284696	137	3725.141	1.778226
4	400.611	0.960375	71	2068.441	1.290327	138	3748.488	1.785357
5	425.009	0.962388	72	2099.202	1.298743	139	3773.125	1.792885
6	451.156	0.964671	73	2122.910	1.305258	140	3797.180	1.800239
7	473.074	0.966683	74	2146.801	1.311849	141	3823.886	1.808406
8	501.052	0.969382	75	2171.815	1.318775	142	3847.157	1.815526
9	523.771	0.971680	76	2200.140	1.326650	143	3873.904	1.823712
10	549.677	0.974414	77	2218.331	1.331724	144	3899.011	1.831399
11	574.419	0.977139	78	2249.944	1.340573	145	3924.745	1.839282
12	602.401	0.980352	79	2272.620	1.346943	146	3947.236	1.846173

13	624.922	0.983038	80	2294.818	1.353197	147	3974.137	1.854418
14	648.928	0.985998	81	2323.298	1.361247	148	4000.000	1.862348
15	674.706	0.989287	82	2348.619	1.368427	149	4025.000	1.870015
16	695.534	0.992026	83	2373.838	1.375599	150	4050.000	1.877685
17	722.973	0.995746	84	2397.572	1.382367	151	4075.000	1.885357
18	743.035	0.998544	85	2423.962	1.389914	152	4100.000	1.893031
19	772.708	1.002803	86	2448.348	1.396906	153	4125.000	1.900707
20	799.365	1.006749	87	2472.638	1.403888	154	4150.000	1.908386
21	827.466	1.011030	88	2497.266	1.410985	155	4175.000	1.916066
22	847.578	1.014168	89	2524.872	1.418959	156	4200.000	1.923748
23	873.161	1.018250	90	2548.532	1.425809	157	4225.000	1.931432
24	898.705	1.022424	91	2571.795	1.432559	158	4250.000	1.939118
25	925.852	1.026964	92	2596.858	1.439846	159	4275.000	1.946805
26	947.130	1.030598	93	2621.377	1.446989	160	4300.000	1.954494
27	976.925	1.035794	94	2644.413	1.453713	161	4325.000	1.962185
28	993.203	1.038685	95	2674.605	1.462545	162	4350.000	1.969877
29	1023.519	1.044166	96	2702.929	1.470848	163	4375.000	1.977571
30	1052.331	1.049490	97	2723.228	1.476809	164	4400.000	1.985265
31	1074.363	1.053635	98	2747.233	1.483869	165	4425.000	1.992962
32	1098.092	1.058169	99	2773.232	1.491529	166	4450.000	2.000659
33	1124.219	1.063244	100	2800.637	1.499617	167	4475.000	2.008358
34	1149.317	1.068199	101	2828.265	1.507785	168	4500.000	2.016058
35	1174.603	1.073268	102	2849.906	1.514192	169	4525.000	2.023759
36	1196.443	1.077708	103	2877.363	1.522333	170	4550.000	2.031461
37	1223.741	1.083336	104	2900.926	1.529330	171	4575.000	2.039165
38	1247.658	1.088336	105	2922.933	1.535873	172	4600.000	2.046869
39	1272.022	1.093495	106	2946.349	1.542843	173	4625.000	2.054574
40	1297.550	1.098971	107	2973.590	1.550963	174	4650.000	2.062280
41	1321.672	1.104208	108	2995.885	1.557616	175	4675.000	2.069987
42	1347.028	1.109779	109	3023.058	1.565735	176	4700.000	2.077695
43	1376.170	1.116263	110	3047.187	1.572953	177	4725.000	2.085404
44	1396.418	1.120818	111	3072.056	1.580401	178	4750.000	2.093113
45	1422.895	1.126834	112	3097.786	1.588115	179	4775.000	2.100823
46	1443.884	1.131650	113	3123.280	1.595766	180	4800.000	2.108534
47	1467.463	1.137109	114	3147.799	1.603132	181	4825.000	2.116246
48	1494.924	1.143531	115	3173.841	1.610964	182	4850.000	2.123958
49	1522.751	1.150106	116	3197.658	1.618133	183	4875.000	2.131670
50	1548.932	1.156353	117	3224.52	1.626227	184	4900.000	2.139383
51	1574.732	1.162564	118	3246.308	1.632797	185	4925.000	2.147097

52	1598.225	1.168268	119	3269.615	1.639831	186	4950.000	2.154811
53	1622.070	1.174102	120	3298.234	1.648475	187	4975.000	2.162526
54	1648.491	1.180618	121	3322.795	1.655900	188	5000.000	2.170241
55	1672.676	1.186628	122	3348.757	1.663755	189	5025.000	2.177956
56	1699.359	1.193309	123	3371.168	1.670541	190	5050.000	2.185672
57	1721.478	1.198885	124	3397.601	1.678550	191	5075.000	2.193388
58	1748.692	1.205793	125	3415.795	1.684066	192	5100.000	2.201105
59	1772.717	1.211933	126	3448.241	1.693909	193	5125.000	2.208821
60	1799.002	1.218694	127	3472.837	1.701377	194	5150.000	2.216538
61	1824.082	1.225186	128	3498.606	1.709206	195	5175.000	2.224256
62	1846.130	1.230926	129	3522.813	1.716565	196	5200.000	2.231973
63	1873.676	1.238138	130	3549.675	1.724736	197	5225.000	2.239690
64	1898.386	1.244646	131	3572.790	1.731771	198	5250.000	2.247408
65	1922.128	1.250931	132	3596.293	1.738928	199	5275.000	2.255126
66	1946.425	1.257396	133	3624.682	1.747578	200	5300.000	2.262844
67	1972.733	1.264432	134	3649.510	1.755147			
Receiver Depth: 2009.758 m								
Source No.	Source offset (m)	Traveltime (s)	Source No.	Source offset (m)	Traveltime (s)	Source No.	Source offset (m)	Traveltime (s)
1	303.261	0.957027	68	1977.755	1.267875	135	3654.610	1.758065
2	328.581	0.958631	69	2001.021	1.274115	136	3679.484	1.765648
3	354.657	0.960413	70	2026.319	1.280931	137	3701.937	1.772497
4	380.983	0.962345	71	2052.794	1.288099	138	3730.246	1.781136
5	404.849	0.964212	72	2073.482	1.293724	139	3753.592	1.788264
6	429.240	0.966231	73	2104.247	1.302125	140	3778.230	1.795790
7	455.469	0.968527	74	2127.948	1.308626	141	3802.290	1.803142
8	477.448	0.970549	75	2151.842	1.315206	142	3828.996	1.811306
9	505.381	0.973249	76	2176.867	1.322123	143	3852.268	1.818424
10	528.180	0.975558	77	2205.177	1.329979	144	3879.018	1.826608
11	554.124	0.978300	78	2223.370	1.335045	145	3904.126	1.834293
12	578.871	0.981028	79	2254.993	1.343881	146	3929.863	1.842174
13	606.897	0.984248	80	2277.647	1.350234	147	3952.356	1.849063
14	629.448	0.986938	81	2299.834	1.356475	148	3979.256	1.857306
15	653.514	0.989906	82	2328.326	1.364515	149	4000.000	1.863664
16	679.317	0.993198	83	2353.659	1.371686	150	4025.000	1.871328
17	700.261	0.995953	84	2378.880	1.378848	151	4050.000	1.878996
18	727.683	0.999669	85	2402.618	1.385607	152	4075.000	1.886665
19	747.801	1.002474	86	2429.010	1.393143	153	4100.000	1.894337
20	777.454	1.006727	87	2453.412	1.400130	154	4125.000	1.902011

21	804.143	1.010675	88	2477.697	1.407100	155	4150.000	1.909687
22	832.193	1.014944	89	2502.335	1.414189	156	4175.000	1.917365
23	852.318	1.018081	90	2529.938	1.422151	157	4200.000	1.925045
24	877.902	1.022158	91	2553.598	1.428992	158	4225.000	1.932727
25	903.481	1.026331	92	2576.873	1.435736	159	4250.000	1.940411
26	930.585	1.030858	93	2601.946	1.443016	160	4275.000	1.948096
27	951.877	1.034488	94	2626.465	1.450151	161	4300.000	1.955783
28	981.685	1.039678	95	2649.516	1.456871	162	4325.000	1.963472
29	997.988	1.042569	96	2679.669	1.465680	163	4350.000	1.971163
30	1028.302	1.048040	97	2707.953	1.473961	164	4375.000	1.978854
31	1057.108	1.053352	98	2728.236	1.479911	165	4400.000	1.986548
32	1079.172	1.057495	99	2752.229	1.486959	166	4425.000	1.994242
33	1102.905	1.062021	100	2778.230	1.494611	167	4450.000	2.001938
34	1129.033	1.067086	101	2805.637	1.502690	168	4475.000	2.009636
35	1154.135	1.072031	102	2833.270	1.510851	169	4500.000	2.017334
36	1179.462	1.077098	103	2854.923	1.517255	170	4525.000	2.025034
37	1201.324	1.081533	104	2882.394	1.525392	171	4550.000	2.032735
38	1228.635	1.087151	105	2905.969	1.532386	172	4575.000	2.040437
39	1252.559	1.092141	106	2927.986	1.538925	173	4600.000	2.048140
40	1276.939	1.097293	107	2951.411	1.545892	174	4625.000	2.055844
41	1302.470	1.102756	108	2978.669	1.554009	175	4650.000	2.063550
42	1326.568	1.107977	109	3000.961	1.560655	176	4675.000	2.071256
43	1351.947	1.113540	110	3028.136	1.568767	177	4700.000	2.078962
44	1381.150	1.120023	111	3052.265	1.575979	178	4725.000	2.086670
45	1401.407	1.124569	112	3077.138	1.583422	179	4750.000	2.094379
46	1427.905	1.130576	113	3102.869	1.591130	180	4775.000	2.102088
47	1448.880	1.135378	114	3128.367	1.598776	181	4800.000	2.109798
48	1472.461	1.140825	115	3152.887	1.606137	182	4825.000	2.117509
49	1499.879	1.147222	116	3178.930	1.613963	183	4850.000	2.125220
50	1527.695	1.153779	117	3202.748	1.621127	184	4875.000	2.132932
51	1553.918	1.160022	118	3229.613	1.629216	185	4900.000	2.140644
52	1579.704	1.166216	119	3251.407	1.635783	186	4925.000	2.148358
53	1603.186	1.171904	120	3274.706	1.642810	187	4950.000	2.156071
54	1627.036	1.177726	121	3303.329	1.651450	188	4975.000	2.163785
55	1653.462	1.184227	122	3327.898	1.658873	189	5000.000	2.171500
56	1677.641	1.190223	123	3353.854	1.666721	190	5025.000	2.179215
57	1704.318	1.196887	124	3376.264	1.673502	191	5050.000	2.186930
58	1726.445	1.202453	125	3402.702	1.681507	192	5075.000	2.194646
59	1753.676	1.209350	126	3420.895	1.687020	193	5100.000	2.202362

60	1777.695	1.215475	127	3453.340	1.696858	194	5125.000	2.210078
61	1803.977	1.222220	128	3477.933	1.704320	195	5150.000	2.217795
62	1829.087	1.228706	129	3503.704	1.712146	196	5175.000	2.225512
63	1851.122	1.234430	130	3527.909	1.719500	197	5200.000	2.233229
64	1878.678	1.241629	131	3554.773	1.727668	198	5225.000	2.240946
65	1903.390	1.248124	132	3577.890	1.734700	199	5250.000	2.248664
66	1927.153	1.254402	133	3601.391	1.741853	200	5275.000	2.256381
67	1951.442	1.260852	134	3629.788	1.750501	201	5300.000	2.264099
Receiver Depth: 2019.927 m								
Source No.	Source offset (m)	Traveltime (s)	Source No.	Source offset (m)	Traveltime (s)	Source No.	Source offset (m)	Traveltime (s)
1	307.433	0.960853	68	1982.824	1.271341	135	3659.735	1.760982
2	332.872	0.962474	69	2006.097	1.277570	136	3684.612	1.768563
3	359.049	0.964273	70	2031.400	1.284375	137	3707.066	1.775409
4	385.343	0.966213	71	2057.867	1.291526	138	3735.376	1.784045
5	409.334	0.968096	72	2078.568	1.297143	139	3758.721	1.791169
6	433.705	0.970121	73	2109.336	1.305528	140	3783.360	1.798692
7	460.001	0.972430	74	2133.030	1.312016	141	3807.424	1.806043
8	482.029	0.974463	75	2156.926	1.318583	142	3834.131	1.814204
9	509.907	0.977163	76	2181.962	1.325491	143	3857.404	1.821319
10	532.777	0.979483	77	2210.257	1.333328	144	3884.155	1.829501
11	558.748	0.982232	78	2228.452	1.338386	145	3909.264	1.837183
12	583.493	0.984962	79	2260.084	1.347209	146	3935.005	1.845062
13	611.554	0.988189	80	2282.716	1.353545	147	3957.499	1.851950
14	634.129	0.990884	81	2304.890	1.359771	148	3984.399	1.860190
15	658.248	0.993859	82	2333.394	1.367801	149	4025.000	1.872632
16	684.072	0.997154	83	2358.739	1.374964	150	4050.000	1.880296
17	705.124	0.999922	84	2383.962	1.382115	151	4075.000	1.887963
18	732.526	1.003635	85	2407.702	1.388864	152	4100.000	1.895632
19	752.696	1.006446	86	2434.097	1.396389	153	4125.000	1.903304
20	782.323	1.010694	87	2458.515	1.403369	154	4150.000	1.910977
21	809.041	1.014643	88	2482.793	1.410327	155	4175.000	1.918653
22	837.034	1.018899	89	2507.442	1.417409	156	4200.000	1.926331
23	857.170	1.022035	90	2535.041	1.425358	157	4225.000	1.934010
24	882.753	1.026106	91	2558.701	1.432190	158	4250.000	1.941692
25	908.363	1.030279	92	2581.986	1.438927	159	4275.000	1.949375
26	935.422	1.034792	93	2607.071	1.446201	160	4300.000	1.957060
27	956.725	1.038419	94	2631.588	1.453325	161	4325.000	1.964747
28	986.543	1.043601	95	2654.653	1.460041	162	4350.000	1.972436

29	1002.868	1.046491	96	2684.768	1.468827	163	4375.000	1.980126
30	1033.179	1.051952	97	2713.012	1.477087	164	4400.000	1.987818
31	1061.975	1.057253	98	2733.279	1.483024	165	4425.000	1.995511
32	1084.068	1.061393	99	2757.260	1.490061	166	4450.000	2.003205
33	1107.805	1.065911	100	2783.262	1.497704	167	4475.000	2.010901
34	1133.931	1.070965	101	2810.670	1.505774	168	4500.000	2.018598
35	1159.036	1.075900	102	2838.309	1.513928	169	4525.000	2.026296
36	1184.402	1.080964	103	2859.972	1.520328	170	4550.000	2.033996
37	1206.284	1.085393	104	2887.458	1.528461	171	4575.000	2.041697
38	1233.606	1.091001	105	2911.043	1.535450	172	4600.000	2.049398
39	1257.536	1.095982	106	2933.070	1.541986	173	4625.000	2.057101
40	1281.929	1.101125	107	2956.504	1.548948	174	4650.000	2.064805
41	1307.463	1.106577	108	2983.778	1.557062	175	4675.000	2.072510
42	1331.536	1.111780	109	3006.069	1.563702	176	4700.000	2.080216
43	1356.935	1.117335	110	3033.245	1.571807	177	4725.000	2.087923
44	1386.199	1.123816	111	3057.374	1.579012	178	4750.000	2.095630
45	1406.463	1.128354	112	3082.250	1.586449	179	4775.000	2.103339
46	1432.981	1.134351	113	3107.982	1.594150	180	4800.000	2.111048
47	1453.941	1.139139	114	3133.483	1.601792	181	4825.000	2.118758
48	1477.524	1.144574	115	3158.005	1.609147	182	4850.000	2.126468
49	1504.896	1.150945	116	3184.048	1.616967	183	4875.000	2.134179
50	1532.702	1.157484	117	3207.868	1.624126	184	4900.000	2.141891
51	1558.966	1.163722	118	3234.734	1.632209	185	4925.000	2.149604
52	1584.736	1.169898	119	3256.536	1.638774	186	4950.000	2.157317
53	1608.206	1.175569	120	3279.827	1.645793	187	4975.000	2.165030
54	1632.059	1.181378	121	3308.451	1.654427	188	5000.000	2.172744
55	1658.491	1.187867	122	3333.029	1.661848	189	5025.000	2.180458
56	1682.662	1.193846	123	3358.978	1.669689	190	5050.000	2.188173
57	1709.332	1.200493	124	3381.389	1.676465	191	5075.000	2.195889
58	1731.466	1.206049	125	3407.830	1.684467	192	5100.000	2.203604
59	1758.713	1.212934	126	3426.021	1.689975	193	5125.000	2.211320
60	1782.727	1.219044	127	3458.467	1.699808	194	5150.000	2.219037
61	1809.004	1.225773	128	3483.057	1.707265	195	5175.000	2.226753
62	1834.144	1.232252	129	3508.829	1.715086	196	5200.000	2.234470
63	1856.165	1.237960	130	3533.031	1.722436	197	5225.000	2.242187
64	1883.729	1.245146	131	3559.898	1.730600	198	5250.000	2.249904
65	1908.443	1.251627	132	3583.016	1.737629	199	5275.000	2.257622
66	1932.226	1.257898	133	3606.516	1.744778	200	5300.000	2.265339
67	1956.508	1.264332	134	3634.919	1.753424			

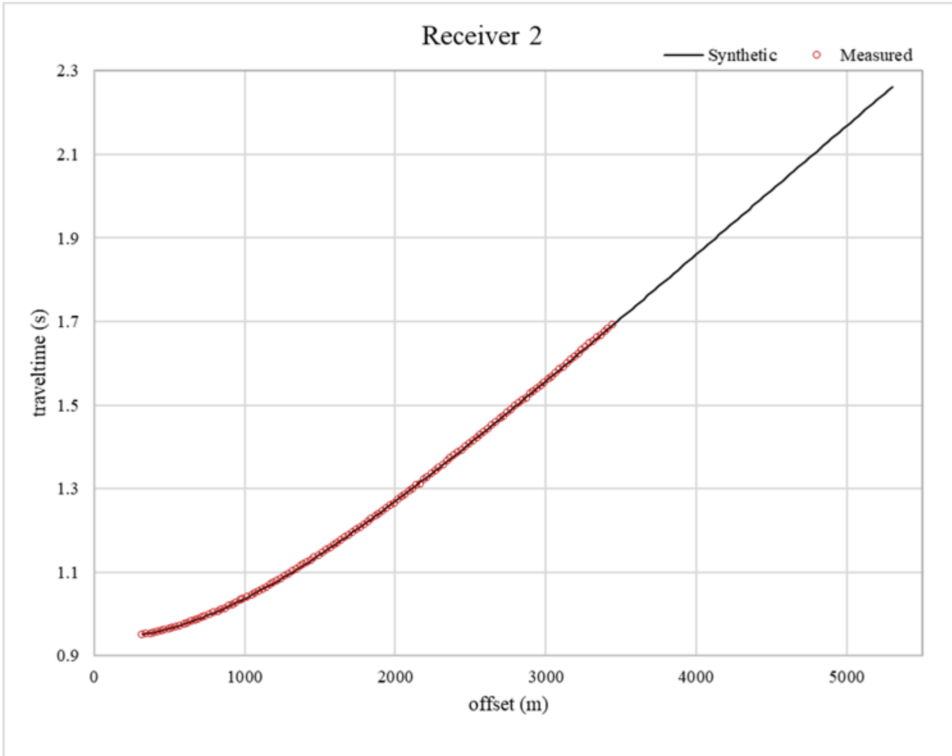

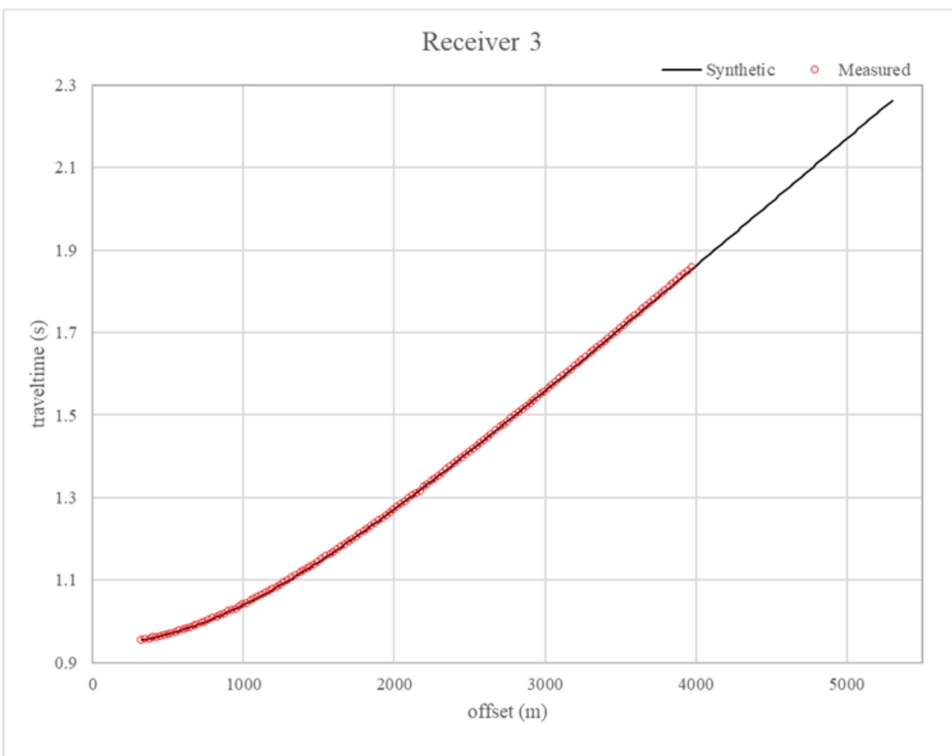

Figure C.1: Comparison of synthetic traveltimes (black line) to measured traveltimes (red circles) for Receivers 2 and 3. The red circles overlie the black dots. For offsets greater than measured offsets the synthetic traveltimes are extrapolated in 25 m intervals.

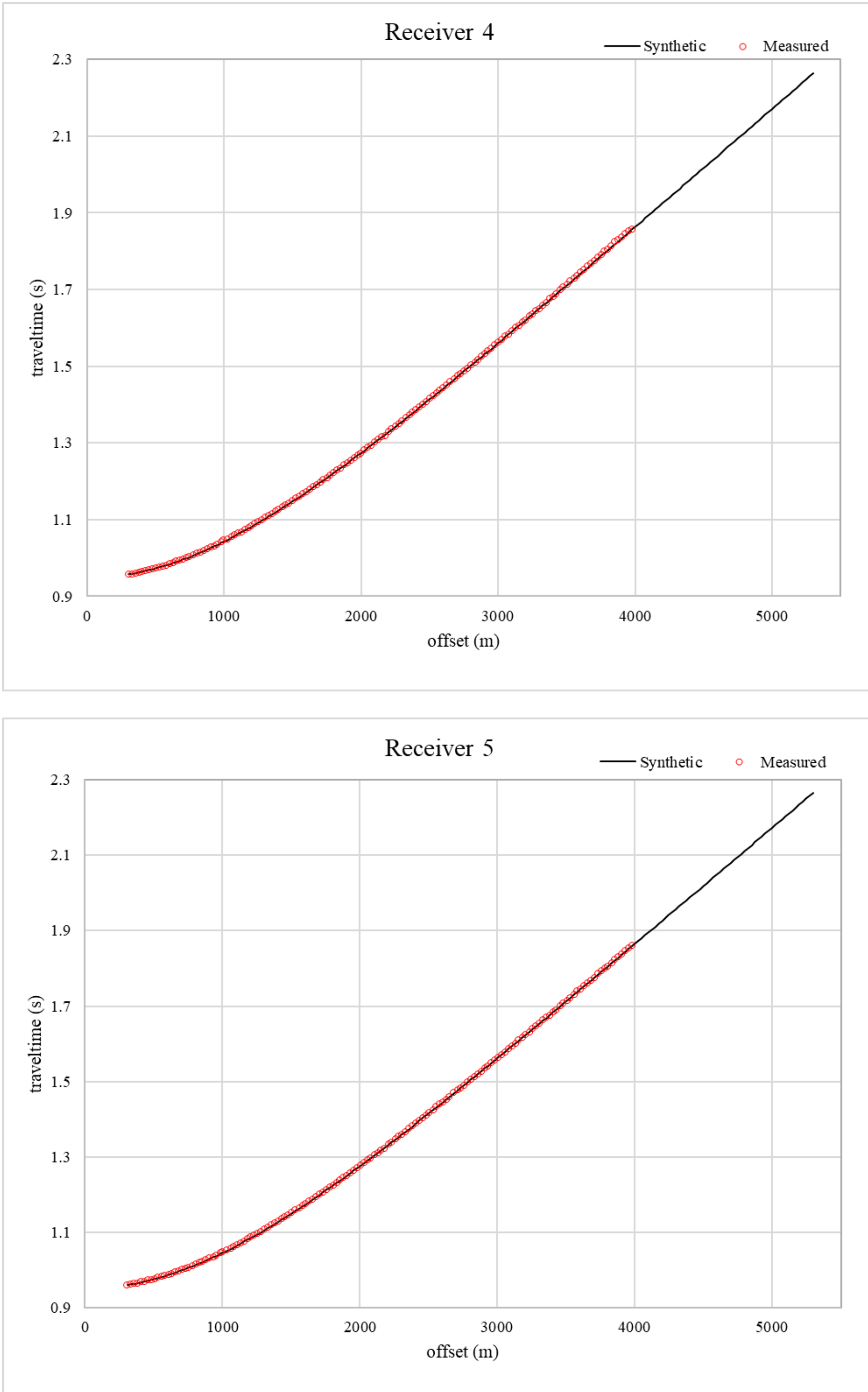

Figure C.2: Comparison of synthetic traveltimes (black line) to measured traveltimes (red circles) for Receivers 4 and 5. The red circles overlie the black dots. For offsets greater than measured offsets the synthetic traveltimes are extrapolated in 25 m intervals.

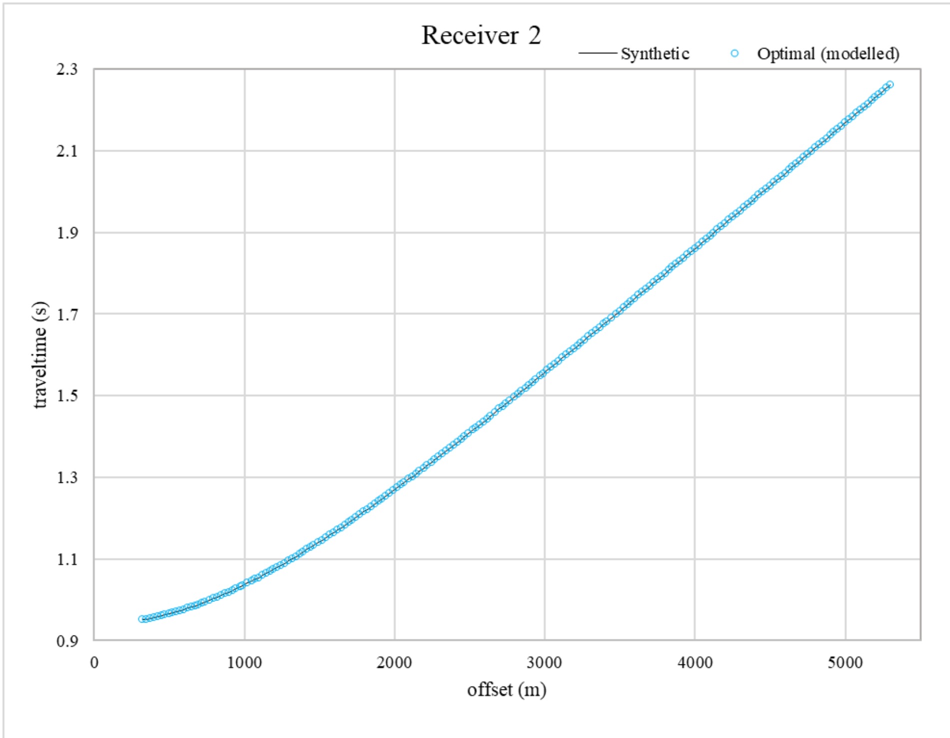

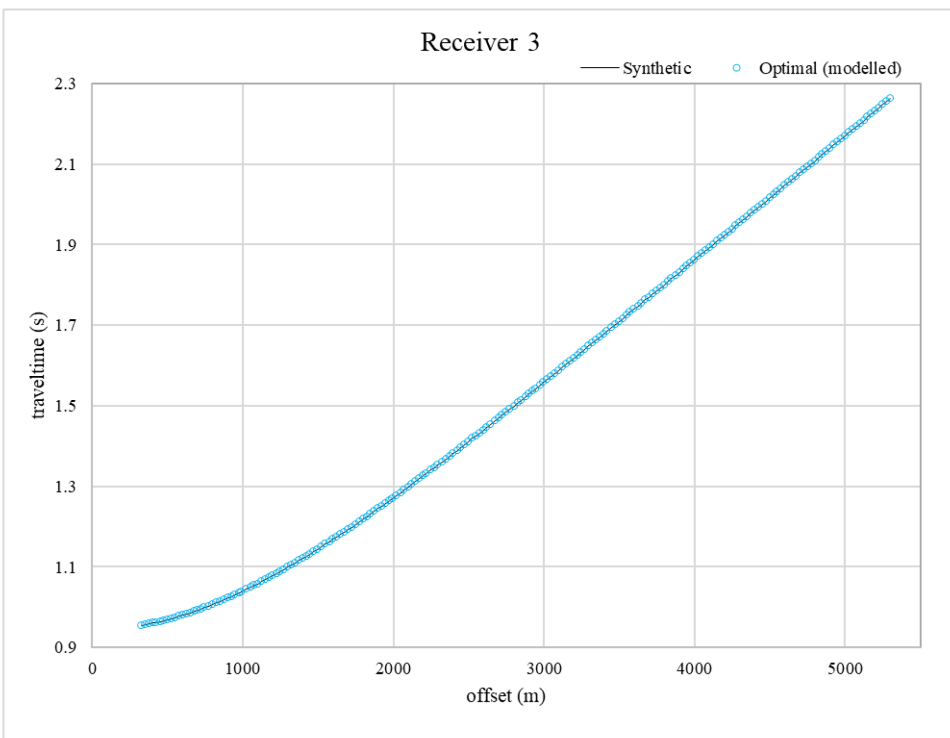

Figure C.3: Comparison of synthetic (black line) to modelled (blue circles) traveltimes for Receivers 2 and 3, for a 4-layer model to source-receiver offsets of 5300 m.

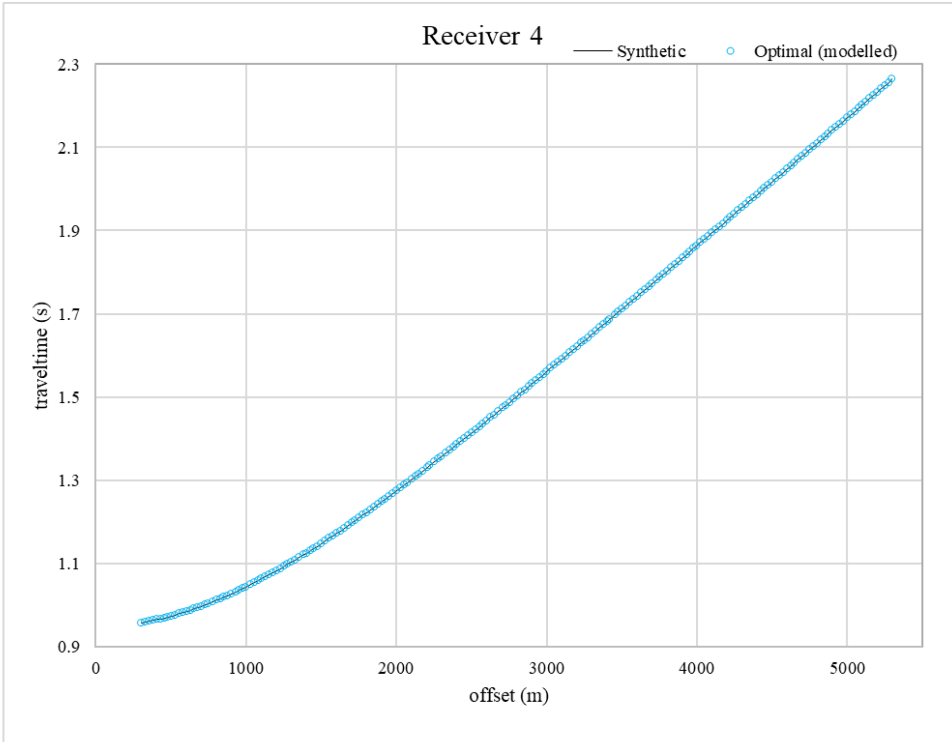

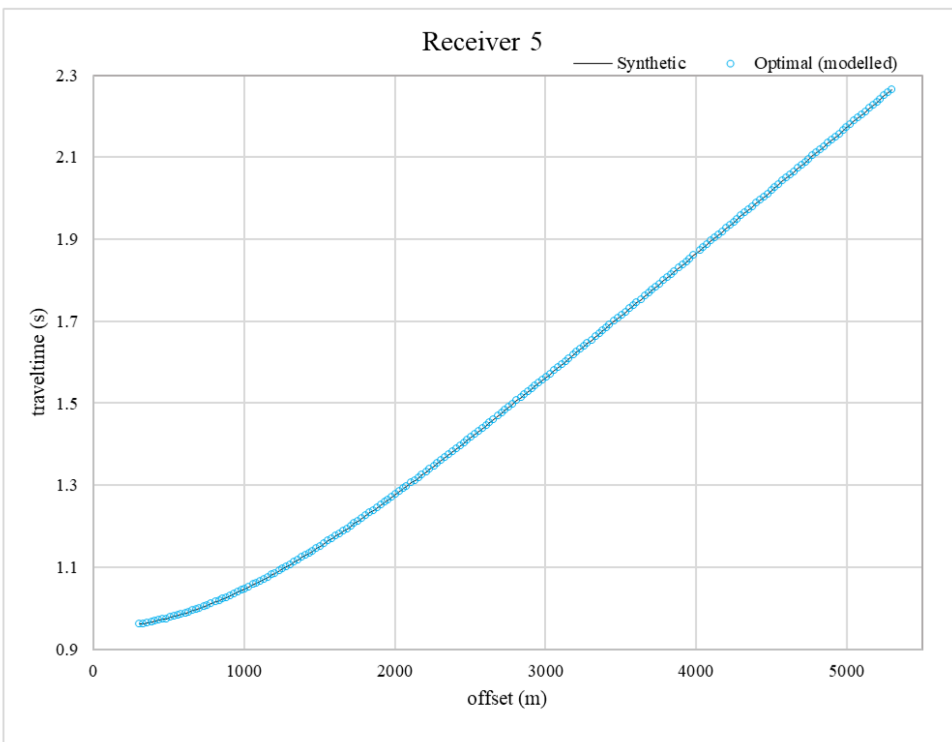

Figure C.4: Comparison of synthetic (black line) to modelled (blue circles) traveltimes for Receivers 4 and 5, for a 4-layer model to source-receiver offsets of 5300 m.

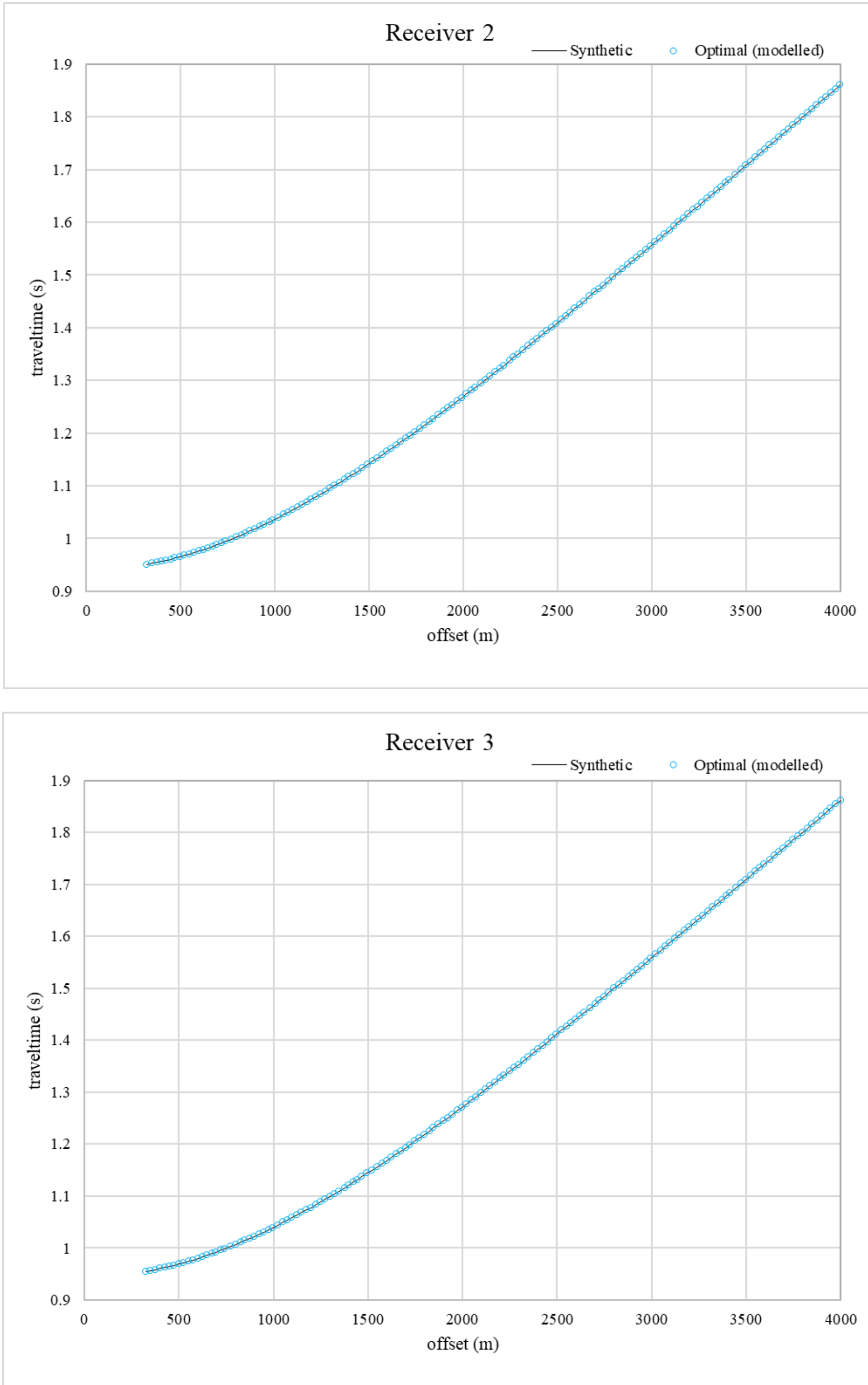

Figure C.5: Comparison of synthetic (black line) to modelled (blue circles) traveltimes for Receivers 2 and 3, for a 4-layer model to source-receiver offsets of 4000 m.

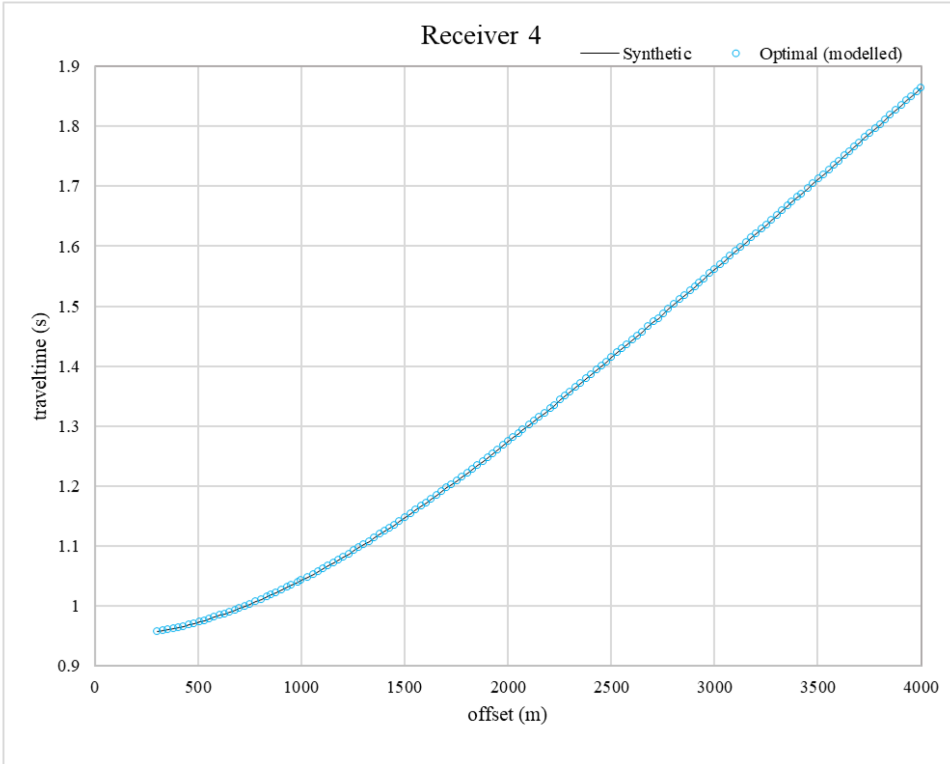

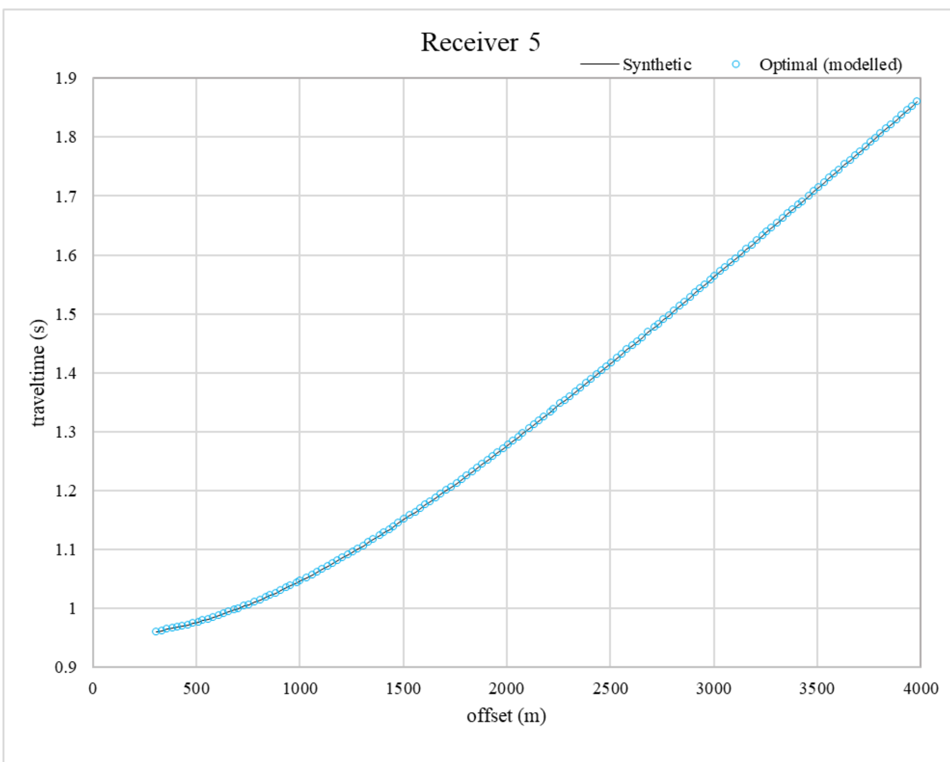

Figure C.6: Comparison of synthetic (black line) to modelled (blue circles) traveltimes for Receivers 4 and 5, for a 4-layer model to source-receiver offsets of 4000 m.

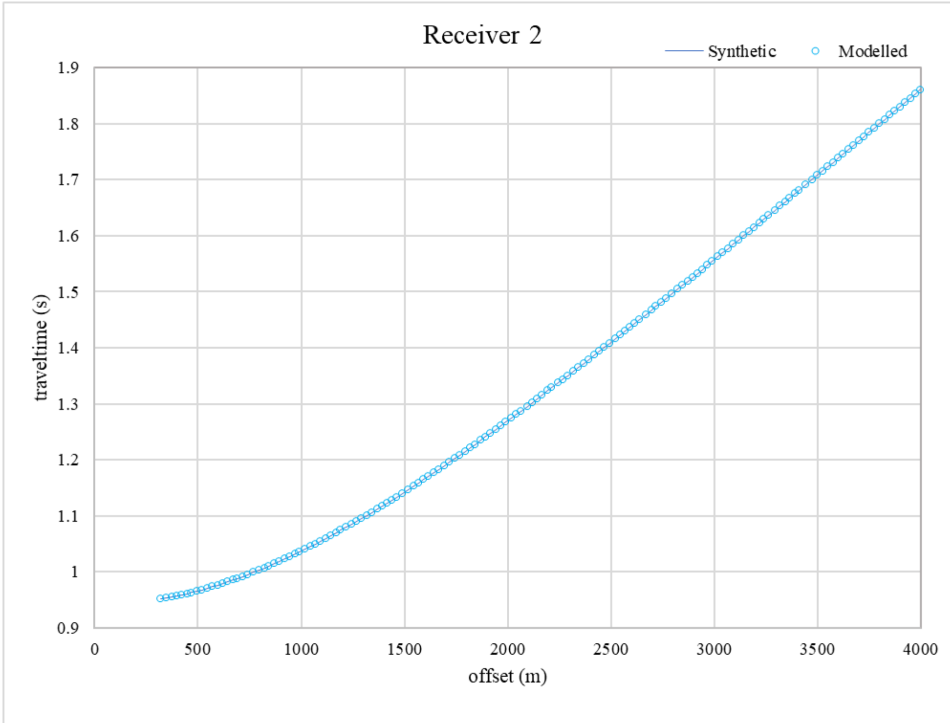

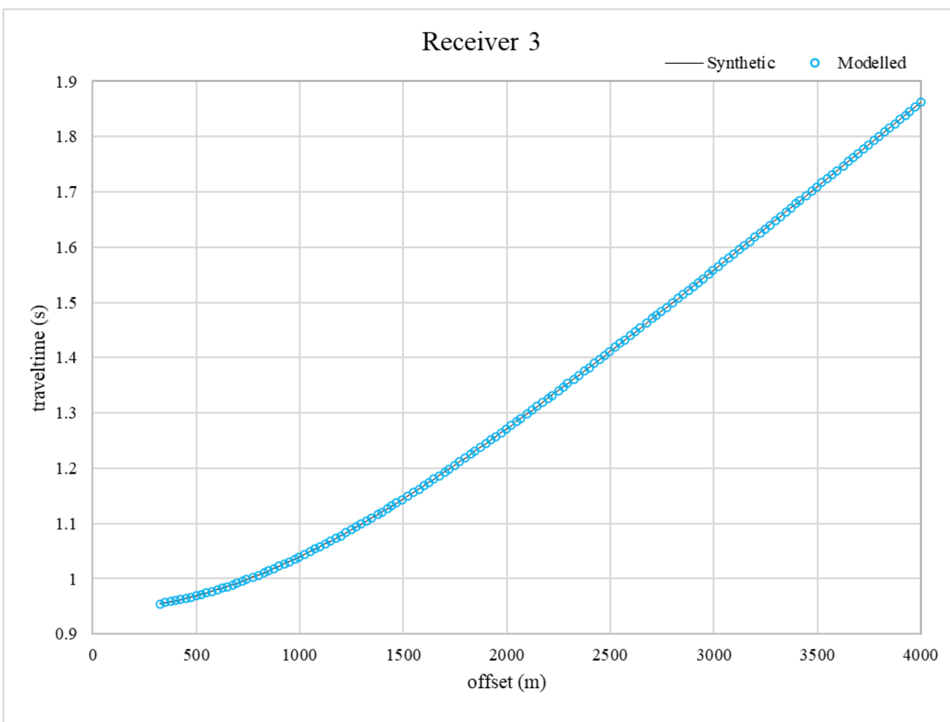

Figure C.7: Comparison of synthetic (black line) to modelled (blue circles) traveltimes for Receiver 2 and 3, for a 3-layer model to source-receiver offsets of 4000 m.

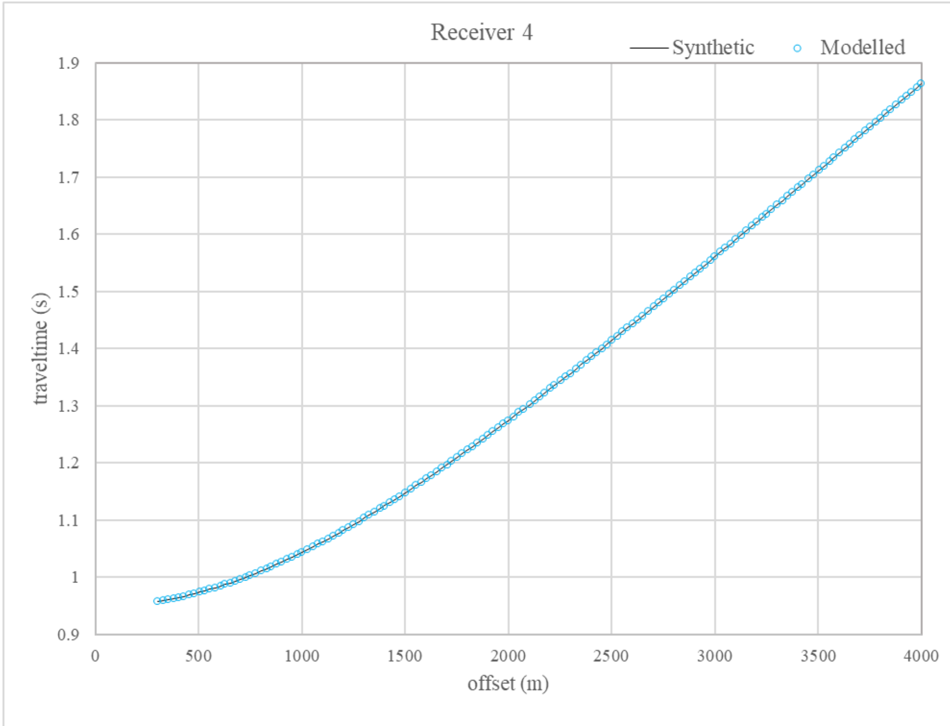

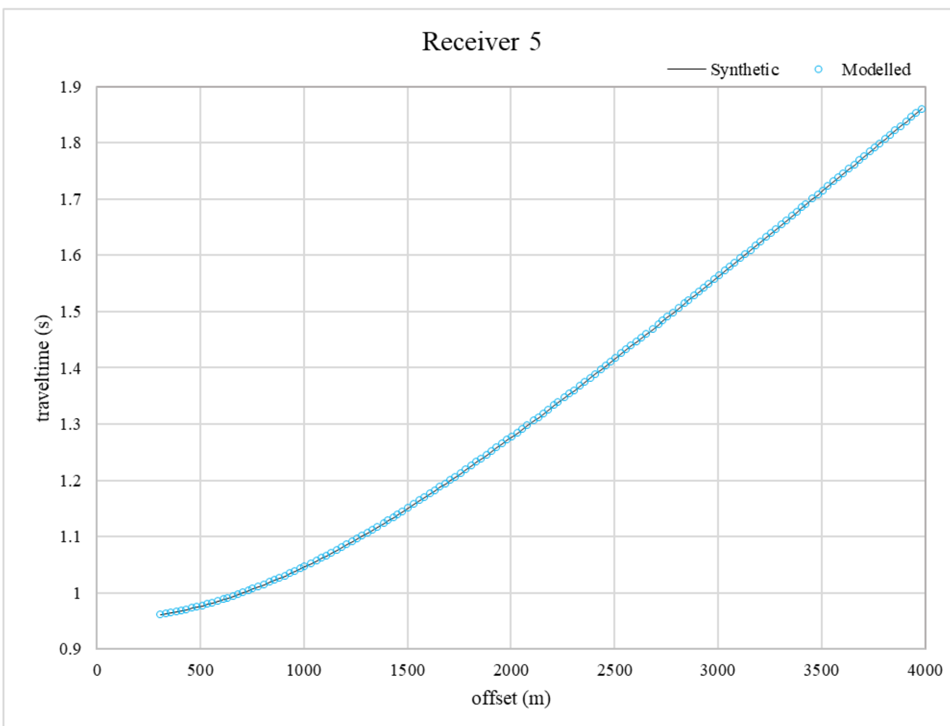

Figure C.8: Comparison of synthetic (black line) to modelled (blue circles) traveltimes for Receiver 4 and 5, for a 3-layer model to source-receiver offsets of 4000 m.

C.2. Noise Profiles

Table C3: Noise profiles.

Receiver Depth: 1979.923 m											
Source offset (m)	Noise Profile 1 (ms)	Noise Profile 2 (ms)	Noise Profile 3 (ms)	Source offset (m)	Noise Profile 1 (ms)	Noise Profile 2 (ms)	Noise Profile 3 (ms)	Source offset (m)	Noise Profile 1 (ms)	Noise Profile 2 (ms)	Noise Profile 3 (ms)
317.805	-0.294	0.110	0.674	1986.236	-0.219	0.139	1.004	3650.000	0.537	1.353	1.040
343.415	-0.146	0.217	0.492	2011.513	0.725	-0.160	-0.421	3675.000	0.685	0.591	-1.280
369.719	-0.463	-0.624	0.253	2038.012	0.270	-0.813	0.344	3700.000	-1.160	-1.500	0.249
393.092	-0.378	-0.607	-0.813	2058.654	0.735	-0.907	-0.960	3725.000	-0.363	-0.740	0.623
417.457	0.811	-0.184	0.678	2089.406	-0.465	-0.823	0.999	3750.000	0.337	-1.220	-0.849
443.392	0.514	-0.534	-0.443	2113.127	-1.200	-0.711	-1.159	3775.000	-0.274	-1.223	-1.033
465.151	0.057	-0.114	0.723	2137.01	0.514	0.988	-0.635	3800.000	1.234	1.487	0.115
493.184	0.446	-0.559	-0.211	2162.001	-0.077	-0.912	-1.293	3825.000	1.454	-0.980	-0.657
515.711	-0.142	-0.528	0.099	2190.353	-1.282	-0.612	0.837	3850.000	-0.908	0.187	1.376
541.511	0.386	-0.396	0.732	2208.538	0.758	-0.258	1.209	3875.000	-0.748	-1.115	-1.528
566.218	-0.767	0.383	-0.837	2240.131	0.751	-0.250	0.503	3900.000	1.210	1.189	-0.073
594.084	0.377	0.438	0.422	2262.848	-0.669	-1.246	-1.284	3925.000	0.342	-1.421	-1.206
616.525	0.971	-0.315	-0.355	2285.069	0.851	-1.148	0.781	3950.000	-0.527	1.380	0.018
640.39	-0.014	0.298	-0.592	2313.522	-1.345	1.060	0.476	3975.000	-0.766	1.078	0.195
666.096	0.098	0.772	0.056	2338.818	0.113	-0.348	-0.122	4000.000	-1.829	-0.950	-1.033
686.674	-0.886	-0.960	0.815	2364.031	0.350	0.355	0.426	4025.000	0.605	0.303	0.431
714.131	0.671	-0.854	-0.900	2387.757	-0.048	0.008	-0.424	4050.000	1.527	0.881	0.024
734.065	0.903	0.358	-0.418	2414.14	1.364	-0.358	-0.151	4075.000	-1.063	0.004	-0.168
763.765	0.086	-0.157	-0.986	2438.493	1.108	-0.074	1.211	4100.000	1.493	1.164	1.732
790.341	0.372	-0.351	-0.407	2462.794	0.631	0.345	-0.902	4125.000	-0.377	0.728	1.660
818.537	-0.213	-0.807	-0.704	2487.398	0.487	0.222	1.190	4150.000	-1.459	-1.147	1.175

838.613	0.717	0.121	0.391	2515.01	0.925	0.015	0.091	4175.000	-1.704	-0.766	1.128
864.183	0.171	-0.570	-0.965	2538.668	-1.156	-0.668	-0.974	4200.000	1.439	-0.775	0.290
889.644	-0.068	-0.989	0.138	2561.908	-1.283	0.045	-0.641	4225.000	-0.815	0.174	-1.374
916.870	-0.410	-0.420	0.942	2586.946	-0.446	-0.915	-0.547	4250.000	-0.857	0.445	-1.203
938.114	0.204	0.815	-0.303	2611.466	-1.103	1.193	0.566	4275.000	-1.010	1.406	-0.956
967.871	0.873	0.567	-0.122	2634.472	1.046	-0.039	-1.002	4300.000	-0.521	1.366	1.511
984.094	0.917	-0.789	-0.867	2664.74	1.414	-1.364	-1.389	4325.000	-0.119	-1.096	-1.277
1014.404	0.192	-0.103	-0.550	2693.145	-0.483	0.493	0.583	4350.000	0.645	-1.811	1.962
1043.220	-0.978	-0.985	0.633	2713.475	-1.047	-1.206	0.093	4375.000	0.385	-1.363	0.727
1065.184	-0.443	-0.013	-0.357	2737.504	-0.770	0.424	-1.185	4400.000	0.176	-1.195	1.405
1088.895	0.629	0.039	0.407	2763.498	0.831	0.387	0.541	4425.000	-0.043	-1.578	-0.728
1115.015	0.109	-0.143	-0.707	2790.900	-0.728	-0.860	0.464	4450.000	0.102	0.180	1.317
1140.098	0.284	0.332	-0.009	2818.515	-0.386	-1.062	0.184	4475.000	-1.012	-0.412	-1.157
1165.295	0.452	-0.815	0.088	2840.130	-0.883	-0.940	1.152	4500.000	-1.545	-1.534	-0.584
1187.085	-0.517	-1.018	0.770	2867.558	0.934	-1.026	0.679	4525.000	0.441	-1.424	0.511
1214.352	-0.037	0.215	0.701	2891.097	-1.425	1.129	-0.189	4550.000	0.604	-0.360	-1.077
1238.248	0.955	-0.161	-0.679	2913.083	1.020	0.097	-0.037	4575.000	1.077	-0.433	-0.879
1262.578	-0.639	0.604	0.384	2936.480	-0.301	-1.255	-1.466	4600.000	-0.982	-0.196	1.014
1288.093	0.666	0.002	1.025	2963.685	-0.212	-1.341	-1.073	4625.000	-1.141	-1.559	0.889
1312.260	0.249	-0.543	0.799	2985.984	-1.536	-0.795	0.657	4650.000	0.030	1.319	-1.869
1337.566	-0.902	1.047	-0.291	3013.154	-1.203	0.928	0.551	4675.000	0.325	1.001	-0.989
1366.579	0.318	-0.070	0.777	3037.280	-1.418	-0.910	0.236	4700.000	-1.596	-1.243	0.450
1386.806	-0.307	-0.087	0.229	3062.143	0.536	-1.267	0.877	4725.000	-1.878	-0.272	-1.119
1413.235	0.425	-0.715	0.583	3087.867	0.891	1.364	-0.216	4750.000	-1.988	2.077	1.966
1434.249	-0.628	-0.562	0.321	3113.355	0.349	1.096	1.575	4775.000	1.187	-1.267	0.292
1457.820	0.607	0.438	0.941	3137.870	-1.525	1.285	-1.302	4800.000	0.543	-1.479	-0.855
1485.368	1.055	0.161	-0.539	3163.910	-1.518	0.286	1.199	4825.000	-0.560	-0.185	1.452

1513.211	-0.713	-0.991	-1.046	3187.722	0.162	1.327	-0.845	4850.000	-0.502	-1.967	0.665
1539.303	-0.386	-0.021	-0.490	3214.578	-1.353	1.561	0.113	4875.000	0.579	0.414	0.802
1565.130	-0.929	0.020	0.262	3236.351	-1.389	0.194	-0.545	4900.000	0.198	-0.682	-0.130
1588.644	-0.916	-0.077	-0.591	3259.675	0.675	-1.167	-1.584	4925.000	1.795	1.394	-1.365
1612.475	0.733	-0.247	-0.720	3288.287	1.358	-0.316	1.231	4950.000	-0.179	1.704	1.882
1638.883	-0.200	-0.330	0.837	3312.831	-1.384	-0.499	0.003	4975.000	1.960	-0.384	-0.374
1663.079	0.304	-0.132	-0.117	3338.804	0.391	-0.358	1.455	5000.000	-1.579	1.675	-0.748
1689.771	-1.056	0.551	-0.166	3361.215	0.001	-0.056	-0.986	5025.000	-1.285	1.240	1.419
1711.871	0.216	-0.809	-0.905	3387.640	1.668	-0.691	-0.683	5050.000	-0.236	1.506	1.893
1739.048	-0.564	0.520	-0.223	3405.836	-1.616	0.825	-0.622	5075.000	1.533	-0.823	2.160
1763.081	-0.945	0.238	-1.059	3438.279	0.635	1.047	1.339	5100.000	0.511	0.089	1.284
1789.370	-0.964	-0.900	0.904	3450.000	-0.412	-0.861	-0.460	5125.000	-2.104	-0.261	0.477
1814.387	0.044	-0.156	0.407	3475.000	0.645	-0.949	-1.138	5150.000	1.605	-0.356	-1.798
1836.461	-0.551	-0.962	-0.534	3500.000	-0.951	1.012	-0.461	5175.000	0.154	1.253	1.979
1863.985	0.600	0.510	-0.535	3525.000	1.551	-1.371	1.713	5200.000	-1.810	2.106	1.435
1888.688	-0.980	-1.236	0.427	3550.000	0.881	-1.132	0.886	5225.000	-1.087	2.193	-2.098
1912.386	1.045	0.134	-0.624	3575.000	0.687	-0.245	0.566	5250.000	1.143	0.519	-0.789
1936.696	1.017	0.840	0.186	3600.000	0.857	-1.049	1.174	5275.000	0.598	1.514	1.930
1962.993	0.990	0.242	1.010	3625.000	0.396	-1.732	0.713	5300.000	1.631	0.065	1.857
Receiver Depth: 1989.809 m											
Source offset (m)	Noise Profile 1 (ms)	Noise Profile 2 (ms)	Noise Profile 3 (ms)	Source offset (m)	Noise Profile 1 (ms)	Noise Profile 2 (ms)	Noise Profile 3 (ms)	Source offset (m)	Noise Profile 1 (ms)	Noise Profile 2 (ms)	Noise Profile 3 (ms)
321.033	0.815	0.337	0.669	1991.090	-0.887	-1.039	-0.889	3675.000	-0.007	1.307	-0.148
346.827	-0.629	0.220	0.059	2016.374	-0.650	-0.827	0.562	3700.000	1.565	-1.238	-1.140
373.160	0.610	-0.736	-0.847	2042.866	-0.787	1.200	0.396	3725.000	1.602	0.961	-1.386
396.718	-0.954	0.423	-0.417	2063.524	0.556	-0.276	0.399	3750.000	-1.657	-0.535	0.777
421.107	0.826	-0.299	0.890	2094.281	-1.048	0.519	0.910	3775.000	0.716	-0.826	-1.542
447.157	-0.307	0.773	-0.932	2117.996	1.228	1.080	0.666	3800.000	-0.967	1.061	1.211

469.001	-0.828	0.010	0.897	2141.883	-0.703	0.629	1.276	3825.000	1.641	-1.033	-0.791
497.013	-0.233	-0.064	0.415	2166.886	0.808	-0.352	-1.063	3850.000	-1.719	-1.480	0.912
519.641	0.808	-0.141	-0.415	2195.224	1.217	0.081	-0.598	3875.000	0.839	1.810	1.391
545.499	-0.278	-0.180	-0.778	2213.413	1.259	0.110	-1.229	3900.000	0.398	-1.586	1.039
570.228	-0.424	0.322	0.010	2245.016	0.646	0.681	-0.243	3925.000	0.803	0.475	0.538
598.156	-0.965	0.430	0.795	2267.713	0.814	0.333	0.817	3950.000	-0.066	0.812	1.366
620.641	-0.215	-0.389	0.187	2289.923	0.935	-1.041	-1.261	3975.000	0.756	1.042	0.875
644.580	0.521	-0.577	-0.858	2318.389	0.113	0.061	0.637	4000.000	-1.463	0.124	-0.770
670.325	0.601	-0.799	0.426	2343.698	1.275	0.435	-0.593	4025.000	-1.587	0.593	1.335
691.031	-0.819	-0.385	0.313	2368.914	0.144	-0.355	1.101	4050.000	1.157	-1.039	1.709
718.482	-0.518	0.260	0.262	2392.644	1.208	0.501	1.084	4075.000	-1.109	1.543	-1.850
738.482	-0.173	-0.820	-0.485	2419.031	0.517	1.107	-0.949	4100.000	-0.839	-1.407	-1.812
768.171	-0.812	-0.710	0.756	2443.401	-0.408	-1.008	1.345	4125.000	-0.042	0.067	1.556
794.790	-0.991	0.515	-0.129	2467.697	-0.306	-1.322	-0.784	4150.000	0.978	-1.296	-0.537
822.941	0.134	-0.906	-0.526	2492.313	1.296	0.572	-0.355	4175.000	-0.866	0.441	-1.644
843.036	-0.887	-0.412	-0.860	2519.922	-0.912	0.016	-0.022	4200.000	-1.504	-1.556	0.488
868.614	0.541	-0.698	0.341	2543.581	0.193	-0.978	-1.363	4225.000	-1.674	-1.681	1.835
894.119	-0.565	-0.607	-0.820	2566.833	-0.764	-0.274	0.422	4250.000	-0.154	-0.633	-1.709
921.307	0.740	-0.419	-0.083	2591.883	0.808	1.418	0.595	4275.000	1.301	-1.664	0.520
942.569	-0.665	-0.131	0.743	2616.403	-1.042	-1.065	-0.543	4300.000	-0.199	0.915	-0.142
972.347	-0.181	0.684	-0.146	2639.425	0.317	-0.158	0.459	4325.000	-0.424	-1.485	0.675
988.598	0.140	0.648	-0.034	2669.654	-1.153	0.994	1.095	4350.000	0.549	0.234	1.177
1018.913	-1.023	-0.068	0.341	2698.020	0.030	-0.389	-0.794	4375.000	1.427	-0.043	-0.261
1047.728	0.026	-0.252	-0.248	2718.334	1.334	0.908	1.070	4400.000	0.708	0.717	0.935
1069.727	0.074	-0.067	0.740	2742.351	-0.761	0.166	0.716	4425.000	0.780	-0.495	1.120
1093.448	-0.644	1.040	-1.028	2768.347	-0.235	0.166	-1.300	4450.000	1.013	-0.821	0.257
1119.573	0.514	-0.741	0.000	2795.751	-0.566	-0.398	1.452	4475.000	-0.977	0.387	-1.251

1144.664	0.194	0.814	-0.129	2823.373	0.784	-0.050	0.337	4500.000	-1.526	0.384	-1.420
1169.907	-0.754	0.724	0.413	2845.001	0.914	1.226	0.624	4525.000	-0.300	-0.978	1.920
1191.722	0.725	-0.156	1.000	2872.444	-0.054	-1.216	0.352	4550.000	1.892	0.572	1.276
1219.006	-0.405	0.109	0.957	2895.995	-0.769	1.236	-1.045	4575.000	1.223	-0.259	-0.163
1242.914	-0.837	-1.020	-0.979	2917.992	-1.207	-1.452	-1.163	4600.000	0.793	0.986	1.275
1267.262	0.954	0.041	1.064	2941.398	1.478	-0.505	0.917	4625.000	1.431	0.140	0.201
1292.784	-0.906	-0.098	-0.143	2968.622	0.306	0.200	0.991	4650.000	0.191	0.346	-1.622
1316.929	-0.190	-0.688	0.107	2990.918	0.960	0.910	0.465	4675.000	0.729	-1.453	0.566
1342.261	0.032	0.098	0.016	3018.09	0.851	0.558	0.582	4700.000	-1.710	0.238	-2.071
1371.339	-0.629	0.182	-0.569	3042.218	-0.082	-1.095	-0.927	4725.000	-1.320	-1.342	-0.856
1391.577	0.080	0.500	0.416	3067.084	-0.354	0.402	0.462	4750.000	1.000	0.481	2.070
1418.030	0.677	-0.342	0.807	3092.811	0.114	0.644	-0.687	4775.000	0.111	-1.161	-0.810
1439.032	-0.558	0.395	0.446	3118.302	-0.485	0.378	-1.230	4800.000	1.279	0.949	-1.088
1462.608	0.332	-0.333	-1.089	3142.820	-0.246	1.178	-0.755	4825.000	0.141	-0.742	-0.285
1490.113	-0.620	-1.096	0.770	3168.861	1.394	-0.759	0.651	4850.000	2.035	0.711	-1.338
1517.949	0.271	-0.565	0.895	3192.675	-0.933	1.191	1.451	4875.000	0.000	1.643	-0.296
1544.086	-0.105	-0.334	-0.380	3219.534	-1.155	1.279	-1.438	4900.000	0.520	0.624	-0.084
1569.900	0.563	0.652	1.085	3241.315	0.896	-0.140	1.025	4925.000	-2.120	-1.669	0.796
1593.404	0.556	0.427	0.921	3264.630	0.856	-1.179	-1.222	4950.000	1.322	-1.388	1.475
1617.242	-0.511	0.467	1.022	3293.246	0.089	0.148	-1.088	4975.000	1.448	0.340	0.735
1643.658	0.404	0.916	0.565	3317.799	-1.119	-1.265	-0.996	5000.000	0.369	0.801	0.942
1667.848	0.034	0.005	-0.282	3343.766	-0.008	0.659	1.303	5025.000	-0.570	0.911	0.665
1694.537	-0.128	0.947	-0.662	3366.177	0.573	1.259	0.395	5050.000	-1.279	-0.769	1.261
1716.647	0.973	-0.744	0.096	3392.607	-1.437	-0.943	0.652	5075.000	-0.118	1.149	-1.707
1743.842	0.031	-0.060	0.572	3410.802	0.927	0.386	0.592	5100.000	-1.865	0.758	-0.894
1767.872	-0.570	1.176	-0.946	3443.246	-1.059	-1.161	-1.052	5125.000	0.168	0.279	-0.970
1794.159	0.470	-0.096	0.611	3475.000	0.535	-1.371	1.125	5150.000	-1.270	1.991	2.071

1819.208	-0.565	0.687	-0.952	3500.000	-0.529	-0.403	-0.496	5175.000	-1.910	-0.415	1.522
1841.269	0.290	0.788	0.260	3525.000	1.151	1.073	-1.331	5200.000	-1.360	-1.164	1.550
1868.805	-1.195	1.163	1.111	3550.000	1.268	0.017	-1.420	5225.000	-1.835	1.958	-2.084
1893.512	0.080	-1.114	0.691	3575.000	-1.202	-1.547	-1.339	5250.000	0.255	1.801	0.240
1917.232	-0.534	1.097	-0.979	3600.000	-0.221	-0.180	-1.466	5275.000	1.975	-1.489	-0.319
1941.535	0.360	0.914	-0.831	3625.000	-0.008	0.275	-0.398	5300.000	0.700	-1.036	0.311
1967.839	0.591	-0.794	0.862	3650.000	-1.647	-0.521	1.718				
Receiver Depth: 1999.699 m											
Source offset (m)	Noise Profile 1 (ms)	Noise Profile 2 (ms)	Noise Profile 3 (ms)	Source offset (m)	Noise Profile 1 (ms)	Noise Profile 2 (ms)	Noise Profile 3 (ms)	Source offset (m)	Noise Profile 1 (ms)	Noise Profile 2 (ms)	Noise Profile 3 (ms)
324.600	-0.413	0.464	-0.440	1995.992	0.980	-0.424	-0.624	3674.382	0.495	-1.414	1.040
350.549	0.003	0.821	-0.320	2021.284	1.227	-1.256	0.652	3696.833	-0.930	0.797	-0.934
376.889	-0.529	-0.686	-0.392	2047.768	-0.816	-0.953	-1.221	3725.141	-1.270	1.495	0.234
400.611	0.158	-0.156	-0.344	2068.441	0.005	-0.747	-0.461	3748.488	0.543	-1.615	-1.109
425.009	-0.314	-0.206	-0.142	2099.202	0.133	-0.966	-0.894	3773.125	-0.550	-0.424	0.673
451.156	-0.885	-0.790	0.113	2122.910	-0.430	0.101	0.903	3797.180	0.366	0.774	0.934
473.074	-0.562	-0.564	0.599	2146.801	-1.260	0.563	-0.286	3823.886	-0.751	1.596	-1.461
501.052	0.819	0.896	-0.219	2171.815	1.225	-0.957	-0.310	3847.157	-0.490	-1.365	-0.088
523.771	-0.347	0.869	-0.881	2200.140	-0.332	0.363	-0.455	3873.904	-1.414	0.125	-1.241
549.677	0.529	-0.637	0.127	2218.331	0.583	0.422	-1.018	3899.011	-1.222	-1.547	-1.700
574.419	-0.432	0.039	-0.975	2249.944	0.133	-0.001	0.505	3924.745	-1.006	0.706	-1.691
602.401	0.636	0.970	-0.321	2272.62	0.669	-0.164	-0.665	3947.236	-0.741	-1.586	-0.209
624.922	0.120	-0.872	0.348	2294.818	-0.013	0.892	-1.133	3974.137	-0.311	-0.648	0.143
648.928	0.772	-0.722	-0.814	2323.298	0.420	1.296	-0.337	4000.000	0.709	0.155	0.628
674.706	-0.172	0.041	0.023	2348.619	1.284	0.554	-0.489	4025.000	-0.771	1.641	-0.203
695.534	-0.540	-0.939	0.682	2373.838	-0.140	-0.190	0.200	4050.000	-0.197	0.172	0.620
722.973	-0.592	0.925	0.277	2397.572	0.382	-0.249	-0.201	4075.000	0.505	-1.050	-1.090
743.035	0.602	-0.455	0.617	2423.962	-0.665	0.611	-1.108	4100.000	0.924	1.671	-1.779

772.708	-0.596	0.890	-0.849	2448.348	-1.141	-1.074	0.955	4125.000	0.000	-1.503	1.173
799.365	-0.596	0.212	0.311	2472.638	1.147	-0.121	-1.033	4150.000	1.321	1.885	0.977
827.466	-0.757	0.479	-0.299	2497.266	0.249	-1.131	0.421	4175.000	-1.887	1.027	1.128
847.578	0.239	0.954	-0.945	2524.872	0.299	0.228	-0.007	4200.000	0.755	0.197	-1.074
873.161	0.276	0.710	0.340	2548.532	-0.472	-0.084	-0.109	4225.000	-1.350	-0.717	1.893
898.705	-0.414	-0.999	0.414	2571.795	-0.369	0.850	-1.194	4250.000	-1.399	-1.786	1.003
925.852	-0.299	0.039	0.902	2596.858	-1.065	0.792	0.791	4275.000	0.159	0.850	-0.649
947.130	-0.169	0.253	-0.822	2621.377	0.880	-0.669	-0.054	4300.000	-1.129	0.733	0.637
976.925	-0.435	0.358	-0.819	2644.413	1.270	1.130	-0.362	4325.000	0.270	-0.154	1.480
993.203	-0.776	-0.413	-0.549	2674.605	-0.857	-0.698	0.885	4350.000	1.766	-0.542	-1.098
1023.519	0.856	-1.021	-0.349	2702.929	-1.112	-1.209	-1.195	4375.000	0.005	-0.497	0.220
1052.331	0.531	-0.699	-0.771	2723.228	-0.025	-1.445	1.348	4400.000	-1.952	1.060	-0.779
1074.363	-0.950	-0.328	-0.789	2747.233	-0.127	0.911	-1.384	4425.000	1.183	0.009	-1.117
1098.092	-0.814	0.349	0.828	2773.232	1.214	0.032	-1.222	4450.000	-1.217	0.655	-0.669
1124.219	0.660	-0.233	-0.398	2800.637	-1.446	0.401	-0.364	4475.000	-1.196	-0.731	-0.433
1149.317	0.708	-0.047	-0.787	2828.265	-0.542	-1.359	-1.025	4500.000	-1.293	-1.365	-1.179
1174.603	0.183	0.318	-1.069	2849.906	-1.175	0.416	-1.389	4525.000	-0.057	2.022	1.884
1196.443	0.372	-0.587	-0.509	2877.363	-0.441	-0.526	0.239	4550.000	-0.565	-0.631	-1.931
1223.741	-0.567	0.532	0.267	2900.926	1.446	-0.243	-0.038	4575.000	1.693	0.501	-0.191
1247.658	0.687	-0.830	0.766	2922.933	0.021	1.381	-0.841	4600.000	-1.451	-0.733	-0.807
1272.022	0.958	-0.670	0.056	2946.349	1.288	0.082	-0.449	4625.000	-0.930	0.752	0.470
1297.550	1.036	-1.059	0.256	2973.590	-0.531	1.116	-0.144	4650.000	-0.527	-1.316	0.273
1321.672	0.067	0.700	0.058	2995.885	0.662	1.379	0.430	4675.000	-0.852	-0.063	-1.620
1347.028	1.097	-0.914	-0.468	3023.058	0.274	-0.406	1.204	4700.000	-1.578	-0.117	-0.860
1376.17	0.099	-0.502	-0.015	3047.187	0.315	-0.345	-1.056	4725.000	0.047	2.002	-0.606
1396.418	-1.007	1.113	-0.134	3072.056	0.136	-0.771	-1.458	4750.000	0.683	1.982	1.602
1422.895	-0.186	-0.592	0.080	3097.786	-1.364	-0.877	-1.011	4775.000	-1.852	-1.417	1.403

1443.884	-0.867	0.406	-0.408	3123.280	-0.853	0.697	-0.614	4800.000	-1.464	-0.461	-0.157
1467.463	-0.739	-0.411	0.324	3147.799	-0.364	-0.915	0.219	4825.000	-1.489	-1.763	1.972
1494.924	1.049	0.719	0.918	3173.841	-0.731	-0.439	-0.491	4850.000	-0.309	2.072	1.327
1522.751	-0.243	0.830	-0.496	3197.658	-0.267	-1.542	0.246	4875.000	0.760	-0.788	0.463
1548.932	-1.049	-0.762	0.258	3224.52	-1.005	-0.804	0.096	4900.000	2.035	-0.334	1.837
1574.732	0.833	-0.035	-0.770	3246.308	1.535	-1.161	1.404	4925.000	0.250	2.130	-0.331
1598.225	0.821	-1.068	0.500	3269.615	0.429	-1.080	-0.863	4950.000	-0.199	-1.940	-1.860
1622.070	0.865	0.936	1.136	3298.234	-1.134	0.275	-0.911	4975.000	-1.062	-1.859	0.874
1648.491	-0.314	0.141	-0.689	3322.795	-1.077	1.052	0.955	5000.000	0.650	0.163	-2.054
1672.676	0.536	0.104	-0.631	3348.757	0.030	0.097	-0.251	5025.000	1.004	0.116	-0.071
1699.359	-0.173	-0.872	-0.737	3371.168	-0.072	1.174	0.844	5050.000	1.947	-1.884	0.820
1721.478	-1.135	-0.146	0.804	3397.601	-0.916	1.460	0.929	5075.000	-0.017	0.206	-1.936
1748.692	-0.175	-0.313	0.252	3415.795	-1.657	1.427	1.031	5100.000	2.133	-0.289	1.415
1772.717	-0.510	1.042	-0.971	3448.241	-0.186	-0.493	-0.875	5125.000	-1.278	-1.891	1.683
1799.002	0.293	-0.486	0.778	3472.837	1.331	1.473	-0.972	5150.000	1.644	0.939	0.043
1824.082	0.982	-0.979	-0.280	3498.606	0.879	1.164	-0.808	5175.000	2.043	1.850	-2.213
1846.130	-0.505	-1.024	0.157	3522.813	-1.609	0.727	0.690	5200.000	-1.427	1.029	-1.553
1873.676	0.413	-0.885	-0.786	3549.675	-0.279	-1.708	0.803	5225.000	0.607	-1.799	-0.883
1898.386	0.095	-0.894	0.106	3572.790	-0.946	1.386	0.809	5250.000	-1.795	-0.534	1.185
1922.128	-0.363	0.910	-0.760	3596.293	-0.001	0.564	-0.306	5275.000	-0.390	-0.808	0.414
1946.425	-0.622	-1.054	-0.414	3624.682	-0.528	-1.548	1.026	5300.000	-1.518	2.018	0.508
1972.733	-0.642	-1.103	0.983	3649.510	0.522	0.418	-0.005				
Receiver Depth: 2009.758 m											
Source offset (m)	Noise Profile 1 (ms)	Noise Profile 2 (ms)	Noise Profile 3 (ms)	Source offset (m)	Noise Profile 1 (ms)	Noise Profile 2 (ms)	Noise Profile 3 (ms)	Source offset (m)	Noise Profile 1 (ms)	Noise Profile 2 (ms)	Noise Profile 3 (ms)
303.261	0.271026	-0.668673	0.541624	1977.755	-0.928588	0.481323	0.107085	3654.610	-1.625820	0.658559	-1.631466
328.581	-0.268953	-0.667026	0.880226	2001.021	0.387378	0.046535	1.033185	3679.484	-1.761009	-0.661354	0.435901

354.657	-0.098	-0.859	-0.043	2026.319	1.252	1.154	-0.670	3701.937	0.019	-0.821	-0.782
380.983	-0.799	0.882	0.270	2052.794	0.191	0.920	-1.189	3730.246	1.692	-0.971	-1.642
404.849	-0.088	0.268	0.352	2073.482	0.857	-0.769	-0.588	3753.592	-0.885	-1.590	-1.403
429.240	-0.247	-0.169	-0.352	2104.247	0.465	-1.090	-0.966	3778.230	-1.601	-0.125	0.636
455.469	-0.372	-0.922	0.633	2127.948	0.329	1.036	-1.150	3802.290	-0.297	0.101	-0.503
477.448	-0.506	0.680	0.152	2151.842	1.255	-0.535	1.042	3828.996	1.783	0.435	0.031
505.381	-0.670	0.094	-0.210	2176.867	1.262	0.760	0.812	3852.268	0.619	-0.578	0.030
528.180	0.267	0.744	-0.450	2205.177	-1.140	0.583	-0.359	3879.018	1.062	-1.735	-1.070
554.124	0.695	0.063	0.811	2223.370	-0.791	-0.761	-0.610	3904.126	0.575	1.530	-0.585
578.871	0.105	0.499	-0.761	2254.993	0.186	0.725	-0.802	3929.863	1.225	-0.451	-1.303
606.897	-0.848	-0.646	-0.942	2277.647	-1.026	0.796	-1.248	3952.356	-1.123	0.686	0.536
629.448	-0.734	-0.597	0.624	2299.834	0.976	0.047	-1.123	3979.256	-1.400	-1.164	0.237
653.514	-0.348	0.159	-0.807	2328.326	-0.511	0.427	-0.410	4000.000	-0.123	-0.985	1.657
679.317	0.308	0.298	0.731	2353.659	0.727	1.208	-1.203	4025.000	-0.809	1.016	1.523
700.261	0.288	0.091	0.115	2378.880	0.641	-0.367	-1.237	4050.000	-0.339	1.839	-0.594
727.683	-0.103	0.516	-0.672	2402.618	0.845	-1.084	1.262	4075.000	1.535	0.386	-1.022
747.801	0.793	0.068	0.481	2429.010	0.749	-0.631	-0.678	4100.000	0.943	0.459	0.142
777.454	0.749	0.690	0.184	2453.412	0.332	0.383	0.712	4125.000	1.684	-0.795	-0.220
804.143	0.334	-0.235	-0.533	2477.697	-0.719	-1.059	0.689	4150.000	0.542	-0.723	0.661
832.193	-0.091	-0.001	0.665	2502.335	0.254	0.961	0.881	4175.000	-0.909	-0.225	-0.077
852.318	-0.225	0.770	0.781	2529.938	-0.806	-1.212	-0.563	4200.000	1.165	-0.225	-0.570
877.902	0.281	0.143	-0.266	2553.598	-0.559	-0.491	0.850	4225.000	1.194	-0.552	0.394
903.481	0.109	-0.064	0.578	2576.873	-1.023	-0.404	-1.244	4250.000	1.863	1.472	0.627
930.585	0.239	0.799	0.227	2601.946	-0.435	0.518	0.342	4275.000	1.931	0.712	1.104
951.877	-0.815	-0.582	-0.919	2626.465	0.515	-1.298	1.217	4300.000	-1.066	0.235	-0.111
981.685	-0.936	-0.204	-0.412	2649.516	-0.864	-0.623	1.264	4325.000	1.141	1.363	0.298
997.988	-0.850	0.404	-0.578	2679.669	-0.210	-0.912	-0.972	4350.000	-0.696	-0.776	0.773

1028.302	0.662	0.902	0.908	2707.953	-1.117	-0.788	1.444	4375.000	1.113	0.288	-0.433
1057.108	0.444	0.299	0.946	2728.236	-1.070	-1.451	0.030	4400.000	0.472	0.059	-0.510
1079.172	0.618	-0.443	0.610	2752.229	1.437	-0.873	0.835	4425.000	0.088	1.052	1.329
1102.905	-0.743	0.473	-0.011	2778.230	-0.157	-1.311	-0.850	4450.000	-0.874	1.306	-1.116
1129.033	-0.758	0.522	0.772	2805.637	1.352	1.298	-0.399	4475.000	-1.171	-0.515	0.199
1154.135	-0.029	0.087	0.879	2833.270	-0.971	-1.135	1.035	4500.000	-1.187	-0.431	-1.242
1179.462	-0.692	-1.002	0.863	2854.923	-0.537	0.369	-0.662	4525.000	0.937	1.867	-0.515
1201.324	-0.994	0.444	0.475	2882.394	-1.413	0.551	0.699	4550.000	-0.288	1.801	-0.808
1228.635	0.247	0.340	-1.070	2905.969	0.784	0.012	1.330	4575.000	0.105	-0.443	1.321
1252.559	0.575	-1.035	1.001	2927.986	0.344	-0.798	-0.210	4600.000	1.778	-1.119	0.290
1276.939	0.818	-0.624	0.626	2951.411	1.021	-0.288	0.693	4625.000	0.036	-1.050	-1.117
1302.470	-0.263	-0.252	-0.185	2978.669	-0.942	-1.381	0.910	4650.000	2.031	-1.549	1.061
1326.568	0.395	-0.723	-0.264	3000.961	-0.896	0.305	0.613	4675.000	-0.025	0.706	-0.213
1351.947	0.680	-1.039	0.073	3028.136	0.076	-1.520	0.996	4700.000	1.946	-0.679	-1.561
1381.150	0.815	-0.666	1.105	3052.265	1.408	-1.566	-0.410	4725.000	-0.661	0.326	1.301
1401.407	-0.936	0.841	0.493	3077.138	0.364	1.009	-1.084	4750.000	-0.606	0.904	-0.130
1427.905	-0.940	1.099	0.208	3102.869	-1.153	0.228	-0.180	4775.000	0.880	1.932	1.812
1448.880	-0.397	-0.120	0.352	3128.367	-1.251	-0.759	0.326	4800.000	1.207	1.700	1.324
1472.461	0.557	-0.195	-0.398	3152.887	1.393	0.310	-0.309	4825.000	-2.077	1.140	-1.964
1499.879	-0.973	-0.574	-0.377	3178.930	-0.602	-0.226	-0.904	4850.000	0.738	-0.358	1.535
1527.695	0.311	0.966	0.195	3202.748	-0.618	-0.151	-0.829	4875.000	1.106	0.142	-0.203
1553.918	0.272	-0.570	0.104	3229.613	-0.058	0.289	-0.618	4900.000	-1.543	-0.481	-0.959
1579.704	-0.046	-0.018	0.678	3251.407	0.637	0.413	0.840	4925.000	-2.075	1.404	-1.713
1603.186	-0.540	0.985	1.129	3274.706	-0.448	-1.416	1.063	4950.000	-0.557	-0.028	-0.045
1627.036	-0.946	-0.171	0.116	3303.329	1.401	1.383	-0.025	4975.000	1.742	-1.410	1.525
1653.462	-0.058	-0.639	-0.076	3327.898	1.206	1.008	0.110	5000.000	0.933	-1.311	0.897
1677.641	0.132	-0.978	0.199	3353.854	0.401	0.944	0.710	5025.000	0.062	0.873	1.553

1704.318	0.953	-0.460	1.132	3376.264	-1.151	-1.187	1.559	5050.000	-1.214	1.102	-1.070
1726.445	0.238	1.069	-1.052	3402.702	-0.017	0.631	0.511	5075.000	-1.013	-1.515	0.696
1753.676	0.680	-0.276	0.917	3420.895	-0.968	1.382	1.030	5100.000	2.182	-2.137	-1.227
1777.695	-0.421	0.909	0.561	3453.340	-1.385	0.957	0.825	5125.000	0.253	-0.735	-1.323
1803.977	0.217	-0.740	0.582	3477.933	-1.263	-0.657	-0.038	5150.000	-0.296	-0.367	-2.094
1829.087	0.034	0.219	-0.353	3503.704	0.809	1.470	0.108	5175.000	-1.740	-0.842	0.828
1851.122	-0.084	1.178	-0.763	3527.909	1.353	0.930	1.302	5200.000	-0.795	0.041	1.976
1878.678	-0.100	0.298	-0.303	3554.773	0.608	-0.290	-1.381	5225.000	1.171	0.980	-0.765
1903.390	0.328	0.024	-0.144	3577.890	-1.286	0.561	1.206	5250.000	-0.326	-1.779	0.660
1927.153	1.055	0.898	-0.186	3601.391	0.504	0.511	-1.320	5275.000	0.680	-0.253	-1.623
1951.442	-0.168	0.239	1.234	3629.788	0.172	0.829	0.293	5300.000	1.679	-1.948	-1.266
Receiver Depth: 2019.927 m											
Source offset (m).	Noise Profile 1 (ms)	Noise Profile 2 (ms)	Noise Profile 3 (ms)	Source offset (m)	Noise Profile 1 (ms)	Noise Profile 2 (ms)	Noise Profile 3 (ms)	Source offset (m)	Noise Profile 1 (ms)	Noise Profile 2 (ms)	Noise Profile 3 (ms)
307.433	-0.576	-0.039	0.505	1982.824	0.003	-0.319	0.943	3659.735	1.734	-1.265	1.272
332.872	-0.847	0.961	-0.892	2006.097	0.630	1.262	0.222	3684.612	0.726	-0.249	-0.125
359.049	-0.306	-0.284	-0.027	2031.400	-0.418	0.946	0.152	3707.066	0.468	0.979	1.695
385.343	0.634	0.127	-0.059	2057.867	-1.049	-0.121	-0.599	3735.376	0.231	0.253	0.905
409.334	0.030	0.564	-0.644	2078.568	1.004	1.067	-0.407	3758.721	-1.419	0.014	-1.444
433.705	-0.289	-0.050	0.621	2109.336	-1.205	-1.149	1.300	3783.360	-0.956	0.928	-0.095
460.001	-0.832	-0.788	0.259	2133.030	-0.427	0.087	-0.188	3807.424	0.637	-1.442	-1.552
482.029	0.069	0.908	-0.527	2156.926	0.263	0.833	-0.580	3834.131	-0.043	-0.975	-1.267
509.907	-0.349	0.839	0.678	2181.962	1.167	1.290	0.485	3857.404	0.383	0.143	-0.130
532.777	0.545	0.834	-0.725	2210.257	-0.576	-0.836	-0.762	3884.155	0.258	1.398	-0.165
558.748	0.626	0.027	0.657	2228.452	0.016	0.158	-1.200	3909.264	-1.366	1.452	1.597
583.493	-0.683	0.944	0.502	2260.084	0.646	-0.113	-0.567	3935.005	0.789	0.805	-0.034
611.554	-0.045	0.851	0.453	2282.716	0.340	1.308	0.496	3957.499	-1.094	-0.867	0.046
634.129	-0.037	-0.663	-0.260	2304.890	-1.190	0.037	1.022	3984.399	0.686	0.664	1.010

658.248	0.339	0.573	-0.590	2333.394	-0.896	-0.910	-0.218	4025.000	0.309	-1.213	1.067
684.072	-0.461	0.504	-0.876	2358.739	-0.253	0.090	-0.202	4050.000	1.598	0.059	-1.413
705.124	0.925	0.627	0.521	2383.962	0.755	0.712	1.078	4075.000	0.092	-0.100	-0.699
732.526	0.945	0.696	0.396	2407.702	-0.756	0.625	-0.873	4100.000	-1.030	1.625	-0.799
752.696	0.903	-0.256	-0.179	2434.097	0.941	0.116	0.774	4125.000	-0.510	1.503	1.137
782.323	0.812	-0.144	-0.555	2458.515	1.375	-0.725	1.296	4150.000	1.870	-1.106	0.472
809.041	-0.781	-0.599	0.090	2482.793	0.889	-0.085	0.684	4175.000	-1.336	0.316	-0.472
837.034	0.149	0.750	-0.149	2507.442	-0.619	-0.879	-0.956	4200.000	-0.237	1.490	1.585
857.170	0.063	0.642	0.251	2535.041	-0.357	1.221	-1.038	4225.000	-1.274	-1.490	1.526
882.753	0.354	0.410	-0.495	2558.701	-1.099	-0.136	-0.615	4250.000	1.579	0.400	-0.273
908.363	0.536	0.773	-0.599	2581.986	-0.997	0.820	-0.303	4275.000	1.495	0.224	-1.930
935.422	0.510	-0.602	-0.800	2607.071	-0.589	-1.203	-0.043	4300.000	-1.304	-0.943	-0.647
956.725	-0.156	-0.979	0.874	2631.588	0.948	1.136	1.075	4325.000	-0.049	-1.490	0.991
986.543	0.315	-0.055	0.382	2654.653	0.093	0.324	-0.821	4350.000	1.333	0.565	1.562
1002.868	0.933	0.024	-0.557	2684.768	-0.126	-0.811	0.353	4375.000	0.434	-1.735	1.213
1033.179	0.571	-0.047	-0.417	2713.012	0.267	-0.181	0.836	4400.000	-0.979	-0.723	-0.618
1061.975	-0.769	0.264	-0.922	2733.279	0.990	0.011	1.449	4425.000	0.332	0.941	1.518
1084.068	-0.270	0.705	0.610	2757.260	-0.909	-0.579	-0.221	4450.000	1.016	-0.486	0.113
1107.805	-0.761	-0.026	0.198	2783.262	-0.466	-0.921	0.617	4475.000	-0.054	1.993	1.844
1133.931	-0.743	0.219	-0.782	2810.670	-0.059	-0.845	0.106	4500.000	-0.284	-1.203	-0.234
1159.036	-0.468	-0.455	0.934	2838.309	1.316	1.109	-1.268	4525.000	-0.538	1.631	1.866
1184.402	0.122	-1.075	0.894	2859.972	0.329	0.688	-1.173	4550.000	1.833	-1.861	-1.223
1206.284	0.680	0.103	-0.281	2887.458	-1.052	-0.654	0.765	4575.000	1.357	-0.722	0.849
1233.606	0.637	0.223	-0.827	2911.043	0.007	-0.209	-1.162	4600.000	-1.457	1.703	-0.680
1257.536	0.602	-0.593	0.521	2933.070	0.832	-1.302	-1.210	4625.000	0.510	-0.657	0.815
1281.929	-0.374	1.023	-0.689	2956.504	-1.255	-0.884	-1.543	4650.000	1.857	1.732	-1.002
1307.463	-0.347	0.770	0.359	2983.778	-1.250	1.501	1.546	4675.000	-0.420	-0.007	-0.110

1331.536	-0.029	0.259	0.686	3006.069	0.258	0.333	-1.397	4700.000	0.277	1.510	0.547
1356.935	-0.390	0.058	0.335	3033.245	0.370	-1.084	-0.649	4725.000	-0.280	-1.868	1.707
1386.199	-0.645	0.225	0.597	3057.374	-1.352	0.611	-0.265	4750.000	0.910	-2.071	0.612
1406.463	-0.743	0.478	-0.834	3082.250	1.162	0.038	0.634	4775.000	-1.747	-0.604	1.171
1432.981	0.959	0.881	-0.289	3107.982	0.291	-0.316	-1.359	4800.000	0.125	0.848	1.972
1453.941	0.957	-0.583	-0.707	3133.483	0.533	-0.990	1.478	4825.000	-1.832	1.161	-0.248
1477.524	1.092	0.003	-0.664	3158.005	0.216	0.032	-0.799	4850.000	1.094	-0.167	0.225
1504.896	-0.106	-0.381	0.094	3184.048	-0.663	1.518	1.006	4875.000	0.089	0.745	-1.622
1532.702	-0.623	0.360	0.383	3207.868	1.352	-0.197	0.433	4900.000	1.147	0.417	0.541
1558.966	0.265	-1.157	1.047	3234.734	0.807	1.292	1.230	4925.000	-0.544	0.725	-0.853
1584.736	-0.741	1.002	0.476	3256.536	1.232	-1.152	-0.149	4950.000	-0.114	-1.327	1.593
1608.206	0.759	0.290	0.598	3279.827	-1.158	-0.097	-0.878	4975.000	1.865	1.405	-0.235
1632.059	-0.603	0.955	-0.051	3308.451	0.055	0.616	-1.043	5000.000	-1.842	0.896	1.213
1658.491	0.501	-0.197	0.444	3333.029	0.362	0.099	-1.038	5025.000	0.919	1.003	-2.101
1682.662	0.611	-0.096	-0.140	3358.978	0.534	-0.939	0.377	5050.000	1.119	-1.962	1.262
1709.332	-0.019	0.837	0.520	3381.389	1.331	0.793	0.350	5075.000	-0.443	1.912	-0.735
1731.466	-0.376	-0.138	-0.918	3407.830	0.533	1.640	-1.450	5100.000	-1.764	0.408	-1.650
1758.713	0.736	-0.195	-0.538	3426.021	1.455	-1.333	0.312	5125.000	1.779	1.422	2.109
1782.727	0.181	-0.596	0.384	3458.467	-1.360	-0.585	1.398	5150.000	-1.266	-0.967	-1.603
1809.004	-0.070	-0.308	0.035	3483.057	-0.758	-0.988	0.418	5175.000	1.951	-0.350	1.086
1834.144	0.469	-0.891	0.588	3508.829	0.700	-0.264	0.786	5200.000	0.620	-0.775	-0.871
1856.165	0.544	0.781	-0.517	3533.031	1.543	1.247	0.276	5225.000	-1.047	0.134	-1.629
1883.729	-0.964	0.610	-0.608	3559.898	-0.266	1.127	0.831	5250.000	0.741	-1.641	1.722
1908.443	0.873	-0.911	-0.868	3583.016	1.467	-0.781	0.479	5275.000	1.227	1.505	0.124
1932.226	0.607	0.765	-0.460	3606.516	-0.557	-0.288	-1.072	5300.000	-2.000	-0.325	0.070
1956.508	0.358	-0.355	-0.749	3634.919	-0.814	0.012	-1.341				

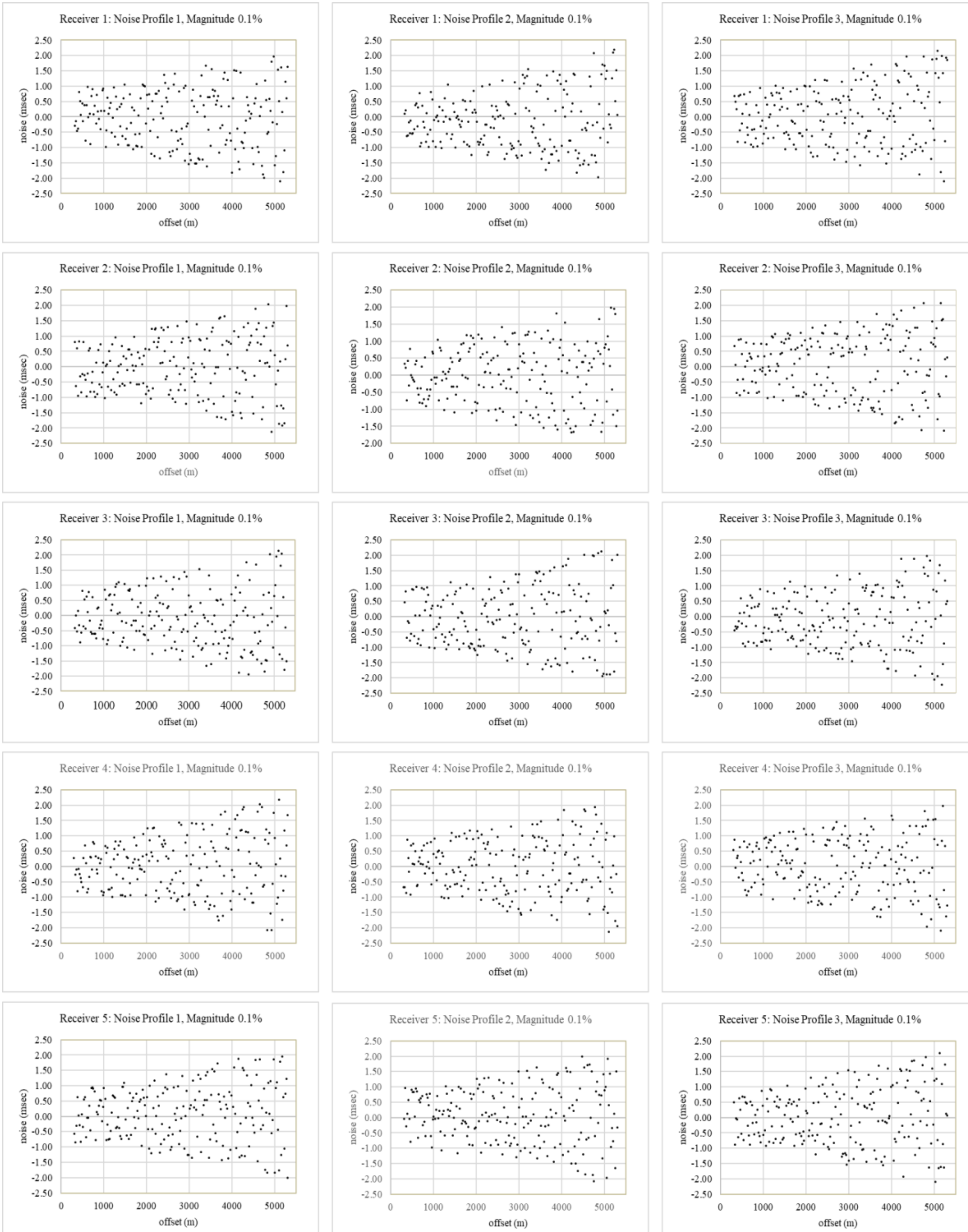

Figure C.9: Noise profiles at magnitude 0.1% for Receivers 1 to 5.

Table C.4: Optimal a, b, χ values, 4-layer model, source-receiver offsets to 4000 m, synthetic data with added noise of magnitude 0.1%, 0.01%, 0.001%, 0.0001% for noise Profiles 2 and 3.

	Used for synthetic traveltimes	Optimal values with no noise added	Noise magnitude			
			0.0001%	0.001%	0.01%	0.1%
			Optimal values with Profile 2 noise added to synthetic traveltimes:			
RSS		6.41×10^{-11}	5.29×10^{-10}	4.59×10^{-08}	4.57×10^{-06}	4.58×10^{-04}
a_1	1279	1200	1165	1396	1420	1554
a_2	1748	1701	1725	1814	1560	1452
a_3	2966	2977	2956	2924	2826	2814
a_4	2597	2597	2596	2596	2584	2620
b_1	0.776	1.242	1.404	0.165	0.587	0.342
b_2	1.023	1.101	1.063	0.913	1.357	1.469
b_3	0.219	0.218	0.222	0.229	0.270	0.364
b_4	0.760	0.759	0.762	0.762	0.781	0.368
χ_1	0.0000	0.0000	0.0000	0.0000	0.0000	0.0000
χ_2	0.0195	0.0213	0.0167	0.0121	0.0025	0.0010
χ_3	0.0585	0.0546	0.0621	0.0731	0.1063	0.0982
χ_4	0.0921	0.0921	0.0922	0.0925	0.0956	0.1274
X	5322	5332	5299	5247	4968	4522
			Optimal values with Profile 3 noise added to synthetic traveltimes:			
RSS		6.41×10^{-11}	4.64×10^{-10}	4.63×10^{-08}	4.64×10^{-06}	4.65×10^{-04}
a_1	1279	1200	1199	1378	1345	1456
a_2	1748	1701	1680	1536	1454	1474
a_3	2966	2977	2990	3090	3091	3043
a_4	2597	2597	2597	2599	2617	2749
b_1	0.776	1.242	1.271	0.588	0.937	0.238
b_2	1.023	1.101	1.134	1.356	1.485	1.495
b_3	0.219	0.218	0.215	0.202	0.232	0.430
b_4	0.760	0.759	0.759	0.752	0.679	0.142
χ_1	0.0000	0.0000	0.0000	0.0000	0.0000	0.0000
χ_2	0.0195	0.0213	0.0238	0.0447	0.0472	0.0434
χ_3	0.0585	0.0546	0.0502	0.0180	0.0146	0.0088
χ_4	0.0921	0.0921	0.0921	0.0921	0.0922	0.0935
X	5322	5332	5295	5452	5198	4295

Table C.5: Optimal a, b, χ values, 3-layer model, source-receiver offsets to 4000 m, synthetic data with added noise of magnitude 0.1%, 0.01%, 0.001%, 0.0001% by profile.

	Used for synthetic traveltimes	Optimal values with no noise added	Noise magnitude			
			0.0001%	0.001%	0.01%	0.10%
			Optimal values with Profile 2 noise added:			
RSS		$6.58\text{x}10^{-11}$	$5.36\ \text{x}10^{-10}$	$4.59\ \text{x}10^{-08}$	$4.57\ \text{x}10^{-06}$	$4.58\ \text{x}10^{-04}$
a_1	1279	1207	1208	1214	1248	1297
a_2	1748					
a_3	2966	2989	2985	2964	2850	2837
a_4	2597	2597	2596	2595	2591	2651
b_1	0.776	1.125	1.124	1.118	1.076	0.975
b_2	1.023					
b_3	0.219	0.215	0.217	0.223	0.258	0.367
b_4	0.760	0.760	0.761	0.762	0.752	0.246
χ_1	0.000	0.016	0.015	0.013	0.001	0.001
χ_2	0.020					
χ_3	0.059	0.051	0.052	0.059	0.098	0.089
χ_4	0.092	0.092	0.092	0.092	0.096	0.127
X	5322	5348	5338	5289	5042	4515
			Optimal values with Profile 3 noise added:			
RSS		$6.58\text{x}10^{-11}$	$5.18\ \text{x}10^{-10}$	$4.65\ \text{x}10^{-08}$	$4.65\ \text{x}10^{-06}$	$4.65\ \text{x}10^{-04}$
a_1	1279	1207	1208	1206	1195	1148
a_2	1748					
a_3	2966	2989	2988	2992	3030	3072
a_4	2597	2597	2597	2599	2621	2759
b_1	0.776	1.125	1.125	1.127	1.139	1.206
b_2	1.023					
b_3	0.219	0.215	0.216	0.217	0.232	0.419
b_4	0.760	0.760	0.759	0.751	0.660	0.101
χ_1	0.000	0.016	0.015	0.016	0.020	0.026
χ_2	0.020					
χ_3	0.059	0.051	0.051	0.050	0.035	0.001
χ_4	0.092	0.092	0.092	0.092	0.092	0.093
X	5322	5348	5343	5331	5205	4325

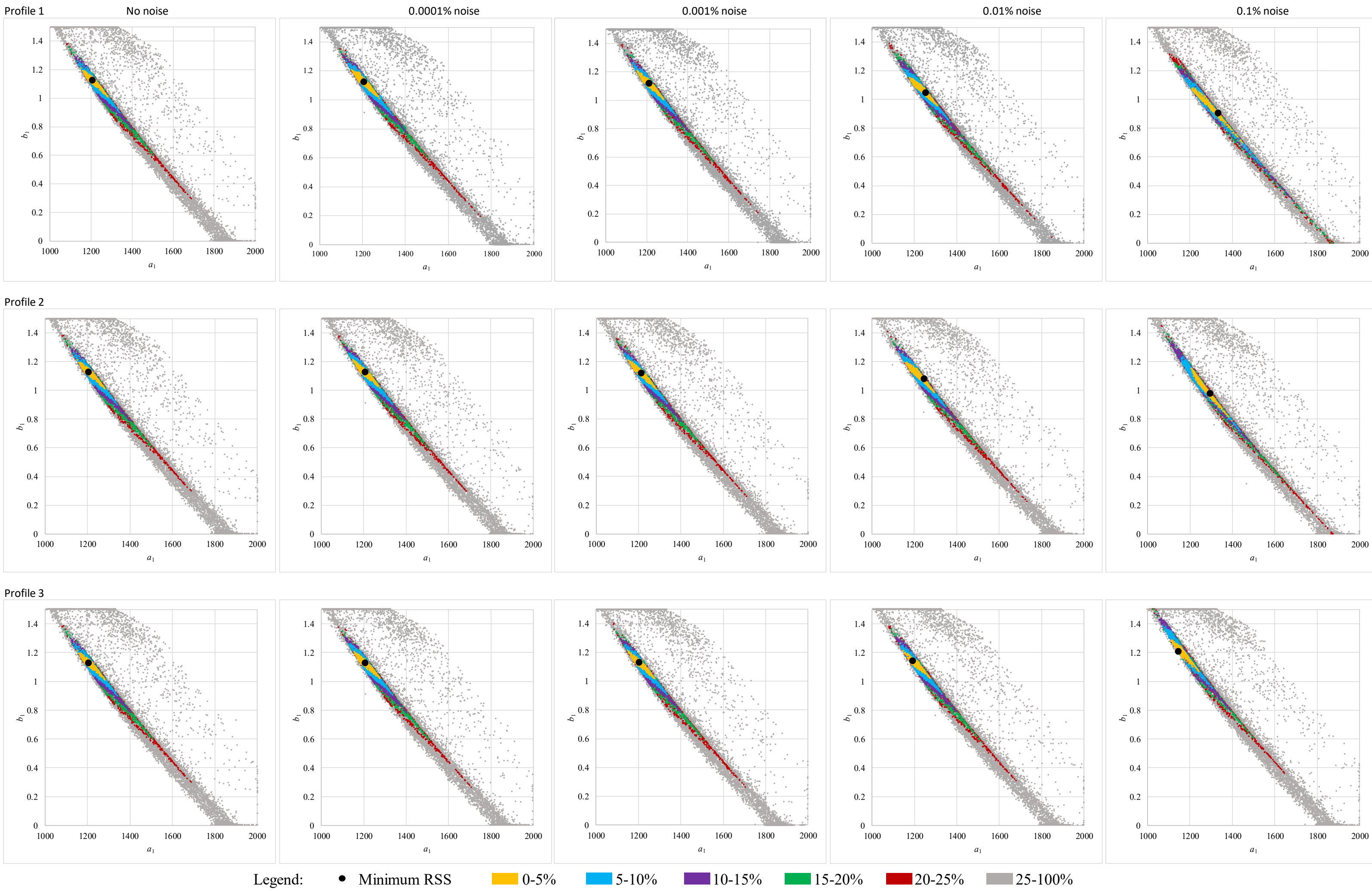

Figure C.10: Cross-plot of parameters, b vs. a, for Layer 1, for noise added as per Profiles 1, 2, and 3, with noise at magnitudes 0, 0.0001%, 0.001%, 0.01%, 0.1%, from left to right. The noise threshold lies between 0.001% noise and 0.01% noise. The colours indicate the distribution of the parameters w.r.t. the percentile of the RSS to the minimum RSS.

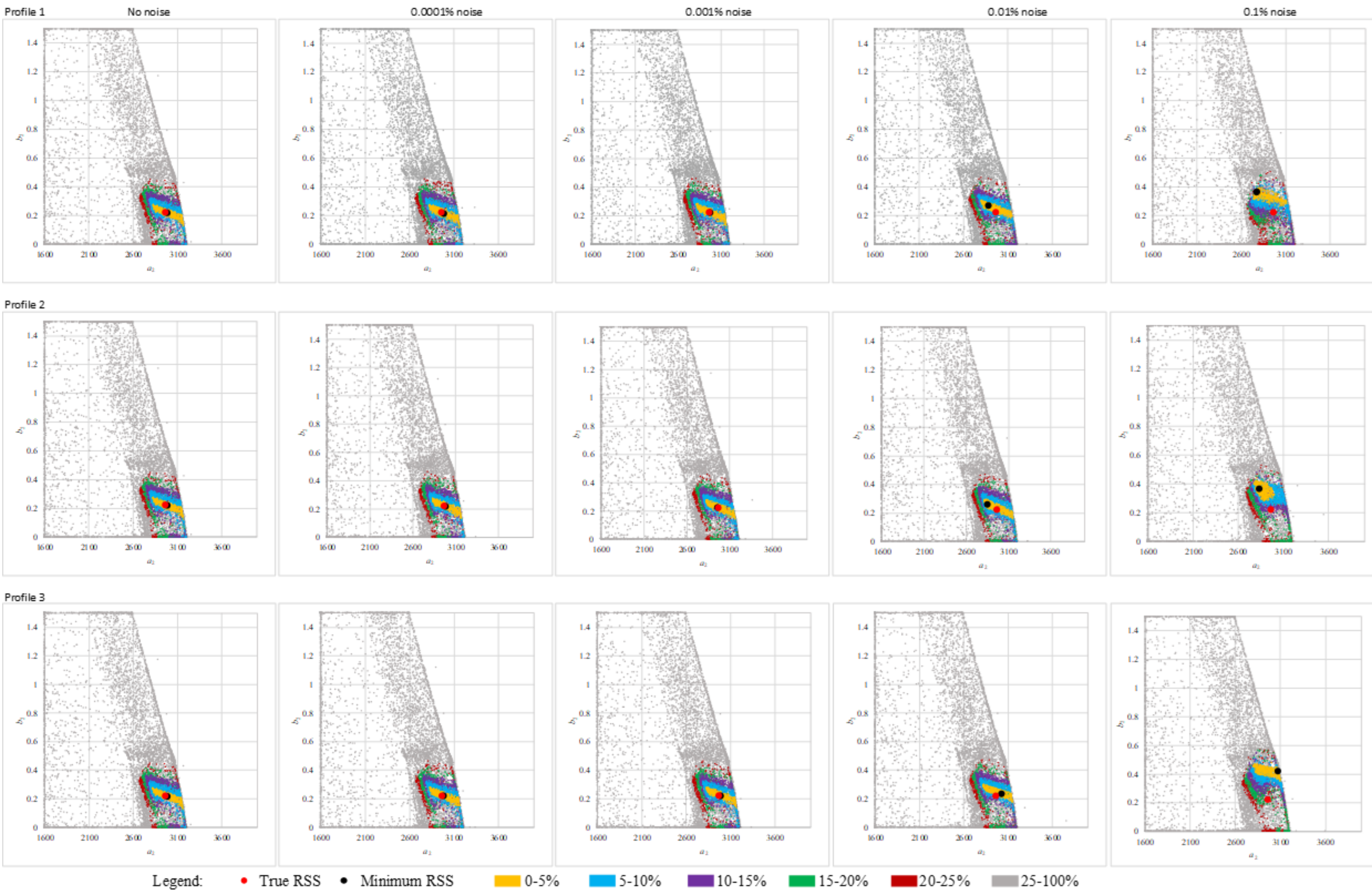

Figure C.11: Cross-plot of parameters, b vs. a, for Layer 2, for noise added as per Profiles 1, 2, and 3, with noise at magnitudes 0, 0.0001%, 0.001%, 0.01%, 0.1%, from left to right. The noise threshold lies between 0.001% noise and 0.01% noise. The colours indicate the distribution of the parameters w.r.t. the percentile of the RSS to the minimum RSS.

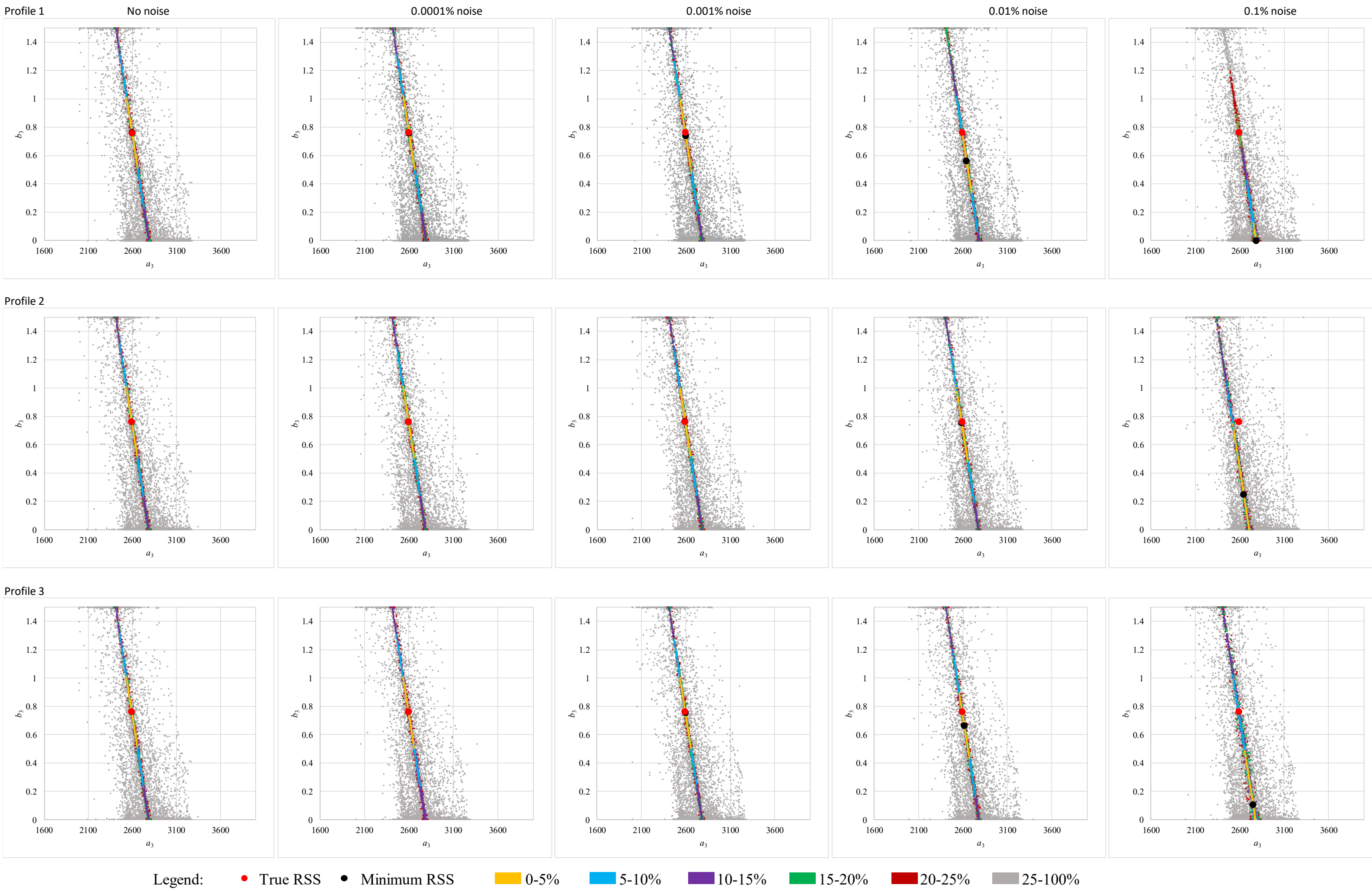

Figure C.12: Cross-plot of parameters, b vs. a, for Layer 3, for noise added as per Profiles 1, 2 and 3, with noise at magnitudes 0, 0.0001%, 0.001%, 0.01%, 0.1%, from left to right. The noise threshold lies between 0.001% noise and 0.01% noise. The colours indicate the distribution of the parameters w.r.t. the percentile of the RSS to the minimum RSS.

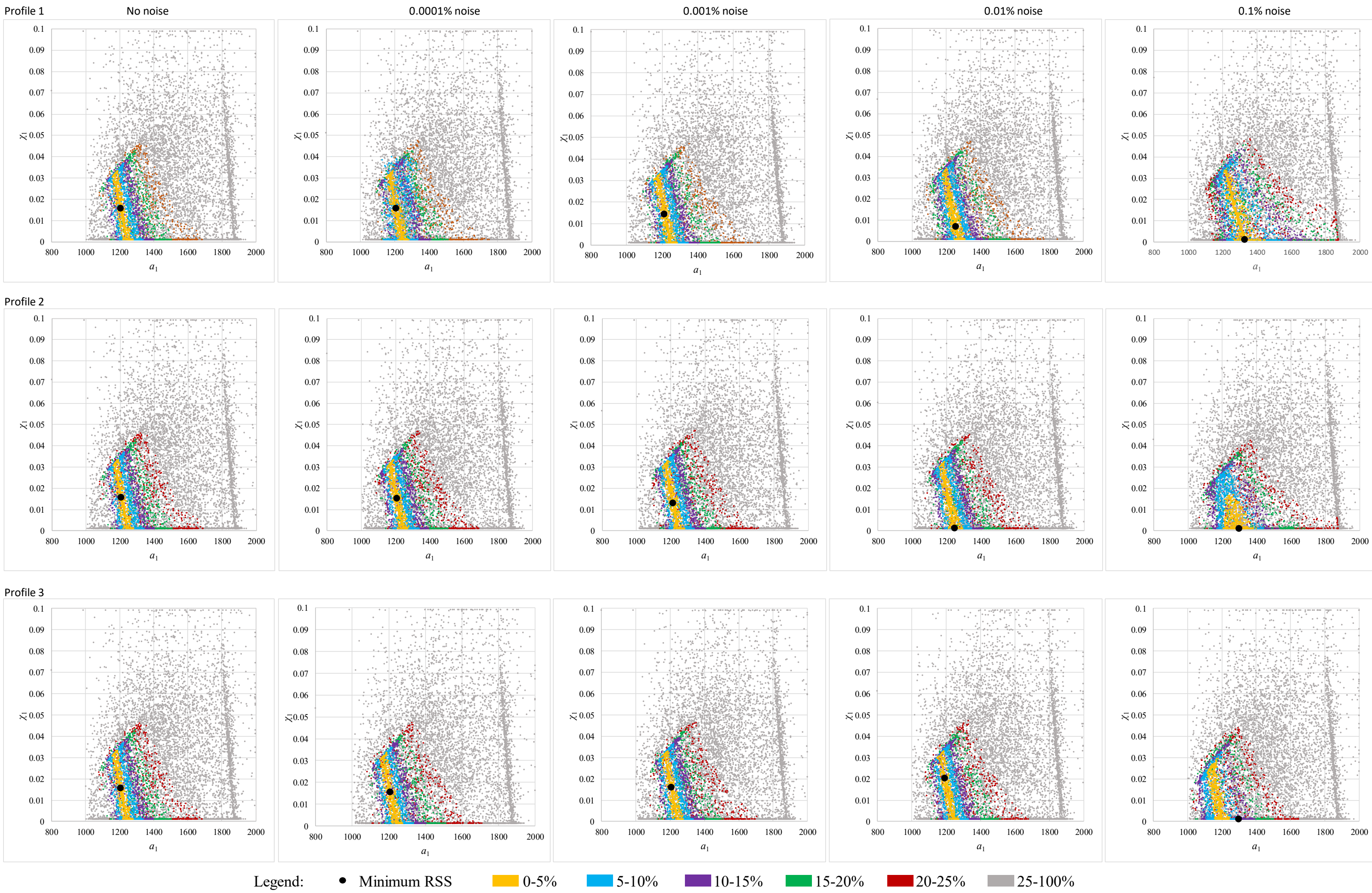

Figure C.13: Cross-plot of parameters, χ vs. a, for Layer 1, for noise added as per Profiles 1, 2, and 3, with noise at magnitudes 0, 0.0001%, 0.001%, 0.01%, 0.1%, from left to right. The noise threshold lies between 0.001% noise and 0.01% noise. The colours indicate the distribution of the parameters w.r.t. the percentile of the RSS to the minimum RSS.

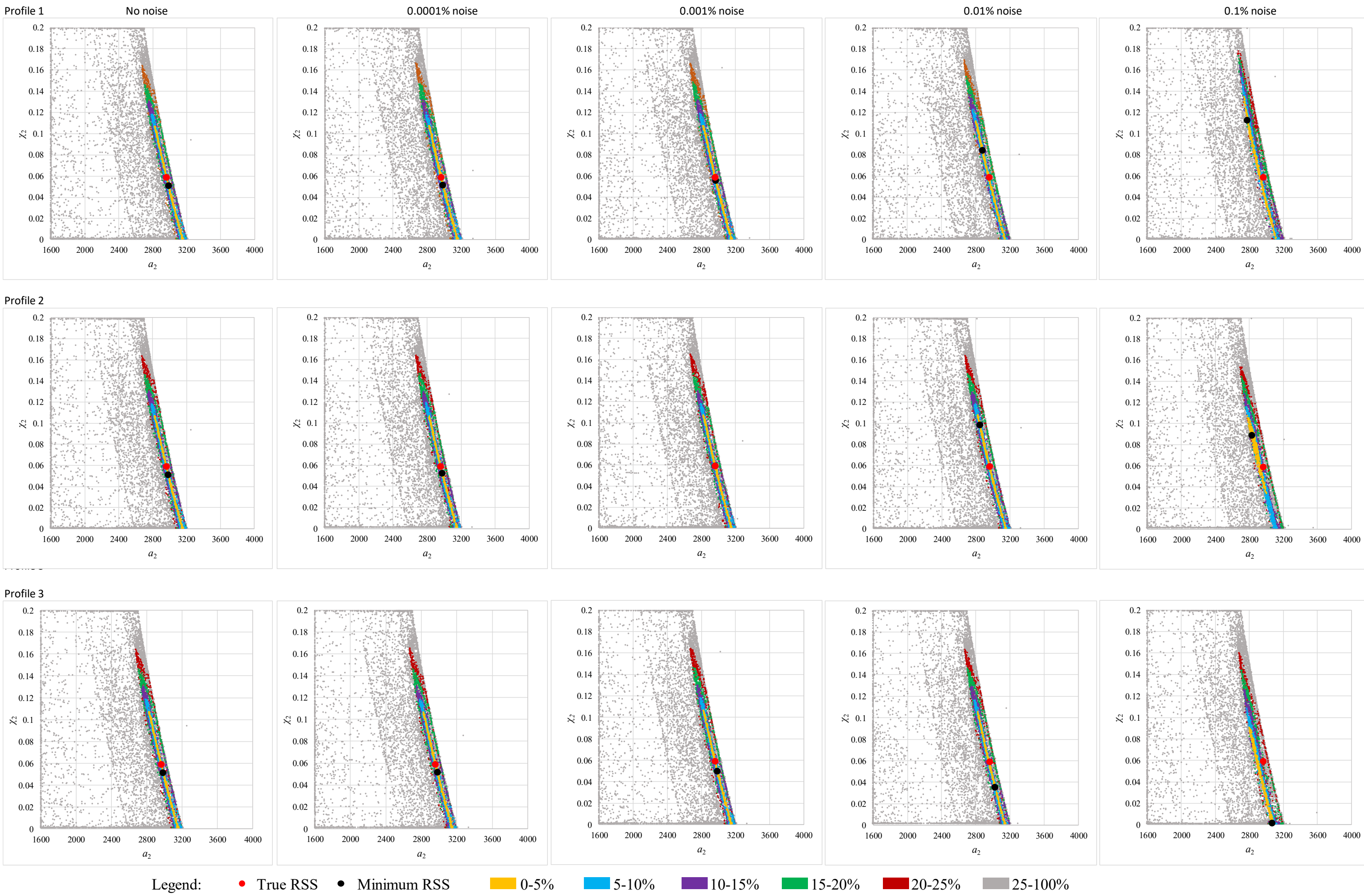

Figure C.14: Cross-plot of parameters, χ vs. a, for Layer 2, for noise added as per Profiles 1, 2, and 3, with noise at magnitudes 0, 0.0001%, 0.001%, 0.01%, 0.1%, from left to right. The noise threshold lies between 0.001% noise and 0.01% noise. The colours indicate the distribution of the parameters w.r.t. the percentile of the RSS to the minimum RSS.

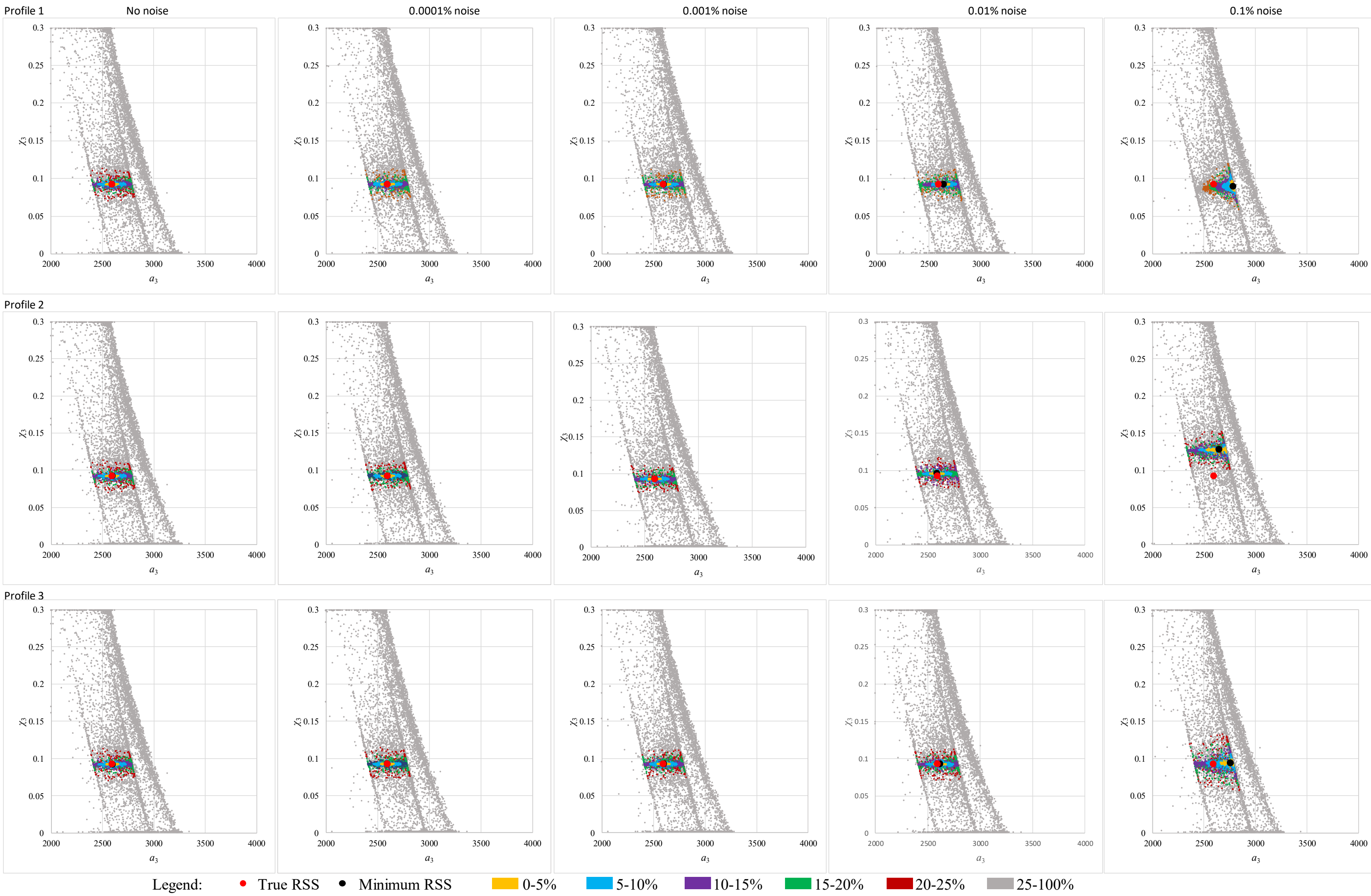

Figure C.15: Cross-plot of parameters, χ vs. a, for Layer 3, for noise added as per Profiles 1, 2, and 3, with noise at magnitudes 0, 0.0001%, 0.001%, 0.01%, 0.1%, from left to right. The noise threshold lies between 0.001% noise and 0.01% noise. The colours indicate the distribution of the parameters w.r.t. the percentile of the RSS to the minimum RSS.

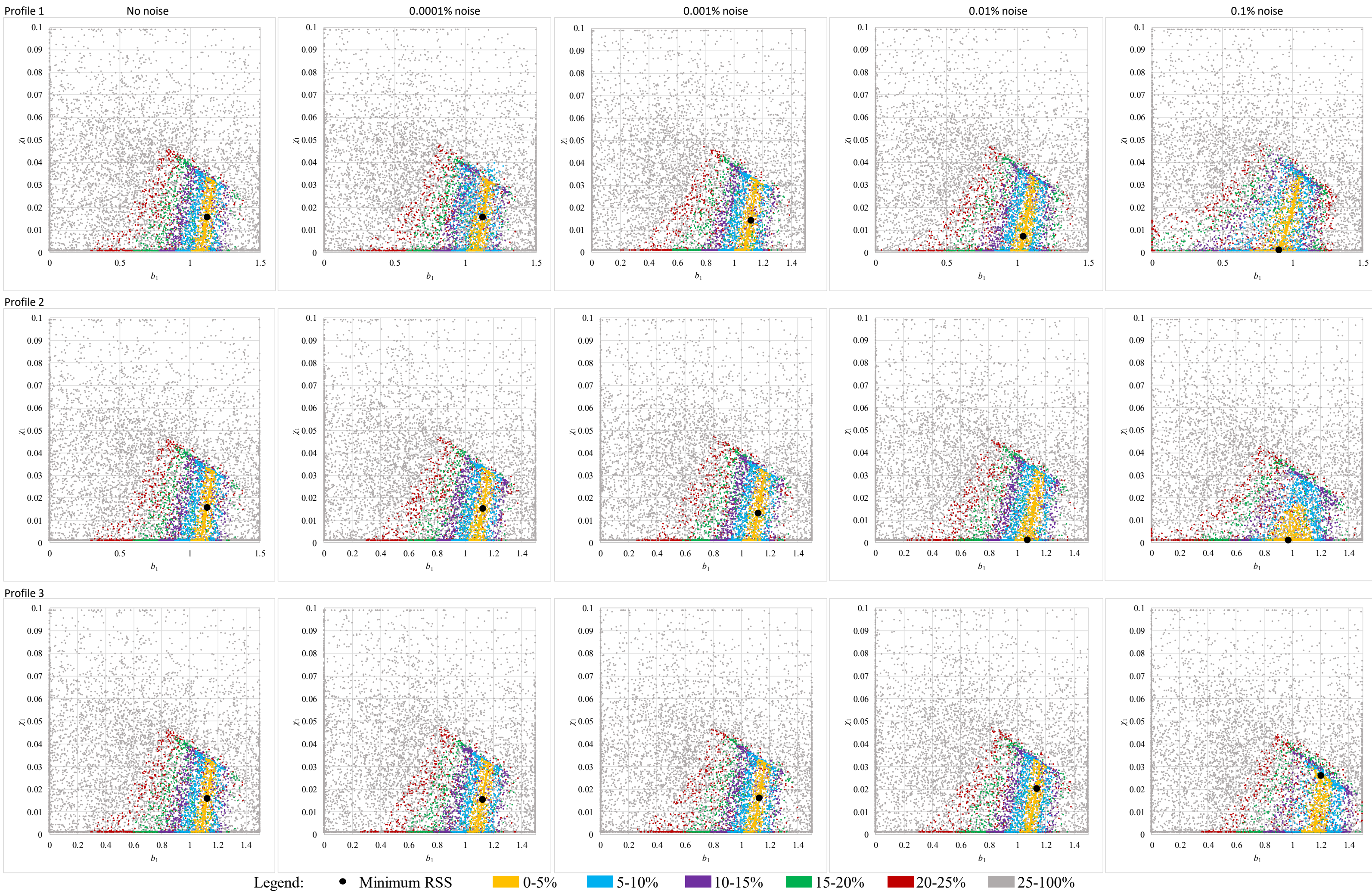

Figure C.16: Cross-plot of parameters, χ vs. b, for Layer 1, for noise added as per Profiles 1, 2, and 3, with noise at magnitudes 0, 0.0001%, 0.001%, 0.01%, 0.1%, from left to right. The noise threshold lies between 0.001% noise and 0.01% noise. The colours indicate the distribution of the parameters w.r.t. the percentile of the RSS to the minimum RSS.

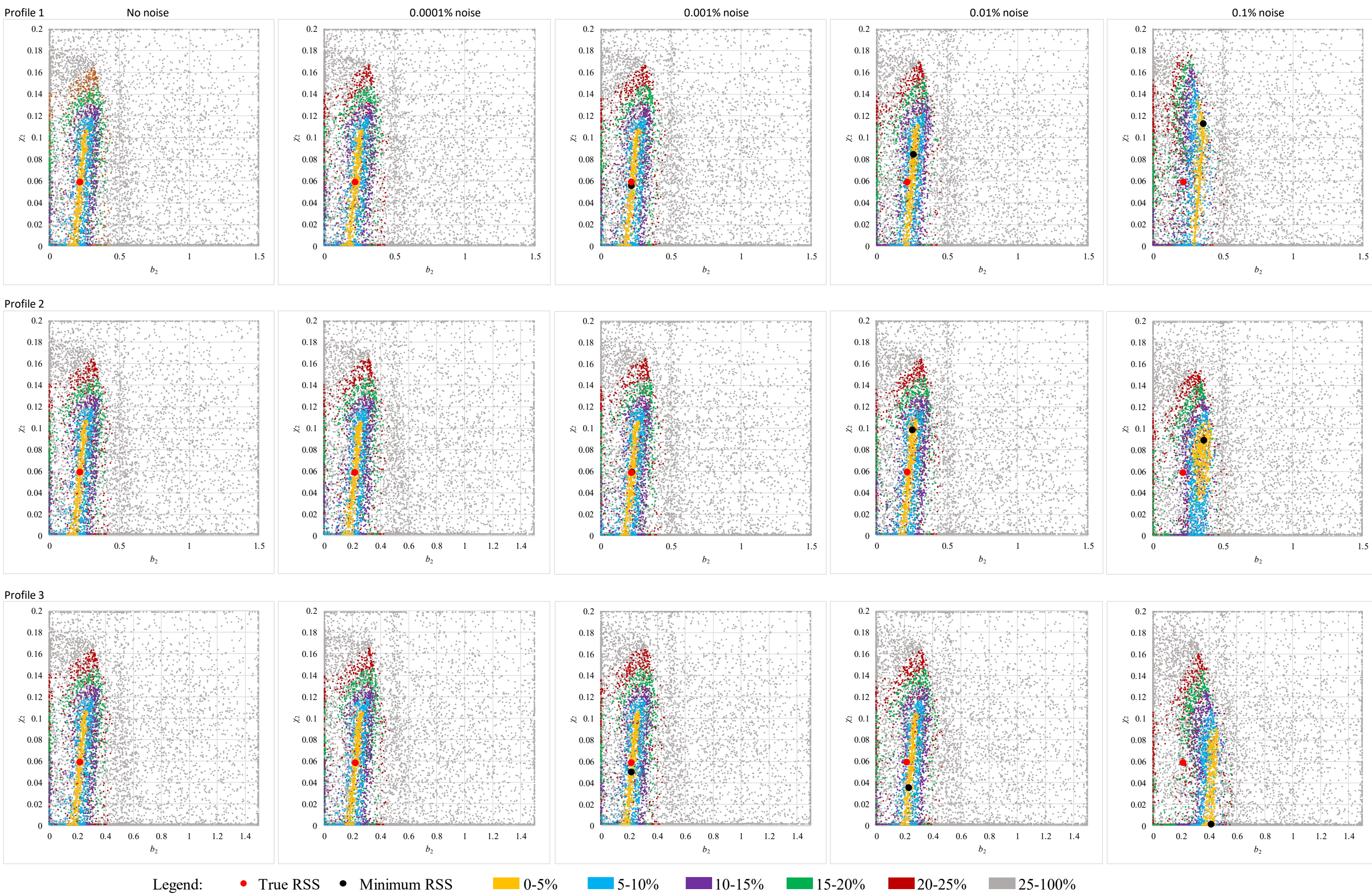

Figure C.17: Cross-plot of parameters, χ vs.b, for Layer 2, for noise added as per Profiles 1, 2, and 3, with noise at magnitudes 0, 0.0001%, 0.001%, 0.01%, 0.1%, from left to right. The noise threshold lies between 0.001% noise and 0.01% noise. The colours indicate the distribution of the parameters w.r.t. the percentile of the RSS to the minimum RSS.

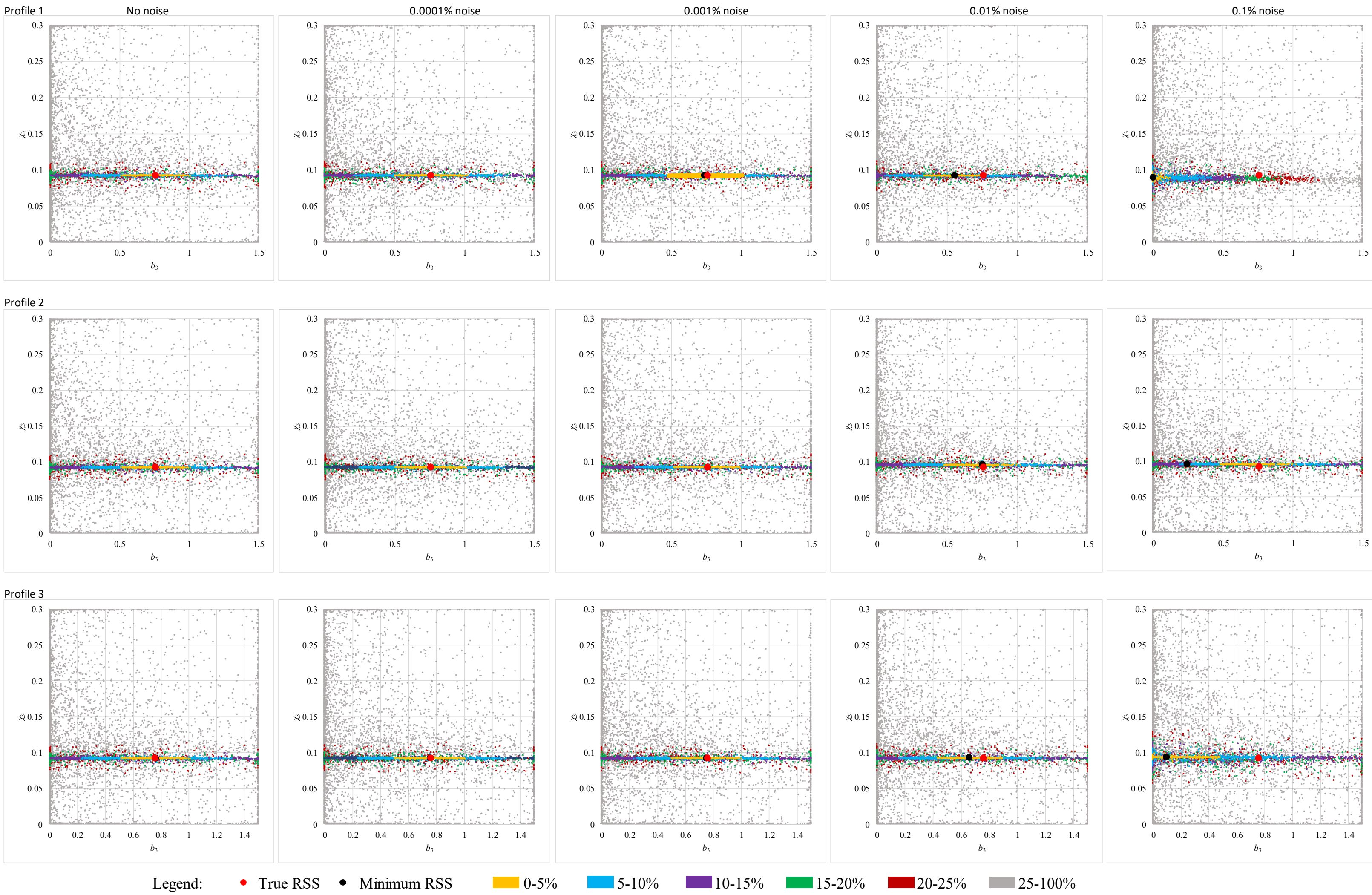

Figure C.18: Cross-plot of parameters, χ vs. b, for Layer 3, for noise added as per Profiles 1, 2, and 3, with noise at magnitudes 0, 0.0001%, 0.001%, 0.01%, 0.1%, from left to right. The noise threshold lies between 0.001% noise and 0.01% noise. The colours indicate the distribution of the parameters w.r.t. the percentile of the RSS to the minimum RSS.

APPENDIX D: Crossplots

D.1 Eight-parameter models

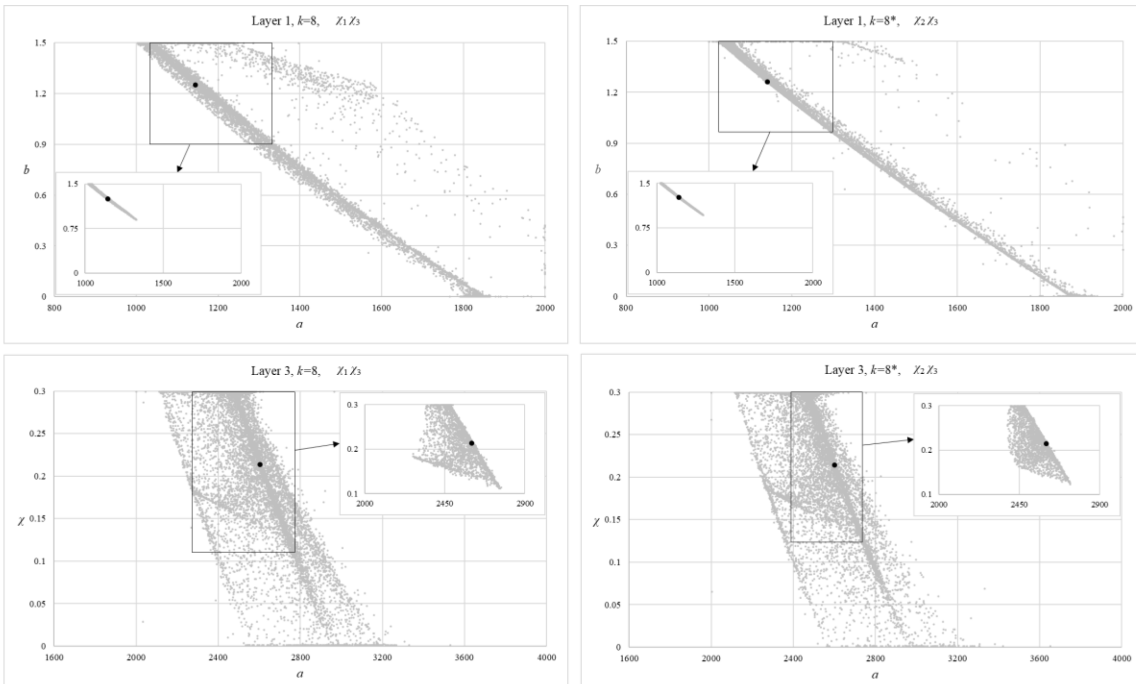

Figure D.1: Crossplots of parameters a (ms^{-1}) versus b (s^{-1}) for the first layer, and a (ms^{-1}) versus χ for the third layer, for the eight-parameter models. For $k = 8$, χ is in first and third layers, for $k = 8^*$, χ is in the second and third layers. a is the speed at the top of the layer. The black boxes encompass the top 25% of the results with respect to the residual sum of squares and correspond to the insets. The dimensions of the insets correspond to the nine-parameter model for comparison. The black dot is where the parameters give the least RSS value.

Table D.1: Correlation coefficients (R) and coefficient of determinations (R^2) corresponding to the insets in Figure D.1.

Layer	Crossplot parameters	Model			
		$k = 8$		$k = 8^*$	
		R	R^2	R	R^2
1	a versus b	-0.9981	0.9963	-0.9989	0.9979
3	a versus χ	-0.4855	0.2358	-0.6374	0.4063

APPENDIX E: Backus and elasticity parameters

E.1 Ten-layer synthetic model – standard Backus parameters – Fermat traveltime

Given elasticity parameters as shown in Table 4.1, equations (1.9) to (1.14) are coded in Excel and give the following for the effective medium:

$$c_{1111}^{\overline{\mathrm{TI}}} = 18.84,\ c_{1133}^{\overline{\mathrm{TI}}} = 10.96,\ c_{1212}^{\overline{\mathrm{TI}}} = 3.99,\ c_{2323}^{\overline{\mathrm{TI}}} = 3.38\ \text{ and }\ c_{3333}^{\overline{\mathrm{TI}}} = 18.43,$$

with units of $10^6\ \mathrm{m^2 s^{-2}}$.

The Fermat traveltime is obtained by taking the thickness of each layer divided by the velocity of the layer, and then summing the resultant travel times,

$$\text{Fermat traveltime} = \sum_{i=1}^{n} \frac{h_i}{\left(v_p\right)_i} = 229.46\ \text{ms},$$

where h_i is the thickness of the layer in m and i is the layer number. In this case, the thickness of each layer is 100 m. Fermat traveltimes are shown in Table E.1.

Table E.1: *P*-wave velocities, v_p, and Fermat traveltimes for a stack of ten, 100 m thick, isotropic layers.

Layer	v_p (kms^{-1})	Fermat traveltime (10^{-3} s)
1	3.25	30.77
2	4.53	22.08
3	5.58	17.92
4	3.85	25.97
5	5.67	17.64
6	4.00	25.00
7	4.05	24.69
8	4.25	23.53
9	5.61	17.83
10	4.16	24.04
	Sum	229.46

E.2 Ten-layer synthetic model – standard Backus parameters – equivalent medium traveltime

This is obtained by taking the thickness of the entire medium and dividing by the velocity of the equivalent medium,

$$\text{equivalent medium traveltime} = \frac{\sum_{i=1}^{n} h_i}{\sqrt{c_{3333}^{\overline{\mathrm{TI}}}}} = \frac{1000\ (\mathrm{m})}{\sqrt{18.43\ (10^6 \mathrm{m}^2\mathrm{s}^{-2})}} = 232.91\ \mathrm{ms}\,,$$

where h_i is the layer thickness for the i th layer. The thickness of each layer is 100 m.

Note:

$$c_{3333}^{\overline{\mathrm{TI}}} = \overline{\left(\frac{1}{c_{1111}}\right)}^{-1} = \left(\frac{\sum_{i=1}^{n} h_i \left(\frac{1}{c_{1111}}\right)_i}{\sum_{j=1}^{n} h_j}\right)^{-1}.$$

E.3 Ten-layer synthetic model – traveltime weighting – equivalent medium traveltime

Here, instead of using thickness as weighting, traveltimes in each layer are used as weights. The traveltime of the equivalent medium is

$$\text{equivalent medium traveltime} = \frac{\sum_{i=1}^{n} h_i}{\sqrt{c_{3333}^{\overline{\mathrm{TI}}}}} = \frac{1000\ (\mathrm{m})}{\sqrt{17.39\ (10^6 \mathrm{m}^2\mathrm{s}^{-2})}} = 239.77\ \mathrm{ms}\,,$$

where here, h_i, represents the traveltime in the *i*th layer and the elasticity parameter is

$$c_{3333}^{\overline{\mathrm{TI}}} = \overline{\left(\frac{1}{c_{1111}}\right)}^{-1} = \left(\frac{\sum_{i=1}^{n} h_i \left(\frac{1}{c_{1111}}\right)_i}{\sum_{j=1}^{n} h_j}\right)^{-1} = \left(\frac{13.19\ (10^{-9}\mathrm{m}^{-2}\mathrm{s}^{3})}{229.46\ (10^{-3}\mathrm{s}\,)}\right)^{-1} = 17.39\ (10^6\mathrm{m}^2\mathrm{s}^{-2})$$

Table E.2: Traveltimes calculated with traveltime weightings for a stack of ten, 100 m thick, isotropic layers.

Layer	c_{1111} (10^6 m^{2}s^{-2})	$\frac{1}{c_{1111}}$ (10^{-6} m^{-2}s^2)	h_j (10^{-3} s)	$h_i\left(\frac{1}{c_{1111}}\right)_i$ (10^{-3} s)
1	10.56	0.095	30.77	2.91
2	20.52	0.049	22.08	1.08
3	31.14	0.032	17.92	0.58
4	14.82	0.067	25.97	1.75
5	32.15	0.031	17.64	0.55
6	16.00	0.063	25.00	1.56
7	16.40	0.061	24.69	1.51
8	18.06	0.055	23.53	1.30
9	31.47	0.032	17.83	0.57
10	17.31	0.058	24.04	1.39
		Sum	229.46	13.19
			$c_{3333}^{\overline{\mathrm{TI}}} =$	17.39

E.4 Ten-layer synthetic model – takeoff angle 30° – standard Backus parameters – Fermat traveltime

Standard Backus parameters for the effective medium are as shown in Section E.1.

The horizontal distance, x_i, in a layer is obtained from the tangent of the incident angle, Θ, for the layer,

$$x_i = h_i tan\Theta_i,$$

where h_i is the thickness of the *i*th layer.

The distance, d_i, in a layer is obtained from the cosine of the incident angle, Θ, for the layer,

$$d_i = h_i cos\Theta_i,$$

The Fermat traveltime is obtained by taking the distance, d_i, travelled in each layer divided by the velocity of the layer, and then summing the resultant travel times.

$$\text{Fermat traveltime} = \sum_{i=1}^{n} \frac{d_i}{(v_p)_i} = 330.52 \text{ ms},$$

where d_i is the distance travelled in the layer and *i* is the layer number. Fermat traveltimes are shown in Table E3.

Table E.3: Fermat traveltimes for a signal travelling through a stack of ten isotropic layers with a takeoff angle of 30°. The bottom of the stack is reached at a horizontal distance of 1072.53 m, with a Fermat traveltime of 330.52 ms.

Layer	v_P (kms^{-1})	Θ (deg)	x (m)	d (m)	Fermat traveltime (10^{-3} s)
1	3.25	30.00	57.74	115.47	35.53
2	4.53	44.18	97.18	139.44	30.78
3	5.58	59.14	167.38	194.98	34.94
4	3.85	36.32	73.51	124.11	32.24
5	5.67	60.73	178.40	204.52	36.07
6	4.00	37.98	78.07	126.87	31.72
7	4.05	38.54	79.66	127.85	31.57
8	4.25	40.83	86.42	132.17	31.10
9	5.61	59.66	170.88	197.99	35.29
10	4.16	39.79	83.29	130.14	31.28
		Sums	1072.53		330.52

E.5 Ten-layer synthetic model – takeoff angle 30° – standard Backus parameters – equivalent medium traveltime

The ray angle, θ, for for a horizontal distance of 1072.53 m, as calculated above, and a total layer thickness of 1000 m is,

$$\theta = tan^{-1}\left(\frac{1072.53}{1000}\right) = 47.00°.$$

From the ray angle, the ray velocity, V, is obtained as described in Section E.9.

Using Excel, the standard Backus elasticity parameters from Section E.1.

$$c_{1111}^{\overline{\mathrm{TI}}} = 18.84,\ c_{1133}^{\overline{\mathrm{TI}}} = 10.96,\ c_{1212}^{\overline{\mathrm{TI}}} = 3.99,\ c_{2323}^{\overline{\mathrm{TI}}} = 3.38\ \text{and}\ c_{3333}^{\overline{\mathrm{TI}}} = 18.43,$$

Using these parameters, the traveltime is computed to be 343.82 ms.

E.6 Ten-layer synthetic model –takeoff angle 30° – modified Backus parameters – equivalent medium traveltime

The distance-weighted Backus elasticity parameters, computed using Excel, are

$$c_{1111}^{\overline{\mathrm{TI}}} = 20.13,\ c_{1133}^{\overline{\mathrm{TI}}} = 4.10,\ c_{1212}^{\overline{\mathrm{TI}}} = 12.06,\ c_{2323}^{\overline{\mathrm{TI}}} = 3.45 \text{ and } c_{3333}^{\overline{\mathrm{TI}}} = 19.76.$$

Using these parameters, the traveltime is computed to be 332.36 ms.

E.7 Ten-layer synthetic model – 7000 m offset – standard Backus parameters – Fermat traveltime

For a 7000 m horizontal offset, the takeoff angle using Excel is 34.97°.

The Fermat traveltime is calculated in similar fashion as shown in Section E.4.

$$\text{Fermat traveltime} = \sum_{i=1}^{n} \frac{d_i}{(v_p)_i} = 1364.97 \text{ ms},$$

where d_i is the distance travelled in the layer and i is the layer number. Fermat traveltimes are shown in Table E4.

Table E.4: Fermat traveltimes for a signal travelling through a stack of ten isotropic layers with to an offset of 7000 m.

Layer	v_P (kms^{-1})	Θ (deg)	x (m)	d (m)	Fermat traveltime (10^{-3} s)
1	3.25	34.97	37.55	122.03	35.53
2	4.53	53.01	36.69	166.22	30.78
3	5.58	79.72	100.38	560.13	34.94
4	3.85	42.76	35.37	136.19	32.24
5	5.67	88.87	891.78	5056.39	36.07
6	4.00	44.86	35.27	141.07	31.72
7	4.05	45.57	35.27	142.86	31.57
8	4.25	48.54	35.54	151.03	31.10
9	5.61	81.58	121.75	683.03	35.29
10	4.16	47.18	35.37	147.14	31.28
		Sums	7000.00	7306.08	1364.97

E.8 Ten-layer synthetic model – 7000 m offset – standard Backus parameters – equivalent medium traveltime

The ray angle, θ, for for a horizontal distance of 7000 m and a total layer thickness of 1000 m is,

$$\theta = tan^{-1}\left(\frac{7000}{1000}\right) = 81.87°.$$

From the ray angle, the ray velocity, V, is obtained as described in Section E.11.

Using Excel, the standard Backus elasticity parameters from Section E.1, the traveltime is computed to be 1631.27 ms.

E.9 Ten-layer synthetic model – 7000 m offset – modified Backus parameters – equivalent medium traveltime

Using Excel, the distance-weighted elasticity parameters are

$$c_{1111}^{\overline{\mathrm{TI}}} = 27.73,\ c_{1133}^{\overline{\mathrm{TI}}} = 21.04,\ c_{1212}^{\overline{\mathrm{TI}}} = 3.52,\ c_{2323}^{\overline{\mathrm{TI}}} = 3.16 \ \text{ and } \ c_{3333}^{\overline{\mathrm{TI}}} = 28.08.$$

Using these parameters, the traveltime is computed to be 1343.15 ms.

E.10 Derivation of the thickness - weighted arithmetic average expression

As per Backus (1962) the average of function of "width" l' is given by,

$$\bar{f}(x_3) = \int_{-\infty}^{\infty} w(\xi - x_3)\, f(\xi)\, \mathrm{d}\xi,$$

where $w(x_3)$ is the weight function.

Let

$$w(y) = \frac{1}{2\sqrt{3}l'} \mathrm{I}_{[-\sqrt{3}l', \sqrt{3}l']} = \begin{cases} \frac{1}{2\sqrt{3}l'} & -\sqrt{3}l' \leq \mathrm{y} \leq \sqrt{3}l' \\ 0 \quad y < -\sqrt{3}l' \text{ or } \mathrm{y} > \sqrt{3}l' \end{cases}.$$

Then, if $Z = 2\sqrt{3}l'$,

$$w(y) = \begin{cases} 1/Z & -Z/2 \leq \mathrm{y} \leq Z/2 \\ 0 & y < -Z/2 \text{ or } \mathrm{y} > Z/2 \end{cases}.$$

Then, if we let the mid-point be $x_3 = Z/2 = \sqrt{3}l'$,

$$w(\xi - x_3) = w(\xi - Z/2)\begin{cases} 1/Z & 0 \leq \xi \leq Z \\ 0 & \xi < 0 \text{ or } \xi > Z \end{cases},$$

and,

$$\bar{f}(Z/2) = \frac{1}{Z}\int_0^Z f(\xi)\, \mathrm{d}\xi = \frac{1}{Z}\sum_{i=1}^{n} h_i f_i\,,$$

where $Z = \sum h_i$ is the total height, and if h_i is constant over all layers,

$$\bar{f}(Z/2) = \frac{1}{n}\sum_{i=1}^{n} f_i\,.$$

E.11 Derivation of the ray velocity from the ray angle

The ray velocity, V, is derived from the ray angle, ϑ, in a transversely isotropic medium, using equations (9.2.19), (9.2.23), (8.4.9), and (8.4.12) from Slawinski (2020a), which in the notation here, using the density-scaled elasticity parameters, are represented as

$$v_{qP} = \sqrt{\left(c_{3333}^{\overline{\mathrm{TI}}} - c_{1111}^{\overline{\mathrm{TI}}}\right)cos^2\vartheta + c_{1111}^{\overline{\mathrm{TI}}} + c_{2323}^{\overline{\mathrm{TI}}} + \sqrt{\Delta}} \tag{E.1}$$

where, ϑ , is the phase angle, discriminant, Δ, is

$$\begin{aligned}\Delta := \left(\left(c_{1111}^{\overline{\mathrm{TI}}} - c_{2323}^{\overline{\mathrm{TI}}}\right)sin^2\vartheta - \left(c_{3333}^{\overline{\mathrm{TI}}} - c_{2323}^{\overline{\mathrm{TI}}}\right)cos^2\vartheta\right)^2 \\ + 4\left(c_{2323}^{\overline{\mathrm{TI}}} + c_{1133}^{\overline{\mathrm{TI}}}\right)^2 sin^2\vartheta cos^2\vartheta\,,\end{aligned} \tag{E.2}$$

(E.3)

$$V(\vartheta) = \sqrt{[v(\vartheta)]^2 + \left[\frac{\partial v(\vartheta)}{\partial \vartheta}\right]^2}\ ,$$

which is the magnitude of the ray velocity in terms of the phase velocity as a function of the phase angle.

$$tan\theta = \frac{tan\vartheta + \frac{1}{v}\frac{\partial v}{\partial \vartheta}}{1 - \frac{tan\vartheta}{v}\frac{\partial v}{\partial \vartheta}}. \tag{E.4}$$

For a given ray angle, θ, equation E.4 is numerically solved for the wavefront normal angle, ϑ, and then equation (E.3) used to solve for ray velocity *V.*

Note:

$$\frac{\partial v(\vartheta)}{\partial \vartheta} = \frac{\frac{D}{C} + A}{B}\ ,$$

where,

$$A = -2\left(c_{3333}^{\overline{\text{TI}}} + c_{1111}^{\overline{\text{TI}}}\right)sin\vartheta cos\vartheta\ ,$$

$$B = 2\sqrt{2}\sqrt{E + \left(c_{3333}^{\overline{\text{TI}}} + c_{1111}^{\overline{\text{TI}}}\right)cos^2\vartheta + c_{1111}^{\overline{\text{TI}}} + c_{2323}^{\overline{\text{TI}}}}\ ,$$

$$C = 2\sqrt{\left[\left(c_{1111}^{\overline{\text{TI}}} - c_{2323}^{\overline{\text{TI}}}\right)sin^2\vartheta - \left(c_{3333}^{\overline{\text{TI}}} - c_{2323}^{\overline{\text{TI}}}\right)cos^2\vartheta\right]^2 + 4\left(c_{1133}^{\overline{\text{TI}}} + c_{2323}^{\overline{\text{TI}}}\right)^2 sin^2\vartheta cos^2\vartheta}\ ,$$

$$\begin{aligned} D = {} & 2\left(2\left(c_{1111}^{\overline{\text{TI}}} - c_{2323}^{\overline{\text{TI}}}\right)sin\vartheta cos\vartheta + 2\left(c_{3333}^{\overline{\text{TI}}} - c_{2323}^{\overline{\text{TI}}}\right)sin\vartheta cos\vartheta\right)\left[\left(c_{1111}^{\overline{\text{TI}}} - c_{2323}^{\overline{\text{TI}}}\right)sin^2\vartheta \right. \\ & \left. - \left(c_{3333}^{\overline{\text{TI}}} - c_{2323}^{\overline{\text{TI}}}\right)cos^2\vartheta\right] + 8\left(c_{1133}^{\overline{\text{TI}}} + c_{2323}^{\overline{\text{TI}}}\right)^2 sin\vartheta cos^3\vartheta \\ & - 8\left(c_{1133}^{\overline{\text{TI}}} + c_{2323}^{\overline{\text{TI}}}\right)^2 sin^3\vartheta cos\vartheta\ , \end{aligned}$$

$$E = \sqrt{\left[\left(c_{1111}^{\overline{\text{TI}}} - c_{2323}^{\overline{\text{TI}}}\right)sin^2\vartheta - \left(c_{3333}^{\overline{\text{TI}}} - c_{2323}^{\overline{\text{TI}}}\right)cos^2\vartheta\right]^2 + 4\left(c_{1133}^{\overline{\text{TI}}} + c_{2323}^{\overline{\text{TI}}}\right)^2 sin^2\vartheta cos^2\vartheta}\ .$$